

Molecular Liquids and Polymers Investigated by Field Cycling ^1H NMR Relaxometry: Impact of Rotational and Translational Dynamics on Relaxation

Von der Universität Bayreuth genehmigte
Abhandlung zur Erlangung des Grades eines
Doktors der Naturwissenschaften (Dr. rer. nat.)

von

Roman Meier

geboren am 29.01.1982 in Prien am Chiemsee

Tag der Einreichung: 13.02.2014

Tag des Kolloquiums: 30.04.2014

1. Gutachter: Prof. Dr. Ernst Rößler

2. Gutachter: Prof. Dr. Franz Fajara

Contents

1 Abstract	1
2 Kurzdarstellung	3
3 Extended Abstract	5
3.1 Introduction	5
3.2 Phenomenological Description of the Rate Dispersion of Glycerol	52
3.3 Intermolecular Relaxation in Glycerol	54
3.4 Application of the Translational Low-Frequency Dispersion to Molecular Liquids	57
3.5 Intermolecular Relaxation in o-Terphenyl	60
3.6 Application of the Translational Low-Frequency Dispersion to Polymers	64
3.7 Derivation of an Isofrictional Quantity in Polymers and its Comparison to Common Theory	66
4 Publications	68
Bibliography	137
Acknowledgements	142

1 Abstract

In this thesis field-cycling nuclear magnetic resonance relaxometry (FC NMR) is applied to measure the spin-lattice relaxation time, T_1 , of proton spins in condensed matter not only at different temperatures but also at different Larmor frequencies, ω . The results are presented by means of six publications, from which the first four deal with viscous molecular liquids while the latter two address melts of linear polymers of various length or molecular mass, M . The spin relaxation rate, $R_1 = 1/T_1$, reflects the molecular dynamics via the fluctuation of a certain interaction. In the present case of protons the spins relax due to magnetic dipole-dipole coupling which may be intra- or intermolecular. Because of the latter the proton relaxation is not only governed by molecular reorientation but also by translation. Contrary to the common assumption that the intramolecular interactions are the most relevant for proton relaxation, it even turns out that especially at low frequencies the relaxation rate actually is dominated by the intermolecular contribution.

The rate dispersion curves, $R_1(\omega)$, obtained by FC ^1H NMR can directly be compared to the results of other techniques like dielectric spectroscopy (DS) or depolarized light scattering (LS). With respect to DS and LS, both solely probing molecular reorientation, $R_1(\omega)$ shows an enhanced intensity at low frequencies for most molecular liquids. This thesis shows that this feature is due to translational dynamics which are only seen by ^1H NMR in combination with a large spectral separation between both types of dynamics. Furthermore it is demonstrated that, besides rotational time constants, τ_{rot} , one can extract self-diffusion coefficients, D , from the rate dispersion, $R_1(\omega)$. This can be done in a simple, model-independent way exploiting the universal translationally driven behavior of $R_1(\omega)$ at low frequencies, which is a consequence of the Fickian diffusion limit at long times. The extracted D show a good agreement with results from field gradient (FG) NMR up to now the most prominent technique to access translational diffusion. To reveal the contribution of intra- and intermolecular relaxation in liquids isotope dilution experiments were done which allow the separation of the total rate, $R_1(\omega)$, into its two respective components, $R_{1,\text{intra}}(\omega)$ and $R_{1,\text{inter}}(\omega)$. It is shown that the intermolecular relaxation in ^1H NMR is not negligible at all even at high frequencies, because, besides the purely translational contribution, $R_{1,\text{inter}}(\omega)$ also contains intermolecularly reflected rotation. This is due to spins placed off the molecules'

center, a phenomenon called ‘eccentricity effect’, and is demonstrated in neat liquids for the first time.

Finally it is shown that from the universal translational low-frequency behavior it is also possible to extract D in the case of polymer melts. Here self-diffusion data in agreement to FG NMR could be collected up to molecular masses where the entanglement of the polymer chains already is established. In addition FC NMR provides time constants, τ_s , on the segmental motion which, in combination with the self-diffusion data, give access to the collective polymer dynamics via an ‘iso-frictional’ quantity, $D\tau_s$, which can be checked against common theories. Depending on the molecular mass three regimes could be identified: the simple liquid behavior, the development of Rouse modes and the final onset of the entanglement regime. Thereby, the pure Rouse regime is only seen in a very small M interval as the Rouse modes slowly evolve with growing M and subsequently entanglement is established for M exceeding the entanglement molecular mass.

In summary, this thesis shows that the intermolecular relaxation channel of the proton spin relaxation is not to be considered as a peculiarity which has to be overcome when collecting information on reorientational/segmental dynamics in condensed matter, but that this feature provides additional information which gives access to translational motion. Thus FC ^1H NMR is a powerful tool for the examination of molecular dynamics in condensed matter and may become a serious competitor to FG NMR regarding monitoring of translational diffusion in neat systems.

2 Kurzdarstellung

In dieser Arbeit wird mit Hilfe von Kernspinresonanz Relaxometrie (FC NMR) die Spin-Gitter-Relaxationszeit, T_1 , von Protonenspins in kondensierter Materie nicht nur bei verschiedenen Temperaturen, sondern auch bei verschiedenen Larmorfrequenzen gemessen. Die Ergebnisse werden anhand von sechs Publikationen präsentiert, von welchen die ersten vier viskose, molekulare Flüssigkeiten behandeln, während sich die letzten beiden mit Schmelzen linearer Polymere von diverser Länge beziehungsweise Molekulargewicht, M , befassen. Die Spinrelaxationsrate, $R_1 = 1/T_1$, spiegelt die molekulare Dynamik durch Fluktuation einer bestimmten Wechselwirkung wider. Im aktuellen Fall von Protonen relaxieren die Spins aufgrund von magnetischer Dipol-Dipol-Kopplung, welche intra- oder intermolekular sein kann. Wegen letzterer wird die Protonenrelaxation nicht nur von molekularer Reorientierung beeinflusst, sondern auch von Translation. Im Gegensatz zur üblichen Annahme die intramolekularen Wechselwirkungen seien am maßgeblichsten für die Protonenrelaxation, stellt sich heraus, dass besonders bei niedrigen Frequenzen der intermolekulare Anteil sogar dominiert.

Die Ratendispersionskurven, $R_1(\omega)$, welche mit FC ^1H NMR gemessen wurden, können direkt mit Ergebnissen von anderen Techniken, wie dielektrische Spektroskopie (DS) oder depolarisierte Lichtstreuung (LS) verglichen werden. Mit Hinsicht auf DS und LS, welche beide nur die molekulare Reorientierung sondieren, zeigt $R_1(\omega)$ bei den meisten molekularen Flüssigkeiten eine vergrößerte Amplitude bei kleinen Frequenzen. Diese Arbeit zeigt, dass diese Eigenschaft aufgrund der Translationsdynamik, die nur von ^1H NMR erfasst wird, in Kombination mit einer großen spektralen Trennung zwischen den beiden Arten von Dynamik auftritt. Außerdem wird aufgezeigt dass, neben rotatorischen Zeitkonstanten, τ_{rot} , auch Selbstdiffusionskoeffizienten, D , aus der Ratendispersionskurve, $R_1(\omega)$, gewonnen werden können. Dies kann in einer einfachen, modelunabhängigen Prozedur durchgeführt werden, welche das universelle, translatorisch bestimmte Verhalten von $R_1(\omega)$ bei kleinen Frequenzen ausnutzt, welches die Konsequenz des Grenzverhaltens von Fickscher Diffusion bei langen Zeiten ist. Die gewonnen D -Werte zeigen eine gute Übereinstimmung mit den Ergebnissen von Feldgradienten-(FG) NMR, bis jetzt die bekannteste Methode um Translationsdiffusion zu erfassen. Um die Anteile von intra- und intermolekularer Relaxation in Flüssigkeiten zu klären wurden Isotopenverdünnungsexperimente durchgeführt, welche die Trennung der

totalen Rate, $R_1(\omega)$, in ihre jeweiligen Komponenten, $R_{1,\text{intra}}(\omega)$ und $R_{1,\text{inter}}(\omega)$, ermöglicht. Es wird belegt, dass sogar bei hohen Frequenzen die intermolekulare Relaxation bei ^1H NMR überhaupt nicht vernachlässigbar ist, weil $R_{1,\text{inter}}(\omega)$ neben dem reinen translativen Beitrag auch intermolekular vermittelte Rotation enthält. Das geschieht wegen Spins, die unzentriert auf dem Molekül platziert sind, ein Phänomen, welches ‘Exzentrizitätseffekt’ genannt wird und zum ersten Mal in reinen Flüssigkeiten gezeigt wird.

Schließlich wird gezeigt, dass es auch im Fall von Polymeren möglich ist mit Hilfe des universellen, translatorisch bestimmten Verhaltens bei kleinen Frequenzen D zu bestimmen. Dabei konnten mit FG NMR übereinstimmende Daten für die Selbstdiffusion bis zu Molekulargewichten gesammelt werden, wo bereits die Verschlaufung der Ketten eingesetzt hat. Weiterhin stellt FC NMR Zeitkonstanten, τ_s , für die Segmentdynamik bereit, welche kombiniert mit den Selbstdiffusionsdaten den Zugriff auf die kollektive Polymerdynamik mittels einer Größe, $D\tau_s$, ermöglicht, welche sich auf gleiche segmentelle Reibungskoeffizienten bezieht und mit gängigen Theorien verglichen werden kann. Je nach Molekulargewicht konnten drei Regimes identifiziert werden: Das Verhalten der einfachen Flüssigkeit, die Entwicklung von Rousemoden und schließlich das Einsetzen der Kettenverschlaufung. Dabei ist das Rouse regime nur über ein kleines Intervall sichtbar, da sich die Rousemoden nur langsam mit steigendem M entwickeln und bald darauf die Verschlaufung einsetzt, wenn M ein bestimmtes Gewicht überschreitet.

Zusammengefasst zeigt diese Arbeit, dass der intermolekulare Relaxationsweg der Protonenspins nicht als eine Eigenart gesehen werden sollte, welche überwunden werden muss, wenn man Information zu Reorientierungs-/Segmentdynamik in kondensierter Materie sammelt, sondern dass diese Eigenschaft zusätzliche Informationen bereitstellt, die es erlauben Translationsdynamik zu erfassen. Deshalb ist FC ^1H NMR eine leistungsfähige Methode zur Untersuchung der molekularen Dynamik in kondensierter Materie und könnte im Feld der Beobachtung von translatorischer Dynamik in reinen Systemen eine ernsthafte Konkurrenz zur FG NMR werden.

3 Extended Abstract

3.1 Introduction

Nuclear magnetic resonance (NMR) relaxometry is a powerful tool for studying dynamics in molecular liquids. The spin-lattice relaxation rate, $R_1 = 1/T_1$, is closely connected to the spectral density which itself is the Fourier transform of a correlation function. As the latter describes the dynamics, spin relaxometry provides access to molecular motion. While in the very beginning of NMR the nucleus most studied was ^1H , later people went more and more towards other nuclei like ^2H or ^{13}C . A reason for this is that the proton relaxation is governed by two-particle interactions where the second particle either can be situated on the same molecule (*i.e.* intramolecular relaxation) or on a different one (*i.e.* intermolecular relaxation). Hence the proton relaxation in molecular liquids generally consists of an intramolecular contribution, $R_{1,\text{intra}}$, and an intermolecular one, $R_{1,\text{inter}}$:

$$R_1 = R_{1,\text{intra}} + R_{1,\text{inter}} \quad (1)$$

The first contribution merely reflects molecular reorientation the latter additionally contains translational motion. Often it was argued that due to the short range nature of the dipole-dipole interaction, which is responsible for proton relaxation, a given proton will feel primarily protons on the same molecule and thus ^1H NMR measures essentially rotational diffusion, an assumption which will be refuted by this thesis. Nevertheless, the intermolecular contribution remained long unexplored in detail and, as said, people often avoided these uncertainties by measuring nuclei with a pure intramolecular relaxation mechanism like ^2H or ^{13}C , which only reflect rotational diffusion like in the case of other techniques, *e.g.* dielectric spectroscopy (DS) and depolarized light scattering (LS). However, contrary to LS and DS common NMR relaxometry only is able to probe the spectral density at one single frequency. With the advent of the fast (*i.e.* electronic) field cycling (FC) technique this changed and it became possible to record the rate dispersion, $R_1(\omega)$, with R_1 taken at different frequencies, ω . Furthermore the commercial availability of Stellar Spinmaster FFC 2000 spectrometers at Stellar s.r.l. since 1997 made FC NMR relaxometry (the abbreviation ‘FC (^1H) NMR’ henceforth refers to relaxometry) gain new momentum. Because this type of spectrometer is best suited to measure protons, especially ^1H NMR relaxometry was rediscovered. Its

frequency range for protons is $10\text{kHz} \leq \omega/2\pi = \nu \leq 20\text{MHz}$. Hence the Stellar FFC relaxometers are well suited to measure viscous liquids. But also the dynamics of more complex systems like polymers are located in this frequency range and with the introduction of that commercial relaxometer people turned to a greater extent to systems like these instead of reexamining the rather old matter of proton relaxation in molecular (simple) liquids.

To overcome the still narrow frequency range covered by FC NMR in preceding publications of the Rössler group in Bayreuth the measured rate dispersions, $R_1(\omega)$, were transformed into the so-called ‘susceptibility representation’, $\chi''_{\text{NMR}}(\omega) \equiv \omega R_1(\omega)$, and then master curves, $\chi''_{\text{NMR}}(\omega \tau_{\text{rot}})$, were constructed by scaling the frequency axis with the rotational time constant, τ_{rot} . The latter procedure assumes ‘frequency-temperature-superposition’ (FTS) to hold and was rarely applied to NMR results so far but is known, *e.g.*, from rheology. The susceptibility master curves cover several decades in frequency and were compared to those from DS and LS. Hereby an additional contribution of the FC ^1H NMR results at low frequencies was found in comparison to the other techniques solely detecting molecular reorientation. Own preliminary work covering several liquids confirmed that this low-frequency extra contribution even is the usual case. This provoked the question what process is reflected there and how it is connected to the fact that ^1H NMR detects, besides intramolecular relaxation, also intermolecular one. Among other experiments the isotope dilution technique can clearly answer this question as it separates intra- and intermolecular relaxation contributions. Another interesting fact is where translational and rotational motion are respectively located, *i.e.*, whether they are spectrally separated which facilitates their separation applying appropriate models. It is the purpose of this thesis to clarify these questions and show how to even benefit from the intermolecular relaxation contribution in ^1H NMR, *e.g.*, when determining self-diffusion coefficients, D .

In Pub. 1 rate dispersion curves, $R_1(\omega)$, of glycerol obtained by FC ^1H NMR are described by applying a model assuming a translational process besides the rotational contribution. The extracted D as well as the rotational time constants, τ_{rot} , are compared with those from other techniques. Pub. 2 experimentally clarifies the shape of the intermolecular relaxation rate dispersion, $R_{1,\text{inter}}(\omega)$, in glycerol by an isotope dilution experiment (*cf.* Sec. 3.1.7). Pub. 3 exploits the universal translationally driven behavior of $R_1(\omega)$ at low frequencies, which is a consequence of the translational diffusion limit at long times, to determine D in a model independent way (*cf.* Sec. 3.1.8). The results obtained on various liquids are compared to the ones from field gradient (FG) NMR, up to now the most prominent technique to access

translational diffusion. Pub. 4 contains an isotope dilution experiment on o-terphenyl (OTP) one of the few systems whose results agree with DS as they show no distinct additional low-frequency contribution. Additionally D was determined for further liquids and a new type of master curve in the rate representation based on the translational diffusion is introduced (*cf.* Sec. 3.1.8). Finally, in Pub. 5 and Pub. 6, the model independent approach to extract D is applied to polymer melts. Again the results are compared with FG NMR.

By means of these six publications this thesis will show that the intermolecular relaxation channel of proton spins is not a handicap of ^1H NMR but it is an enhancement from which additional information on translational diffusion in condensed matter can be obtained. It will show that FC ^1H NMR is capable to access, besides rotational, also translational molecular dynamics which may render it a serious competitor with FG NMR at least in neat systems.

3.1.1 Phenomenology of Rotational Dynamics in Liquids

Besides NMR, depolarized light scattering (LS) [1-4] and various other techniques, especially dielectric spectroscopy (DS) [5-7] has a longstanding tradition in the study of reorientational dynamics in molecular liquids. DS measures the complex dielectric permittivity, $\hat{\varepsilon}(\omega) = \varepsilon'(\omega) - i\varepsilon''(\omega)$. Most descriptive hereby is the dielectric loss, $\varepsilon''(\omega)$, which is given by the dielectric susceptibility, $\chi''(\omega)$, and is connected to the spectral density via the fluctuation-dissipation theorem [8]:

$$\varepsilon''(\omega) \propto \chi''(\omega) \equiv \omega \cdot J_{\text{DS}}(\omega) \quad (2)$$

The spectral density is the Fourier transform of the correlation function, $C^{(1)}$, [9]:

$$J_{\text{DS}}(\omega) = J^{(1)}(\omega) = 1/2 \int_{-\infty}^{\infty} C^{(1)}(t) \cdot e^{-i\omega t} dt$$

where

$$C^{(1)}(t) \propto \langle P_1\{\cos[\theta(t)]\} P_1\{\cos[\theta(0)]\} \rangle \quad (3)$$

if neglecting cross relaxation. The brackets $\langle \rangle$ denote the ensemble average, $P_1(x) = x$ the Legendre polynomial of rank $l = 1$ and θ the orientation of the molecular dipoles. Thus the molecular reorientation in liquids is essentially probed via the correlation of the projection of the molecular dipoles. Commonly correlation functions are normalized to give $C(0) = 1$, as consequence their Fourier transform yields normalized spectral densities:

$\int_0^{\infty} J(\omega) d\omega = \pi/2$ with $J(0) = \tau_{\text{rot}}$, where τ_{rot} is the time constant giving the time scale of the decay of the reorientational correlation.

Like in FC NMR most DS experiments are done on viscous or supercooled liquids since standard equipment usually operates at frequencies $\nu = \omega/2\pi < 1\text{GHz}$. Figure 1a exemplarily shows typical results on two liquids, namely glycerol and 3-fluoroanilin by plotting their dielectric losses, ε'' , taken at different temperatures versus frequency, ν .

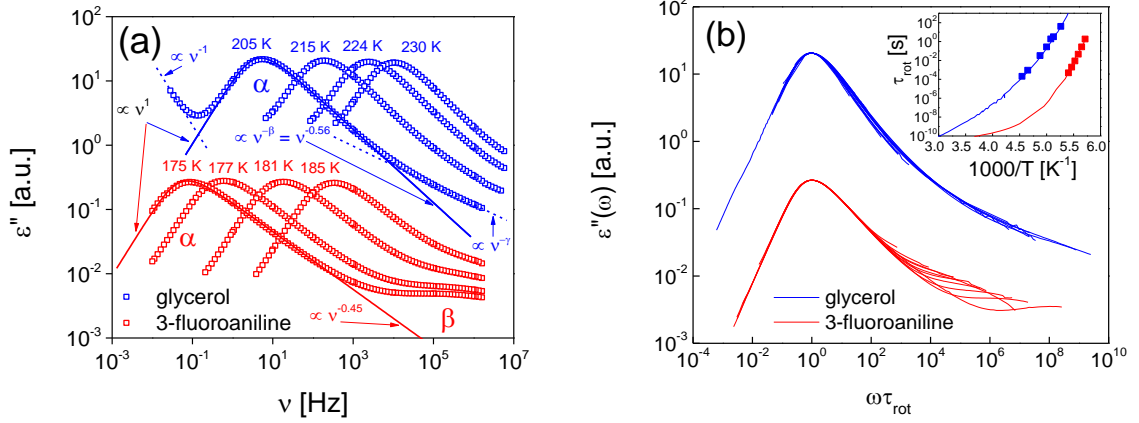


Figure 1a: The dielectric loss, $\varepsilon''(\nu)$, of glycerol (blue open squares, data taken from Ref. [7]) and 3-fluoroanilin (red open squares, data taken from Ref. [10]) at temperatures as indicated. The solid lines are fits using Eq. 6, the dotted lines are power laws. **Figure 1b:** Master curves for glycerol (184 K - 288 K) and 3-fluoroaniline (172 K - 187 K) obtained by plotting the dielectric loss versus the reduced frequency, $\omega \tau_{\text{rot}}$; inset: squares: corresponding τ_{rot} versus inverse temperature, lines: accessory data from Refs. [4] and [6].

The most prominent feature of the curves is the main peak commonly known as α -peak. The α -process is associated with the structural relaxation in the liquid, which is observed in terms of molecular reorientation by DS. Therefore the rotational correlation times obtained by DS are often labeled as τ_{α} . For molecular liquids $\tau_{\text{rot}} \equiv \tau_{\alpha}$ is valid, whereas in polymers τ_{α} does not refer to the reorientation of a whole molecule, as the α -process is associated with segmental dynamics in this case (*cf.* Sec. 3.1.9). People early noticed that the rotational dynamics in liquids cannot be described in terms of isotropic rotational diffusion, which results in an exponential correlation loss and finally yields the ‘Debye spectral density’ (*cf.* Figure 4, black dotted line, as susceptibility):

$$J_{\text{rot,Debye}}(\omega) = \frac{\tau_{\text{rot}}}{1 + (\omega \tau_{\text{rot}})^2} \quad (4)$$

The rotational time constant is given by:

$$\tau_{\text{rot}} = \tau_{\text{rot}}^{(l)} = \frac{1}{l(l+1)D_{\text{rot}}} \quad (5)$$

Its connection to the rotational diffusion coefficient, D_{rot} (which is connected to the mean-square angular deviation: $\langle \theta^2 \rangle \propto D_{\text{rot}} \cdot t$), depends on the rank, l , of the associated correlation function. In case of DS $l = 1$ (*cf.* Eq. 3) and thus $\tau_{\text{rot}} = \tau_{\text{rot}}^{(1)} = 1/(2D_{\text{rot}})$.

In contrast to rotational diffusion, the experimental shape around the main peak can be described with the phenomenological function which was proposed by Davidson and Cole in 1951 [11, 12] (CD function; *cf.* Figure 1a, solid lines and Figure 4, red dotted line, as susceptibility):

$$J_{\text{DS}}(\omega) \cong J_{\text{rot}}(\omega) \equiv \frac{\sin[\beta \cdot \arctan(\omega \tau_{\text{CD}})]}{\omega \cdot [1 + (\omega \tau_{\text{CD}})^2]^{\frac{\beta}{2}}} \quad (6)$$

Here, τ_{CD} is a time constant and $0 < \beta \leq 1$ is a parameter which controls the asymmetric broadness of the respective susceptibility peak. For $\beta = 1$ the expression is reduced to the Debye spectral density (Eq. 4). The function can be interpreted as some sort of cooperative rotational diffusion which results in a retarded, non-exponential correlation loss. This sort of reorientation is addressed as ‘rotational dynamics’ in this thesis. In fact the CD function is very similar to the Kohlrausch function, which is given by a stretched exponential correlation loss in the time domain, where the stretching parameter is commonly also labeled as $0 < \beta \leq 1$ [5]. In both susceptibility curves this parameter manifests itself as power-law $\propto \omega^{-\beta}$ at the high frequency-flank of the susceptibility peaks (*cf.* Figure 1a, solid lines) while the low-frequency side agrees among the curves regardless of the value of β (*cf.* Figure 4, dotted lines). The CD function can mathematically be interpreted as a superposition of Debye spectral densities weighted with a certain distribution of correlation times. Hence, in the following τ_{rot} is defined as the mean correlation time, which in the case of the CD function is given by:

$$\tau_{\text{rot}} \equiv \langle \tau \rangle = \beta \tau_{\text{CD}} \quad (7)$$

As a liquid is cooled down (and crystallization is avoided) it may get in the supercooled regime and hereby the dynamics slows down. As seen in Figure 1a the main relaxation process (α -peak) shifts towards lower frequencies with decreasing temperature. When its shape remains unchanged by a variation of temperature as one may already anticipate visually from Figure 1a one can collapse curves taken at different temperatures onto a common master

curve, $\chi''(\omega\tau_{\text{rot}})$, by scaling the frequency axis with the appropriate time constants, τ_{rot} . This approach is well known, *e.g.* from rheology [13] and is believed to reflect a fundamental feature of cooperative dynamics in liquids and supercooled liquids [14, 15]. Commonly it is referred to as ‘frequency-temperature superposition’ (FTS). Figure 1b demonstrates its applicability to the DS measurements on glycerol (blue lines) and 3-fluoroaniline (red lines). The measurements on glycerol were taken between 184K and 288K the ones on 3-fluoroaniline between 172K and 187K and all curves coincide in the area of the α -peak which proofs the validity of FTS regarding the α -process.

For both systems the dependence of the corresponding τ_{rot} on inverse temperature is shown in the inset of Figure 1b where again the blue symbols refer to glycerol and the red ones to 3-fluoroaniline. With the accessory data from Refs. [4] and [6] (lines) it is obvious that τ_{rot} is not linear in this representation versus $1/T$. This demonstrates that $\tau_{\text{rot}}(T)$ generally cannot be described in terms of a thermally activated process (*i.e.* Arrhenius law). The behavior of $\tau_{\text{rot}}(T)$ can be interpreted as a rising apparent activation energy when the system is driven deeper into the supercooled regime [4, 16]. However, it can fairly well be described by the phenomenological Vogel-Fulcher-Tammann (VFT) function [17-19]:

$$\tau_{\text{rot}}(T) = \tau_0 e^{B/(T-T_0)} \quad (8)$$

where τ_0, T_0 (with $T_0 < T_g$; T_g : *cf.* below) and B are parameters depending on the particular system.

By further cooling a supercooled liquid its rotational correlation time will eventually reach a value of $\tau_{\text{rot}} = 100\text{s}$. The respective temperature conventionally defines the glass transition temperature, T_g , where the viscosity is such high ($\approx 10^{12} \text{Pa}\cdot\text{s}$) that the system is to be considered a solid. As the liquid virtually undergoes no structural changes the glass transition is deemed to be a mere kinetic phenomenon.

In Figure 1a several other relaxation features are visible. At high frequencies the dielectric loss of glycerol (blue open squares) undergoes a change in the power law behavior from $\propto \nu^{-\beta}$ to $\propto \nu^{-\gamma}$ with $\gamma < \beta$. This additional process is called excess wing. An examination of the master curve of glycerol (*cf.* Figure 1b, blue lines) shows that FTS essentially also holds with respect to the excess wing. In the case of 3-fluoroaniline the situation is different. In Figure 1a (red open squares) even a distinct peak is seen at high frequencies reflecting a relaxation mechanism usually called β -process. Figure 1b (red lines) demonstrates that FTS fails with the β -process. The reason for that is a different dependence of the time constants on temperature: Unlike the α -process the β -process is describable by an Arrhenius behavior

which causes the spectral separation between them to increase with decreasing temperature. Since all liquids either show a mere excess wing or an additional β -process, Kudlik et al. [6] suggested a classification into type-A systems and type-B systems, respectively. The origin of these processes and their connection among each other and to the main relaxation process has been a matter of research and debate since nearly fifty years now. As this thesis focuses besides molecular reorientation mainly on the translational diffusion in liquids and supercooled liquids, which is found at lower frequencies than the rotational main peak, we will not go further into the field of the secondary processes.

Finally, in Figure 1a there is a crossover of the glycerol curve taken at 205 K to a power-law behavior $\propto \nu^{-1}$ (indicated by a dotted blue line) at lowest frequencies. This is an intrinsic peculiarity of the DS technique itself which stems from the conductivity contribution of ionic impurities. In favorable cases one may subtract the contribution as it was done for the glycerol curve in Figure 2b, which reaches to the lowest frequencies. There are also approaches to get rid of the impurities, *e.g.* the ‘DC cleaning’, an application of high DC voltage to the sample before measuring [20]. In spite of these counter-measures its occurrence limits the accessible range in the low-frequency side of the α -peak. Of course, NMR is not hampered by this issue and thus may be well suited for measurements in this regime.

3.1.2 NMR Relaxation (intramolecular) and Rotational Dynamics

The relaxation of spins with a dipole moment (*e.g.* the ^1H spin) is mediated by fluctuations of the dipole-dipole interaction with other spins. These arise due to alternation of length, r , and angle, $\Omega \equiv [\theta, \varphi]$ (given by polar angle, θ , and the azimuthal angle, φ), of the spin-to-spin vector with respect to the external field which stems from the molecular motion. Hence, the spin-lattice relaxation rate, R_1 , gives information about the molecular dynamics. Analogous to DS it is expressed in terms of time correlation functions or spectral densities. But here terms due to dipole-dipole coupling, which is a tensorial interaction, enter and the correlation function is of rank $l = 2$. Assuming that no internal degrees of freedom exist in the molecule, *i.e.* that the molecule is rigid, for the intramolecular relaxation (*i.e.* relaxation due to coupling between spins located on the same molecule) one merely has to correlate the angle [21, 22]:

$$C_{\text{intra}}(t) = C^{(2,m)}(t) \propto \langle Y_{2,-m}[\Omega(t)] Y_{2,m}[\Omega(0)] \rangle \quad (9)$$

$Y_{2,m}$ denotes a spherical harmonic of rank $l = 2$. In the case of liquids, which are isotropic, $C_{\text{intra}}(t)$ becomes independent of m and of the azimuthal angle, φ . In this case it can be

simplified to an expression which only differs from the dielectric one (*cf.* Eq. 3) by entering of the orientation via Legendre polynomials, P_l , of rank $l = 2$ instead of rank $l = 1$ [21]:

$$C_{\text{intra}}(t) = C^{(2)}(t) \propto \langle P_2\{\cos[\theta(t)]\} P_2\{\cos[\theta(0)]\} \rangle \quad (10)$$

The Fourier transform of the correlation function yields the spectral density, $J_{\text{intra}}(\omega) = J^{(2)}(\omega)$, which again is normalized to $\pi/2$.

In the case of dipolar coupling of like spins (*i.e.* homonuclear coupling, AA) time-dependent second order perturbation theory gives the famous Bloembergen-Purcell-Pound (BPP) expression for the intramolecular relaxation rate [21, 23]:

$$R_{1,\text{intra}}^{\text{AA}}(\omega) = \frac{K_{\text{intra}}^{\text{AA}}}{5} \cdot [J_{\text{intra}}(\omega) + 4J_{\text{intra}}(2\omega)]$$

with

$$K_{\text{intra}}^{\text{AA}} = 2I_A(I_A + 1) \left(\frac{\mu_0}{4\pi} \hbar \gamma_A^2 \right)^2 \sum_i \frac{1}{r_i^6} \quad (11)$$

Here, I_A is the spin quantum number, γ_A the gyromagnetic ratio and r_i the distance of a reference nucleus A to the i -th nucleus A. The summation goes over all other nuclei A on the molecule. The Larmor frequency is given by $\omega = \gamma_A B_r$ with B_r being the external magnetic field in which the spin of nucleus A relaxes (*i.e.* relaxation field). In the case of dipole-dipole coupling to different spins (*i.e.* heteronuclear coupling, AB) the expression (Solomon-Bloembergen-Morgan (SBM) expression) is (assuming spin B to be always in thermal equilibrium) [21, 22, 24]:

$$R_{1,\text{intra}}^{\text{AB}}(\omega) = \frac{K_{\text{intra}}^{\text{AB}}}{10} \cdot \left[J_{\text{intra}} \left(\omega \left| 1 - \frac{\gamma_B}{\gamma_A} \right| \right) + 3J_{\text{intra}}(\omega) + 6J_{\text{intra}} \left(\omega \left(1 + \frac{\gamma_B}{\gamma_A} \right) \right) \right]$$

with

$$K_{\text{intra}}^{\text{AB}} = \frac{4}{3} I_B(I_B + 1) \left(\frac{\mu_0}{4\pi} \hbar \gamma_A \gamma_B \right)^2 \sum_i \frac{1}{r_i^6} \quad (12)$$

where I_B is the spin quantum number of the nucleus B and γ_B its gyromagnetic ratio. The summation goes over all nuclei B of the molecule. Like in Eq. 11, $\omega = \gamma_A B_r$. Assuming the additivity of homo- and heteronuclear relaxation rates the whole intramolecular relaxation rate is given by $R_{1,\text{intra}}(\omega) = R_{1,\text{intra}}^{\text{AA}}(\omega) + R_{1,\text{intra}}^{\text{AB}}(\omega)$ where more terms (*i.e.* $R_{1,\text{intra}}^{\text{AC}}(\omega), R_{1,\text{intra}}^{\text{AD}}(\omega), \dots$) follow in the case of further other relevant nuclei (*i.e.*, C, D, ...) being present. The intramolecular coupling constants ($K_{\text{intra}}^{\text{AA}}, K_{\text{intra}}^{\text{AB}}, \dots$) are chosen to give with $J_{\text{intra}}(0) = \tau_{\text{rot}}$:

$$R_{1,\text{intra}}(0) = (K_{\text{intra}}^{\text{AA}} + K_{\text{intra}}^{\text{AB}} + \dots) \cdot \tau_{\text{rot}} \equiv K_{\text{intra}} \tau_{\text{rot}} \quad (13)$$

As already said, besides $R_{1,\text{intra}}(\omega)$, relaxation due to interactions of spins situated on different molecules with an intermolecular relaxation rate, $R_{1,\text{inter}}(\omega)$, also does occur so that the overall rate is given by [21]:

$$R_1(\omega) = R_{1,\text{intra}}(\omega) + R_{1,\text{inter}}(\omega) \quad (14)$$

For the sake of simplicity when comparing results from ^1H NMR to other techniques probing rotation it was often argued that the intermolecular part is negligible and in first order $R_1(\omega) \approx R_{1,\text{intra}}(\omega)$ holds. The most important reason given was the short range nature of the dipole-dipole interaction. Because of it one would expect the major contribution to relaxation from the nearest protons most probably belonging to the same molecule [25]. This thesis will refute this assumption and clarify the impact of $R_{1,\text{inter}}(\omega)$ on the overall $R_1(\omega)$.

3.1.3 NMR and other Techniques

For a long time the role of intermolecular relaxation in ^1H NMR stayed unexplored in detail and people turned to nuclei which only provide an intramolecular relaxation channel such as ^2H or ^{13}C to exclude translational influences on the spectral densities measured and so to provide a better comparability to other techniques like DS or LS solely probing rotation. While ^{13}C predominantly relaxes via dipole-dipole interaction with the neighboring, directly bonded protons, regarding ^2H NMR the spin relaxation is mediated by the coupling of the deuteron's quadrupole moment to an electric field gradient [22]. In molecular systems this gradient stems from charge distributions in the bonds and thus the relaxation mechanism of ^2H , just like the one of ^{13}C , is intramolecular solely reflecting the reorientation of the bond(s) and thus of the whole presumably rigid molecule. The connection between the ^2H relaxation rate and the spectral density, J_{intra} , is analogous to Eq. 11, only the prefactor has to be adapted due to the different kind of coupling. For ^{13}C Eq. 12 applies.

As DS provides information on rotational dynamics based on a rank $l = 1$ correlation function and NMR does in terms of rank $l = 2$ it is a crucial point how this influences the results. Concerning the rotational time constants usually a good agreement $\tau_{\text{rot}}^{(1)} \cong \tau_{\text{rot}}^{(2)}$ is found in spite of the theoretical prediction of $\tau_{\text{rot}}^{(1)}/\tau_{\text{rot}}^{(2)} = 3$ (*cf.* Eq. 5) for the case of isotropic rotational diffusion [26]. For example, Dries et al. [27] compared ^2H NMR measurements on o-terphenyl (OTP) with results from DS and found equal τ_{rot} in the liquid and the moderately supercooled regime. Blochowicz et al. [28] yielded analogue results on glycerol and tricresyl

phosphate. As, like ^2H NMR, LS also probes molecular reorientation in terms of a rank $l = 2$ correlation function soon also comparisons with results from LS were done: Brodin and Rössler [29] published LS results on glycerol and τ_{rot} is found to be alike the one from DS. The same is reported by Petzold and Rössler on OTP [30]. Just recently, Schmidke et al. [4] demonstrated the consent of τ_{rot} from LS to other techniques (particularly DS and NMR) for a huge variety of liquids. Besides the above mentioned liquids it contains for example 2-methyl tetrahydrofuran, ethyl benzene, toluene, propylene glycol, propylene carbonate, benzophenone, salol and several others. As proposed by the experiments, in the following we will not distinguish between τ_{rot} obtained by different techniques or in terms of different ranks in this thesis: $\tau_{\text{rot}}^{(1)} \cong \tau_{\text{rot}}^{(2)} = \tau_{\alpha} = \tau_{\text{rot}}$.

Concerning the spectral shapes of $J^{(1)}(\omega)$ and $J^{(2)}(\omega)$ in the regime of the α -relaxation the situation is more difficult. In the case of LS the spectra can be directly compared to these from DS as done in Ref. [29] with glycerol. Like in DS the α -peak in the susceptibility of LS can be described with a CD function (Eq. 6). However it is broader which corresponds to a smaller value β in the case of LS. A similar result is given in Ref. [28] for ^2H NMR versus DS for glycerol. In Ref. [31] results on tricresyl phosphate obtained by DS, photon correlation spectroscopy (PCS) and ^{31}P NMR are compared in susceptibility representation. Like LS and ^2H NMR the latter two reflect molecular reorientation in terms of rank $l = 2$. As the employed ^{31}P NMR data consisted of stimulated echo decays [32] the direct output of ^{31}P NMR was a correlation function like in the case of PCS. Hence for comparison to DS the data had to be Fourier transformed, a process which could be omitted for ^{31}P NMR if it was experimentally possible to do relaxometry at different Larmor frequencies. Again the susceptibility peaks of ^{31}P NMR and DSC show a broadening at high frequencies compared to DS. It seems that molecular reorientation is reflected as a broader peak in terms of rank $l = 2$. Nevertheless, as the α -relaxation seen by NMR can be described with Eq. 6 using an appropriate β , from now on we describe the intramolecular spectral density also with the CD function: $J_{\text{intra}}(\omega) \cong J_{\text{rot}}(\omega)$. In Pub. 2 and Pub. 4 it will be demonstrated that this also holds for the intramolecular part of the proton relaxation.

As said, in NMR relaxometry for a direct comparison of the spectral shapes obtained by techniques like DS and LS one needs frequency dependent relaxation data, $R_1(\omega)$. As, besides a few exceptions [33, 34], most of the FC NMR data are still collected via proton relaxation, it is an objective of this thesis to show that the intermolecular relaxation pathway of ^1H NMR does not hamper the gathering of information on rotational motion in liquids but provides

additional ones on translation. This is achieved via extensively measuring the frequency dispersion of the proton relaxation rate $R_1(\omega)$ in various systems by FC ^1H NMR.

3.1.4 Field-Cycling NMR Relaxometry – Development & State of the Art

First frequency dependent ^1H NMR measurements on neat liquids were published by the group of Noack [35, 36]. Employing a spectrometer that operated on separate channels they could measure at 12 different Larmor frequencies ω in the range of 50kHz to 160MHz. As the NMR signal amplitude follows a dependence $\propto \omega^2$ they had to use a 50ml(!) sample of liquid to get a satisfying signal-to-noise ratio at the lowest frequencies [37]. This fact already indicates the problems of acquiring relaxation dispersion curves on a conventional way. However, the group of Noack accomplished a then unmatched abundance of data on glycerol but had problems to describe it with models available at those days. After unsuccessfully trying with several rotational models they eventually turned to the translational spectral density given by Abragam [21] (*cf.* Eq. 20, Sec. 3.1.6). Claiming in Ref. [35] that proton relaxation due to rotation prevails as the diffusion coefficients are small in glycerol, while suggesting in Ref. [36] that relaxation is mostly driven by diffusion Hausser and Noack leave the reader in confusion and conclude that there are still open questions. However the statement that in contrast to DS the CD spectral density is not sufficient to describe the proton relaxation in molecular liquids is still up-to-date as it is confirmed by more advanced NMR techniques like FC NMR as done in a publication by Gainaru et al. [25], in an own preliminary report [38] as well as in the present work, where the reasons for this more complex spectral shape revealed by ^1H NMR relaxometry will be analyzed.

The crucial point of FC NMR is the switching of the external magnetic field. This allows the relaxation to take place at a desired relaxation field, B_r , while the signal can be acquired at a rather high detection field, B_d , to get a large signal amplitude. This ‘field cycling’ can either be accomplished mechanically or electronically. In the first case the sample is moved between sites bearing different fields (sample shuttle technique) [39-41]. This results in rather long switching times (*i.e.* the time when the desired field is achieved and stable) of about 200ms which constitutes the lower limit of accessible relaxation times. On the other hand, as cryomagnets can be employed one can measure at comparatively high fields which also entails a better spectral resolution.

The electronic method, *i.e.* ‘fast field cycling’ (henceforth simply abbreviated ‘FC’) NMR uses electromagnets where the current is tuned. Here the switching time is on the order of

some milliseconds but it is not possible to reach field strengths like accomplished by cryomagnets. The pioneering work was done in the eighties by Noack [42] and later by Kimmich and Anorado [43]. However, this technique gained genuine momentum not until the introduction of a commercial FC NMR spectrometer by Stelar s.r.l., Italy in 1997.

The instrument operating in Bayreuth is the Stelar Spinmaster FFC 2000 [44] and the data presented in this work were measured in a proton frequency interval of $10\text{kHz} \leq \nu \leq 20\text{MHz}$. A few measurements at very low frequencies were done in Darmstadt by a home-built spectrometer [45, 46] which allows to reach frequencies as low as $\nu \cong 200\text{Hz}$. These measurements are contained in Pub. 5 and Pub. 6, where the objective was to cover slow polymer dynamics.

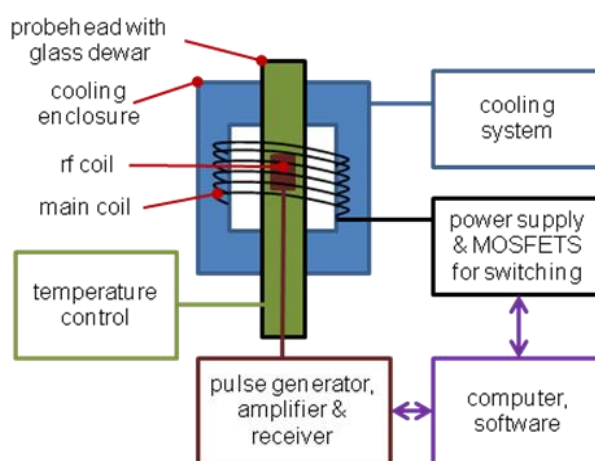


Figure 2: Schematic setup of the Stelar Spinmaster FFC 2000 spectrometer

The principal mode of operation of the Spinmaster spectrometer is given in Figure 2. The external field, B , is generated by the main solenoid coil. It is connected to the power supply via MOSFETs which allow switching its current. It can reach values up to 350A . A part of the MOSFETs has a contrary polarity that allows compensating overshooting. So magnetic fields up to 0.5T can be set and stabilized within at most 3ms . The high current requires a cooling of the main coil and the MOSFETs. This happens with two independent, thermally coupled loops. The first one consists of a special cooling fluid (Solvay Galden) which surrounds the coil and is also pumped through a copper structure on which the MOSFETs are set. This fluid passes a heat exchanger that transfers the heat to a tap water circuit.

The probehead is equipped with a saddle coil that allows to introduce the glass tube with the sample directly from the top of the main magnet. The walls of the probehead are a glass

dewar which enables temperature control to maintain temperatures between 160K and 420K with an accuracy better than about $\pm 1\text{K}$. Above room temperature a dried air flow is heated, below evaporated liquid nitrogen is used instead. By a software provided by Stelar one can control the external field, apply pulses and read out the signal.

The standard procedure to obtain the rate dispersion is implemented in the software. It consists of many cycles running a basic sequence. One is shown exemplarily in Figure 3. First the sample is polarized in a high polarization field, B_p . This field is hold sufficiently long that equilibrium magnetization is reached, *i.e.* several times of the relaxation time at the polarization field, $T_1(\omega = \gamma_H B_p)$. As noted in Sec. 3.1.2 the frequency, ω , is given by B via the gyromagnetic ratio, γ_H (for protons in this case). After maintaining B_p long enough B is switched to a lower field, B_r , and M will decay towards the new equilibrium value, $M(\infty)$, on the timescale of $T_1(\omega = \gamma_H B_r)$. After a delay time, τ , a 90° pulse is applied at a high field, B_d . The magnitude of the acquired free induction decay (FID) is $\propto M(\tau)$. Via a variation of τ one obtains the whole magnetization curve which usually is monoexponential for ^1H . This kind of fit yields $R_1(\omega) = 1/T_1(\gamma_H B_r)$. Doing this with different B_r one can measure $R_1(\omega)$ up to about $\nu = \omega/2\pi = 9\text{MHz}$.

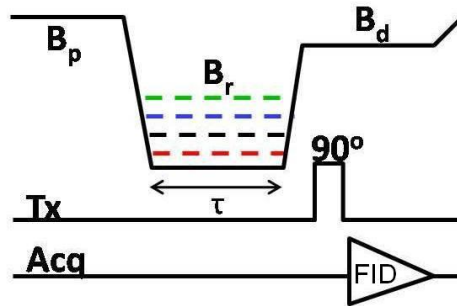


Figure 3: Basic prepolarized sequence

At higher fields one uses the so called ‘nonpolarized sequence’ which equilibrates the sample without external field and then observes the build-up of magnetization. By the combination of both kind of sequences it is possible to cover a proton frequency range of $10\text{kHz} \leq \nu \leq 20\text{MHz}$. While the upper limit is given apart from the power supply by the performance of the main coil and the MOSFETs and the capacity to cool them, the lower one is given by the magnetic earth field and stray fields in the laboratory mostly from surrounding cryomagnets in the present case. In Darmstadt the home-built spectrometer is actually able to measure from 30MHz down to 200Hz by employing an active stray field compensation [45, 46].

However, depending on the relaxation rate dispersion the lowest field may also be limited by the switching time as the relaxation time, $T_1(\omega)=1/R_1(\omega)$, decreases with decreasing frequency and may eventually reach values in order of 1 ms. In this case the magnetization reaches its equilibrium before one even can start acquiring the FID.

3.1.5 Data Representation and Refinement

In order to directly compare the results from FC NMR to others, especially from DS, it is useful to employ an alternative way of data representation besides the common relaxation rate. While the proton-proton relaxation rate, $R_1(\omega)$, is given by a linear combination of spectral densities $J(\omega)$ (cf. Eq. 11), the dielectric loss, $\varepsilon''(\omega)$, is a susceptibility quantity which is related to the spectral density via the dissipation-fluctuation theorem (Eq. 2). Hence, it is possible to convert $R_1(\omega)$ to a here called ‘NMR susceptibility’, $\chi''_{\text{NMR}}(\omega)$, simply by multiplying it with its frequency. In contrast to the ‘rate representation’, $R_1(\omega)$, this form of data representation is henceforth called ‘susceptibility representation’:

$$\omega R_1(\omega) = K[\chi''(\omega) + 2\chi''(2\omega)] \equiv 3K \cdot \chi''_{\text{NMR}}(\omega) \quad (15)$$

Here only proton-proton coupling is considered; the prefactor 3 ensures the normalization, $\int \chi''_{\text{NMR}}(\omega) d(\ln\omega) = \pi/2$,

which follows from the normalization of $J(\omega)$ via

$$\int \omega J(\omega) d(\ln\omega) = \int \chi''(\omega) d(\ln\omega) = \pi/2.$$

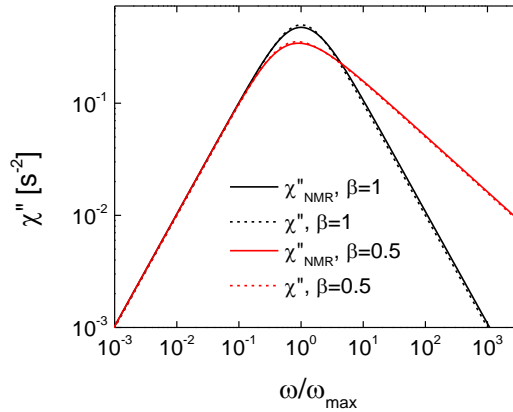


Figure 4: Comparison of the NMR susceptibility, $\chi''_{\text{NMR}}(\omega)$, (Eq. 15) with the basic one, $\chi''(\omega) = \omega \cdot J(\omega)$, for two different stretching parameters, β , (cf. Eq. 6).

The comparability of $\chi''(\omega)$ and $\chi''_{\text{NMR}}(\omega)$ is demonstrated in Figure 4. It shows the susceptibilities exemplarily based on a Debye (Eq. 4) and a CD spectral density (Eq. 6) versus

a scaled frequency which fixes the peak position at $\omega/\omega_{\max} = 1$. It is obvious that in a double logarithmic scale the slight broadened shape of $\chi''_{\text{NMR}}(\omega)$ due to the linear combination in Eq. 15 is virtually not visible. Of course, in an absolute frequency scale the peak of $\chi''_{\text{NMR}}(\omega)$ is slightly shifted to lower frequencies with respect to $\chi''(\omega)$ but this is accounted for by applying the whole BPP expression (Eq. 11) to NMR data when extracting τ_{rot} by fitting.

The comparability of NMR relaxation data with other frequency domain techniques is one advantage of the susceptibility representation, another one is that analogically to DS it is easy to construct master curves in this form provided that FTS applies as yet demonstrated for many cases by DS (*cf.* Sec. 3.1.1, Figure 1b). In practice one applies a fit using Eq. 15 with a CD spectral density (Eq. 6) to a NMR susceptibility dataset covering the susceptibility peak which, as will be demonstrated later in this Section, reflects rotational dynamics and hence gives the rotational time constant, τ_{rot} . With the obtained τ_{rot} this curve is plotted versus $\omega\tau_{\text{rot}}$. The NMR susceptibilities obtained at other temperatures are shifted along the frequency axis to provide the best overlap with the previous one. The shift factor is τ_{rot} at the respective temperature. Of course it is advisable to crosscheck these results with other techniques like DS and LS. Commonly they agree which proves the general applicability of FTS [25, 38].

Besides of the extended access to τ_{rot} this technique also considerably enhances the covered frequency range. This renders FC NMR competitive to DS in spite of its comparatively narrow frequency window. A third advantage is that the master curves can be transformed into dipolar correlation functions, $C_{\text{DD}}(t/\tau_{\text{rot}})$, via Fourier transformation, which is not possible with curves covering only a few decades in frequency:

$$C_{\text{DD}}(t/\tau_{\text{rot}}) \propto \int_0^{\infty} \frac{\chi''_{\text{NMR}}(\omega\tau_{\text{rot}})}{\omega\tau_{\text{rot}}} \cos(\omega t) dt \quad (16)$$

As the master curve is scaled by τ_{rot} the correlation function is likewise. Strictly $C_{\text{DD}}(t/\tau_{\text{rot}})$ consists of a linear combination like $C(t/\tau_{\text{rot}}) + 4C(t/2\tau_{\text{rot}})$ (*cf.* Eq. 15) but as in the case of susceptibilities (*cf.* Figure 4) in a double logarithmic plot this difference does virtually not affect the shape.

An instructive comparison of measurements on glycerol by FC ^1H NMR, DS and LS merged into master curves was published by Gainaru et al. in 2008 [25]. Though mainly focused on the secondary processes on the high-frequency flank it gives valuable information on the rotational main peak itself as seen by the different techniques. Figure 5a presents DS data compared to a NMR susceptibility, $\chi''_{\text{NMR}}(\omega)$, on an absolute frequency scale at first. The peak

positions of both profiles taken at $T = 262$ K (red line: DS, red symbols: FC NMR) agree. This is a direct proof that the susceptibility maximum of $\chi''_{\text{NMR}}(\omega)$ reflects molecular reorientation like DS. It also serves as justification for the identification of the shift parameter with the rotational time constant when constructing susceptibility master curves, $\chi''_{\text{NMR}}(\omega\tau_{\text{rot}})$. (The fact that $\chi''_{\text{NMR}}(\omega)$ is based on the BPP equation (*cf.* Eq. 15) while the DS curves are not can be omitted in this illustration)

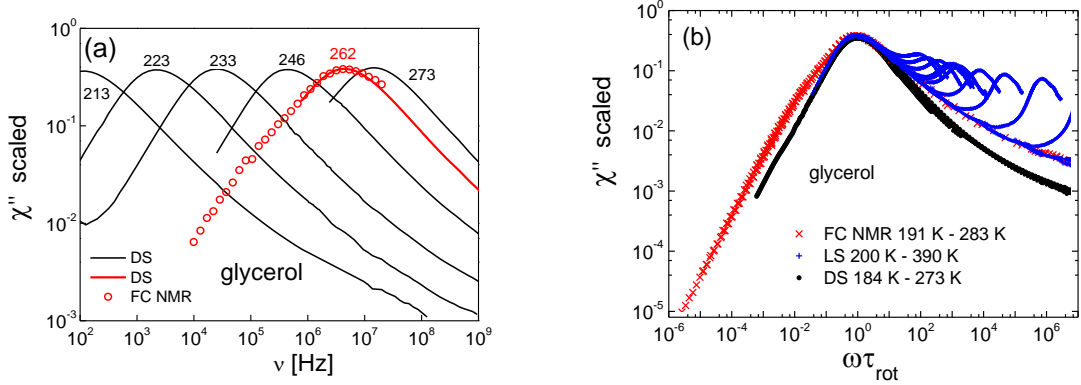


Figure 5a: Dielectric loss of glycerol (lines) taken at different temperatures as indicated and one NMR susceptibility, $\chi''_{\text{NMR}}(\omega)$, taken at 262 K (red dots) versus absolute frequency. Adapted from [25].
Figure 5b: Susceptibility master curves, $\chi''(\omega\tau_{\text{rot}})$, of glycerol obtained by FC ^1H NMR (red crosses), DS (black dots) and LS (blue dots). Adapted from [25].

As the overlap of both curves in Figure 5a is only a narrow frequency interval in the maximum region (FC NMR covers lower, DS higher frequencies), for comparison of the shape Figure 5b shows the master curves of all three techniques. In case of LS the peak seen at high frequencies is a so-called microscopic peak which is revealed by LS in the GHz – THz regime. Apart from these microscopic peaks one can see that FC NMR (red crosses) and LS (blue dots) agree on the high frequency side, while DS (black dots) exhibits a narrower peak. This feature supports the findings of Refs. [28, 29, 31] (*cf.* Sec. 3.1.3) as it again indicates the susceptibility peak being broader when measuring the rank $l = 2$ correlation instead of $l = 1$. The rotational correlation times, τ_{rot} , agree among all methods. But unlike in Ref. [28] where ^2H NMR was compared with DS the ^1H NMR results exhibit a sort of additional intensity at low frequencies (‘shoulder’), while LS and DS do not (*cf.* Figure 5b). In the main peak region (*i.e.* $\omega\tau_{\text{rot}} \cong 1$) all spectra are reproduced via a CD susceptibility, at low frequency (*i.e.* $\omega\tau_{\text{rot}} < 1$) it only fails with the FC ^1H NMR results due to the retarded crossover to the simple liquid behavior (*i.e.* $\propto \omega^1$). As already mentioned (*cf.* Sec. 3.1.4) the failure of the CD

function to reproduce ^1H NMR measurements was already recognized by the group of Noack [35, 36]. As one can clearly attribute the molecular reorientation to the main peak of the ^1H NMR susceptibility (*cf.* Figure 5a) the additional feature of the ^1H NMR master curves on the low-frequency side appears to represent a slower process only seen by proton relaxation.

A preliminary study [38] compared results from FC ^1H NMR to DS for a variety of other liquids. It covers homologues of glycerol (propylene glycol, 2,3-butanol, threitol, xylitol, sorbitol) as well as non-alcoholic liquids (OTP, tristyrene, 3-fluoroaniline, m-toluidine). Except for OTP and tristyrene the results of which agree rather well with DS (disregarding the smaller β in the CD function reflected at high frequencies) a distinct additional relaxation contribution of different magnitudes was found at low frequencies for the other systems. As OTP and tristyrene are the only systems without H-bonds, this indeed seemed to indicate clusters due to H-bonds being responsible for this feature as proposed in Ref. [25]. Nevertheless the discussion in Ref. [38] proposes translational motion as possible agent. The latter assumption will be proven in this thesis.

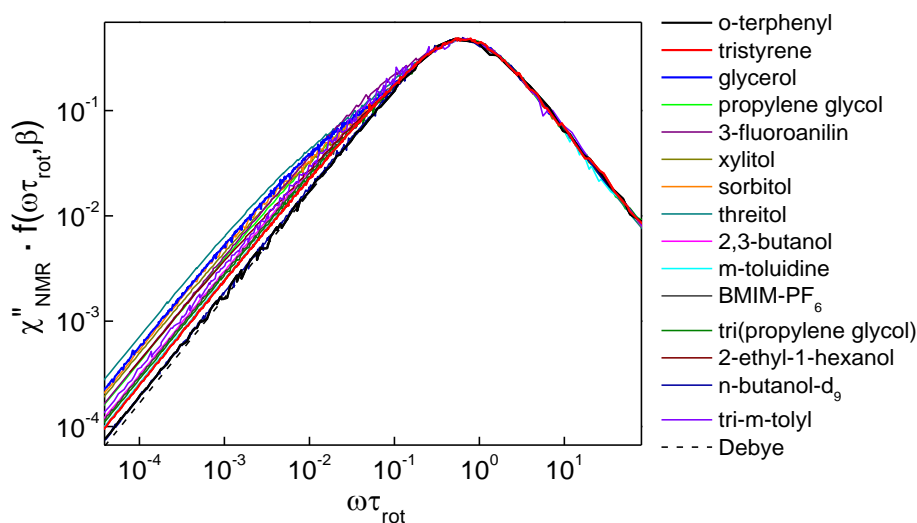


Figure 6: Susceptibility master curves for different liquids in ‘second scaling’ representation (*cf.* Ref. [38]). The part of the curves (at low frequencies) which do not agree with the Debye susceptibility (black dashed line) are not given by a CD function and reflect the excess contribution. Adapted from [38].

Besides the systems considered in Ref. [38] Figure 6 shows further examples of liquids which were measured afterwards. Also a ionic liquid, 1-butyl-3-methylimidazolium hexafluorophosphate (BMIM- PF_6), is included. A special scaling (referred to as ‘second

scaling') was applied which makes the susceptibility curves agreeing with a normalized Debye susceptibility (black dashed line, *cf.* Eq. 4) in the interval where a CD function (Eq. 6) applies, *i.e.* at high frequencies. A more detailed description can be found in Ref. [38]. This representation facilitates the comparison of the excess contribution of different systems. From Figure 6 it is clear that the majority of liquids shows it with varying magnitude. It is the purpose of this thesis to demonstrate that the extra contribution at low frequencies originates from intermolecular relaxation mediated by molecular translation and even allows to quantify translational diffusion in liquids.

3.1.6 Intermolecular Relaxation – Models

As already noted in Sec. 3.1.2, besides rotation also translational motion enters ^1H NMR relaxation rates via intermolecular dipole-dipole interaction. In contrary to intramolecular relaxation where the inter spin distances are considered to be constant, for the intermolecular correlation function fluctuations in time of both the orientation, $\Omega \equiv [\theta, \varphi]$, and the length, r , of the spin-spin axis, \mathbf{r} , have to be taken into account [22]:

$$C_{\text{inter}}(t) \propto \left\langle \frac{Y_{2,0}(\Omega(t))}{r^3(t)} \frac{Y_{2,0}(\Omega(0))}{r^3(0)} \right\rangle \quad (17)$$

where $Y_{2,m}(\Omega)$ again denotes a spherical harmonic (here we set $m=0$ without loss of generality, because the correlation function is independent of m in isotropic systems (*cf.* Eq. 9)).

Since the early days of NMR there have been many calculations of $C_{\text{inter}}(t)$ based on various model assumptions. For that matter the ensemble average is approximated by employing probability functions, $g(r)$ and $P(\mathbf{r}_0, \mathbf{r}, t)$ [21, 47]:

$$C_{\text{inter}}(t) \propto \iint \frac{Y_{2,0}(\Omega(t))}{r^3(t)} \frac{Y_{2,0}(\Omega(0))}{r^3(0)} g(r(0)) P(\mathbf{r}_0, \mathbf{r}, t) d\mathbf{r} d\mathbf{r}_0 \quad (18)$$

Hereby is $\mathbf{r}_0 \equiv [\Omega(0), r(0)]$ and $\mathbf{r} \equiv [\Omega(t), r(t)]$. The pair distribution function of the liquid, $g(r=|\mathbf{r}|)$, accounts for the probability that a second spin is placed at a distance $r(0)$ with respect to the considered one and $P(\mathbf{r}_0, \mathbf{r}, t)$ is the conditional probability that a spin-spin vector is \mathbf{r} at time, t , given that it was \mathbf{r}_0 at time zero. Integration over \mathbf{r} and \mathbf{r}_0 gives the expectation for $Y_{2,0}(\Omega(t))/r^3(t) \cdot Y_{2,0}(\Omega(0))/r^3(0)$ and thus for $C_{\text{inter}}(t)$. Therefore $P(\mathbf{r}_0, \mathbf{r}, t)$ determines the dynamics. It is obtained by solving the differential equation describing the actual diffusion model. The calculation of $C_{\text{inter}}(t)$ is tedious and often not possible in an

analytical way especially with an arbitrary $g(r)$. Hence the models which are introduced here employ a uniform spin density which only excludes the volume of closest approach of two spins, d : $g(r)=0$ for $r < d$ and $g(r)=1$ else. As the bulkiness of the spin bearing molecules imposes a distance of closest approach, d can be taken as measure for the molecules' diameter in the pure liquid

In real liquids $g(r)$ shows a first maximum around d as the volume exclusion by a considered molecule renders an accumulation of molecules (and thus spins) in the direct surrounding, *i.e.* first coordination shell. The first coordination shell itself causes a second coordination shell which is reflected as a smaller maximum in $g(r)$ and so on, which results in a damped oscillatory function. Finally, $g(r)=1$ for large r (compared to the correlation length in the liquid) like in the case of a simple distance of closest approach. As large r go along with long times, no differences regarding the shape of spectral densities to those based on the crude assumption (*i.e.* $g(r)=0$ for $r < d$ and $g(r)=1$ else) are expected at low frequencies. But as the aggregation of molecules in the first coordination shell also means a concentration of spins at rather short distances, the spectral density is most likely enhanced as a whole compared to the one, where a simple distance of closest approach in connection with an uniform spin density was assumed. Hence, $g(r)$ only affects the zero-frequency limit of the spectral density but not its first order behavior [47].

Formerly one of the most employed expression is given by Abragam [21] first published in 1961. It assumes that $P(\mathbf{r}_0, \mathbf{r}, t)$ (*cf.* Eq. 18) obeys the diffusion equation, $\partial P / \partial t = D_{12} \nabla^2 P$. Here, $D_{12} = D_1 + D_2$ is the relative diffusion coefficient which is the sum of the self-diffusion coefficients of the two participating species. For identical molecules in a neat liquid one has $D_{12} = 2D$. Analogical to the rotational time constant, τ_{rot} , it is useful to define a translational one:

$$\tau_{\text{trans}} = d^2 / (2D) \quad (19)$$

Abragam [21] presents an analytical expression for the spectral density. Normalized to $\pi/2$ it is given by:

$$J_{\text{Abrgm}}(\omega) = 3\tau_{\text{trans}} \int_0^\infty J_{3/2}^2(u) \frac{u \cdot du}{u^4 + \omega^2 \tau_{\text{trans}}^2} \quad (20)$$

with $J_l(u)$ being a Bessel function. A graphic description of this model is as follows: The spins are present with uniform density undergoing continuous translational diffusion. Thereby, each spin is placed in the center of a sphere with diameter d and trajectories of

other spins with $r < d$ simply vanish. With no interaction at $r = d$ imposed, each spin always diffuses independently, *i.e.* $\partial P/\partial t = D_{12} \nabla^2 P$ always is valid. The spheres are allowed to interpenetrate while spins with overlapping spheres do not couple to each other. As constructed, $J_{\text{Abrgm}}(\omega)$ is solely affected by translational motion.

Another early result on relaxation via translational diffusion was published by Torrey in 1953 [48]. The motional model is isotropic jump diffusion characterized by the mean squared jump length, $\langle l^2 \rangle$, and the mean time between two jumps, τ_{jump} . The self-diffusion coefficient is thus given as $D = \langle l^2 \rangle / 6\tau_{\text{jump}}$ (*cf.* Eq. 37). Like in Abragam's formulation [21] d is imposed while the spins move independently. However, after normalization this spectral density has two independent parameters, instead of one. The analytical expression for the spectral density, $J_{\text{Ttry}}(\omega)$, is lengthy so we refrain from showing it but we will discuss it by means of own numerical calculations within the model. We find it most convenient to define the two parameters as $\langle l^2 \rangle / d^2$ and $\tau_{\text{trans,Ttry}} \equiv \tau_{\text{jump}} \cdot (5/4 + 3d^2 / \langle l^2 \rangle)$ because in this notation for $\tau_{\text{trans,Ttry}} = \tau_{\text{trans}}$ one yields $J_{\text{Ttry}}(\omega) = J_{\text{Abrgm}}(\omega)$ in the limit of continuous diffusion, *i.e.* $\langle l^2 \rangle / d^2 \rightarrow 0$.

The definition of $\tau_{\text{trans,Ttry}}$ can be reasoned via the zero-frequency development given in [48], $J_{\text{Ttry}}(0) \propto \tau_{\text{jump}} [1 + 12d^2 / (5\langle l^2 \rangle)]$ and the respective value for $\langle l^2 \rangle / d^2 \rightarrow \infty$ which gives for the normalized spectral density: $J_{\text{Ttry}}(0) = 1/2 \cdot \tau_{\text{jump}}$. Along $J_{\text{Abrgm}}(0) = 2/5 \cdot \tau_{\text{trans}}$ the condition finally is $J_{\text{Ttry}}(0) = \tau_{\text{jump}} [1/2 + 6d^2 / (5\langle l^2 \rangle)] = 2/5 \cdot \tau_{\text{trans,Ttry}}$.

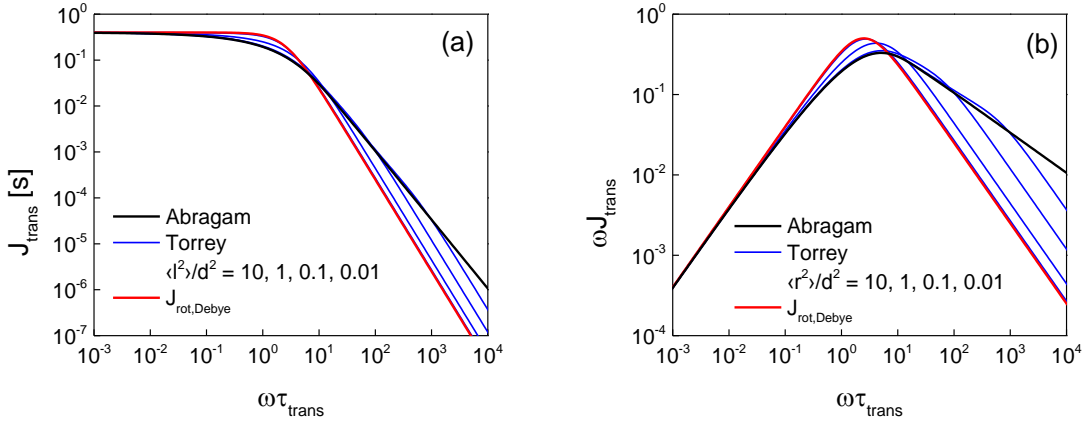


Figure 7a: Comparison of $J_{\text{Abrgm}}(\omega \tau_{\text{trans}})$ (black line, Eq. 20) with $J_{\text{Ttry}}(\omega \tau_{\text{trans,Ttry}})$ for different ratios of mean squared flight distance and squared distance of closest approach, $\langle l^2 \rangle / d^2$, (blue lines); the red line is a Debye spectral density. **Figure 7b:** Same as in Figure 7a but in susceptibility representation.

Figure 7 shows $J_{\text{Ttry}}(\omega\tau_{\text{trans,Ttry}})$ (cf. Figure 7a, blue lines) and the corresponding susceptibility representation (cf. Figure 7b, blue lines) for different ratios $\langle l^2 \rangle / d^2$. The black lines are the respective results for $J_{\text{Abrgm}}(\omega\tau_{\text{trans}})$ the red ones refer to a Debye spectral density (Eq. 4). The ratio $\langle l^2 \rangle / d^2$ is the crucial parameter in Torrey's model and, as mentioned, $J_{\text{Abrgm}}(\omega\tau_{\text{trans}})$ is contained as limiting case for $\langle l^2 \rangle / d^2 \rightarrow 0$, when the jump diffusion becomes continuous. In Figure 7a one can see that the characteristic high-frequency behavior of $J_{\text{Abrgm}}(\omega\tau_{\text{trans}}) \propto \omega^{-3/2}$ is followed by $J_{\text{Ttry}}(\omega\tau_{\text{trans,Ttry}})$ until higher frequencies when $\langle l^2 \rangle / d^2$ is smaller before the curve bends into a final behavior $\propto \omega^{-2}$. The equivalent behavior is seen in Figure 7b. As noted by Sholl [47] when the jump distance becomes large with respect to the distance of closest approach, $J_{\text{Ttry}}(\omega\tau_{\text{trans,Ttry}})$ converges towards a Debye spectral density (red lines in Figure 7).

As said, Torrey's treatment [48], like Abragam's [21], assumes an independent motion of spins. In 1975 Ayant et al. [49] showed that results obtained under this assumption are only valid for large diffusion paths, $\mathbf{r} - \mathbf{r}_0$, *i.e.* long times, t , and accordingly only for small frequencies, ω . Independently from Hwang and Freed [50], who published the same model in 1975, their treatment imposes reflecting wall boundary conditions, *i.e.* $(\partial P / \partial r)_{r=d} = 0$, thus describing hard spheres with a diameter, d . This is the first model with a realistic physical background: Hard spheres with each a spin in their centers undergo translational diffusion until they are reflected when hitting another sphere, *i.e.* $r = d$. Besides the fact that the spheres are not allowed to interpenetrate no other forces are implied. Thus this model will be addressed as force-free hard-sphere (FFHS) model throughout this thesis. For long times r becomes large, consequently the influence of the reflecting wall boundary ceases and $P(\mathbf{r}_0, \mathbf{r}, t)$ of the FFHS model finally also obeys the diffusion equation, $\partial P / \partial t = D_{12} \nabla^2 P$. Therefore differences between J_{Abrgm} and the FFHS model are expected at high frequencies. The FFHS model is purely translational and its normalized spectral density is given by:

$$J_{\text{trans}}(\omega) = \frac{54}{\pi} \int_0^\infty \frac{u^2}{81 + 9u^2 - 2u^4 + u^6} \frac{u^2 \tau_{\text{trans}}}{u^4 + (\omega\tau_{\text{trans}})^2} du \quad (21)$$

τ_{trans} is given alike in Abragam's solution [21] by Eq. 19.

Figure 8 compares the FFHS model ([49, 50]) against the expression of Abragam ([21]). While the behavior at low frequencies is alike, the difference between the two models indeed manifests itself mainly at high frequencies. The FFHS model shows a limiting behavior of $\propto \omega^{-2}$ whereas with Abragam's expression it is $\propto \omega^{-2/3}$. In the susceptibility representation

(*cf.* Figure 8b) this results in a broader peak for the latter case which leads to a smaller peak height due to normalization. Hwang and Freed [50] compared the FFHS model to two alternative results employing more realistic assumptions for $g(r)$. While the shape of the spectral densities only shows minor differences at higher frequencies their overall magnitude gets enhanced with respect to the FFHS model. This may result in a systematic underestimation of d when applying the FFHS model to experimental data.

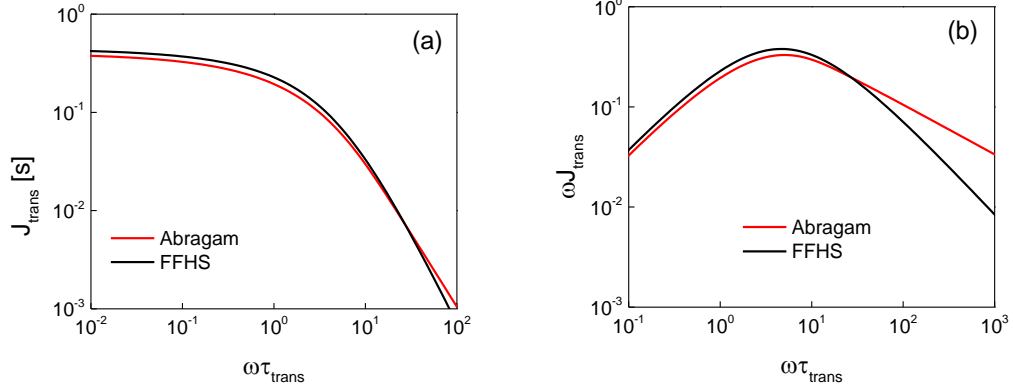


Figure 8a: Comparison of $J_{\text{Abrgm}}(\omega\tau_{\text{trans}})$ (Eq. 20, red line) to $J_{\text{trans}}(\omega\tau_{\text{trans}})$ (Eq. 21, black line);

Figure 8b: Same as in Figure 8a but in the susceptibility representation.

Later in 1977 Ayant et al. improved the FFHS model [51]. They calculated the spectral density, $\tilde{J}_{\text{inter}}(\omega)$, for hard spheres again carrying one spin, which, however, is placed off-centered with a distance, ρ . The eccentricity, $0 \leq e \equiv d/(2\rho) < 1$, of a spin on a molecule renders an influence of rotation on the spin-spin vector, \mathbf{r} . Hence the intermolecular part generally contains both, translation and rotation, and the resulting spectral density is not anymore called $J_{\text{trans}}(\omega)$, which refers to a purely translational spectral density. For the rotational dynamics isotropic rotational diffusion is assumed. The expression for $\tilde{J}_{\text{inter}}(\omega)$ is quite long and we refrain from giving it explicitly. In Pub. 4 the eccentricity model is discussed in detail using exemplary numerical calculations, furthermore it is applied to describe the intermolecular relaxation contribution, $R_{1,\text{inter}}(\omega)$, of OTP and glycerol- h_5 (*i.e.* perdeuterated glycerol, $\text{CH}_5(\text{OD})_3$) derived by isotope dilution experiments which will be discussed below (*cf.* Sec. 3.1.7). Nevertheless, we will sum up the most important aspects here.

In Figure 9a $\tilde{J}_{\text{inter}}(\omega\tau_{\text{trans}})$ according to Ref. [51] is plotted exemplarily for different values for the spin eccentricity, e . Figure 9b shows the corresponding curves in susceptibility

representation. In the case when the spin is placed in the center of the sphere (*i.e.* $e = 0$) only the translational diffusion drives the intermolecular relaxation and the model gets reduced to the simple FFHS case (Eq. 21) (*cf.* Figure 9, black solid lines). Otherwise (*i.e.* $0 < e < 1$) one has to introduce the correlation time for the rotational motion τ_{rot} . Altogether, the eccentricity model has three independent parameters, τ_{trans} , τ_{rot} and e .

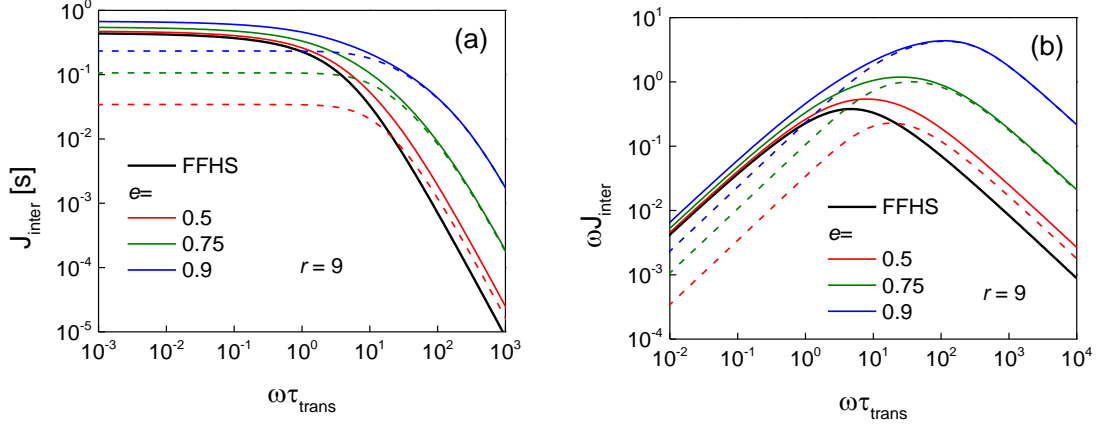


Figure 9a: Spectral density as given by the eccentricity model of Ayant et al. [51] for different eccentricities, e , of the spin position (solid lines); dashed lines: rotational part (*cf.* text below). **Figure 9b:** Same curves as in Figure 9a but in susceptibility representation.

Assuming simple hydrodynamics of a sphere rotating and translating in a viscous medium Ref. [21] gives the following ratio between the two time constants, *i.e.* the spectral separation between rotational and translational dynamics, henceforth called Debye-Stokes-Einstein (DSE) relation:

$$r \equiv \frac{\tau_{\text{trans}}}{\tau_{\text{rot}}} = 9 \quad (22)$$

Applying Eq. 5 with $l = 2$ and Eq. 19 it follows from the combination of the Stokes-Einstein relation

$$D = (k_B T) / (6\pi\eta R_H) \quad (22a)$$

for the translational dynamics with the Einstein relation

$$D_{\text{rot}} = (k_B T) / (8\pi\eta R_H^3) \quad (22b)$$

for rotational dynamics when identifying the hydrodynamic radius, R_H , with the model-based distance of closest approach: $R_H = d/2$. Hereby, η is the shear viscosity.

This ratio, $r = 9$, is also assumed in Figure 9. Compared to the FFHS spectral density a growing rotational part emerges at high frequencies with increasing e . This is best recognized in the susceptibility representation (*cf.* Figure 9b). In Figure 9 the rotational share (*i.e.* $\tilde{J}_{\text{inter}}(\omega\tau_{\text{trans}}) - J_{\text{trans}}(\omega\tau_{\text{trans}})$) is plotted with dashed lines. Its magnitude rises with eccentricity. Thus $\tilde{J}_{\text{inter}}(\omega)$ for an arbitrary e is not normalized (indicated by the tilde).

Besides the complexity of its expression another burden of the eccentricity model is the assumption of rotational diffusion (*i.e.* exponential correlation loss) for the molecular reorientation which leads to a slope $\propto \omega^{-1}$ of the rotational part (and therefore of $\omega \cdot \tilde{J}_{\text{inter}}$) at high frequencies in the susceptibility representation (*cf.* Figure 9b, dashed lines). This contradicts experimental results on liquids which usually find a stretched exponential correlation decay and thus higher slopes at the high-frequency side of the rotational susceptibility (*cf.* Secs. 3.1.1, 3.1.3 and 3.1.5). Hence, in Pub. 4 we define an approximation for the exact solution of the eccentricity problem using the FFHS model and a CD function allowing for $\beta < 1$:

$$\tilde{J}_{\text{inter}} \cong J_{\text{trans}} + f \cdot J_{\text{rot}} \quad (23)$$

The phenomenological parameter f gives the strength of the rotational contribution with respect to the translational one and can directly be linked to the eccentricity, e (*cf.* Pub. 4). Furthermore we note that the apparent spectral separation gets larger with increasing e . In Figure 9b it can be easily seen that the position of the rotational peak (*cf.* dotted lines) shifts to higher frequencies as e gets larger. Hence a description of the eccentricity model in terms of Eq. 23 yields an apparent ratio, $r_{\text{app}} = \tau_{\text{trans}}/\tau_{\text{rot}}$, which is dependent of e . This feature is also addressed in Pub. 4.

First experimental evidence for the eccentricity effect was given by Albrand et al. in 1981 [52]. They measured the spin-lattice relaxation rate, R_1 , of ^{13}C in neopentane ($\text{C}(\text{CH}_3)_4$). Due to the large chemical shift its possible to distinguish between the centered carbons and the off-centered ones. To avoid the necessity of separating different relaxation mechanisms di-tert-butyl nitroxide (DTBN) was added to the neat liquid in different concentrations. DTBN contains an unpaired electron and thus provides an efficient intermolecular relaxation channel which renders all others negligible. The result is given in Figure 10, where R_1 is plotted versus the concentration of DTBN for the centered carbons (a) and the off-centered ones (b). As expected both values grow linearly with increasing concentration of radicals, but more

important is the fact that the off-centered carbons always have a larger R_1 than the centered ones. This is a direct proof of the relaxation enhancement due to eccentricity.

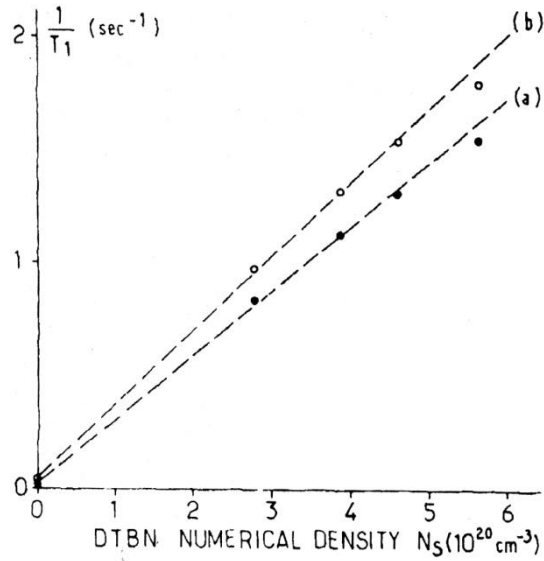


Figure 10: Spin-lattice relaxation rate, R_1 , of ^{13}C in neopentane versus the concentration of di-tert-butyl nitroxide (DTBN) measured at 303K and 25.16 MHz. Curve (a) refers to the centered carbons, (b) to the off-centered ones. Taken from [52].

Nevertheless, this effect was not revealed in neat liquids so far. To do so, one has to separate the intramolecular relaxation channel from the intermolecular one. As mentioned this can be obtained via an isotope dilution experiment as done in Pub. 2 and Pub. 4, where the eccentricity effect was revealed by means of the dispersion of $R_{1,\text{inter}}(\omega)$ for the first time. Though the details of the isotope dilution experiment will not be discussed until the following Section, Figure 11 presents its results in case of glycerol- h_5 (*i.e.* $\text{CH}_5(\text{OD})_3$) in terms of susceptibility master curves as presented in Pub. 2, because it is a clear and vivid demonstration of the eccentricity effect in a neat liquid.

Figure 11a presents the separation of the total susceptibility master curve ($\nu \cdot R_1(\omega \tau_{\text{rot}})$, black squares) into the intramolecular contribution ($\nu \cdot R_{1,\text{intra}}(\omega \tau_{\text{rot}})$, red squares) and the intermolecular one ($\nu \cdot R_{1,\text{inter}}(\omega \tau_{\text{rot}})$, blue squares). It confirms that the intramolecular part is purely rotational as it is given by a CD function. The proof for eccentricity is best seen in Figure 11b where only the intermolecular susceptibility is given. The crucial point is the broadness of the peak which results in the necessity of the incorporation of two processes to interpolate the whole curve. The black line in Figure 11b is a fit based on Eq. 23 which

assumes, besides the purely translational part (FFHS model, green line) also a rotational one (CD function, red line). A comparison of the location of the intramolecular rotational peak to the alleged intermolecular rotational contribution confirms its rotational origin, as their positions agree. To our knowledge, this is the first proof of the eccentricity effect in neat liquids.

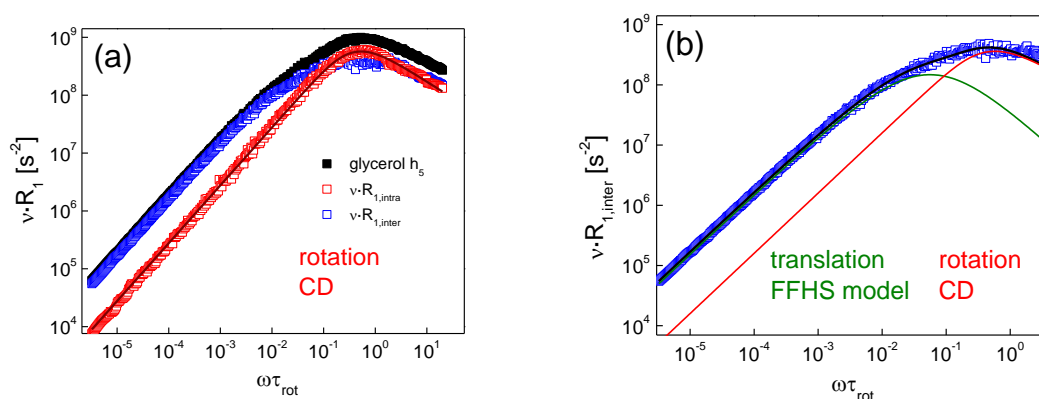


Figure 11a: Susceptibility master curve of glycerol- h_5 (black solid squares) and its separation into intra- (red open squares) and intermolecular contributions (blue open squares). The red line is a fit of the intramolecular contribution using the CD function. **Figure 11b:** Intermolecular part of the susceptibility master curve. Black solid line: interpolation according to Eq. 23, green solid line: translational part (FFHS model), red solid line: rotational part (CD function). Adapted from Pub. 2.

3.1.7 The Isotope Dilution Experiment and Its History

Since the mid-fifties there have been various attempts to isolate the rotational contribution to proton spin relaxation, *i.e.* to suppress the intermolecular relaxation contribution. Giulotto et al. [53] and Mitchell and Eisner [54, 55] diluted a proton bearing liquid in another one without protons. As a consequence the solvent virtually does not support proton relaxation and should suppress the intermolecular dipole-dipole interactions of the solute as a considered proton on one molecule sees less and less protons on neighboring ones as the concentration of the solvent increases. But the introduction of another substance changes the viscosity and consequently the relaxation rate. It was tried to account for this by scaling R_1 with viscosity or employing elaborate models (*e.g.* [56]). Nevertheless it became obvious that more profound modifications of molecular dynamics happen with dilution and no results on the neat liquid can be deduced. Furthermore the authors did not distinguish between intra- and intermolecular relaxation but between rotational and translational one. But as shown in the previous section (*cf.* Sec. 3.1.6) the pure translational motion generally cannot be isolated via

dilution experiments due to the eccentricity effect. So the evidence on molecular dynamics was rather inconclusive and very much dependent on the chosen system of the mixture. In the following the term ‘isotope dilution’ refers exclusively to a mixture of a proton bearing liquid dissolved in its fully deuterated counter-part. By example we will see in Sec. 3.1.8 that the dilution with a chemical different solvent is not at all comparable to an isotope dilution experiment in our sense, where the solute has essentially the same chemical properties as the solvent.

The first isotope dilution experiment was carried out by Bonera and Rigamonti [57]. They measured spin-lattice relaxation of mixtures of acetone and benzene with their respective deuterated counterparts. As the dynamics almost does not change with deuteration this is a much more significant experiment. An increasing introduction of deuterated molecules suppresses the intermolecular relaxation as the interaction of deuterons and protons is much weaker than that between protons among themselves (*cf.* Eqs. 27 and 28, Sec. 3.1.8). Hence, when the dilution with deuterons is not extremely high their contribution to the relaxation rate, $R_1(x_H; \omega)$, can be neglected and one finds the following linear dependence on the molar concentration of the proton bearing species, x_H :

$$R_1(x_H; \omega) = R_{1,\text{intra}}(\omega) + x_H \cdot R_{1,\text{inter}}(\omega) \quad (24)$$

The measurement of $R_1(\omega)$ for different concentrations, x_H , and the extrapolation $x_H \rightarrow 0$ yields $R_{1,\text{intra}}(\omega)$ and thus $R_{1,\text{inter}}(\omega)$.

Bonera and Rigamonti [57] were able to achieve this separation for an extended temperature interval but as they were confined to a single Larmor frequency their insight into molecular dynamics was limited. From the extracted $R_{1,\text{intra}}$ they calculated correlation times, τ_{rot} , using reasonable values for the spin-spin distances, r_i , and assuming the extreme narrowing condition, *i.e.* when $\omega\tau_{\text{rot}} \ll 1$ one finds $J_{\text{rot}}(\omega) \cong \tau_{\text{rot}}(T)$ and thus $R_{1,\text{intra}}$ only dependent on the temperature (*cf.* Eq. 11). The result was compared to an estimation for τ_{rot} given by the Einstein relation (Eq. 22b). Satisfactory agreement was only found, in the case of benzene. For acetone the estimate was higher than the calculation using $R_{1,\text{intra}}$. The results for $R_{1,\text{inter}}$ were compared to a frequency independent estimate for the intermolecular relaxation rate given in Ref. [23]. Again the results on acetone did not match at all due to a very much higher experimental value of $T_{1,\text{inter}} = 90\text{s}$ (!) at 298K. Both deviations were explained by a fast methyl group rotation. An analogue experiment was published by Harmon and Muller in 1969

on ethane [58]. They found their results for $R_{1,inter}$ very well describable by the model of Torrey [48] which was improved by a more realistic radial distribution function, $g(r)$.

An important step represents the publication of Kintzinger and Zeidler in 1973 on glycerol [59]. They made basically the same experiment as presented in Pub. 2 in this thesis, namely an isotope dilution experiment on glycerol- h_5 (*i.e.* $CH_5(OD)_3$) in its fully deuterated counterpart (glycerol- h_0). The deuteration of all the hydroxyl groups avoids an exchange of OD/OH. Employing different kinds of spectrometers they were able to cover 10 different frequencies. The intramolecular contribution was identified to be describable via a CD spectral density. Concerning the intermolecular part it was more difficult. Though it was known that it reflects both translational and rotational dynamics they tried the Torrey model [48] because there was no model describing the impact of eccentricity in those days. Contrary to Harmon and Muller [58] the Torrey model fails with the richer dataset of Kintzinger and Zeidler.

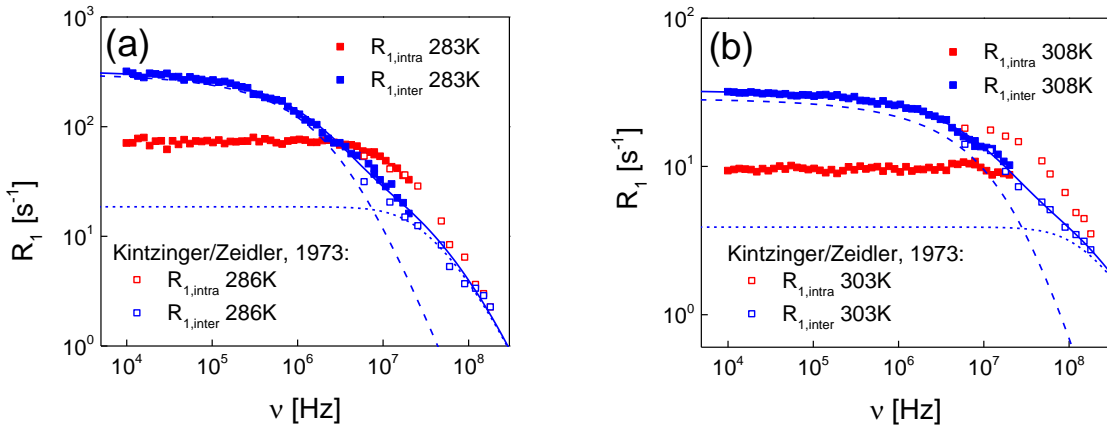


Figure 12: Intra- and intermolecular relaxation of glycerol- h_5 at 283 K / 286 K (Figure 12a) and 308 K / 303 K (Figure 12b). The data plotted in open squares is taken from Ref. [59] the solid squares reflect measurements done for Pub. 2. Fits of the eccentricity model of Ayant et al. [51] (solid blue lines) and its separation into translational part (dashed blue lines) and rotational part (dotted blue lines) are included.

Figures 12a and 12b show the separation of intra- and intermolecular contribution of glycerol- h_5 for two similar temperatures respectively. They compare our measurements done in the course of Pub. 2 (solid squares) to these from Kintzinger and Zeidler [59] (open squares). Included are fits with the eccentricity model of Ayant et al. [51] (solid blue lines) for the intermolecular parts, which are itself separated in rotational parts ($\tilde{J}_{inter}(\nu) - J_{trans}(\nu)$), dotted

blue lines) and translational ones ($J_{\text{trans}}(\nu)$, dashed blue lines). One can see the difference between the frequency intervals accessible by the Stellar Spinmaster FFC 2000 spectrometer in Bayreuth and the spectrometers used by Kintzinger and Zeidler. In the latter case only rather high frequencies are covered while the Stellar relaxometer is capable to measure down to 10 kHz. A comparison to the rotational parts of the fits (dotted blue lines) and to $R_{1,\text{intra}}(\omega)$ (red symbols) shows that the interval covered by Kintzinger and Zeidler hardly exceeds the rotation dominated regime and so they missed also the discovery of the excess contribution at low frequencies best seen in master curves (*cf.* Figures 5b and 6). Besides the much denser frequency grid provided by the Stellar Spinmaster FFC 2000 spectrometer this demonstrates clearly the advantages concerning accessing the translational motion in supercooled liquids, because only covering low frequencies makes the quantification of the translational motion possible as shown in the next section.

We further note that in 2003 Friedrich et al. [60] published another work on glycerol employing the isotope dilution technique. They diluted glycerol- h_8 (*i.e.* fully protonated glycerol) in glycerol- h_0 and evaluated $R_{1,\text{intra}}$ at a fixed frequency for different temperatures arguing that the effect due to OH/OD exchange is small. The result $R_{1,\text{intra}}$ from ^1H NMR was compared to measurements on ^2H and ^{13}C both, as noted, relaxing only via intramolecular channels. On the lines of previous works the data solely reflecting molecular reorientation was describable employing the CD spectral density (Eq. 6).

Finally we note that there are isotope dilution experiments on polymers, *e.g.* Collignon and Sillescu [61] employed a conventional NMR spectrometer measuring polyethylene while Lindner et al. [62] measured polystyrene. Kehr et al. [63] employed FC NMR for the first time on poly(ethylene oxide) and polybutadiene and Herrmann et al. [34] investigated polybutadiene and poly(dimethyl siloxane) also by FC NMR.

3.1.8 Low-Frequency Limit of the Relaxation Rate and its Applications

Translational spectral densities show a universal low-frequency behavior, namely linearity in the square root of frequency, $\sqrt{\omega}$. This is the result of an intrinsic feature of translational diffusion and found for every model as long as $P(\mathbf{r}_0, \mathbf{r}, t)$ (*cf.* Eq. 18) obeys the diffusion equation, $\partial P/\partial t = D_{12} \nabla^2 P$, for large distances, $\mathbf{r} - \mathbf{r}_0$, and long times, t , [47]. In the correlation function this feature manifests itself in a power-law behavior $C_{\text{trans}} \propto t^{-3/2}$ at long times, t , a fact well known for long [52].

Figure 13a shows the correlation function of the models discussed for the intermolecular relaxation (*cf.* Sec 3.1.6) obtained by cosine transform of their spectral densities (*cf.* Eq. 16). For comparison an exponential correlation loss is also plotted (red line) which corresponds to a Debye spectral density (Eq. 4). It is the only curve which does not show the translational behavior $\propto t^{-3/2}$ at long times which is indicated by the dashed line. Even Torrey's model with a large jump distance (cyan line) finally obeys the power-law after following the rotational correlation function quite long. The curve for the eccentricity model (purple line) shows a correlation loss due to rotation at short times, but eventually also obeys the translational power-law at long times.

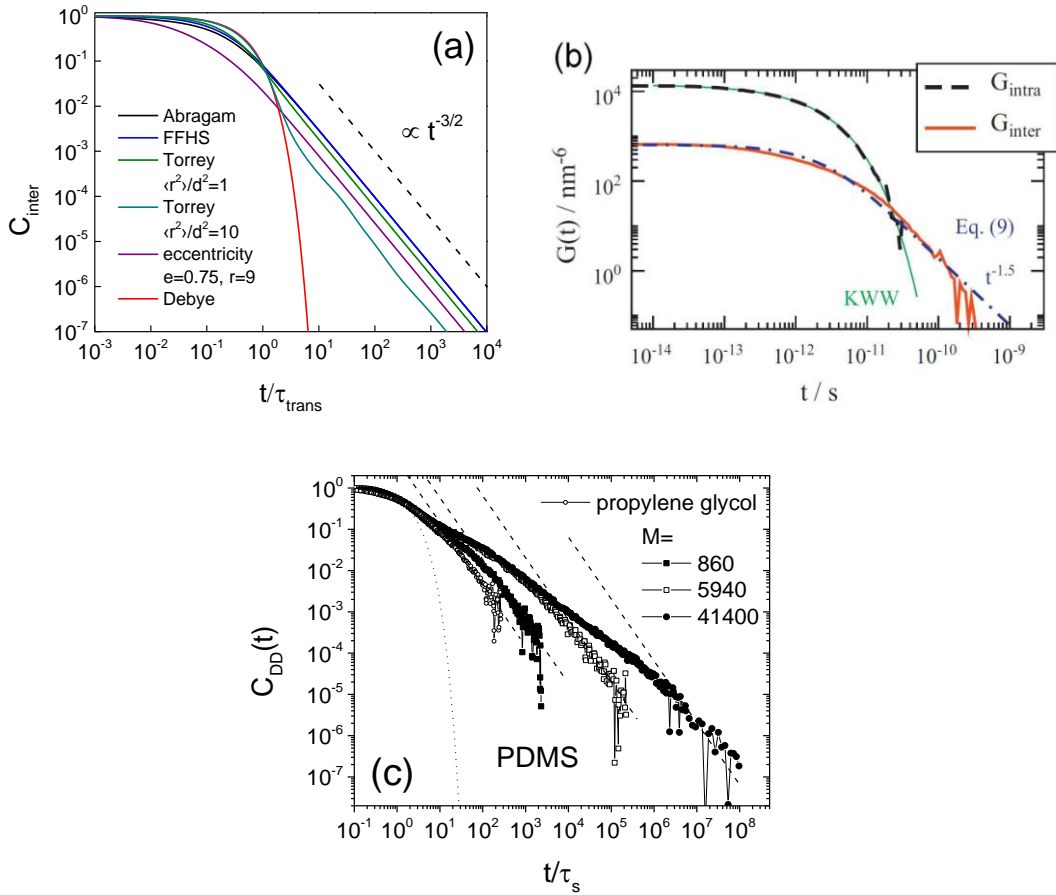


Figure 13a: Intermolecular correlation functions versus reduced time, $C_{\text{inter}}(t/\tau_{\text{trans}})$, for the models discussed in Sec. 3.1.6 derived from the spectral densities, $J_{\text{inter}}(\omega\tau_{\text{trans}})$, via cosine transform (*cf.* Eq. 16), for comparison an exponential correlation loss (rotational diffusion), $C_{\text{rot}}(t/\tau_{\text{rot}})$, is also plotted (red line). **Figure 13b:** Intra- and intermolecular correlation function derived by MD simulation on di(propylene oxide). Taken from Ref. [64]. **Figure 13c:** Dipolar correlation functions, $C_{\text{DD}}(t/\tau_{\text{rot}})$, for PG and PDMS with different molecular masses derived via Eq. 16; dashed lines: power laws $\propto t^{-3/2}$. Dotted line: Kohlrausch function. Taken from Pub. 6.

Due to the growth of computing capacity this behavior $C(t) \propto t^{-3/2}$ at long times could also be identified in recent molecular-dynamics (MD) simulations of liquids and polymers. Figure 13b shows a MD simulation on di(propylene oxide) done by Henritzi et al. [64]. The dashed black line is the intramolecular correlation function, the solid red line the intermolecular correlation function. The former was interpolated by a stretched exponential (Kohlrausch function, *cf.* Sec. 3.1.1) (green solid line) while the latter was fitted to the correlation function which corresponds to the FFHS model (Eq. 21) (blue dashed-dotted line). The interpolation with the stretched exponential works almost perfectly while the intermolecular part shows slight deviations to the FFHS correlation function. This may be due to the eccentricity effect which is omitted by the FFHS model. However, the most important fact in this context is the crossover of the intermolecular correlation function (red solid line) to the behavior $C(t) \propto t^{-3/2}$ at longest times which reflects translational diffusion in the hydrodynamic limit.

In Pub. 6 this power-law is firstly demonstrated at experimental data. Via Eq. 16 the susceptibility master curves of propylene glycol (PG) and of a polymer, poly(dimethyl siloxane) (PDMS) with different molecular masses, M , were transformed into the corresponding dipolar correlation functions, $C_{DD}(t/\tau_{rot})$. Figure 13c shows the results. At short correlation times the loss is given by a stretched exponential (dotted line) while at sufficient long times the power-law $C(t) \propto t^{-3/2}$ is established for every system. While for the liquid systems (PG, PDMS with $M = 860 \text{ g/mol}$) this happens at shorter times, for higher M the crossover gets more and more protracted due to additional polymer dynamics. In Pub. 5, Pub. 6 and Sec. 3.1.9 the polymer dynamics are addressed in more detail.

Concerning the spectral densities this feature of the correlation function at long times comes into effect at low frequencies where it is reflected as a first order linear behavior in $\sqrt{\omega}$. For example, the series expansion for the FFHS spectral density (Eq. 21) is as follows [50]:

$$J_{\text{trans}} = \frac{4\tau_{\text{trans}}}{9} \left(1 - \frac{3\sqrt{2}}{8} \sqrt{\omega\tau_{\text{trans}}} + \frac{1}{12\sqrt{2}} (\omega\tau_{\text{trans}})^{3/2} + \dots \right) \quad (25)$$

While the first order of the expansion in frequency of any translational spectral density thus is $\propto \sqrt{\omega}$, a rotational one is $\propto \omega^2$ as seen exemplarily at the series expansion of a Debye spectral density (Eq. 4):

$$J_{\text{rot}} = \tau_{\text{rot}} \left(1 - (\omega\tau_{\text{rot}})^2 + \dots \right) \quad (26)$$

This crucial difference between J_{trans} and J_{rot} is well known for a long time, *e.g.*, it was given by Harmon in 1970 [65]. Due to experimental restrictions it has not been systematically and extensively applied so far. The present work will fill this gap as Pub. 3 – Pub. 6 apply the consequences of this feature to the rate dispersion data of a variety of systems.

By dipole-dipole coupling of a considered nucleus in a bulk liquid to identical nuclei, J_{trans} contributes to the translational part of the relaxation rate, $R_{1,\text{inter}}^{\text{trans}}(\omega)$, via (BPP expression, *cf.* Eq. 11):

$$R_{1,\text{inter,AA}}^{\text{trans}}(\omega) = \frac{K_{\text{inter,AA}}}{5} [J_{\text{trans}}(\omega) + 4J_{\text{trans}}(2\omega)]$$

with

$$K_{\text{inter,AA}} = \frac{8\pi}{3} I_A (I_A + 1) \frac{N_A}{d^3} \left(\frac{\mu_0}{4\pi} \hbar \gamma_A^2 \right)^2 \quad (27)$$

Hereby, N_A is the spin density of nuclei A; d denotes the distance of closest approach. When coupled to different nuclei the contribution to $R_{1,\text{inter}}^{\text{trans}}(\omega)$ is as follows (SBM expression, *cf.* Eq. 12):

$$R_{1,\text{inter,AB}}^{\text{trans}}(\omega) = \frac{K_{\text{inter,AB}}}{10} \left[J_{\text{trans}} \left(\omega \left| 1 - \frac{\gamma_B}{\gamma_A} \right| \right) + 3J_{\text{trans}}(\omega) + 6J_{\text{trans}} \left(\omega \left(1 + \frac{\gamma_B}{\gamma_A} \right) \right) \right]$$

with

$$K_{\text{inter,AB}} = \frac{16\pi}{9} I_B (I_B + 1) \frac{N_B}{d^3} \left(\frac{\mu_0}{4\pi} \hbar \gamma_A \gamma_B \right)^2 \quad (28)$$

where N_B represents the spin density of nuclei B. As the rotational contribution to the total rate dispersion yet goes with the square in frequency, $\propto \omega^2$ (*cf.* Eq. 26), $R_1(\omega)$ is dominated by the translational contribution $\propto \sqrt{\omega}$ at sufficiently low frequencies. Hence, from Eqs. 25, 27 and 28 follows (assuming the additivity of $R_{1,\text{inter,AA}}^{\text{trans}}(\omega)$ and $R_{1,\text{inter,AB}}^{\text{trans}}(\omega)$):

$$R_1(\omega) = R_1(0) - \frac{B}{D^{3/2}} \cdot \sqrt{\omega}$$

with

$$B = \frac{2\pi}{45} \left(\frac{\mu_0}{4\pi} \hbar \gamma_A \right)^2 \cdot \left\{ \left(1 + 4\sqrt{2} \right) I_A (I_A + 1) \gamma_A^2 N_A + \frac{1}{3} \sum_X \left[\left(\sqrt{\left| 1 - \frac{\gamma_X}{\gamma_A} \right|} + 3 + 6\sqrt{1 + \frac{\gamma_X}{\gamma_A}} \right) I_X (I_X + 1) \gamma_X^2 N_X \right] \right\} \quad (29)$$

The summation over X accounts for all species of different nuclei (*i.e.* B, C, ...) which undergo dipole-dipole coupling with the nucleus A. We note that Eq. 29 implies that there is no ‘extreme narrowing’ in ¹H NMR, *i.e.* $R_1(\omega)$ is always frequency dependent even at lowest frequencies. The introduction of the coupling constant cancels out the model specific parameters (d and τ_{trans}) of J_{trans} and the prefactor of the term $\propto \sqrt{\omega}$ becomes model independent providing direct access to D . As said, it is also independent of the form of the radial distribution function, $g(r)$, [47]. Thus the first-order behavior of $R_1(\omega)$ is universal. $R_1(0)$ includes, besides the translational contribution, *i.e.* $R_{1,\text{inter}}^{\text{trans}}(0) = 4/9 \cdot K_{\text{inter}} \tau_{\text{trans}}$ with

$$K_{\text{inter}} = K_{\text{inter,AA}} + K_{\text{inter,AB}} + \dots = \frac{8\pi}{3} \frac{1}{d^3} \left(\frac{\mu_0}{4\pi} \hbar \gamma_A \right)^2 \left\{ I_A (I_A + 1) \gamma_A^2 N_A + \frac{2}{3} \sum_X [I_X (I_X + 1) \gamma_X^2 N_X] \right\} \quad (30)$$

also all rotational parts, *i.e.* $(K_{\text{intra}} + f \cdot K_{\text{inter}}) \cdot \tau_{\text{rot}}$, which are supposed to be a constant offset to the overall rate dispersion at low frequencies (*cf.* Eqs. 23, 25 - 28):

$$R_1(0) = R_{1,\text{intra}}^{\text{rot}}(0) + R_{1,\text{inter}}^{\text{rot}}(0) + R_{1,\text{inter}}^{\text{trans}}(0) = (K_{\text{intra}} + f \cdot K_{\text{inter}}) \cdot \tau_{\text{rot}} + \frac{4}{9} K_{\text{inter}} \tau_{\text{trans}} \quad (31)$$

where the intramolecular rotational part is $R_{1,\text{intra}}^{\text{rot}}(0) = K_{\text{intra}} \cdot \tau_{\text{rot}}$ and the intermolecular rotational part is $R_{1,\text{inter}}^{\text{rot}}(0) = f \cdot K_{\text{inter}} \cdot \tau_{\text{rot}}$

As a result of Eq. 29 one can directly calculate the self-diffusion coefficient from the slope, $m \equiv dR_1/d\sqrt{\omega}$, at low frequencies, when simply plotting the relaxation rate against the square root of frequency:

$$D = (B/m)^{2/3} \quad (32)$$

Except physical constants, B only contains the spin densities, N_X , which are easily accessible in most cases (*cf.* Eq. 6 in Pub. 6).

Unlike the treatment given in from Pub. 3 - Pub. 6 where only proton-proton coupling has to be considered (the H-D coupling *e.g.* in glycerol- h_3 (*i.e.* $\text{CD}_5(\text{OH})_3$) is negligible as will be shown in Chap. 3.4) the examination given above is improved as it also includes heteronuclear coupling. As further shown exemplarily in Chap. 3.4 the analysis of rate dispersions obtained by ¹⁹F NMR for the liquid 3-fluoroaniline requires the full expression in Eq. 29.

As said, the effect of translational diffusion on the relaxation dispersion is well known for a long time but, as it will be shown in the following, only since the recent years the

experimental possibilities are potent enough to take systematically advantage from it. One of the first attempts to extract D from the proton relaxation rate dispersion in bulk liquids was published by Harmon in 1970 [65]. Figure 14a shows his R_1 data plotted as open squares against the square-root of frequency. The dashed line is the linear fit from which D was obtained. The solid squares reflect a recent FC ^1H NMR measurement from Ref. [25] at the same temperature. Both datasets agree well. The slight deviations among them may be attributed to minor temperature differences. Nevertheless the data from FC ^1H NMR covering lower frequencies allows much better to estimate the linear regime of $R_1(\sqrt{\nu})$ at this temperature. It turns out that the linearity only holds until $\sqrt{\nu}/\text{Hz} \approx 1000$. After that further dispersion sets in which does not stem from the long time diffusion as it is not linear in $\sqrt{\nu}$. This renders Harmon's fit represented by the dashed line problematic. It gives $D=1.9 \cdot 10^{-12} \text{ m}^2/\text{s}$ while the solid line fit yields $D=1.3 \cdot 10^{-12} \text{ m}^2/\text{s}$. Thus Harmon overestimated D due to the smaller absolute slope of the fit resulting from the fact that no data at sufficiently low frequencies could be obtained.

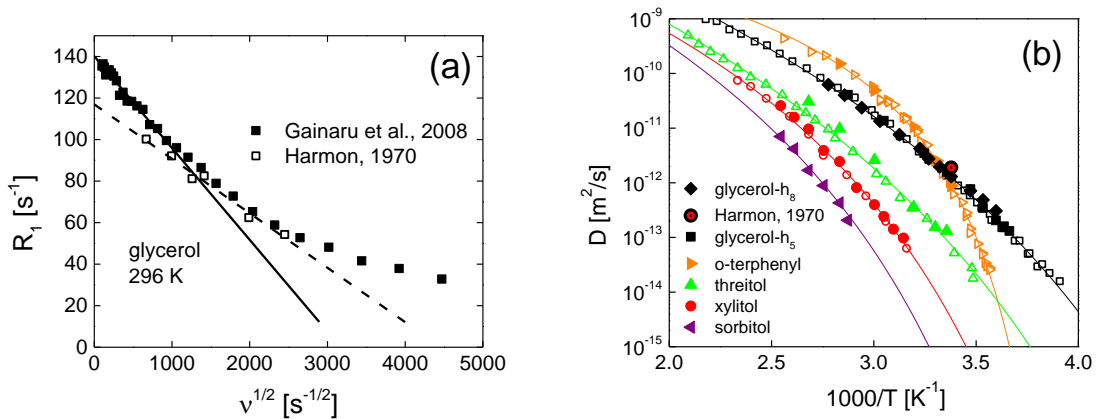


Figure 14a: Proton relaxation rate versus square root of frequency for glycerol at $T = 296$ K; solid squares data from Ref. [25]; open squares: data from Ref. [65]. Solid Line: linear fit of the low-frequency data, dashed line: fit applied in Ref. [65]. **Figure 14b:** Result for D versus inverse temperature for different liquids as derived from the low-frequency slope of $R_1(\sqrt{\nu})$ (solid symbols), open symbols reflect data from FG NMR ([66, 67]). Red/black circle: result from Ref. [65]. Solid lines: VFT laws for D (cf. Eq. 8). Adapted from Pub. 3.

Figure 14b presents our results for D (black solid symbols) on glycerol and other liquids as published in Pub. 3. They agree well with the available data from FG NMR (black open symbols). Additionally the result of Harmon [65] (red/black circle) is included. As explained,

the point lies slightly above the others, however the effect is small on the logarithmic scale. This points out the robustness of the present analysis.

For the sake of completeness we mention that previously this low-frequency analysis was also applied to solutions of paramagnetic nitroxide radicals. For example, Fries et al. [68] reexamined the system of DTBN in neopentane (*cf.* Sec. 3.1.6 and Ref. [52]). As it contains an unpaired electron DTBN is a radical and hence it provides a very effective relaxation channel for the proton spins of neopentane, which is intermolecular, of course. The universal low-frequency behavior in the solution thus is enhanced and could be revealed in spite of neopentane being in the non-viscous regime around room temperature, where the low-frequency dependence, $R_1(\sqrt{\omega})$, of pure neopentane would be very weak and hardly resolvable.

Unlike Ref. [68] or Ref. [69] where the spin-electron coupling was simply accounted for by the Solomon-Bloembergen-Morgan (SBM) expression (Eq. 28), Ref. [70] also considers hyperfine coupling of the electron spin to the spin of a nucleus in the radical molecule, in this case ^{15}N with spin $I=1/2$. The hyperfine coupling results in two additional regimes of linearity in $R_1(\sqrt{\omega})$ found at lower frequencies than that one imposed by the SBM expression, which is only valid when the Larmor frequency of the electron spin is very large compared to the amplitude of the hyperfine coupling. The three regimes were also found experimentally. Later Kruk et al. [71] generalized the treatment given in Ref. [70] and extended it for ^{14}N with spin $I=1$. In Ref. [72] not only the three linear regimes were identified experimentally but also the difference between the two nitrogen isotopes affecting the slope of the linear regime at lowest frequencies was resolved.

Apart from the enhancement of the relaxation rate another advantage of the admixture of radicals is the large gyromagnetic ratio of the electron spin with respect to the proton's, which favors the probing of fast translational dynamics. Thus the introduction of paramagnetic substances promises an extension of the covered dynamic range compared to the one accessible in the pure liquid. However this approach only determines the relative diffusion coefficient, $D_{12} = D_1 + D_2$, between the solvent and the radical. One can get self-diffusion coefficients for the radical, D_2 , by acquiring diffusion data on the neat solvent, D_1 , from references assuming that due to the small concentration of the radical the bulk dynamics is not affected. Hence, this approach cannot provide information on the neat liquid in a straightforward manner.

We further note that the low-frequency behavior of $R_1(\omega)$ was also derived for translational diffusion in two-dimensional and one-dimensional systems. The former is $R_1(\omega) \propto D^{-1} \ln(\omega^{-1})$, while the latter is $R_1(\omega) \propto (\omega D)^{-1/2}$ [47]. Diffusion processes in two dimensions were identified in lithium intercalation compounds using ^7Li NMR relaxometry and β -radiation detected NMR relaxation [73]. Moreover, one-dimensional translational diffusion was identified in the intermetallic compound $\text{Li}_{12}\text{Si}_7$ also employing ^7Li NMR relaxometry [74].

Another application of the universal low-frequency behavior is a new ansatz for the construction of master curves in the rate representation instead of $\chi''_{\text{NMR}}(\omega \tau_{\text{rot}})$, which is presented in Pub. 4. Eq. 29 suggests that plotting the ratio $R_1(\omega)/R_1(0)$ against the square root of an appropriate reduced frequency, $\omega \tau_{\text{res}} \equiv x^2$, should bring the translation dominated part of every dataset onto a common $1-x$ behavior as

$$R_1(\omega)/R_1(0) = 1 - \sqrt{\omega \tau_{\text{res}}}$$

with

$$\tau_{\text{res}} = \left(\frac{B}{D^{3/2} \cdot R_1(0)} \right)^2 \quad (33)$$

holds (*cf.* Eq. 29). While the susceptibility master curves, $\chi''_{\text{NMR}}(\omega \tau_{\text{rot}})$, always rely on FTS the rate dispersion master curves are exact at low frequencies as, by construction, all datasets coincide in the $1-x$ behavior. When FTS applies (*i.e.* $r = \text{const.}$ and the spectral shape of each translational and rotational contribution stays unchanged) the curves for a given system taken at different temperatures should also coincide beyond the linear regime, when the higher order terms of the translational and rotational spectral densities come into effect. As in this representation master curves from different systems will all coincide in the low-frequency $1-x$ regime, comparing them at higher frequencies can be a powerful tool. Especially the interplay between rotational and translational contribution can be put into perspective as it is crucial for the direction in which the master curve leaves the linear behavior coming from low frequencies.

By taking into account the second order of the expansion of the FFHS model (Eq. 25) and the first order of the Debye (Eq. 26) one can define a quantity, c , which is a crucial indicator for the shape of $R_1(\omega)/R_1(0) = f(\sqrt{\omega \tau_{\text{res}}})$. Considering mere proton-proton coupling one can give the following threshold value for c , which designates the two areas, where the curve is ‘rotationally dominated’ or ‘translationally dominated’ (*cf.* Pub. 4):

$$c \equiv \xi \cdot r^{5/2} = \frac{918}{\sqrt{2+16}} \approx 53 \quad (34)$$

with $\xi = K_{\text{inter}} / (K_{\text{intra}} + f \cdot K_{\text{inter}})$ and r being the spectral separation (Eq. 22). Thus ξ is the ratio of ‘translational coupling’, K_{inter} , and ‘rotational coupling’, $K_{\text{intra}} + f \cdot K_{\text{inter}}$. Figure 15 adapted from Pub. 4, where this issue is discussed in detail (*cf.* Chap. 3.5) exemplarily shows the impact of c on the shape of the curve. The translational part is given by the FFHS model (Eq. 21) the rotational part by a Debye spectral density (Eq. 4). The Debye spectral density was chosen on the lines of the fact that the derivation of the threshold for c (Eq. 34) is based on it by the use of the series expansion given in Eq. 26.

When $c < 53$ the curve will most likely bend downwards (‘rotationally dominated shape’, blue line, $c = 27$) when leaving the linear behavior (dashed line). As r enters c with a power of 2.5 while ξ only does linearly, a downward bent curve in this representation is a strong indication towards a narrow spectral separation of rotational and translational contributions and experimentally found, *e.g.*, for OTP and tristyrene as shown in Pub. 4. For the present $\xi = 0.11$, a realistic assumption, this feature vanishes when the spectral separation is only slightly increased (red line). As $c = 55$ is close to the threshold given in Eq. 34 the curve is neither decisively bent downwards nor upwards. A further increase of r makes the curve clearly bent upwards (‘translationally dominated shape’, black solid line) like seen in the case of glycerol (*cf.* Pub. 4).

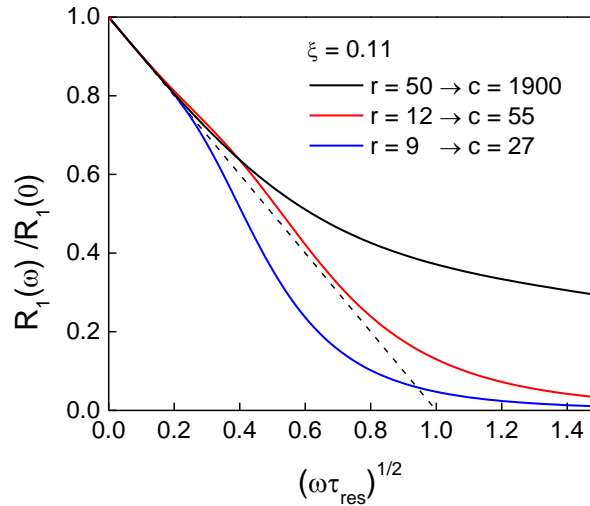


Figure 15: Master curves in rate representation for the model system consisting of a Debye (Eq. 4) and a FFHS spectral density (Eq. 21) for different spectral separation, r . Adapted from Pub. 4.

Figure 16a represents the data of the isotope dilution experiment on glycerol-h₅ in glycerol-h₀ from Pub. 3 now firstly in terms of rate representation master curves, $R_1(\omega)/R_1(0)(\sqrt{\omega\tau_{\text{res}}})$. This has not been done so far as this type of data representation was not introduced until Pub. 4. In the present context it is of interest to compare it with a system which is diluted by a chemically different, protonless substance like also done in Refs. [53-55] (*cf.* Sec. 3.1.7). For this sake, Figure 16b shows so far unpublished data on the system of propylene glycol (PG) diluted with deuterated chloroform (Chld). The molar ratios of the solutes, glycerol-h₅ and PG, are given by x_{H} and x_{PG} , respectively. As constructed all curves agree in the linear low-frequency behavior $1-x$ (black solid lines) and datasets from a given sample taken at different temperatures collapse giving a master curve for each dilution ratio, x_{H} or x_{PG} . The comparison of the development of the master curves due to dilution points out towards fundamental differences between an isotope dilution experiment and a dilution experiment with another proton-free solvent. Unlike glycerol-h₅ in glycerol-h₀, PG with Chld shows a crossover from the translationally dominated shape to the rotationally dominated shape with increasing dilution.

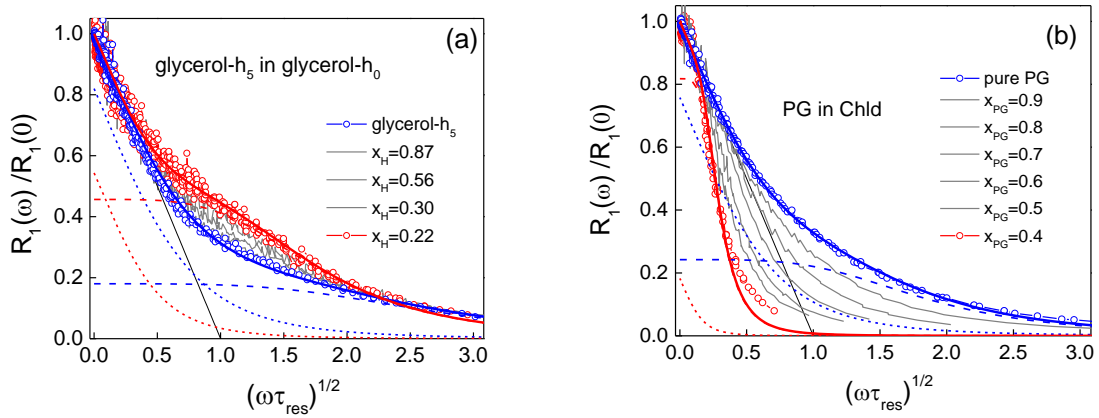


Figure 16a: Rate dispersion master curves, $R_1(\omega)/R_1(0)(\sqrt{\omega\tau_{\text{res}}})$, of glycerol-h₅ diluted in glycerol-h₀ for different molar ratios, x_{H} , of glycerol-h₅, black solid line: low-frequency behavior, blue/red solid lines: fits employing a Debye function for the rotational part (dashed lines) and the FFHS model for the translational part (dotted lines). Data taken from Pub. 3. **Figure 16b:** Same as in Figure 16a, but with a new system: PG in Chld. The molar ratio of PG is given by x_{PG} .

In Sec. 3.1.7 we already noted that the introduction of another substance alters the viscosity and the authors of Refs. [53-55] tried to account for that by scaling it out. In the case of PG with Chld the viscosity decreases with decreasing x_{PG} , *i.e.* the dynamics gets faster with introduction of Chld and in Figure 16 this effect is accounted for by the employment of the

rescaled frequency axis. The development of the master curves with dilution hence stems from a variation of the shape of the entire spectral density.

The blue lines with open circles in Figure 16 represent the respective pure substance, the red lines with open circles are the results of the most diluted samples and the grey solid lines show intermediate dilution ratios. The development in Figure 16a (isotope dilution, glycerol-h₅ in glycerol-h₀) can quite easily be rationalized: With advancing dilution the intermolecular part gets more suppressed (*cf.* Eq. 24) and alongside with it the included translational contribution. Meanwhile, the purely rotational intramolecular contribution to the whole curve remains unchanged and thus its share grows. The gain of the red curve compared to the pure substance (blue curve) thus is connected to a growth of the proportion of the ‘rotational coupling’ (*i.e.* $K_{\text{intra}} + f \cdot K_{\text{inter}}$) and thus to a diminishment of ξ in Eq. 34. Nevertheless the high spectral separation $r \approx 40$ of glycerol-h₅ (*cf.* Pub. 1) prevents a downward bent curve after the $1-x$ behavior at low frequencies, regardless of ξ . This explanation is proven by applying fits (red and blue solid lines) employing a Debye spectral density (Eq. 4) for the rotational contributions (inter- as well as intramolecular) (dashed lines) and a FFHS spectral density (Eq. 21) for the translational one (dotted lines) like already plotted in Figure 15. (For the sake of simplicity we only consider proton-proton coupling.) On the linear scale in Figures 16a and 16b the fits based on the Debye spectral density work fine. As this representation focuses on low frequencies with respect to the rotational regime deviations are only visible at the highest reduced frequencies where the fact that the Debye spectral density does not support stretching becomes relevant.

As the absolute coupling is eliminated by dividing by $R_1(0)$ and likewise is the absolute timescale by the introduction of the reduced time scale, $\sqrt{\omega \tau_{\text{res}}}$, the remaining parameters for the fits are the ratios ξ and r . As expected the fits in Figure 16a have a common $r = 38$ and differ only in the ratios of coupling: $\xi = 0.27$ for pure glycerol-h₅ and $\xi = 0.07$ for the highest dilution, $x_{\text{H}} = 0.22$, indicating a diminished ‘translational coupling’. The parameter c is in both cases well above the threshold given in Eq. 34: $c \cong 2400$ and $c \cong 600$, respectively. In the case of PG in Chld (*cf.* Figure 16b) the situation alters very much. The fit parameters for pure PG are: $r = 20$, $\xi = 0.35$ and consequently $c \cong 650$ which is quite similar to glycerol-h₅. While the master curve of pure PG is bent upwards the diluted samples show a rising downwards curvature which suggests a decreasing spectral separation, r , an effect not observed for glycerol-h₅ in glycerol-h₀ (*cf.* Figure 16a). This is confirmed by the fit for $x_{\text{PG}} = 0.4$: $r = 9$, $\xi = 0.06$ and thus $c \cong 14$. As a free fit would yield a even lower r , the

value $r=9$ was set. While contrary to glycerol-h₅ in glycerol-h₀ a decreasing r with decreasing x_{PG} is obvious, the trend in ξ is analogous to the isotope dilution experiment.

This data representation shows that dilution with a chemically different substance may result in profound changes of the dynamics and hence is not an experiment on the lines of an isotope dilution experiment. In the case of PG in Chld it suggests that the main aspect is the narrowing of the spectral separation with increasing dilution.

Finally, as an outlook, a more accurate approach to quantify the spectral separation shall be mentioned because it is not included in the Publications. As $R_1(0)$ is a linear combination of τ_{rot} and τ_{trans} (cf. Eq. 31) while the low-frequency slope, m , only depends on the translational motion (cf. Eqs. 29 and 32), one can gather information on the quantity $D\tau_{\text{rot}} = d^2/(2r)$ (cf. Eqs. 19 and 22) which is also, like the model-based r , a measure for the rotational-translational coupling in the liquid, when relating both parameters of the linear fit, $R_1(0)$ and m , as follows (cf. Eqs. 19, 31 and 32):

$$\frac{R_1(0)}{m^{2/3}} = \frac{D\tau_{\text{rot}}(K_{\text{intra}} + f \cdot K_{\text{inter}}) + \frac{2}{9} K_{\text{inter}} d^2}{B^{2/3}} = \text{const. when } r = \text{const.} \quad (35)$$

This quantity should be constant when FTS applies or at least when translational-rotational coupling holds, *i.e.* $r(T) = \text{const.}$, which is a weaker condition than FTS as the shape of the spectral densities still may change without an alternation of the spectral separation.

Assuming that the spin densities, N_X , the intramolecular coupling constant, K_{intra} , and the ‘molecules’ diameter’, d , (and therefore K_{inter} , cf. Eq. 30) are constant in the considered temperature range, *i.e.*, that no structural changes in the liquid occurs, one has to relate a temperature dependence of $R_1(0)/m^{2/3}$ solely to a change in $D\tau_{\text{rot}}$:

$$\frac{R_1(0)}{m^{2/3}} \propto D\tau_{\text{rot}} + \frac{\frac{2}{9} K_{\text{inter}}}{K_{\text{intra}} + f \cdot K_{\text{inter}}} \cdot d^2 = D\tau_{\text{rot}} + \text{const.} \quad (36)$$

One can obtain absolute results on $D\tau_{\text{rot}}$ for all profiles, $R_1(\omega)$, taken at higher temperature when one low-temperature profile is available, which allows to extract both τ_{rot} and D via fitting. Figure 17 taken from Pub. 1 exemplarily shows the result of this procedure, besides glycerol-h₈ also two perdeuterated species are depicted. Pub. 1 proves that $R_1(\omega)$ of glycerol can almost perfectly be interpolated by a combination of CD function (Eq. 6) and FFHS model (Eq. 21) with τ_{rot} and D agreeing with other methods. Besides τ_{rot} and D the fit also yields K_{inter} (and therefore d , cf. Eq. 30) and the overall rotational coupling $K_{\text{intra}} + f \cdot K_{\text{inter}}$.

With these parameters, K_{inter} and $K_{\text{intra}} + f \cdot K_{\text{inter}}$, Eq. 35 allows the calculation of $D\tau_{\text{rot}}$ for other datasets taken at higher temperatures where the rotational dispersion is not any more contained in the actual frequency window as one only needs the result of the linear fit of $R_1(\sqrt{\omega})$ at low frequencies, m and $R_1(0)$. This is similar to the susceptibility master curve procedure (*cf.* Sec. 3.1.5), but it does not assume a constant spectral separation and it fastens on translational instead of rotational motion.

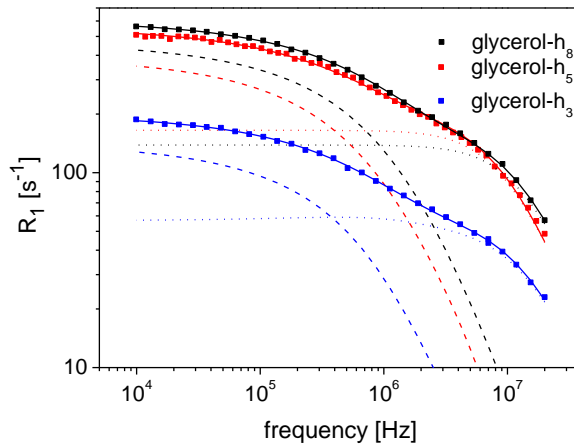


Figure 17: Rate dispersion curve of glycerol-h₈, glycerol-h₅ and glycerol-h₃ at 278 K; solid lines: fits only distinguishing between rotation based on a CD function (dotted lines) and translation based on the FFHS model (dashed lines). Taken from Pub. 1.

This procedure for determining $D\tau_{\text{rot}}$ can exemplarily be used to reexamine the difference between the isotope dilution experiment (glycerol-h₅ in glycerol-h₀) and the admixture of a chemically different deuterated solvent (PG in Chld). Figure 18a shows the results of the various dilutions of glycerol-h₅ in glycerol-h₀ (solid squares) and of glycerol-h₈ (blue stars, data from Pub. 4) compared to combined results from FG NMR and DS (Ref. [66], black circles). The black open squares depict an own compilation of available literature data on D and τ_{rot} (Refs. [25, 28, 29, [75]-[77]]). The parameters of the required fits of a low-temperature profile, K_{inter} and $K_{\text{intra}} + f \cdot K_{\text{inter}}$ are given in Pub. 1 and Pub. 2. The first observation is that our result on glycerol-h₈ well agrees with those from the references. Furthermore it reveals that the isotope dilution, like the partial deuteration in the case of glycerol-h₅, has no effect on $D\tau_{\text{rot}}$.

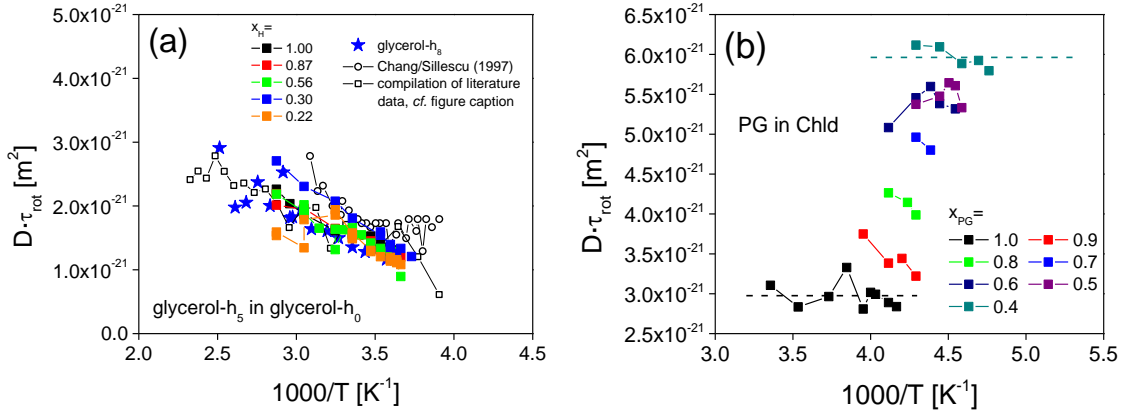


Figure 18a: $D\tau_{rot}$ for glycerol-h₅ in glycerol-h₀ (solid squares) and glycerol-h₈ (blue stars, data from Pub. 4). For comparison data from Ref. [66] were included (open circles), the open squares represent an own compilation of available data in the literature (Refs. [25, 28, 29, 75-77]). **Figure 18b:** Analogue data on the system PG in Chld.

Figure 18b presents the data of the system PG in Chld. While isotope dilution seems not to affect $D\tau_{rot}$ it gets higher with dilution in the case of PG in Chld. When applying fits to the low-temperature profiles in order to obtain K_{inter} and $K_{intra} + f \cdot K_{inter}$ for all PG concentrations, x_{PG} , the condition $K_{inter} \propto x_{PG}$ was imposed which led to a global $d \cong 4.13 \cdot 10^{-10}$ m. Thus considering $D\tau_{rot} = d^2/(2r)$ a rise in $D\tau_{rot}$ reflects a decreasing spectral separation, r . For pure PG it gives a mean $r \cong 39$ (c.f. dashed black line in Figure 18b) for PG in Chld with $x_{PG} = 0.4$ the average in temperature (c.f. dashed cyan line in Figure 18b) gives $r \cong 14$. This suggests that the dilution with Chld makes the PG molecules better obey the Stokes-Einstein-Debye relation, $r = 9$.

Summing up, in case of the isotope dilution experiment we find $r \cong \text{const.}$, while for PG in Chld r decreases with increasing dilution with Chld. As unlike in the case of glycerol-h₅ in glycerol-h₀ Chld does not support hydrogen bonds this is an indication that hydrogen bonds are responsible for a big spectral separation and thus indirectly for the low-frequency excess contribution found in the susceptibility master curves of various hydrogen-bonded liquids.

For high temperatures $T > 1.2T_g$ commonly translational and rotational coupling is considered to hold in molecular liquids, i.e. $D\tau_{rot} = \text{const.}$, while when approaching T_g , $D\tau_{rot}$ rises considerably, which led to the term ‘enhanced translation’ close to the glass temperature [66, 67], because a rise in $D\tau_{rot}$ reflects a decreasing spectral separation, r , which represents an acceleration of translational dynamics with respect to rotational one. Despite the fact that all the data on glycerol presented in Figure 18a are measured well above $1.2T_g$ one can distinguish a slight dependence of $D\tau_{rot}$ on temperature. Our results as well as the references

suggest a rising spectral separation, r , with decreasing temperature, *i.e.* a slowing down of translation with respect to rotation in the liquid and moderately supercooled liquid before the anticipated but not experimentally covered contrary process (enhanced translation) sets in close to T_g [66].

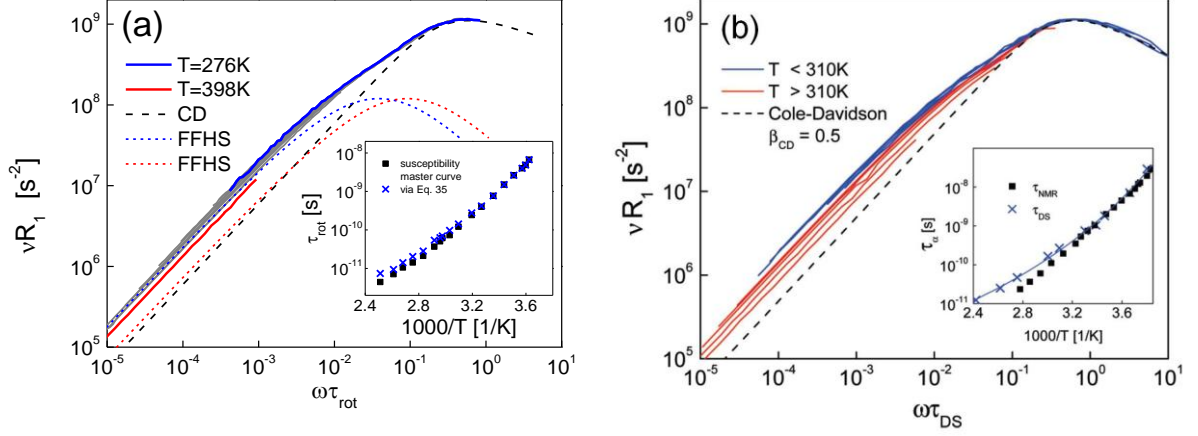


Figure 19a: NMR susceptibility of glycerol-h₈ (data from Pub. 4) plotted versus scaled frequency, $\omega\tau_{\text{rot}}$, the factor τ_{rot} is obtained via calculations along Eq. 35; blue and red solid lines taken at temperatures as indicated, grey lines taken at intermediate temperatures, dashed solid line: CD susceptibility, dotted lines: FFHS model, inset: comparison of τ_{rot} derived via Eq. 35 (blue exes) with results from susceptibility master curve construction (black solid squares). **Figure 19b:** Analogous figure employing results from DS ($\tau_{\text{DS}} = \tau_{\text{rot}}$) instead of the ones derived by Eq. 35. Taken from Ref. [38].

As the susceptibility master curves assume FTS and thus omit effects of temperature on the spectral separation it is of interest to compare the rotational time constants, τ_{rot} , derived with the present method (given by $D\tau_{\text{rot}}$ and D) to the ones which are yielded via the construction of susceptibility master curves. Figure 19a illustrates the differences of both approaches for glycerol-h₈. The inset compares τ_{rot} from the susceptibility master curve procedure assuming FTS (and thus $r = \text{const.}$) for translation and rotation (black solid squares) with the result of the presently discussed method (blue exes). The main picture shows the master curve $\chi''_{\text{NMR}}(\omega\tau_{\text{rot}})$ where the latter rotational correlation times derived from $D\tau_{\text{rot}}$ were used for scaling. It is immanent that using the former would make all datasets coincide.

Like Figure 18a, Figure 19a also suggests that the spectral separation gets narrower with increasing temperature. This shall be pointed out by the model functions inserted. The dashed black line is a CD susceptibility to account for the rotational part (intra- and intermolecularly mediated), whereas the dotted lines represent the translational share in terms of the FFHS model. The first one (blue dotted line) located at lower frequencies is placed to account

(together with the rotational peak) for the curve taken at lowest temperature (blue line), where the spectral separation seems to be rather wide. The second one (red dotted line) is shifted to higher frequencies in order to account for the curve taken at highest temperature (red line) therefore representing a narrower spectral separation.

As a further evidence for this change in spectral separation serves Figure 19b, which is taken from Ref. [38]. It is analogous to Figure 19a, only that it employs τ_{rot} obtained without the assumption of FTS from DS experiments. The result is equivalent.

3.1.9 Polymer Dynamics

This thesis will show that the translationally driven, universal low-frequency dispersion can also be found in polymers and thus self-diffusion coefficients can be extracted via Eq. 32, too. The main difference between simple liquids and polymers are several polymer specific dynamical regimes, which occur between the fast α -process (structural relaxation) and the slowest motion, the translational diffusion. In the case of polymers the former is connected to the reorientation of the polymer segments (with a time constant $\tau_s = \tau_\alpha$) while in liquids it reflects molecular reorientation ($\tau_{\text{rot}} = \tau_\alpha$). When going from simple liquids to oligomers and eventually from oligomers to polymers by increasing the molecular mass, M , a rising number of additional processes arise.

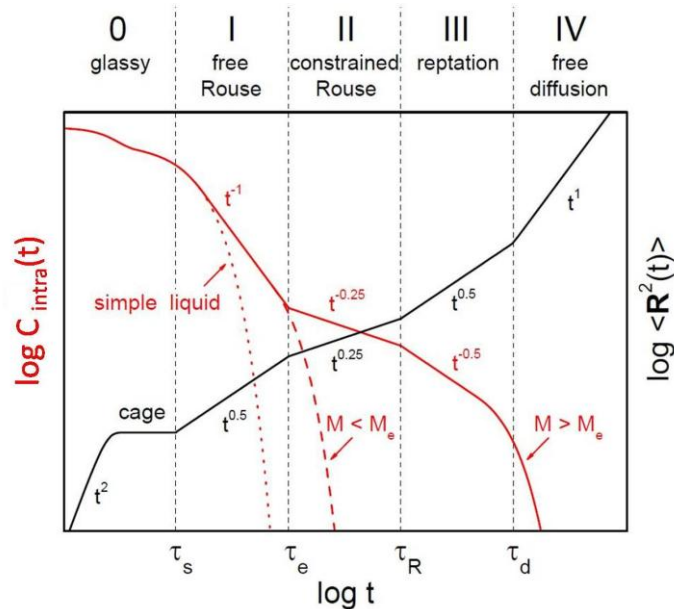


Figure 20: Schematic dependence of the logarithm of the intramolecular (segmental) correlation function, $C_{\text{intra}}(t)$, and the mean-square displacement, $\langle \mathbf{R}^2(t) \rangle$, on time as expected within the tube-reptation model. For $C_{\text{intra}}(t)$ also the expectations for an unentangled polymer (dashed line) and for a simple liquid (dotted line) are given. Adapted from Ref. [79].

At the beginning of the polymerization, *i.e.* the molecule is integrated into short chains of monomers, their local reorientation is not fully isotropic anymore and cannot fully extinct the whole correlation. The remaining correlation decays via slower processes which are identified as chain modes. They are most commonly described by the free Rouse model, which assumes the polymer being a chain of beads connected by entropic springs [78].

Figure 20 shows its predictions for the rank $l = 2$ correlation function, $C_{\text{intra}}(t)$, (left axis, red curve). One sees the correlation loss for a simple liquid (dotted line) due to molecular/segmental reorientation (regime 0, glassy dynamics) and for the free Rouse chain (dashed line) (regime I), the latter protracted because of the slower modes involved. With higher molecular masses the chains will start to feel each other and get entangled among themselves. This happens when the entanglement mass, M_e , is exceeded, and the free Rouse regime is joined by the constrained Rouse (II) and the reptation (III) regime at longer times. Regime II is described as hindered chain modes in a tube which consists of the other chains, regime III describes the one dimensional motion (*i.e.* reptation) of the chain along these tubes [80]. In the case of regime I – III being present normal (Fickian) translational diffusion (IV in Figure 20) can be observed only after a quite long time (*i.e.* τ_d , when reptation already has performed), which is needed to dissolve one tube and set up another (*cf.* Figure 20, red solid line).

The advantage of the employment of the universal translational low-frequency is obvious: Because of its model independent approach one can avoid considering all the previous polymer dynamics. Here a quantification of D by fitting the whole rate dispersion employing certain models, *e.g.* FFHS model with CD function like done in Pub. 1 for simple liquids, would be very tedious in the best case. Nevertheless the experimental results have to cover regime IV, which becomes increasingly difficult the higher M is. This shall be further clarified by means of the predictions on the mean square displacement, $\langle \mathbf{R}^2(t) \rangle$, for the different regimes in Figure 20 (right axis, black curve). The simple liquid only has the ballistic regime (free flight of the particle) at very short times, after which the cage of the surrounding molecules starts to take effect. The latter's influence extends to longer times, when approaching T_g but finally one will see normal translational diffusion, whose main feature is that the mean square displacement grows linearly in time. The rate of the growth of $\langle \mathbf{R}^2(t) \rangle$ is given by the self-diffusion coefficient, D , via:

$$\langle \mathbf{R}^2(t) \rangle = 6D \cdot t \quad (37)$$

In contrary to simple liquids for polymers after the α -process (regime 0, glassy dynamics) several subdiffusive (*i.e.* $\langle \mathbf{R}^2(t) \rangle \propto t^\gamma$ with $\gamma < 1$) regimes (I-III in Figure 20), are consecutively inserted with growing M , which retards the final crossover to regime IV described by Eq. 5. For this reason with a given experimental setup one only can access D up to a certain molecular mass, as above the translational dynamics is such retarded that the universal low-frequency behavior is located below the lowest frequencies measurable and cannot anymore be shifted into the covered frequency window by applying higher temperatures.

For many systems (*e.g.* poly(dimethyl siloxane), polyisoprene, polybutadiene) yet it is possible to cover M values beyond M_e (*i.e.* entangled polymers) and one can identify a crossover of the power-law behavior $\propto M^{-\alpha}$ of the transport coefficients at M_e which is predicted by the theories (*cf.* Pub. 5, Pub. 6).

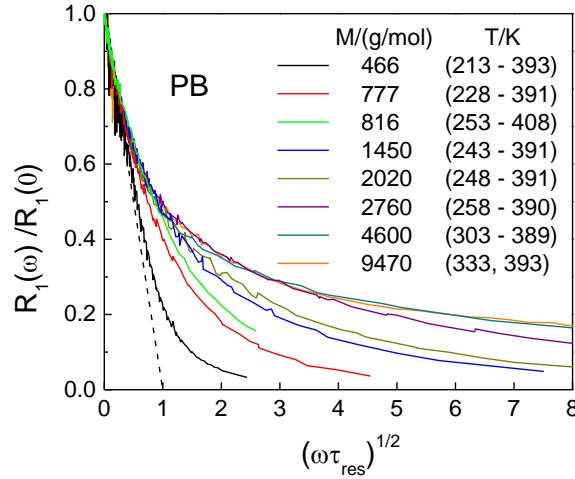


Figure 21: Master curves in rate representation, $R_1(\omega)/R_1(0)(\sqrt{\omega\tau_{\text{res}}})$, for polybutadiene (PB) with different molecular masses, $466 \leq M/(\text{g/mol}) \leq 9470$. Taken from Pub. 5.

Figure 21 shows the rate dispersion master curves for polybutadiene (PB) with different molecular masses, M , as presented in Pub. 5. With the assistance of the relaxometer in Darmstadt the universal low-frequency behavior could be detected for PB with molecular masses up to $M = 9470 \text{ g/mol}$ (*i.e.* PB9470). For higher M the translational regime was not contained in the accessible frequency interval. For each system the datasets taken at different temperatures collapse onto a common master curve and, as constructed, all of them coincide in the low-frequency behavior but show differences at higher reduced frequencies. While PB466 (solid black curve in Figure 21) still is a simple liquid, the highest M considered

(cyan and orange curves in Figure 21) clearly exceed the entanglement molecular mass, $M_e = 1900 \text{ g/mol}$ [81], and therefore should feature polymer dynamics. Their development with growing molecular masses can easily be seen in Figure 21 as a systematic change of the master curves.

The master curve of the low- M system in principle merely shows two dynamical processes: translation and rotation. The dispersion due to the latter causes the curve to approach zero at intermediate reduced frequencies. With an increase of M the curve bends more and more upwards and finally seems to approach a finite value of $R_1(\omega)/R_1(0)$ at highest frequencies of the presently covered interval. This behavior demonstrates the arising of polymer dynamics in between the segmental dynamics and translational diffusion which shifts the former to higher reduced frequencies with respect to the translation. Eventually it is spectrally separated from translation to such an extent that the dispersion due to segmental dynamics is not anymore contained in the covered frequency interval and thus acts like a constant underground like seen in the case of PB9470 (Figure 21, orange line).

In the following a short introduction to each of the six publications is given.

3.2 Phenomenological Description of the Rate Dispersion of Glycerol (Pub. 1)

This publication presents FC ^1H NMR measurements on fully protonated glycerol (glycerol- h_8) and two perdeuterated varieties, namely glycerol- h_5 (*i.e.* $\text{CH}_5(\text{OD})_3$) and glycerol- h_3 (*i.e.* $\text{CD}_5(\text{OH})_3$) taken in a broad temperature range. To further clarify the intermolecular contribution, firstly a translational model is consulted to account for the intermolecular relaxation contribution to the whole rate dispersion curve. It turns out that this provides a consistent analysis of all samples.

The experimental results are analyzed in terms of the model functions given in the introduction. The rotational part is described by a CD function (Eq. 6) while the translational one by the FFHS model (Eq. 21). For glycerol- h_8 only the BPP equations (Eqs. 11 and 27) are employed. For the perdeuterated samples also heteronuclear dipolar coupling is considered which requires the SBM equations (Eqs. 12 and 28) in addition. As Pub. 1 does not yet take into account eccentricity effects the intermolecular rotational contribution is included into the intramolecular coupling constants $(C_{\text{intra}}^{\text{HH}})^2$ for glycerol- h_8 and $(C_{\text{intra}}^{\text{HH,red}})^2$ and $(C_{\text{intra}}^{\text{HD}})^2$ for the partially deuterated samples which were global, temperature independent fit parameters. Thereby, $(C_{\text{intra}}^{\text{HD}})^2$ was a fixed multiple of $(C_{\text{intra}}^{\text{HH,red}})^2$. Since the labeling in Pub. 1 differs from the notation given in Chap. 3.1 we may identify:

$$\frac{2}{5} I_{\text{H}} (I_{\text{H}} + 1) (C_{\text{intra}}^{\text{HH,red}})^2 = \frac{1}{5} (K_{\text{intra}}^{\text{HH}} + f \cdot K_{\text{inter}}^{\text{HH}})$$

$$\frac{2}{15} I_{\text{D}} (I_{\text{D}} + 1) (C_{\text{intra}}^{\text{HD}})^2 = \frac{1}{10} (K_{\text{intra}}^{\text{HD}} + f \cdot K_{\text{inter}}^{\text{HD}})$$

The suggested separation between inter- and intramolecular contribution in Pub. 1, $R_{1,\text{intra}}$ and $R_{1,\text{inter}}$, has strictly to be transferred into rotational and translational ones, R_1^{rot} and R_1^{trans} . However, as revealed in Pub. 2, this is only a problem of labeling concerning the coupling and does not affect the results on the molecular dynamics, *i.e.* $\tau_{\text{R}} = \tau_{\text{rot}}$ and D . The major results of Pub. 1 are as follows:

- The rate dispersion curves, $R_1(\omega)$, for all samples are perfectly describable by a combination of a CD spectral density and the FFHS model with a distance of closest approach, d , which only changes slightly with temperature.

- For all samples the results for the rotational correlation times, τ_{rot} , agree with ones from DS and the obtained self-diffusion coefficients, D , agree with those from FG NMR. The spectral separation is found to be $r \approx 50$ considerably exceeding the DSE relation, *i.e.* $r = 9$ (Eq. 22). Thus FC ^1H NMR is capable to monitor both translational and rotational dynamics in liquids. In fair approximation translational-rotational coupling holds (*i.e.* $r(T) = \text{const.}$) though a slight trend of r to decrease with increasing temperature can be distinguished (*cf.* Sec. 3.1.8).

The previous two points (*i.e.* good interpolation of data and agreement of τ_{rot} and D) proof the validity of this phenomenological separation which however distinguishes between rotational and translational parts instead of intra- and intermolecular ones as it is demonstrated by isotope dilution experiments in Pub. 2 and Pub. 4. Thus in Pub. 1 for the first time $R_1(\omega)$ is consistently fitted and self-diffusion data is presented obtained by FC ^1H NMR in liquids.

3.3 Intermolecular Relaxation in Glycerol (Pub. 2)

As the attempted separation between intra- and intermolecular contributions in Pub. 1 was based on models, Pub. 2 reveals the intermolecular contribution, $R_{1,\text{inter}}(\omega)$, model independently by an isotope dilution experiment (*cf.* Sec. 3.1.7). So Pub. 2 serves as a retrospective justification for the separation done in Pub. 1 because it shows that it can be identified as a distinction between rotational and translational parts instead of intra- and intermolecular ones. This is done by disclosing the eccentricity effect which is subsequently shown to be describable on the lines of the intramolecular rotational contribution. Thus the separation into rotational and translational contribution gives correct quantitative estimations for both types of molecular dynamics.

As said in Sec. 3.1.7, in principle the experiment in this publication is a rerun of the one already performed in by Kintzinger and Zeidler [59]. Glycerol-h₅ was diluted in its fully deuterated counter-part, glycerol-h₀. Thereby, glycerol-h₅ was used to prevent proton exchange at the hydroxyl groups. As shown in Sec. 3.1.7 we still were able to obtain new results as the FC NMR technique covers lower frequencies than those Kintzinger and Zeidler were able to reach using conventional equipment. Their rate dispersion curves do not cover the translational dominated frequency regime (*cf.* Figure 12), they essentially only saw rotation. Pub. 2 fills this experimental gap.

For five different dilution ratios $1 \leq x \equiv x_{\text{H}} \leq 0.22$ (with x being the mole fraction of glycerol-h₅) rate dispersion curves were recorded in a broad temperature range. The results are analysed in terms of global fits to rate dispersion curves considering also the heteronuclear coupling of protons to deuterons on the one hand and in terms of susceptibility master curves on the other hand where the extrapolation $x \rightarrow 0$ is performed (*cf.* Eq. 24 multiplied with frequency). Regarding the global fits for the intermolecular spectral density the approximation for the eccentricity model given in Eq. 23 is used. Based on the notation given in Chap. 3.1 we identify:

$$\frac{2}{5} I_{\text{H}} (I_{\text{H}} + 1) (C_{\text{intra}}^{\text{HH,red}})^2 = \frac{1}{5} K_{\text{intra}}^{\text{HH}}$$

$$\frac{2}{15} I_{\text{D}} (I_{\text{D}} + 1) (C_{\text{intra}}^{\text{HD}})^2 = \frac{1}{10} K_{\text{intra}}^{\text{HD}}$$

In the applied fitting procedure the distance of closest approach, d , the strength of the rotational contribution due to eccentricity, f , $(C_{\text{intra}}^{\text{HH,red}})^2$ and $(C_{\text{intra}}^{\text{HD}})^2$ are global fit parameters,

i.e. their value does not change with temperature or dilution ratio. The appropriate spin densities for protons and deuterons are given by the spin density of glycerol-h₈, the ratio of protons and deuterons in the case of glycerol-h₅ and the particular dilution ratio.

The parameter β , which describes the broadening of the (both intra- and intermolecular mediated) rotational spectral density (CD function, Eq. 6) and the spectral separation, r , are only allowed to vary with temperature. The rotational time constants, τ_{rot} , being identical for the intra- and intermolecular J_{rot} and fixing τ_{trans} via r , are free fit parameters. Included into the fit procedure are measurements of each dilution ratio x at four temperatures $273 \leq T/\text{K} \leq 283$ where both the rotational and translational dispersions are contained in the frequency window. The global fits and the analysis using susceptibility master curves yield consistent results:

- The most prominent loss of relaxation rate or susceptibility with increasing dilution with glycerol-h₀ happens at low frequencies. The intermolecular relaxation obviously prevails here. The extrapolation $x \rightarrow 0$ leaves the intramolecular contribution which is given by a CD function. This is a direct proof of the intermolecular origin of the excess contribution at low frequencies, where about 80% of the magnitude is intermolecular.
- The model used in Pub. 1 (*i.e.* FFHS model for intermolecular and CD function for intramolecular part instead of translational and rotational part, respectively) fails to describe the whole dataset, due to a significant decrease of $R_1(x; \omega)$ with x in the rotational regime. Without eccentricity (*i.e.* model used in Pub. 1) the rate dispersion curves for different x would coincide in the rotational regime. Thus, the global fits are not possible until the introduction of an intermolecular modulated (as thus x -dependent) rotational contribution via $\tilde{J}_{\text{inter}}(\omega)$ (Eq. 23), which contains the same J_{rot} which is also employed for the intramolecular part. The quality of the fits is very good and the obtained D agree with FG NMR. This loss with increasing dilution at the rotational regime is an evidence for the eccentricity effect. As noted in Sec. 3.1.6 (*cf.* Figure 11b) an inspection of the intermolecular part of the susceptibility master curve is a further demonstration of the eccentricity effect as it shows besides a pure translational part, which is responsible for the excess contribution, a rotational one. A comparison of the rotational contribution due to eccentricity to the intramolecular part shows that the positions of the peaks coincide as expected from the fact that they

reflect the same process. These results validate the separation for neat liquids as done in Pub. 1 and it becomes clear why it leads to consistent self-diffusion coefficients.

We note that the found value $f = 2.68$ can be related to an (effective) eccentricity of $e = 0.75$ (*cf.* Pub. 4). The value for the intramolecular proton-proton coupling constant $(C_{\text{intra}}^{\text{HH,red}})^2 = 1.1 \cdot 10^{10} \text{ Hz}^2$ is smaller than $(C_{\text{intra}}^{\text{HH,red}})^2 = 1.55 \cdot 10^{10} \text{ Hz}^2$ given in Pub. 1 for glycerol- h_5 , because the latter misleadingly also accounts for the rotational contribution due to eccentricity. In consistence with Pub. 1 the spectral separation $r \approx 50$ is found to slightly decrease with increasing temperature.

To summarize, Pub. 2 shows the differences between the separation of rotation and translation and intra- and intermolecular contributions. While the intramolecular part is purely rotational it is generally not possible to extract the mere translational contribution with an isotope dilution experiment because of the eccentricity effect, which, to our knowledge, is demonstrated in neat liquids for the first time by Pub. 2.

Pub. 3 will show that translation can also be quantified in a model-independent way without the necessity of a sufficiently large spectral separation, r . In Pub. 4, which contains an isotope dilution experiment on OTP, we apply the exact solution of the eccentricity model by Ayant et al. [51] instead of Eq. 23.

3.4 Application of the Translational Low-frequency Dispersion to Molecular Liquids (Pub. 3)

As demonstrated in Sec. 3.1.8 the translationally driven low-frequency behavior of the relaxation rate (Eq. 29) gives a handle to extract easily and in a model independent way self-diffusion coefficients, D , in neat liquids. Pub. 3 shows the results of this method for glycerol, OTP, threitol, xylitol and sorbitol (*cf.* Figure 14b).

We note, that Pub. 3 employs a different kind of normalization of the intermolecular spectral density. The prefactor $1/d^3$ is included in the expression for $J_{\text{inter}}(\omega)$ which renders the first order of its series expansion model independent. When $1/d^3$ is contained in the prefactor K_{inter} like formulated in Sec. 3.1.8 (*cf.* Eq. 30) the model dependent parameters in $J_{\text{inter}}(\omega)$ like d and τ_{trans} do not cancel out until plugged into the expression for the relaxation rate to give a first order term which only depends on D like in Eq. 29.

We summarize the results:

- The comparison of $R_{1,\text{intra}}(\omega)$ from Pub. 2 to results from DS again confirms the purely rotational shape. Contary, the whole rate, $R_1(\omega)$, significantly differs from profiles obtained by DS as the former exhibit a distinctive linear behavior at low frequencies when plotted versus $\sqrt{\omega}$, while DS profiles start flatly when coming from low frequencies. This comparison also demonstrates on the basis of experimental data that at sufficient low frequencies the slope of $R_1(\sqrt{\omega})$ is purely translational driven as the rotational contributions are constant there. So D can be evaluated directly from the whole relaxation rate.
- The linear part of $R_1(\sqrt{\omega})$ at low frequencies can be identified for all liquids considered. The results on D determined from the slope, $dR_1/d\sqrt{\omega}$, agree well to available results from FG NMR (*cf.* Figure 14b).

As the covered liquids (besides glycerol-h₅ where the H-D coupling has an insignificant contribution which can be omitted) only contain protons as active nuclei, Eq. 6 in Pub. 3 only considers proton-proton coupling and therefore is consistent to Eq. 29 with only the first summand preserved in the expression for B . As Pub. 4 - Pub. 6 also only consider proton-proton coupling, the negligible influence of H-D coupling on the result of D shall be clarified exemplarily with glycerol-h₃, which has a relatively high deuteron spin density. Furthermore we demonstrate a case, where heteronuclear coupling has significant influence.

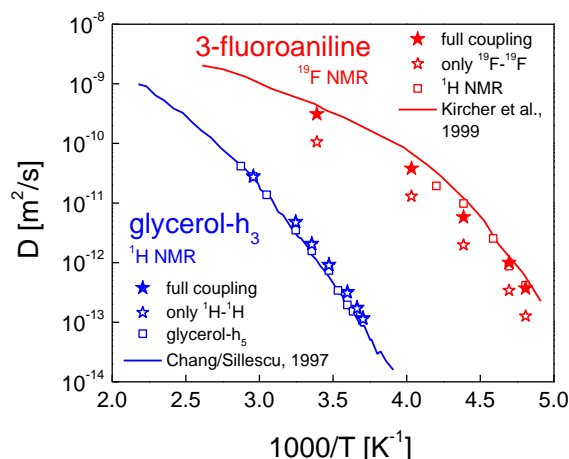


Figure 22: Self-diffusion coefficient, D , vs. inverse temperature for 3-fluoroaniline and glycerol- h_3 as derived from the low-frequency analysis of $R_1(\sqrt{\omega})$. Solid stars: results accounting for heteronuclear coupling; open stars: results omitting heteronuclear coupling. Open squares: see text. Solid lines: FG NMR data from Ref. [66] (glycerol) and Ref. [82] (3-fluoroaniline).

Figure 22 shows the low-frequency analysis of FC ^1H NMR data of glycerol- h_3 published in Pub. 1. The result, where the full coupling (Eq. 29 with second term due to deuterium) is incorporated (blue solid stars) is compared to the result where the H-D coupling is omitted (blue open stars). We see an almost perfect match of both datasets, a thorough scrutinization reveals a slightest trend of D being smaller when only homonuclear coupling is considered. The blue solid lines are measurements by FG NMR [66] and one sees that D of glycerol- h_3 seems to be slightly higher. This may be due to proton exchange in the hydroxyl groups. The fact that glycerol- h_5 (blue open squares) better agrees with the results from FG NMR supports this claim.

The second example shows 3-fluoroaniline measured with FC ^{19}F NMR a result which is so far unpublished. Like ^1H , the spin of ^{19}F ($I = 1/2$) relaxes via dipole-dipole interaction. As its gyromagnetic ratio is only slightly lower than that of a proton spin, the measurement with the Stellar relaxometer is straight forward and does not need hardware adaption. Every molecule only contains one fluorine in contrast to six hydrogen atoms. This fact in combination with the similar gyromagnetic ratios renders the contribution due to ^{19}F - ^1H coupling significant, as demonstrated in Figure 22, where the red solid stars represent the complete treatment whereas the red open stars depict the result when only ^{19}F - ^{19}F coupling is considered. With respect to FG NMR [82] (solid red line) only the accurate treatment fairly agrees. For comparison results derived by FC ^1H NMR are included (red open squares) also accounting for ^1H - ^{19}F coupling. They quite well agree to the results of FG NMR and to the full analysis of the FC

^{19}F NMR data. The slight deviations to FG NMR may be due to the fact that the SBM equation (Eq. 28) assumes that the other spins are always in equilibrium when the considered spin relaxes, which is problematic as ^{19}F and ^1H spins relax on similar time scales.

We finally note that, as shown in Pub. 3, this low-frequency analysis also works for OTP which is known to show no distinct low-frequency excess contribution attributed to the translational motion and therefore agrees well with results from DS. So one is tempted to ask how the intermolecular part of OTP does look like, which obviously contains the translational part that enables the analysis done in Pub. 3 but does not result in a low-frequency shoulder like in the case of glycerol. For this reason Pub. 4 presents an isotope dilution experiment on OTP.

3.5 Intermolecular Relaxation in o-Terphenyl (Pub. 4)

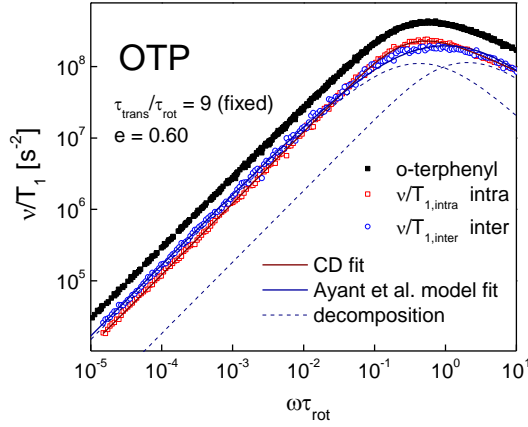


Figure 23: Susceptibility master curve of OTP (black solid squares) and its separation into intra- (red open squares) and intermolecular contributions (blue open squares). The red line is a fit of the intramolecular contribution using the CD function; the blue line is a fit of the intermolecular contribution by the eccentricity model of Ayant et al. [51]. Taken from Pub. 4.

As OTP shows no low-frequency excess contribution an isotope dilution experiment was performed with OTP in order to clarify the relaxation contributions according to intra- and intermolecular interactions. Contrary to Pub. 2, the intermolecular contribution is described by the eccentricity model of Ayant et al. [51]. The eccentricity model is also compared to the approximation given in Eq. 23, which was used to describe the results in Pub. 2. In addition the rate master curve approach (*cf.* Sec. 3.1.8, Eq. 33) is introduced and its shape is discussed. Hereby is shown, that the quantity $c \equiv \xi \cdot r^{5/2}$ (*cf.* Eq. 34) is the decisive parameter characterizing the behavior of the master curve beyond the linear regime, *i.e.* $c < 53$ suggests a ‘rotationally dominated shape’ while $c > 53$ suggests a ‘translationally dominated shape’. In the former case going to higher $\sqrt{\omega \tau_{\text{res}}}$ the master curve leaves the linear regime in downward direction while it deviates in upwards direction for the latter case. By mistake in Pub. 4, Eq. 15 the threshold $c \approx 40$ is given, $c \approx 53$ like in Eq. 34 is correct. This stems from a mistake in Pub. 4, Eq. 10c, where $1/135$ should read correctly $1/(135\sqrt{2})$. Apart from the ‘rescaled correlation time’, τ' , given by

$$\tau' = \left(\frac{40}{3(\sqrt{2} + 8)} \right)^2 \tau_{\text{res}} \cong \left(\frac{1}{0.7} \right)^2 \tau_{\text{res}}$$

the formalism in Pub. 4 is consistent with the one in Sec. 3.1.8 only considering proton-proton coupling. As for exclusive homonuclear coupling $K_{\text{inter}}d^3 = 60B/(1+4\sqrt{2})$ is valid (*cf.* Eqs. 29 and 30), using the expression for $R_1(0)$ given in Eq. 31 one can easily confirm the connection between τ' (Pub. 4, Eq.13) and τ_{res} (Eq. 33) given above. We furthermore note that in Pub. 4 the FFHS model is addressed as ‘hard-sphere free diffusion (HSFD) model’.

The major results are:

- The comparison between the exact solution of the eccentricity model from Ayant et al. [51] and the approximation given in Eq. 23 shows that the rotational part of the former (derived by subtraction of the corresponding FFHS contribution) is not given by a Debye (Eq. 4) or CD (Eq. 6) spectral density. Because it includes the rotational correlation time in terms of different ranks, l , its susceptibility peak is broadened, however as rotational diffusion is assumed the high-frequency slope is $\propto \omega^{-1}$ like in the case of a Debye susceptibility. The parameter f of the approximation initially rises slowly for small e , while later the increase rapidly gets steeper. For large $e > 0.85$ the magnitude of the rotational part exceeds the translational one by more than one decade as $f > 10$. The apparent spectral separation, r_{app} , which is needed for the approximation (Eq. 23) to interpolate the eccentricity model described by r also rises slowly at first with e , then gets steeper and may reach values a decade higher than r for the unphysical case of a spin placed on the surface of the hard-sphere. The behavior for different r is similar. However, while for small r the apparent ratio, r_{app} , is always higher than r (*e.g.* $r_{\text{app}}(r=9; e \rightarrow 0) \cong 19$) while for larger r it is smaller for small e and will cross r only at even higher e . For example $r_{\text{app}} = r$ at $e = 0.31$ for $r = 20$ while for $r = 50$ this holds at $e = 0.65$.
- Concerning the isotope dilution experiment, unlike in Pub. 2 in the case of glycerol-h₅ the loss of relaxation rate in OTP with decreasing proton concentration is not significantly larger at low frequencies than at high ones. The contributions of intra- and intermolecular relaxation are quite similar as seen in Figure 23, a fact which explains the absence of the low-frequency excess contribution. Nevertheless the linearity of the relaxation rate at low frequencies due to translational diffusion can be identified for $R_1(\sqrt{\omega})$ as well as for $R_{1,\text{inter}}(\sqrt{\omega})$. It is demonstrated that the rotational contribution does not interfere with the low-frequency linearity, as $R_{1,\text{intra}}(\sqrt{\omega})$ is constant there. The intermolecular part of the susceptibility of OTP is well describable with the eccentricity model but unlike in the case of glycerol-h₅ the resulting

parameters are rather inconclusive. Furthermore the peak position of the intramolecular susceptibility of OTP does not match the one of the intermolecular rotational contribution according to the eccentricity model (*cf.* Figure 23).

- The rate dispersion master curves show a distinct ‘rotationally dominated shape’ only for OTP and tristyrene, while glycerol and its homologues have the ‘translationally dominated shape’. As the behavior of the master curve is dominated by the spectral separation (*cf.* Eq. 34) this is most likely because the former two substances are one of the few in which the DSE relation (Eq. 22), *i.e.* $r = 9$, approximately holds.
- Self-diffusion coefficients, D , derived from the low-frequency behavior in $R_1(\sqrt{\omega})$ for several additional systems not covered in Pub. 3 also agree well to available data from FG NMR.

Since the apparent spectral separation, r_{app} , considerably rises with e , one may argue that the high spectral separation (exceeding the DSE relation, $r = 9$, Eq. 22) of translation and rotation experimentally found, *e.g.* for glycerol, is due to the eccentricity effect. However the large value $r \approx 50$ is confirmed by the rotational intramolecular contribution obtained by the isotope dilution experiment (*cf.* Pub. 2) in combination with the model-independent access to D via the low-frequency behavior in $R_1(\sqrt{\omega})$ (*cf.* Pub. 3). Furthermore, for $r = 50$ even $r_{\text{app}} < r$ may hold at intermediate e as shown above.

In this context we want to call in mind some results on glycerol-h₅ and glycerol-h₃ in Pub. 1. The fact that $33 \leq r \leq 54$ for the former while $50 \leq r \leq 71$ for the latter may be connected to the eccentricity effect, as the hydroxyl protons of glycerol-h₃ are supposed to be more off-centered than the ones of glycerol-h₅. Anyway, the connection of eccentricity and spectral separation calls for further investigations.

We further note that in Ref. [66] the issue of spectral separation is also addressed, however in terms of ‘apparent hydrodynamic radii’. The results are in agreement to our finding that OTP approximately fulfills the DSE relation (Eq. 22) while glycerol does not as $r \approx 50$. With Eq. 22a Ref. [66] deducts apparent hydrodynamic radii, $R_{\text{H}}^{\text{trans}}$, using D from FG NMR measurements and η from literature. The particular value $R_{\text{H}}^{\text{trans}}$ is compared to $R_{\text{H}}^{\text{rot}}$, the analog result employing τ_{rot} from ²H NMR measurements [83], Eq. 22b (alongside with Eq. 5 and $l = 2$) and again η from literature. For OTP the result is $R_{\text{H}}^{\text{trans}} \cong R_{\text{H}}^{\text{rot}} = 0.23 \text{ nm}$ while for glycerol $R_{\text{H}}^{\text{trans}} = 0.16 \text{ nm}$ and $R_{\text{H}}^{\text{rot}} = 0.096 \text{ nm}$ is found. This means that in the case of OTP Eqs. 22a and 22b simultaneously hold using the same R_{H} which reflects $r \cong 9$ in our notation. In case of glycerol the fact that $R_{\text{H}}^{\text{trans}} > R_{\text{H}}^{\text{rot}}$ renders the translational motion

comparatively slower than the rotational one and indicates that r exceeds the DSE prediction in Eq. 22.

In summary one can state that in terms of models the relaxation dispersion in simple liquids is well understood now. The intramolecular part is proven to be purely rotational, while the intermolecular part contains translational and rotational dynamics, the latter due to the eccentricity effect. We find two opposites: glycerol has a large spectral separation, thus the intermolecular contribution is distinctively bimodal which results in this ‘shoulder’ found in the whole susceptibility at low frequencies. OTP has a small spectral separation and thus in a double logarithmic scale the intermolecular part does not differ much from the intramolecular one. As a result no distinct low-frequency shoulder is visible. However, when plotting $R_{1,\text{inter}}(\sqrt{\omega})$ or $R_1(\sqrt{\omega})$ one can identify the translational contribution by means of the linear low-frequency behavior, which allows to extract D without any models. The independence of models is very favorable for more complex systems and in the next Sections it is demonstrated that this approach for determining D can also be applied to polymers.

3.6 Application of the Translational Low-Frequency Dispersion to Polymers (Pub. 5)

This publication shows in form of a short letter, that the translationally driven low-frequency behavior can also be identified in polymers and that one can obtain self-diffusion coefficients, D , up to molecular masses, M , which exceed the entanglement mass, M_e . In polymers with even higher M the time scale where translational diffusion sets in (*i.e.* the time when Eq. 37 applies) gets very large, as the longer the polymer chain is the more sub-diffusive regimes will retard the onset of translational diffusion (*cf.* Figure 20). Eventually the linear regime in $R_1(\sqrt{\omega})$ will not appear in the experimental accessible frequency window but at lower frequencies. Consequently one can increase the maximum M where translation is experimentally coverable by extending the minimum frequency of the FC relaxometer. With the home-built relaxometer in Darmstadt [45, 46] $R_1(\nu)$ was measured at frequencies as low as $\nu = 200\text{Hz}$. As the present publication and Pub. 6 deal with polymers, in these cases the experimental data obtained by the Stellar FC relaxometer were amended by low-frequency data obtained in Darmstadt to increase the maximum M where translational diffusion can be identified in $R_1(\sqrt{\omega})$.

The formalism in Pub. 5 is identical to the one given in Chap. 3.1 only considering proton-proton coupling. The focus was on linear polybutadiene (PB). We summarize the results:

- It is demonstrated that the linear regime at low frequencies can be identified in $R_1(\sqrt{\omega})$, though a comparison of the low- M systems to ones with a higher M makes clear that the linear regime gets smaller with rising M . The results cover about three decades in D and are in good agreement with data obtained by FG NMR. The limitations due to M are reflected in the temperature range, where this analysis can be performed. While it is quite broad for PB with the lowest $M = 466\text{g/mol}$ (*i.e.* PB466) in case of the largest $M = 9470\text{g/mol}$ (*i.e.* PB9470) the analysis was confined to a few high temperatures, where the linear regime is only just revealed with the aid of the relaxometer in Darmstadt.
- The dependence of the self-diffusion coefficients on the molecular mass, $D(M)$, is derived by cuts at a specific temperature, in the present case where reference data were available. The agreement with FG NMR is good and the combination of the reference data with our results taken at comparative low M reveals a crossover in the power-

law behavior $\propto M^{-\alpha}$. The position of the resulting kink in the double-logarithmic plot of $D(M)$ agrees with M_e , hence it reflects the crossover from Rouse to entanglement behavior. This suggests that the two or three highest M experimentally covered in Pub. 5 by FC NMR are already entangled.

Regarding the power-laws in $D(M)$ one can compare the exponents to predictions of polymer models. However these commonly refer to ‘isofrictional’ quantities and D fulfills this condition only well above M_e . We will see in Pub. 6 that the product $D\tau_s$ is an isofrictional quantity and the results will be compared to present models.

3.7 Derivation of an Isofrictional Quantity in Polymers and its Comparison to Common Theory (Pub. 6)

Besides the coverage of four more types of linear polymers, *i.e.* poly(dimethyl siloxane) (PDMS), polystyrene (PS), polyisoprene (PI) and poly(propylene glycol) (PPG), in Pub. 6 the determination of the isofrictional quantity, $D\tau_s$, is an advancement compared to Pub. 5.

The fact that $D\tau_s$ is an isofrictional quantity can be reasoned as follows: The dependence of D on temperature, T , and M can be factorized [81, [84]]: $D(T, M) = F(M)/\xi(T, M)$. The quantity ξ denotes the monomeric friction coefficient which is another measure for segmental dynamics, *i.e.* $\xi \propto \tau_s$ holds. Generally, it depends on both T and M . The collective polymer dynamics is reflected by F , which only depends on M and is an iso-frictional quantity. Consequently, $D\tau_s(M) \propto F(M)$ also is. For small M the monomeric friction coefficient depends on M as does the glass transition temperature, T_g , itself, which governs the local (glassy) dynamics. For large M both T_g and ξ get insensitive to M and iso-thermal and iso-frictional quantities become equivalent.

The formalism in Pub. 6 is consistent with the one given above in this thesis, however we have to note a misprint: in Eq. 3 in Pub. 6 the exponent $(\dots)^2$ is missing (*cf.* Eq. 33). In principle, one could directly obtain $D\tau_s$ via the procedure given in Sec. 3.1.8, but as this method is based on quite crude assumptions for simple liquids the segmental relaxation times, τ_s , are derived by the construction of susceptibility master curves under the assumption of FTS. Here is an account of the most important results:

- The complementarity of the segmental time constants, τ_s , obtained by FC ^1H NMR with the ones measured by DS was already demonstrated for PDMS, PI, PPG and PG in Refs. [[85]-[88]] which also present the respective NMR susceptibility master curves. In case of PS the susceptibility master curves are shown in Pub. 6, the corresponding τ_s are complement to results from DS taken at lower temperatures and agree well to LS measurements.
- Firstly, the dipolar correlation function, C_{DD} , for PDMS with different M and propylene glycol is derived from the respective susceptibility master curves via Eq. 16. (*cf.* Figure 13c) In all cases a power-law $\propto t^{-3/2}$ is found at sufficiently long times. For PDMS it gets clear that the crossover to the long-time behavior is the more retarded the higher M is. This is due to additional polymer specific dynamics which

occur between the correlation loss due to segmental relaxation and the translational diffusion. The build-up of polymer dynamics with rising M is also demonstrated for PS and PDMS in terms of rate dispersion master curves. (*cf.* Figure 21 for PB).

- From the low-frequency behavior of $R_1(\sqrt{\omega})$ self-diffusion coefficients, $D(T)$, can be obtained. Their agreement to available literature data obtained by FG NMR is good.
- The dependence $D(M)$, an ‘iso-thermal’ quantity, derived by taking cuts at a certain temperature also agrees well to results from FG NMR. Exemplarily for PDMS the product $D\tau_s$ is verified to be an isofrictional quantity by demonstrating its mere dependence on M via showing that $D\tau_s$ is constant in T . This proves the cancellation of the influence of ξ in $D\tau_s$. The equivalence of iso-thermal and iso-frictional quantities for large M can be seen for the polymers where M is covered up to the entanglement regime: For $M > M_e$ both quantities, D and $D\tau_s$, show the same M -dependence, *i.e.* $\propto M^{-\alpha}$ with $\alpha \cong 2.2$, which is somewhat above the prediction of the tube-reptation model, $\alpha = 2$. The correction by including τ_s comes into effect for smaller M : depending on the system a narrow and thus indistinct Rouse regime, *i.e.* $D\tau_s \propto M^{-\alpha}$ with $\alpha = 1$ and the low- M limit of the monomeric liquid where $D\tau_s$ becomes M -independent is resolved. The best results could be obtained on PDMS where the intermolecular relaxation is rather strong [34]. Here the entanglement regime, a short interval reflecting Rouse dynamics and the crossover to the simple-liquid behavior is covered. The difference between the iso-thermal and the iso-frictional quantity is most remarkable at PS. While $D(M)$ shows a very steep M -dependence, $D\tau_s(M)$ suggests that only for $M = 1920 \text{ g/mol}$ first effects due to polymer dynamics are revealed, *i.e.* first Rouse modes are established. This feature can be related to a strong dependence of the glass transition temperature, T_g , of PS on M .

To sum up, the present work demonstrates that FC ^1H NMR is capable to probe local (segmental) as well as collective dynamics in polymers. The results can be compared to models and the crossover to the simple liquid behavior may give an answer to the widely discussed question: When does a liquid become a polymer?

4 Publications

List of included publications as referred to in this thesis

- Pub. 1** Translational and Rotational Diffusion of Glycerol by Means of Field Cycling ^1H NMR Relaxometry.
Kruk, D; Meier, R.; Rössler, E.A.
J. Phys. Chem. B **2011**, *115*, 951.
- Pub. 2** Intermolecular Relaxation in Glycerol as Revealed by Field Cycling ^1H NMR Relaxometry Dilution Experiments.
Meier, R.; Kruk, D; Gmeiner, J; Rössler, E.A.
J. Chem. Phys. **2012**, *136*, 034508.
- Pub. 3** Nuclear Magnetic Resonance Relaxometry as a Method of Measuring Translational Diffusion Coefficients in Liquids.
Kruk, D; Meier, R.; Rössler, E.A.
Phys. Rev. E **2012**, *85*, 020201.
- Pub. 4** Inter- and Intramolecular Relaxation in Molecular Liquids by Field Cycling ^1H NMR Relaxometry.
Meier, R.; Kruk, D; Bourdick, A.; Schneider, E.; Rössler, E.A.
Appl. Magn. Reson. **2012**, *44*, 153.
- Pub. 5** Long-Time Diffusion in Polymer Melts Revealed by ^1H NMR Relaxometry.
Meier, R; Herrmann, A.; Kresse, B.; Privalov, A.F.; Kruk, D.; Fujara, F.; Rössler, E.A.
ACS Macro Lett. **2013**, *2*, 96.
- Pub. 6** Iso-Frictional Mass Dependence of Diffusion of Polymer Melts Revealed by ^1H NMR Relaxometry.
Meier, R; Herrmann, A.; Hofmann, M.; Schmidtke, B.; Kresse, B.; Privalov, A.F.; Kruk, D.; Fujara, F.; Rössler, E.A.
Macromolecules **2013**, *46*, 5538.

Individual contributions to joint publications

- Pub. 1** I conducted all experiments for glycerol-h₅ and glycerol-h₃. Glycerol-h₈ was measured by C. Gainaru. D. Kruk and I performed all analysis during my Ph.D. studies.
- Pub. 2** I conducted all experiments. The results for glycerol-h₅ are already contained in Pub. 1. I performed all analysis during my Ph.D. studies.
- Pub. 3** I conducted all experiments, except for glycerol-h₈ and OTP which were partly measured by C. Gainaru and S. Kariyo. However the data from Figure 1 are from Pub. 2 and the self-diffusion coefficients for glycerol-h₅ are based on data already given in Pub. 1. Furthermore the data on xylitol, sorbitol and threitol is own preliminary work published in Ref. [38]. I performed all analysis during my Ph.D. studies.
- Pub. 4** I conducted all experiments where the data shown in Figure 6, 9a and 10 were obtained. The data of Figure 1b, 8b and 9b was already given in Pub. 2 while the data contained Figure 1a, 11 and 12 are partly published in Ref. [38]. OTP and tristyrene were measured by S. Kariyo while triphenyl phosphate was measured by A. Bourdick. Some profiles contained in Figure 7a and 8a were measured by E. Schneider. I performed all analysis during my Ph.D. studies.
- Pub. 5** The experimental data were obtained by A. Herrmann and published in Refs. [34] and [88]. I performed all analysis during my Ph.D. studies.
- Pub. 6** I performed all measurements on the samples given in Table 2. On PS1920 and PI9910 low-frequency measurements were conducted by B. Kresse and me in Darmstadt. The other data were obtained by S. Kariyo, A. Abou Elfadl, A. Herrmann and M. Hofmann and were published in Refs. [85-91]. The segmental time constants from DS were obtained by J. Hintermeyer and published in Ref. [92]. I performed all analysis during my Ph.D. studies.

Other publications

- Universal Polymer Dynamics Revealed by Field Cycling ^1H NMR.
Herrmann, A.; Kariyo, S.; Abou Elfadl, A.; Meier, R.; Gmeiner, J.; Novikov, V.N.;
Rössler, E.A.
Macromolecules **2009**, *42*, 5236.
- Comparative Studies of the Dynamics in Viscous Liquids by Means of Dielectric Spectroscopy and Field Cycling NMR.
Meier, R.; Kahlau, R.; Kruk, D.; Rössler, E.A.
J. Phys. Chem. A **2010**, *114*, 7847.
- Nuclear-Magnetic-Resonance Measurements Reveal the Origin of the Debye Process in Monohydroxy Alcohols.
Gainaru, C.; Meier, R.; Schildmann, S.; Lederle, C.; Hiller, W.; Rössler, E.A.;
Böhmer, R.
Phys. Rev. Lett. **2010**, *105*, 258303.
- Translational Diffusion in Paramagnetic Liquids by ^1H NMR Relaxometry: Nitroxide Radicals in Solution
Kruk, D.; Korpała, A.; Kubica, A.; Meier, R.; Rössler, E.A.; Moscicki, J.
J. Chem. Phys **2012**, *138*, 024506.
- Evolution of the Dynamic Susceptibility in Molecular Glass Formers: Results from Light Scattering, Dielectric Spectroscopy, and NMR.
Petzold, N.; Schmidtke, B.; Kahlau, R.; Bock, D.; Meier, R.; Micko, B.; Kruk, D.;
Rössler, E.A.
J. Chem. Phys **2012**, *138*, 12A510.
- Intermolecular Spin Relaxation and Translation Diffusion in Liquids and Polymer Melts: Insight from Field-Cycling ^1H NMR Relaxometry.
Meier, R.; Kruk, D.; Rössler, E.A.
Chem. Phys. Chem. **2013**, *14*, 3071.

Publication 1

Translational and Rotational Diffusion of Glycerol by Means of Field
Cycling ^1H NMR Relaxometry

Kruk, D; Meier, R.; Rössler, E.A.

J. Phys. Chem. B **2011**, *115*, 951.

Copyright 2011 by The American Chemical Society

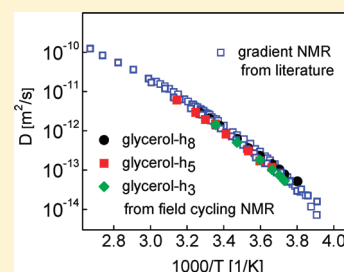
DOI: 10.1021/jp110514r

Translational and Rotational Diffusion of Glycerol by Means of Field Cycling ^1H NMR Relaxometry

D. Kruk,[†] R. Meier, and E. A. Rössler*

Experimentalphysik II, Universität Bayreuth, 95440 Bayreuth, Germany

ABSTRACT: Field cycling (FC) ^1H NMR relaxometry has been applied to study translational and rotational dynamics of nondeuterated ($-h_8$) and partially deuterated ($-h_3$ and $-h_5$) glycerol in a broad temperature range. We demonstrate that a low-frequency excess intensity observed in the relaxation dispersion stems from intermolecular dipole–dipole interactions mediated by translational dynamics, whereas the main relaxation is attributed to rotational dynamics. A theoretical description of the relaxation processes is formulated accounting for ^1H – ^1H as well as ^1H – ^2H relaxation channels for the partially deuterated systems. While the intermolecular spectral density is derived from the force-free-hard-sphere model (Fick diffusion with appropriate boundary conditions) of translational motion, the intramolecular relaxation contribution is described by a Cole–Davidson spectral density. This ansatz reproduces very well the dispersion profiles obtained from FC ^1H NMR. Moreover, the approach allows extracting the diffusion coefficient D , which is in good agreement with results from gradient ^1H NMR. Thus, ^1H NMR relaxometry has the potential to become an alternative method for measuring the diffusion coefficient in viscous liquids.



1. INTRODUCTION

With the emergence of a commercial electronic field cycling (FC) nuclear magnetic resonance (NMR) spectrometer, this technique gained new momentum for relaxation studies of condensed matter.^{1,2} FC NMR monitors the dispersion of the spin–lattice relaxation time $T_1(\omega)$. A frequency range from 10 kHz to 20 MHz can be now routinely covered by ^1H NMR relaxometry. In our previous publication,³ subsequently referred to as paper 1, we have compared the results of ^1H NMR relaxometry and dielectric spectroscopy (DS) for several viscous (supercooled) liquids. While the DS susceptibility spectra can be well interpolated by a Cole–Davidson (CD) function yielding correlation times that are attributed to the rotational dynamics involved in the structural relaxation (α -process), the corresponding ^1H NMR relaxation spectra, in contrast, show in addition to the α -relaxation peak a low-frequency excess contribution. Its amplitude varies among the systems. For some liquids essentially no such low-frequency excess contribution is found, and in this case both NMR and DS susceptibilities are very similar and well interpolated by a single CD function. The excess contribution shows similar temperature dependence as does the α -process; i.e., the seemingly two relaxation processes cannot be separated by changing temperature.

Discussing several possibilities to explain the low-frequency excess contribution to the ^1H dispersion spectrum we have been left with arguments supporting the idea that the low-frequency contribution is caused by translational motion, i.e., by diffusion of the liquid molecules, cf., paper 1. ^1H NMR relaxometry probes the fluctuations of the dipole–dipole interaction between pairs of nuclei. Due to an intermolecular contribution, ^1H NMR relaxation data may thus reflect, in addition to the molecular reorientation also translational motion. In the case of the hydrodynamic model of a (molecular) sphere rotating and

translating in a viscous medium, Abragam derived the relationship $\tau_{\text{trans}}/\tau_{\text{R}} = 9$, where τ_{R} is the rotational correlation time of rank two and τ_{trans} is the corresponding time constant of translational diffusion.⁴ The ratio is close to the experimental finding in paper 1 yielding $\tau_{\text{ex}}/\tau_{\alpha} = 20$ – 30 , being essentially temperature independent for a given liquid, and thus indicating rotational–translational coupling in the moderately viscous liquid not too close to the glass transition temperature T_{g} .⁵ In other words, intra- and intermolecular relaxation contributions are spectrally shifted with respect to each other, and this facilitates their separation without performing isotope dilution experiments as usually is done.^{6–9}

In the present publication we attempt to quantitatively describe the inter- and intramolecular relaxation dispersion of differently protonated glycerol ($-h_8$, $-h_5$, and $-h_3$) by assuming appropriate spectral densities. In particular, for the intermolecular spectral density we apply the so-called force-free hard-sphere diffusion model introduced by Hwang and Freed¹⁰ and Ayant et al.,¹¹ which provides a spectral density being distinctly of non-Debye character. For the intramolecular spectral density a CD function is chosen. We shall demonstrate that this approach gives an almost perfect interpolation of the total relaxation spectra. Moreover, it allows determining the diffusion coefficient D over a broad temperature range, which well agrees with data obtained from gradient NMR.^{12,13} Though some model assumptions are involved in the applied description, NMR relaxometry may become an alternative, and in some cases complementary method to gradient NMR.

Received: November 3, 2010

Revised: December 14, 2010

Published: January 18, 2011

2. RELAXATION PROCESSES IN VISCOUS LIQUIDS: THEORETICAL BACKGROUND

In this section the theory of ^1H spin–lattice relaxation in liquids, including intermolecular and intramolecular components is summarized. The description begins with nondeuterated systems, and it is subsequently extended to partially deuterated molecules.

2.1. Intramolecular and Intermolecular Proton Relaxation: Nondeuterated Systems. The observed proton spin–lattice relaxation, described by a relaxation rate $R_1^{\text{HH}} = (T_1^{\text{HH}})^{-1}$, contains intramolecular and intermolecular contributions:

$$R_1^{\text{HH}} = R_{1,\text{intra}}^{\text{HH}} + R_{1,\text{inter}}^{\text{HH}} \quad (1)$$

The intramolecular relaxation rate, $R_{1,\text{intra}}^{\text{HH}}$, results from fluctuations of dipole–dipole interactions between nuclei (in this case protons) belonging to the same molecule. It is given as the well-known combination of intramolecular spectral densities, $J_{\text{intra}}(\omega)$:^{4,14,15}

$$R_{1,\text{intra}}^{\text{HH}} = \frac{2}{5} I_{\text{H}}(I_{\text{H}} + 1) (C_{\text{intra}}^{\text{HH}})^2 [J_{\text{intra}}(\omega_{\text{H}}) + 4J_{\text{intra}}(2\omega_{\text{H}})] \quad (2)$$

where ω_{H} is the proton frequency. The effective dipole–dipole constant, $C_{\text{intra}}^{\text{HH}}$, fulfills the condition $(C_{\text{intra}}^{\text{HH}})^2 \leq (C_{\text{intra,rigid}}^{\text{HH}})^2 = \sum_i [(\mu_0/4\pi)(\gamma_{\text{H}}^2 \hbar^2 / r_i^3)]^2$. Here r_i is the distance between a “reference” proton and the i th proton in the molecule, the summation goes over all neighboring protons, the spin quantum number is $I_{\text{H}} = 1/2$, and γ_{H} is the proton gyromagnetic factor. The quantity $C_{\text{intra,rigid}}^{\text{HH}}$ gives the coupling constant in the limit of no motion (second moment).⁴ The spectral density, $J_{\text{intra}}(\omega)$, depends upon the motional model applied to describe the fluctuations of the intramolecular dipole–dipole couplings. Neglecting any kinds of internal motion, for viscous liquids governed by cooperative dynamics, the CD spectral density is commonly used:¹⁶

$$J_{\text{intra}}(\omega) = \frac{\sin[\beta \arctan(\omega\tau_{\text{CD}})]}{\omega[1 + (\omega\tau_{\text{CD}})^2]^{\beta/2}} \quad (3)$$

where $\tau_{\text{R}} = \tau_{\text{CD}}\beta$ is the rotational correlation time, while $0 < \beta \leq 1$ is a phenomenological stretching parameter. This spectral density represents the Fourier transform of the normalized rotational correlation function $C_{\text{intra}}(t)$ for the rank-two Wigner rotation matrices describing the molecular reorientation. By normalization it is understood that $C(t=0) = 1$ and $\int_0^\infty J(\omega) d\omega = \pi/2$.

The intermolecular relaxation pathway is mediated by relative translational diffusion of the participating molecules, since it results from fluctuations of dipole–dipole interactions between nuclei belonging to different molecules. In this case the correlation function reflects changes not only in the orientation of the dipole–dipole vectors but also in the interspin distance, explicitly the non-normalized intermolecular correlation function is given by^{1,4,15,17,18}

$$\tilde{C}_{\text{inter}}(t) = \left\langle \frac{D_{0,m}^{2*}(\Omega(t))}{r^3(t)} \frac{D_{0,m}^2(\Omega(0))}{r^3(0)} \right\rangle \quad (4)$$

Here, the rank-two Wigner rotation matrices $D_{0,m}^2$ describe the orientation of the internuclear axis in the laboratory frame via the Euler angle Ω . Again, the form of the correlation function depends on the assumed diffusion model. For a force-free

diffusion with a uniform distribution of the molecules (treated as hard spheres) outside the distance of closest approach, d , and under the assumption of the reflecting wall boundary condition at $r = d$, the correlation function for translational diffusion takes the closed analytical form:^{10,11}

$$\begin{aligned} \tilde{C}_{\text{inter}}(t) &= 72N_{\text{H}} \frac{1}{d^3} \int_0^\infty \frac{u^2}{81 + 9u^2 - 2u^4 + u^6} \exp\left(-\frac{u^2 t}{\tau_{\text{trans}}}\right) du \\ &= \frac{4\pi}{3} N_{\text{H}} \frac{1}{d^3} C_{\text{inter}}(t) \end{aligned} \quad (5)$$

where N_{H} is the number of interacting spins (protons in this case) per unit volume (i.e., $(4\pi/3)N_{\text{H}}$ is the number of spins per unit sphere), while $\tau_{\text{trans}} = d^2/D_{12}$, where D_{12} is the relative translational diffusion coefficient defined as a sum of self-diffusion coefficients of the participating molecules. Thus for identical molecules it is twice larger than the self-diffusion coefficient, $D_{12} = 2D$. The spectral density $J_{\text{inter}}(\omega)$ is given as Fourier (cosine) transform of the normalized correlation function $C_{\text{inter}}(t)$ ¹⁷

$$\begin{aligned} J_{\text{inter}}(\omega) &= 72 \frac{3}{4\pi} \int_0^\infty \left[\int_0^\infty \frac{u^2}{81 + 9u^2 - 2u^4 + u^6} \exp\left(-\frac{u^2 t}{\tau_{\text{trans}}}\right) du \right] \cos(\omega t) dt \\ &= 72 \frac{3}{4\pi} \int_0^\infty \frac{u^2}{81 + 9u^2 - 2u^4 + u^6} \frac{u^2 \tau_{\text{trans}}}{u^4 + (\omega\tau_{\text{trans}})^2} du \end{aligned} \quad (6)$$

The intermolecular ^1H – ^1H relaxation rate is given, in analogy to eq 1, as

$$\begin{aligned} R_{1,\text{inter}}^{\text{HH}}(\omega_{\text{H}}) &= \frac{2}{5} I_{\text{H}}(I_{\text{H}} + 1) N_{\text{H}} \frac{4\pi}{3} \frac{1}{d^3} \left(\frac{\mu_0}{4\pi} \gamma_{\text{H}}^2 \hbar^2 \right)^2 [J_{\text{inter}}(\omega_{\text{H}}) \\ &\quad + 4J_{\text{inter}}(2\omega_{\text{H}})] \end{aligned} \quad (7)$$

The model of translational motion represented by eq 6 is highly simplified. It assumes that the nucleus carrying the spin is placed in the center of the molecule. This implies that the fluctuations of the interspin vector (in terms of its orientation and its length) are entirely caused by the translational motion. Actually, if the spin of interest is placed at a different position in the molecule (not in its center) molecular tumbling also leads to changes of the interspin vector.¹⁹ In this work we do not account for such noncentricity effects. In consequence, the distance of closest approach, d , included in eqs 5 and 7, being on the order of the molecular size, has a meaning of an effective quantity. Assuming further the Stokes–Einstein–Debye relation for a (molecular) sphere rotating and translating in a viscous medium, the model predicts a relationship between the rank-two rotational correlation time τ_{R} and the translational correlation time: $\tau_{\text{trans}}/\tau_{\text{R}} = 9$.⁴ This implies that the spectral densities of the intra- and intermolecular relaxation are shifted in frequency with respect to each other.

2.2. Susceptibility Representation and Comparison with Dielectric Spectroscopy. It is interesting and useful to find analogies between the description of NMR relaxation and the way in which dielectric spectroscopy (DS) results are typically analyzed. In DS one measures a susceptibility function, $\chi''(\omega)$, instead of a spectral density, $J(\omega)$. These two quantities are related via the fluctuation–dissipation theorem: $\chi''(\omega) = \omega J(\omega)$. This implies that one can rewrite eq 1 in the susceptibility

representation, employing eqs 2 and 7

$$\begin{aligned} \chi''_{\text{NMR}}(\omega_{\text{H}}) = & \frac{2}{5} I_{\text{H}}(I_{\text{H}} + 1)(C_{\text{intra}}^{\text{HH}})^2 [\chi''_{\text{intra}}(\omega_{\text{H}}) + 2\chi''_{\text{intra}}(2\omega_{\text{H}})] \\ & + \frac{2}{5} I_{\text{H}}(I_{\text{H}} + 1) N_{\text{H}} \frac{4\pi}{3} \frac{1}{d^3} \left(\frac{\mu_0}{4\pi} \gamma_{\text{H}}^2 \hbar \right)^2 [\chi''_{\text{inter}}(\omega_{\text{H}}) \\ & + 2\chi''_{\text{inter}}(2\omega_{\text{H}})] \end{aligned} \quad (8)$$

We note that the appearance of the two susceptibility terms ($\chi''(\omega)$ and $\chi''(2\omega)$) in each relaxation contribution leads only to slight broadening with respect to a single susceptibility as probed in DS. In DS one does not detect effects of translational motion. Thus, an appropriate comparison between DS and NMR (adjusted to the susceptibility representation) considerably helps to identify the intermolecular contribution to the NMR relaxation, i.e., to decompose the overall relaxation into the intramolecular and intermolecular contributions. Nevertheless, at this stage one should be aware that while NMR relaxometry results are related to a rank-two correlation functions, in DS one probes the correlation functions of rank one.

2.3. Phenomenological Analysis and the NMR Relaxation Model. In paper 1 we attempted to describe the NMR relaxation data for glycerol (and several other liquids) in a phenomenological way in terms of a sum of two CD spectral densities. For convenience of the reader we repeat the applied formula below (eq 6 of paper 1)

$$\begin{aligned} \chi''_{\text{NMR}}(\omega_{\text{H}}) = & K\{(1-S)[\chi''_{\alpha}(\omega_{\text{H}}) + 2\chi''_{\alpha}(2\omega_{\text{H}})] + S[\chi''_{\text{ex}}(\omega_{\text{H}}) \\ & + 2\chi''_{\text{ex}}(2\omega_{\text{H}})]\} \end{aligned} \quad (9)$$

introducing a factor S describing the relative contributions of these two processes and a coupling constant K . The first term on the right-hand side of eq 9 corresponds to the rotational motion (α -process), while the second term was supposed to describe the low-frequency excess intensity, the origin of which was then not specified; now we attribute it to the intermolecular relaxation. Comparing eqs 8 and 9, one can set up a relationship between the previous and current quantities:

$$K(1-S) = \frac{2}{5} I_{\text{H}}(I_{\text{H}} + 1)(C_{\text{intra}}^{\text{HH}})^2 \quad (10a)$$

$$KS = \frac{2}{5} I_{\text{H}}(I_{\text{H}} + 1) N_{\text{H}} \frac{4\pi}{3} \frac{1}{d^3} \left(\frac{\mu_0}{4\pi} \gamma_{\text{H}}^2 \hbar \right)^2 \quad (10b)$$

In the low frequency limit, assuming that the extreme narrowing condition ($\omega\tau \ll 1$) has been reached, the ratio between the intramolecular and intermolecular contributions to the overall relaxation rate can be estimated on the basis of eqs 2 and 7 as

$$\begin{aligned} \frac{R_{1,\text{inter}}^{\text{HH}}}{R_{1,\text{inter}}^{\text{HD}}} = & \frac{3}{4\pi} S \frac{\tau_{\text{trans}}}{\tau_{\text{R}}} \left(72 \int_0^{\infty} \frac{du}{81 + 9u^2 - 2u^4 + u^6} \right) \\ = & 0.45S \frac{\tau_{\text{trans}}}{\tau_{\text{R}}} = 0.45S \frac{d^2}{D_{12}\tau_{\text{R}}} \end{aligned} \quad (11)$$

Since τ_{trans} is at least an order of magnitude longer than τ_{R} in the low-frequency range the intermolecular contribution to the relaxation is comparable with the intramolecular part; in many

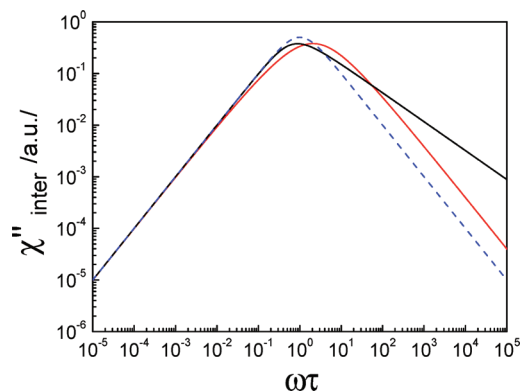


Figure 1. Normalized susceptibility function for translational diffusion, eq 6 (red line), compared with the CD function (black line), $\beta_{\text{CD}} = 0.56$, and Debye function (dashed blue).

cases (shown later) the intermolecular relaxation rate even dominates the intramolecular one.

It is important to notice that the spectral density for the translational motion (eq 6) leads to a susceptibility function of a spectral shape that is distinct from a CD function. Figure 1 shows a simulated intermolecular susceptibility, χ''_{inter} ; a CD function is shown for comparison.

The last remark of this section concerns the meaning of the S parameter. In paper 1, it has been introduced in connection to a two-step correlation function. However, the intra- and intermolecular contributions to relaxation are associated with different kinds of correlation functions; the two-step description proposed in paper 1 should be treated utterly formally.

2.4. Intramolecular and Intermolecular Proton Relaxation: Partially Deuterated Systems. The description of ^1H spin-lattice relaxation in partially deuterated liquids is more complicated than for fully protonated molecules presented above. Now, the observed relaxation rate, $R_1^{\text{H}}(\omega_{\text{H}})$, results from four relaxation pathways

$$\begin{aligned} R_1^{\text{H}}(\omega_{\text{H}}) = & R_{1,\text{intra}}^{\text{H}}(\omega_{\text{H}}) + R_{1,\text{inter}}^{\text{H}}(\omega_{\text{H}}) \\ = & R_{1,\text{intra}}^{\text{HH}}(\omega_{\text{H}}) + R_{1,\text{intra}}^{\text{HD}}(\omega_{\text{H}}) + R_{1,\text{inter}}^{\text{HH}}(\omega_{\text{H}}) + R_{1,\text{inter}}^{\text{HD}}(\omega_{\text{H}}) \end{aligned} \quad (12)$$

The first two terms, $R_{1,\text{intra}}^{\text{HH}}$ and $R_{1,\text{intra}}^{\text{HD}}$ describe the ^1H – ^1H and ^1H – ^2H contributions to the intramolecular relaxation, respectively, while the next two terms, $R_{1,\text{inter}}^{\text{HH}}$ and $R_{1,\text{inter}}^{\text{HD}}$ correspond to the intermolecular relaxation and, in analogy, describe its proton–proton and proton–deuteron parts, respectively. $R_{1,\text{intra}}^{\text{HH}}$ and $R_{1,\text{inter}}^{\text{HH}}$ are given by eqs 2 and 7, respectively. The ^1H – ^2H contribution to the intramolecular relaxation is given as^{14,15}

$$\begin{aligned} R_{1,\text{intra}}^{\text{HD}}(\omega_{\text{H}}) = & \frac{2}{15} I_{\text{D}}(I_{\text{D}} + 1)(C_{\text{intra}}^{\text{HD}})[J_{\text{intra}}(\omega_{\text{H}} - \omega_{\text{D}}) \\ & + 3J_{\text{intra}}(\omega_{\text{H}}) + 6J_{\text{intra}}(\omega_{\text{H}} + \omega_{\text{D}})] \end{aligned} \quad (13)$$

where $(C_{\text{intra}}^{\text{HD}})^2 \leq (C_{\text{intra,rigid}}^{\text{HD}})^2 = \sum_j (\mu_0/4\pi)(\gamma_{\text{H}}\gamma_{\text{D}}\hbar)/(r_j^3)^2$, γ_{D} and ω_{D} are the ^2H gyromagnetic ratio and the Larmor frequency, respectively, and $I_{\text{D}} = 1$. The sum again goes over all neighboring deuterons in the molecule. Since the same motion is responsible for the fluctuations of the ^1H – ^1H as well as of ^1H – ^2H intramolecular dipolar interactions, the spectral densities of eq 13 can also be described by the CD function (eq 3).

The $^1\text{H}-^2\text{H}$ contribution to the intermolecular relaxation is given as

$$R_{1,\text{inter}}^{\text{HD}}(\omega_{\text{H}}) = \frac{2}{15} I_{\text{D}}(I_{\text{D}} + 1) \frac{4\pi}{3} N_{\text{D}} \frac{1}{d^3} \left(\frac{\mu_0}{4\pi} \gamma_{\text{H}} \gamma_{\text{D}} \hbar \right)^2 \times [J_{\text{inter}}(\omega_{\text{H}} - \omega_{\text{D}}) + 3J_{\text{inter}}(\omega_{\text{H}}) + 6J_{\text{inter}}(\omega_{\text{H}} + \omega_{\text{D}})] \quad (14)$$

where N_{D} is now the concentration of deuterons per unit volume. The intermolecular spectral density, $J_{\text{inter}}(\omega)$, for the force-free-hard-sphere model of the translational motion is defined by eq 6.

Let us now consider a partially deuterated liquid (for example, glycerol- h_5 with OD groups instead of OH ones or glycerol- h_3 with deuterons instead of the nonhydroxyl protons) and denote by N the entire number of spins per unit volume (not distinguishing between ^1H and ^2H). In such a case the intra- and intermolecular contributions should be appropriately modified, yielding

$$R_1^{\text{H}}(\omega_{\text{H}}) = R_{1,\text{intra}}^{\text{HH}}(\omega_{\text{H}}) + R_{1,\text{intra}}^{\text{HD}}(\omega_{\text{H}}) + R_{1,\text{inter}}^{\text{HH}}(\omega_{\text{H}}) + R_{1,\text{inter}}^{\text{HD}}(\omega_{\text{H}}) = \frac{2}{5} I_{\text{H}}(I_{\text{H}} + 1) (C_{\text{intra}}^{\text{HH,red}})^2 [J_{\text{intra}}(\omega_{\text{H}}) + 4J_{\text{intra}}(2\omega_{\text{H}})] + \frac{2}{15} I_{\text{D}}(I_{\text{D}} + 1) (C_{\text{intra}}^{\text{HD}})^2 [J_{\text{intra}}(\omega_{\text{H}} - \omega_{\text{D}}) + 3J_{\text{intra}}(\omega_{\text{H}}) + 6J_{\text{intra}}(\omega_{\text{H}} + \omega_{\text{D}})] + \frac{2}{5} I_{\text{H}}(I_{\text{H}} + 1) nN \frac{4\pi}{3} \frac{1}{d^3} (C_{\text{inter}}^{\text{HH}})^2 [J_{\text{inter}}(\omega_{\text{H}}) + 4J_{\text{inter}}(2\omega_{\text{H}})] + \frac{2}{15} I_{\text{D}}(I_{\text{D}} + 1) (1 - n)N \frac{4\pi}{3} \frac{1}{d^3} \left(\frac{\gamma_{\text{H}}}{\gamma_{\text{D}}} C_{\text{inter}}^{\text{HH}} \right)^2 \times [J_{\text{inter}}(\omega_{\text{H}} - \omega_{\text{D}}) + 3J_{\text{inter}}(\omega_{\text{H}}) + 6J_{\text{inter}}(\omega_{\text{H}} + \omega_{\text{D}})] \quad (15)$$

The factor n denotes the fraction of protons in the molecule, and for example, it is equal $n = 5/8$ for glycerol- h_5 , and $n = 3/8$ for glycerol- h_3 ; $1 - n$ denotes then the fraction of deuterons. Then the intramolecular proton–proton contribution is weighted by nN , while $C_{\text{inter}}^{\text{HH}} = (\mu_0/4\pi)\gamma_{\text{H}}^2\hbar$. In eq 15 we do not distinguish between $^1\text{H}-^1\text{H}$ and $^1\text{H}-^2\text{H}$ distances of closest approach. In the first term of this equation the reduced dipole–dipole coupling, $C_{\text{intra}}^{\text{HH,red}}$, has been used, accounting for the partial deuteration of the molecule (which obviously reduces the effective proton–proton dipole–dipole coupling). To reduce as much as possible the number of parameters involved in this description, the intramolecular $^1\text{H}-^2\text{H}$ dipole–dipole coupling can be approximated as

$$(C_{\text{intra}}^{\text{HD}})^2 \cong \left(\frac{\gamma_{\text{D}}}{\gamma_{\text{H}}} \right)^2 ((C_{\text{intra}}^{\text{HH}})^2 - (C_{\text{intra}}^{\text{HH,red}})^2) \quad (16)$$

3. INTERPRETATION OF THE ^1H RELAXATION DISPERSION FOR GLYCEROL

In this section we present an interpretation of ^1H relaxation data for glycerol- h_8 , glycerol- h_3 , and glycerol- h_5 in terms of the model described in section 2. We begin with glycerol- h_8 ; the experimental data for this case have been presented in paper 1.

Table 1

temp (K)	τ_{R} (s)	β	d (Å)	D (m ² /s)	$d^2/(2D\beta\tau_{\text{R}})$
Glycerol- h_8					
263	3.2×10^{-8}	0.68	3.59	5.14×10^{-14}	58
268	2.2×10^{-8}	0.61	3.59	7.71×10^{-14}	62
270	1.5×10^{-8}	0.67	3.57	1.03×10^{-13}	62
273	1.1×10^{-8}	0.67	3.56	1.42×10^{-13}	61
278	7.3×10^{-9}	0.65	3.52	2.33×10^{-13}	56
283	4.9×10^{-9}	0.66	3.47	3.63×10^{-13}	51
288	2.5×10^{-9}	0.69	3.30	6.25×10^{-13}	50
296	1.3×10^{-9}	0.69	3.20	1.34×10^{-12}	43
301	8.4×10^{-10}	0.68	3.17	2.04×10^{-12}	43
306	6.4×10^{-10}	0.61	3.07	2.93×10^{-12}	40
Glycerol- h_5					
273	1.5×10^{-8}	0.69	3.57	1.17×10^{-13}	54
278	1.0×10^{-8}	0.69	3.52	1.71×10^{-13}	52
283	7.0×10^{-9}	0.63	3.37	3.06×10^{-13}	41
293	2.8×10^{-9}	0.66	3.33	7.65×10^{-13}	40
298	1.6×10^{-9}	0.65	3.33	1.49×10^{-12}	37
303	1.2×10^{-9}	0.67	3.32	1.94×10^{-12}	36
308	8.7×10^{-10}	0.65	3.32	2.95×10^{-12}	33
318	4.3×10^{-10}	0.66	3.33	6.02×10^{-12}	33
Glycerol- h_3					
268	3.4×10^{-8}	0.65	3.97	5.35×10^{-14}	67
270	2.5×10^{-8}	0.61	3.95	7.44×10^{-14}	69
273	1.8×10^{-8}	0.61	3.95	1.02×10^{-13}	71
278	9.7×10^{-9}	0.67	3.95	1.80×10^{-13}	67
288	3.3×10^{-9}	0.66	3.87	5.05×10^{-13}	68
298	1.6×10^{-9}	0.61	3.74	1.42×10^{-12}	50

Assuming that the observed relaxation is a sum of intramolecular and intermolecular contributions we have attempted to reproduce the relaxation dispersion data in terms of eq 2 for the rotational motion and of eq 7 for the translational motion. The adjustable parameters are $C_{\text{intra}}^{\text{HH}}$, τ_{R} , β , and d , D . The intramolecular dipole–dipole coupling constant, $C_{\text{intra}}^{\text{HH}}$, is assumed constant for all temperatures. The density of protons, $N_{\text{H}} = 6.6 \times 10^{-2} \text{ \AA}^{-3}$, is evaluated from the molecular mass and the density of glycerol (the volume of one glycerol molecule is 121 \AA^3).²⁰ The obtained parameters are collected in Table 1. The intramolecular dipole–dipole constant is found to be $2/5 I_{\text{H}}(I_{\text{H}} + 1) (C_{\text{intra}}^{\text{HH}})^2 = 5.84 \times 10^9 \text{ Hz}^2$ while the effective coupling constant resulted from the phenomenological analysis performed in paper 1 (cf. also eq 9) is equal to $K(1 - S) = 5.89 \times 10^9 \text{ Hz}^2$, which is in very good agreement (eq 10a). The relaxation data and the corresponding fits are presented in Figure 2. In comparison with the analysis presented in paper 1 (a sum of two CD contributions) the fits are now almost perfect.

To explicitly show the intermolecular contribution to the overall relaxation, in Figure 3 we show a decomposition of the relaxation dispersion data into the intermolecular and intramolecular at $T = 278 \text{ K}$ (this figure also contains data for glycerol- h_5 and glycerol- h_3 discussed later). The ratio between the intermolecular and intramolecular relaxation rates reaches in the low-frequency limit the value of $R_{1,\text{inter}}^{\text{HH}}/R_{1,\text{intra}}^{\text{HH}} \cong 3$.

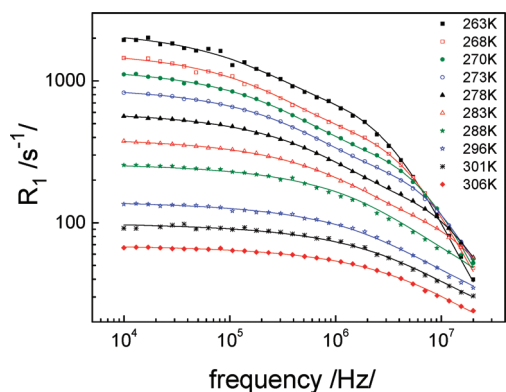


Figure 2. ^1H spin–lattice relaxation dispersion data for glycerol- h_8 and corresponding theoretical curves obtained as least-squares fits of the superposition of intramolecular and intermolecular contributions (eqs 2 and 7).

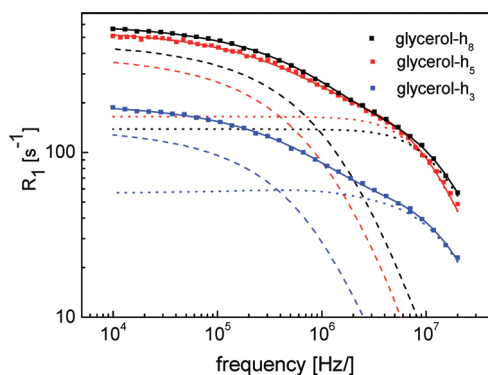


Figure 3. Decomposition of relaxation dispersion data for differently protonated glycerol at 278 K into intramolecular (dotted lines) and intermolecular (dashed lines) parts. Solid line: model fit.

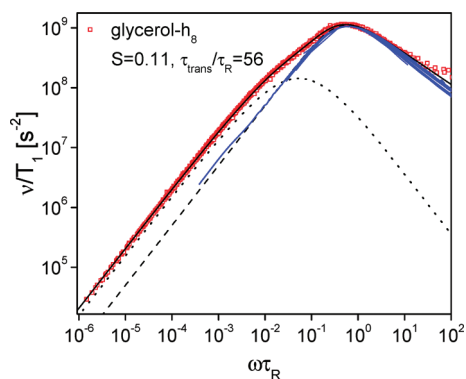


Figure 4. Susceptibility master curve for glycerol- h_8 , obtained by applying frequency–temperature superposition (cf. paper 1). The curve has been reproduced (solid line) using the model of eq 6 for the intermolecular relaxation and a CD function for the intramolecular contribution. Dashed and dotted lines show the intramolecular and intermolecular parts, respectively. For comparison the master curve from dielectric spectroscopy is included (blue), not showing the low-frequency excess intensity.

To establish a line of analogy between the current analysis of the relaxation dispersion data for individual temperatures and the phenomenological interpretation of master curves (obtained by

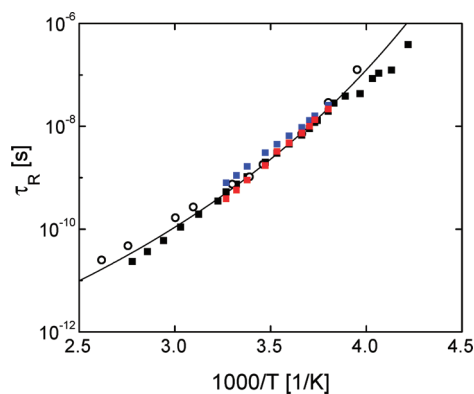


Figure 5. Comparison of rotational correlation times τ_R obtained from the present analysis (red squares) with correlation times obtained from the phenomenological approach in paper 1 (blue squares), from the NMR master curves (black squares), and from dielectric spectroscopy results¹⁸ (open circles). The interpolating line represents a fit with Vogel–Fulcher–Tammann equation.

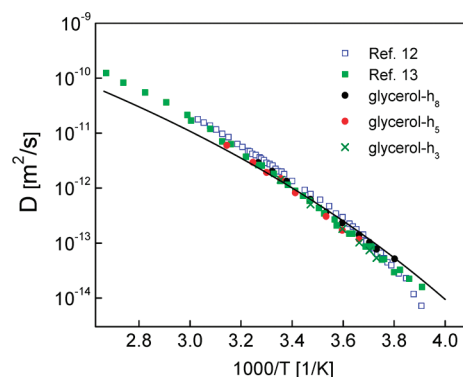


Figure 6. Comparison of translational diffusion coefficients obtained from the current analysis of differently protonated glycerol, and from NMR gradient methods taken from refs 12 and 13. Solid line: estimation of $D(T)$ from the VFT fit of $\tau_R(T)$ (in Figure 5) assuming translational–rotational coupling.

applying frequency–temperature superposition) shown in paper 1, we have attempted to describe the master curve for glycerol- h_8 in terms of eq 8 with $\chi''_{\text{inter}} = \omega J_{\text{inter}}(\omega)$, where $R_{\text{inter}}^{\text{HH}}(\omega)$ is given by eq 6 (the intramolecular part is described by a CD function). The result is shown in Figure 4. The average ratio $\tau_{\text{trans}}/\tau_R \cong 56$ matches well the average of the values for the individual temperatures (Table 1).

Coming back to the analysis of the individual relaxation dispersion data, we compare the obtained rotational correlation times, τ_R , with the values presented in paper 1, which stem from DS and from the construction of the NMR master curve (cf. Figure 4). The comparison is shown in Figure 5. The obtained rotational correlation times are now somewhat shorter than these reported in paper 1 and better follow the Vogel–Fulcher–Tammann (VFT) relation.²¹ The obtained translational diffusion coefficient D are compared with the corresponding values measured using the NMR static field gradient technique^{12,13} (Figure 6). The D values agree very well among the different methods. Assuming that translational–rotational coupling holds, one is able to estimate the translational diffusion coefficients for higher temperatures (than it has been measured) on the basis of the lower temperature results. For this purpose we have used the

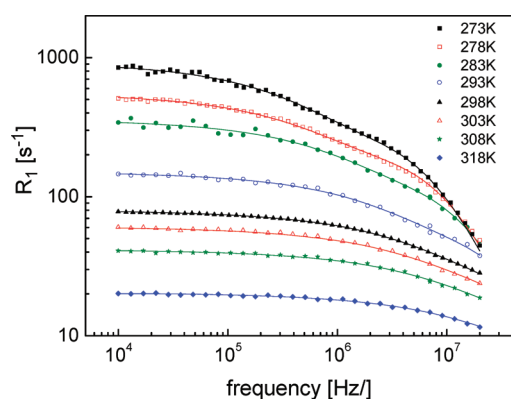


Figure 7. ^1H spin–lattice relaxation dispersion data for glycerol- h_5 and corresponding theoretical curves obtained as least-squares fits of the superposition of intramolecular and intermolecular contributions (eq 15).

rotational correlation times τ_R from the VFT fit (solid line in Figure 5), the distance of closest approach, $d = 3.07 \text{ \AA}$ (Table 1) and the ratio, $d^2/2D\tau_R = r = 40$ both for 306 K. The calculated D values are included in Figure 6 as solid line. For higher temperatures they somewhat deviate from the literature field gradient results, in fact as expected because of the tendency of the d and r values to decrease with temperature. Nevertheless, the deviations do not exceed a factor 2.

Next we turned our attention to the case of glycerol- h_5 . In the analysis, two dipole–dipole couplings are used, $(C_{\text{intra}}^{\text{HH}})^2$ and $(C_{\text{intra}}^{\text{HH,red}})^2$ (eq 15). The second coupling constant, $(C_{\text{intra}}^{\text{HH,red}})^2$, is chosen as an adjustable parameter ($(C_{\text{intra}}^{\text{HH,red}})^2$ denotes here the contribution to the overall coupling constant, $(C_{\text{intra}}^{\text{HH}})^2$, generated by the nondeuterated part of the molecule, while $(C_{\text{intra}}^{\text{HH}})^2$ is fixed to the value previously obtained for glycerol- h_8 , $(C_{\text{intra}}^{\text{HH}})^2 = 1.97 \times 10^{10} \text{ Hz}^2$. For the $(C_{\text{intra}}^{\text{HD}})^2$ value the relationship of eq 16 is employed. The same value of the coupling constant $(C_{\text{intra}}^{\text{HH,red}})^2$ is assumed for all temperatures. The other adjustable parameters are τ_R , β , d , and D . The proton fraction is set to $n = 5/8$. The results are collected in Table 1; for the coupling constant, $(C_{\text{intra}}^{\text{HH,red}})^2 = 1.55 \times 10^{10} \text{ Hz}^2$. The relaxation dispersion data and the fitted curves for glycerol- h_5 are shown in Figure 7. The translational diffusion coefficients for glycerol- h_5 are compared with the values for glycerol- h_8 in Figure 6. The results agree very well with those obtained for glycerol- h_8 .

It is interesting to compare the relaxation data and the corresponding intramolecular and intermolecular contributions to the overall relaxation for the case of glycerol- h_8 and for glycerol- h_5 ; such a comparison is shown in Figure 3. As one can see, the overall relaxation rates are not very much different. This is consistent with the obtained values of the dipole–dipole coupling constants, $(C_{\text{intra}}^{\text{HH,red}})^2 \cong 0.8(C_{\text{intra}}^{\text{HH}})^2$. This relationship can be understood when one notices that a major contribution to the effective dipole–dipole coupling stems from the protons bound to the distant carbons (the distance between the $-\text{CH}_2$ protons is short compared to other interproton distances). The relatively larger intramolecular contribution in the case of glycerol- h_5 originates from the somewhat longer rotational correlation time compared to fully protonated glycerol- h_8 .

Finally, we take into consideration the complementary case of glycerol- h_3 . Again we have performed five-parameter fits with adjustable τ_R , β , d , and D and the coupling constant $(C_{\text{intra}}^{\text{HH,red}})^2$

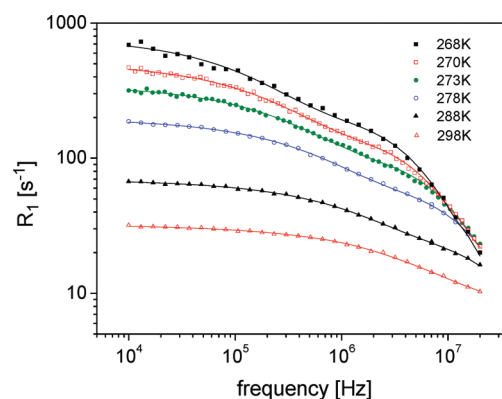


Figure 8. ^1H spin–lattice relaxation dispersion data for glycerol- h_3 and corresponding theoretical curves obtained as least-squares fits of the superposition of intramolecular and intermolecular contributions (eq 15).

assumed to be temperature independent (in this case $(C_{\text{intra}}^{\text{HH,red}})^2$ is associated with the part of the molecule containing the OH groups). The dipole–dipole coupling corresponding to fully protonated glycerol molecule has again been set to $(C_{\text{intra}}^{\text{HH}})^2 = 1.97 \times 10^{10} \text{ Hz}^2$, while for the $(C_{\text{intra}}^{\text{HD}})^2$ value eq 16 has again been used; $n = 3/8$. The obtained results are collected in Table 1, while the relaxation dispersion data and the fitted curves for glycerol- h_3 are shown in Figure 8.

For the dipole–dipole coupling constant corresponding to the protonated part of the molecule it has been obtained $(C_{\text{intra}}^{\text{HH,red}})^2 = 0.58 \times 10^{10} \text{ Hz}^2$. The sum of the independently obtained dipole–dipole coupling constant for the protonated parts of glycerol- h_5 and glycerol- h_3 gives $2.13 \times 10^{10} \text{ Hz}^2$, which is in acceptable agreement with $(C_{\text{intra}}^{\text{HH}})^2 = 1.97 \times 10^{10} \text{ Hz}^2$. In analogy to glycerol- h_8 and glycerol- h_5 the decomposition of the relaxation data for glycerol- h_3 (278 K) into the intramolecular and intermolecular contributions is presented in Figure 3. The obtained translational diffusion coefficients for glycerol- h_3 are also shown in Figure 6 for comparison. The values are consistent with the previous results for glycerol- h_8 and glycerol- h_5 .

4. DISCUSSION

Applying the force-free-hard-sphere diffusion model for the intermolecular relaxation contribution and a CD function for the intramolecular part, we can quantitatively reproduce the relaxation spectra of differently deuterated glycerol. As one can see from Figures 2, 7, and 8 (glycerol- h_8 , h_5 , and h_3 , respectively), the theoretical curves agree very well with the experimental results. The quality of the fits is better than when attempting to reproduce the relaxation dispersion data in terms of two CD functions, as previously done in paper 1. The very good agreement with the experimental data proves that the spectral density of eq 6 captures the essential features of the translational motion, despite the simplifying assumptions leading to this model. This description yields $D(T)$ values that agree well with those measured by gradient NMR (Figure 6). The results obtained for nondeuterated and partially deuterated molecules are consistent; for the latter case the rotational and translational correlation times are somewhat longer compared to the protonated molecules, as expected from the molecular mass. The effective distance of closest approach, d , is, in all cases, on the order of the molecular radius (3.07 \AA).²⁰ The d value changes

somewhat with temperature, it becomes shorter for higher temperatures (Table 1).

The force-free-hard-sphere model of translational diffusion applied here is entirely based on the concept of a single correlation time. As has been explained in section 2.1, the assumption that the spin is placed in the molecular center means that one neglects effects of molecular tumbling on the changes of the intermolecular vector in terms of its length and its orientation. We suppose that the slight temperature dependence of the distance of closest approach is a consequence of the simplified character of the applied model, i.e., of neglecting the noncentricity effects. Due to a considerable influence of rotational motion on the intermolecular correlation function, it becomes more “rotational-like” and, as a consequence, the intra- and intermolecular contributions to relaxation are spectrally less separated. We believe that this explains why one does not observe a distinct low-frequency excess intensity for some liquids, for instance, for *o*-terphenyl.

The ratio $\tau_{\text{trans}}/\tau_{\text{R}}$ decreases somewhat with temperature as one can see from Table 1, being anyway much larger than the factor 9. This value stems from the Stokes–Einstein–Debye equation assuming the force-free-hard-sphere model (section 2), while glycerol molecules can hardly be considered as hard spheres with spins in their center and therefore one should not treat the factor 9 as “a reference”. As one can see from the table, the $\tau_{\text{trans}}/\tau_{\text{R}} = r$ ratio is somewhat larger for glycerol- h_3 compared to glycerol- h_8 and glycerol- h_5). Still, the analysis indicates that translational-rotational coupling holds in a fair approximation in the investigated temperature range, which is actually well above the glass transition temperature T_{g} of the liquid. Only close to T_{g} translational–rotational coupling is expected to break down.⁵

5. CONCLUSIONS

It has been demonstrated that ¹H NMR relaxation dispersion for nondeuterated and partially deuterated glycerol can be consistently interpreted as a superposition of intramolecular and intermolecular contributions. The intramolecular part has been described in terms of CD spectral densities, while for the intermolecular dipole–dipole correlation function the force-free-hard-sphere model of translational diffusion has been applied. The spectral shape of the intermolecular spectral density resulting from this model leads to very good agreement with the experimental data. The extracted translational diffusion coefficients have been compared with the results of gradient NMR, again being in an excellent agreement with them. The analysis shows that NMR relaxometry can serve as a credible way to determine the diffusion coefficient and the rotational correlation times by means of a single experiment. Thus, NMR relaxometry has the potential to become an alternative method measuring the diffusion coefficient in viscous liquids.

AUTHOR INFORMATION

Permanent Addresses

[†]Institute of Physics, Jagiellonian University, Reymonta 4, 30-059 Krakow, Poland.

REFERENCES

- (1) Kimmich, R.; Anardo, E. *Prog. NMR Spectrosc.* **2004**, *44*, 257.
- (2) Herrmann, A.; Abou Elfadl, A.; Meier, R.; Novikov, V. N.; Rössler, E. A. *Macromolecules* **2009**, *42*, 5236.

- (3) Meier, R.; Kahlau, R.; Kruk, D.; Rössler, E. A. *J. Phys. Chem. A* **2010**, *114*, 7847.
- (4) Abragam, A. *The Principles of Nuclear Magnetism*; Oxford University Press: Oxford, U.K., 1961; p 302.
- (5) Fujara, F.; Geil, B.; Sillescu, H.; Fleischer, G. *Z. Phys. B-Condens. Matter* **1992**, *88*, 195.
- (6) Zeidler, M. D. *Ber. Bunsen-Ges. Phys. Chem.* **1965**, *69*, 659.
- (7) Kintzinger, J. P.; Zeidler, M. D. *Ber. Bunsen-Ges. Phys. Chem.* **1972**, *77*, 98.
- (8) Lindner, P.; Rössler, E.; Sillescu, H. *Makromol. Chem.* **1981**, *182*, 3653.
- (9) Kehr, M.; Fatkullin, N.; Kimmich, R. *J. Chem. Phys.* **2007**, *126*, 094903.
- (10) Hwang, L. P.; Freed, J. H. *J. Chem. Phys.* **1975**, *63*, 4017.
- (11) Ayant, Y.; Belorizky, E.; Alizon, J.; Gallice, J. *J. Phys. (Paris)* **1975**, *36*, 991.
- (12) Chang, I.; Sillescu, H. *J. Phys. Chem.* **1997**, *101*, 8794.
- (13) Chen, B.; Sigmund, E. E.; Halperin, W. P. *Phys. Rev. Lett.* **2006**, *96*, 145502.
- (14) Slichter, C. P. *Principles of Magnetic Resonance*; Springer-Verlag: Berlin, 1990.
- (15) Kowalewski, J.; Mäler, L. *Nuclear Spin Relaxation in Liquids: Theory, Experiments, and Applications*; Taylor & Francis: New York, 2006.
- (16) Böttcher, C. J. F.; Bordewijk, P. *Theory of electric polarization*; Elsevier: Amsterdam, 1973; Vol. 2.
- (17) Kruk, D. *Theory of Evolution and Relaxation of Multi-Spin Systems*; Arima: Bury St. Edmunds, U.K., 2007.
- (18) Kowalewski, J.; Kruk, D.; Parigi, G. *Adv. Inorg. Chem.* **2005**, *57*, 41.
- (19) Ayant, Y.; Belorizky, E.; Fries, P.; Rosset, J. *J. Phys. (Paris)* **1977**, *38*, 325.
- (20) Lide, D. R., Ed. *CRC Handbook of Data on Organic Compounds*, 3rd ed.; CRC Press: Boca Raton, FL, 1994.
- (21) Blochowicz, T.; Gainaru, C.; Medick, P.; Tschirwitz, C.; Rössler, E. A. *J. Chem. Phys.* **2006**, *124*, 134503.

Publication 2

Intermolecular Relaxation in Glycerol as Revealed by Field Cycling ^1H
NMR Relaxometry Dilution Experiments.

Meier, R.; Kruk, D; Gmeiner, J; Rössler, E.A.

J. Chem. Phys. **2012**, *136*, 034508.

Copyright 2012 by The American Institute of Physics

DOI: 10.1063/1.3672096

Intermolecular relaxation in glycerol as revealed by field cycling ^1H NMR relaxometry dilution experiments

R. Meier,¹ D. Kruk,^{1,2} J. Gmeiner,¹ and E. A. Rössler^{1,a)}

¹*Experimentalphysik II, Universität Bayreuth, 95440 Bayreuth, Germany*

²*Faculty of Mathematics and Computer Science, University of Warmia and Mazury in Olsztyn, Sloneczna 54, PL-10710 Olsztyn, Poland*

(Received 7 October 2011; accepted 5 December 2011; published online 19 January 2012)

^1H spin-lattice relaxation rates $R_1 = 1/T_1$ have been measured for partly deuterated glycerol- h_5 diluted in fully deuterated glycerol- h_0 for progressively lower concentrations of glycerol- h_5 . By means of the field cycling (FC) technique relaxation dispersion data, $R_1(\omega)$, have been collected for several temperatures in the frequency range of 10 kHz–20 MHz. In order to disclose the spectral shape of the intra- and intermolecular relaxation, extrapolation of the relaxation data to the zero concentration limit has been performed. The paper confirms that the low frequency excess contribution to the total relaxation rate $R_1(\omega)$ previously reported for several liquids is of intermolecular origin and reflects translational motion, whereas the high-frequency part is attributed to molecular rotation. Thus, intra- and intermolecular relaxation contributions are spectrally separated. The intermolecular relaxation itself contains also a contribution from rotational motion, which is due to non-central positions of the interacting nuclei in the molecule. This eccentricity effect is quantitatively reproduced by treating the intermolecular spectral density as a sum of translational-like (described by the free diffusion model) and rotational-like contributions (described by a Cole-Davidson function). Applying frequency-temperature superposition master curves as well as individual relaxation dispersion data, $R_1(\omega)$, are analyzed. It is demonstrated that, in spite of the rotational influence, the translational diffusion coefficients, $D(T)$, can be extracted from the ^1H relaxation dispersion which gives ^1H NMR relaxometry the potential to become a routine technique determining the diffusion coefficient in liquids. © 2012 American Institute of Physics. [doi:10.1063/1.3672096]

I. INTRODUCTION

In recent years, field cycling (FC) nuclear magnetic resonance (NMR) relaxometry has become a powerful tool for investigating dynamics in condensed matter.^{1,2} Due to availability of commercial FC spectrometers this technique gained new momentum. Field cycling ^1H NMR allows routine measurements of spin-lattice relaxation time dispersion $T_1 = T_1(\omega)$ in a frequency range of 10 kHz–20 MHz.

In our two recent publications we have compared the results of ^1H NMR relaxometry and dielectric spectroscopy (DS) for several viscous liquids.^{3,4} It is well known that DS spectra for such systems can be described in terms of a Cole-Davidson spectral density providing correlation times of the reorientational dynamics involved in the structural relaxation (α -process) which is determined by the glass transition phenomenon.^{5,6} ^1H NMR susceptibility spectra, i.e., relaxation dispersion data transformed to the susceptibility representation, show, in addition to the α -relaxation peak, a low-frequency excess contribution (a kind of a shoulder) the amplitude of which varies for different liquids. We have attributed this low-frequency process to intermolecular relaxation mediated by translational motion of the molecules, while the main relaxation peak originates from intramolecular relaxation associated with reorientational dynamics.⁴ As

^1H NMR relaxation probes fluctuations of dipole-dipole interactions between pairs of protons, one has to distinguish between proton sites within the same molecule (intramolecular) and in different molecules (intermolecular). Thus, the overall relaxation rate $R_1 = 1/T_1$ is a sum of intramolecular and intermolecular relaxation rates, $R_{1,\text{intra}}$ and $R_{1,\text{inter}}$, respectively. It is expected that the intermolecular relaxation is dominated by the relative translational motion of the spins located on different molecules.

Assuming a Cole-Davidson susceptibility for the intramolecular part reflecting reorientational dynamics, while the intermolecular part of the overall ^1H relaxation rate $R_1(\omega)$ has been described by the force-free-hard-sphere model,^{7,8} i.e., Fickian diffusion with appropriate boundary conditions, we have been able to describe quantitatively the T_1 dispersion data for differently deuterated glycerol over a large temperature range.⁴ Thereby, we have extracted values of the diffusion coefficient, $D(T)$. The values obtained are in good agreement with those from pulse field gradient NMR.^{9,10} This shows that FC ^1H NMR has the potential to become an alternative method of measuring diffusion coefficients in liquids. Here, we note that a similar analysis has already been attempted by Kintzinger and Zeidler.¹¹ The authors pointed out that describing the intermolecular relaxation of glycerol in terms of Torrey's jump model of translation diffusion¹² one gets values of the diffusion coefficients which are larger than those independently measured. The essential

^{a)} Author to whom correspondence should be addressed. Electronic mail: ernst.roessler@uni-bayreuth.de.

difference between Torrey and Hwang/Freed models is the specification of the boundary conditions that influences the form of the resulting correlation function.

The above outlined interpretation of FC ^1H NMR dispersion data of simple liquids relies on the fact that the intra- and intermolecular relaxation contributions exhibit distinct dispersion features, i.e., they are spectrally shifted.^{15–17} For the hydrodynamic model of a (molecular) sphere rotating and translating in a viscous medium Abragam¹³ derived the relationship $\tau_{\text{trans}}/\tau_{\text{rot}} = 9$, where τ_{trans} is the correlation time of translational diffusion and $\tau_{\text{rot}} = \tau_{\alpha}$ is the rotational correlation time that can be identified with the time constant of the α -process. Experimentally, we have observed $\tau_{\text{trans}}/\tau_{\text{rot}} = 30\text{--}60$.⁴ This ratio is essentially temperature independent as expected for translational-rotational coupling to hold for moderately viscous liquids.¹³

Yet, the ultimate proof of our approach can only be given if one is able to separate the intra- and intermolecular relaxation in a model free way. This is usually done by performing so-called isotope dilution experiments.^{17–19} Substituting protonated molecules by their deuterated counterpart allows suppressing the intermolecular dipole-dipole interactions. Then by extrapolating the results to the infinite dilution limit one can isolate the intramolecular relaxation for a given frequency and temperature, thereby obtaining the intermolecular part. Up to our knowledge, such experiments have been rarely performed by FC ^1H NMR.^{11,20} In the present contribution we use isotope dilution to separate intra- and intermolecular relaxation in the glass former glycerol. As it will be demonstrated, because the interacting protons belonging to different molecules are not placed in the molecular center the intermolecular relaxation is also affected by molecular rotation. This is referred to as the eccentricity effect.²¹ Thus, the intermolecular relaxation is influenced by both translational and rotational motion. In the simple diffusion model mentioned above the eccentricity effect is not taken into account. In other words, it is assumed that the protons are in the center of a (spherical) molecule treated as a hard sphere. The eccentricity has been discussed in the literature,^{22,23} however, no systematic studies have been performed, so far. In this work we explicitly show the combined effects of the translational and rotational motions on the intermolecular relaxation. The translational diffusion coefficient can be extracted from the relaxation dispersion results in spite of the rotational influence.

II. RELAXATION THEORY FOR ISOTOPICALLY DILUTED SYSTEMS

A description of ^1H spin-lattice relaxation for non-deuterated and partially deuterated liquids has been given in Ref. 4. Here we shall extend it to the case when a partially deuterated (or non-deuterated) liquid is diluted in its fully deuterated counterpart, for instance, glycerol- h_8 /glycerol- h_0 , or glycerol- h_5 /glycerol- h_0 (h_8 denotes non-deuterated glycerol, h_5 with deuterated hydroxyl groups and h_0 – fully deuterated). As already explained, the observed relaxation rate, $R_1^H(\omega_H)$ (ω_H denotes the proton Larmor frequency) is a sum of intramolecular, $R_{1,\text{intra}}^H(\omega_H)$, and intermolecular,

$R_{1,\text{inter}}^H(\omega_H)$, contributions, i.e.,

$$R_1^H(\omega_H) = R_{1,\text{intra}}^H(\omega_H) + R_{1,\text{inter}}^H(\omega_H). \quad (1)$$

For partially deuterated molecules the intramolecular as well as intermolecular relaxation results from ^1H - ^1H (HH) and ^1H - ^2H (HD) dipole-dipole interactions; that means

$$R_{1,\text{intra}}^H(\omega_H) = R_{1,\text{intra}}^{HH}(\omega_H) + R_{1,\text{intra}}^{HD}(\omega_H), \quad (2a)$$

$$R_{1,\text{inter}}^H(\omega_H) = R_{1,\text{inter}}^{HH}(\omega_H) + R_{1,\text{inter}}^{HD}(\omega_H). \quad (2b)$$

The ^1H - ^1H relaxation contributions are expressed as the well-known combination of spectral densities for a system of two equivalent spins with corresponding proportionality constants

$$R_{1,\text{intra}}^{HH}(\omega_H) = \frac{2}{5} I_H (I_H + 1) (C_{\text{intra}}^{HH})^2 \times [J_{\text{intra}}(\omega_H) + 4J_{\text{intra}}(2\omega_H)], \quad (3a)$$

$$R_{1,\text{inter}}^{HH}(\omega_H) = \frac{2}{5} I_H (I_H + 1) N_H \frac{4\pi}{3} \frac{1}{d^3} \left(\frac{\mu_0}{4\pi} \gamma_H^2 \hbar \right)^2 \times [J_{\text{inter}}(\omega_H) + 4J_{\text{inter}}(2\omega_H)], \quad (3b)$$

where C_{intra}^{HH} denotes an effective intramolecular dipole-dipole coupling constant, $I_H = 1/2$, γ_H is the proton gyromagnetic ratio, other symbols have their obvious meaning. The parameter d (Eq. (3b)) is the distance of closest approach of the interacting nuclei (for identical molecules $d = 2a$, where a is the molecular radius), while $\frac{4\pi}{3} N_H$ is the number of protons per unit sphere. The intramolecular spectral density, $J_{\text{intra}}(\omega)$, reflects rotational dynamics of the molecules. For viscous liquids one typically assumes a Cole-Davidson form of the susceptibility function $\chi''_{\text{intra}}(\omega)$ related to $J_{\text{intra}}(\omega)$ as $\chi''_{\text{intra}}(\omega) = \omega J_{\text{intra}}(\omega)$, i.e.,²⁴

$$J_{\text{intra}}(\omega) = J_{\text{rot}}(\omega) = \frac{\sin[\beta \arctan(\omega\tau_{CD})]}{\omega[1 + (\omega\tau_{CD})^2]^{\frac{\beta}{2}}}, \quad (4)$$

where $\tau_{\text{rot}} = \tau_{CD}\beta$ is the rotational correlation time, while $0 < \beta \leq 1$ is a phenomenological stretching parameter. In Ref. 4 the intermolecular spectral density, $J_{\text{inter}}(\omega)$, reflecting the translational motion has been described according to the model proposed by Hwang and Freed⁷ and Ayant *et al.*⁸ as hard spheres with the nuclei of interest assumed to be placed in their centers. In consequence, the following form of $J_{\text{inter}}(\omega)$ has been used:^{25,26}

$$J_{\text{inter}}(\omega) = J_{\text{trans}}(\omega) = 72 \frac{3}{4\pi} \int_0^\infty \frac{u^2}{81 + 9u^2 - 2u^4 + u^6} \frac{u^2 \tau_{\text{trans}}}{u^4 + (\omega\tau_{\text{trans}})^2} du \quad (5)$$

with $\tau_{\text{trans}} = \frac{d^2}{D_{12}}$, where D_{12} is the relative translational diffusion coefficient defined as a sum of self-diffusion coefficients of the participating molecules (for identical molecules $D_{12} = 2D$). We note that $J_{\text{intra}}(\omega)$ and $J_{\text{inter}}(\omega)$ are normalized, i.e., $\int_0^\infty J_{\text{intra}}(\omega) d\omega = \pi/2$. As already explained in Sec. I the assumption that the interacting nuclei (spins) are placed in the center of the molecule implies that the fluctuations of the

intermolecular vector (in terms of its orientation and length) are entirely caused by the translational motion. However, for polyatomic molecules with nuclei placed at different positions in the molecule the fluctuations of the intermolecular dipole-dipole interactions are also mediated by rotational dynamics (besides the translational motion). The ^1H - ^2H contributions to the intra- and intermolecular relaxation are given as

$$R_{1,\text{intra}}^{HD} = \frac{2}{15} I_D (I_D + 1) (C_{\text{intra}}^{HD})^2 [J_{\text{intra}}(\omega_H - \omega_D) + 3J_{\text{intra}}(\omega_H) + 6J_{\text{intra}}(\omega_H + \omega_D)], \quad (6a)$$

$$R_{1,\text{inter}}^{HD}(\omega_H) = \frac{2}{15} I_D (I_D + 1) \frac{4\pi}{3} N_D \frac{1}{d^3} \left(\frac{\mu_0}{4\pi} \gamma_H \gamma_D \hbar \right)^2 \times [J_{\text{inter}}(\omega_H - \omega_D) + 3J_{\text{inter}}(\omega_H) + 6J_{\text{inter}}(\omega_H + \omega_D)], \quad (6b)$$

where γ_D and ω_D are the deuteron gyromagnetic factor and the deuteron Larmor frequency, respectively, and $I_D = 1$, while $\frac{4\pi}{3} N_D$ is the number of deuterons per unit sphere.

Let us now consider a partially deuterated liquid (for example, glycerol- h_5) mixed with its fully deuterated counterpart (glycerol- h_0 in this case). Combining the invoked expressions for intramolecular and intermolecular relaxation rates, one gets the following expression for the overall ^1H spin-lattice relaxation rate:

$$\begin{aligned} R_1^H(\omega_H) &= R_{1,\text{intra}}^{HH}(\omega_H) + R_{1,\text{intra}}^{HD}(\omega_H) \\ &\quad + R_{1,\text{inter}}^{HH}(\omega_H) + R_{1,\text{inter}}^{HD}(\omega_H) \\ &= \frac{2}{5} I_H (I_H + 1) (C_{\text{intra}}^{HH,\text{red}})^2 \\ &\quad \times [J_{\text{intra}}(\omega_H) + 4J_{\text{intra}}(2\omega_H)] \\ &\quad + \frac{2}{15} I_D (I_D + 1) (C_{\text{intra}}^{HD})^2 [J_{\text{intra}}(\omega_H - \omega_D) \\ &\quad + 3J_{\text{intra}}(\omega_H) + 6J_{\text{intra}}(\omega_H + \omega_D)] \\ &\quad + \frac{2}{5} I_H (I_H + 1) n x N \frac{4\pi}{3} \frac{1}{d^3} \left(\frac{\mu_0}{4\pi} \gamma_H^2 \hbar \right)^2 \\ &\quad \times [J_{\text{inter}}(\omega_H) + 4J_{\text{inter}}(2\omega_H)] \end{aligned}$$

$$\begin{aligned} &+ \frac{2}{15} I_D (I_D + 1) (1 - n x) N \frac{4\pi}{3} \frac{1}{d^3} \left(\frac{\mu_0}{4\pi} \gamma_H \gamma_D \hbar \right)^2 \\ &\quad \times [J_{\text{inter}}(\omega_H - \omega_D) + 3J_{\text{inter}}(\omega_H) \\ &\quad + 6J_{\text{inter}}(\omega_H + \omega_D)]. \quad (7) \end{aligned}$$

The factor n denotes the fraction of protons in the molecule (for instance, $n = 5/8$ for glycerol- h_5), thus $(1 - n)$ is the fraction of deuterons, while x is the mole fraction of molecules which contain ^1H (not fully deuterated molecules); $x = 1$ means that there are no fully deuterated molecules, while for $x = 0$ all molecules are fully deuterated. For $x = 1$ this expression is identical with Eq. (15) of Ref. 4; $nN = N_H$ and $(1 - n)N = N_D$. The dilution (reflected by the factor x) obviously affects only the intermolecular relaxation. The intramolecular part remains unchanged. The meaning of $C_{\text{intra}}^{HH,\text{red}}$ has already been explained in Ref. 4; it is a reduced dipole-dipole coupling constant after accounting for partial deuteration of the molecule. In the case of isotopic dilution the ^1H - ^1H contribution to the intermolecular relaxation is reduced by the fraction x , i.e., $n \rightarrow nx$, while the ^1H - ^2H contribution is weighted by the factor $(1 - nx)$. To explain this, let us consider a reference ^1H nucleus. The intermolecular ^1H - ^2H contribution stems from its interactions with ^2H nuclei of the partially deuterated molecules and of the fully deuterated molecules. The first contribution is now weighted by the factor $(1 - n)x$ and the second one by $(1 - x)$; summing them up one gets $(1 - nx)$ appearing in the fourth term of Eq. (7). Although for highly protonated systems, $x \rightarrow 1$, the $R_{1,\text{inter}}^{HD}$ contribution can be neglected compared to $R_{1,\text{inter}}^{HH}$, it becomes progressively more relevant for decreasing x (see Fig. 1).

To analyze the intermolecular contribution to the overall relaxation as a function of x let us assume that $n = 1$. This means that we consider a system containing a fraction x of fully protonated molecules and $(1 - x)$ of fully deuterated molecules. Figure 1 shows simulations in terms of Eq. (1) of ^1H spin-lattice relaxation rates versus x for a set of parameters suiting well to the case of glycerol- h_8 /glycerol- h_0 (parameters for glycerol have been obtained in Ref. 4). As τ_{trans} is significantly longer than τ_{rot} the intermolecular relaxation contribution is observed at low frequencies and progressively suppressed by isotope dilution. For $x = 0$ the intermolecular

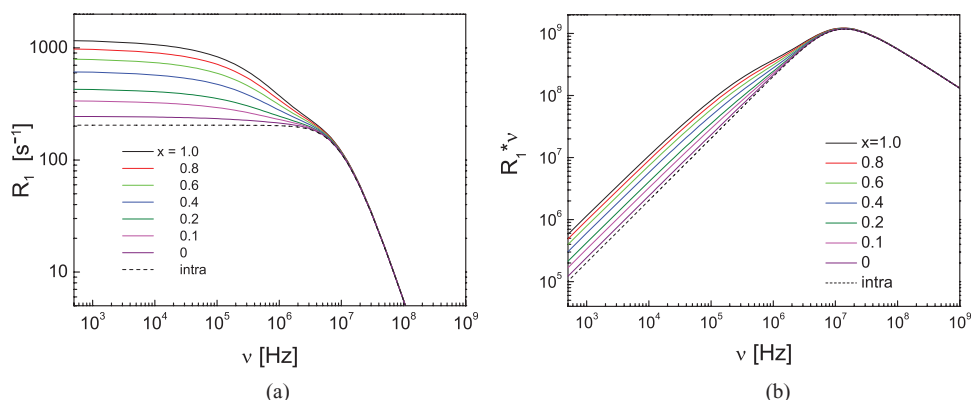


FIG. 1. Theoretical predictions for the overall relaxation dispersion (a) and for the susceptibility representation of the data (b) for glycerol- h_8 ($n = 1$) dissolved in glycerol- h_0 for different mole fractions x of glycerol- h_8 , according to Eq. (7). It has been assumed that $(C_{\text{intra}}^{HH})^2 = 1 \times 10^9 \text{ Hz}^2$, $\beta = 0.65$, $D = 1.0 \times 10^{-13} \text{ m}^2/\text{s}$, $d = 3.0 \text{ \AA}$, and $\tau_{\text{rot}} = 1.0 \times 10^{-8} \text{ s}$.

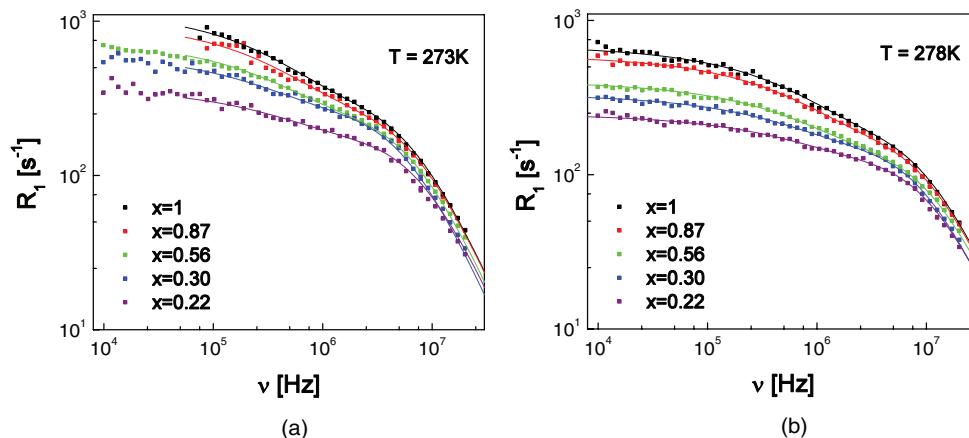


FIG. 2. Relaxation dispersion data for glycerol- h_5 /glycerol- h_0 for different mole fractions, x , of the partially protonated molecules at $T = 273$ K (a) and $T = 278$ K (b). Solid lines: fits according to Eq. (9). The parameters obtained are given in Table I.

contribution stems entirely from ^1H - ^2H dipole-dipole interactions.

The theoretical predictions are compared with the results of dilution experiments in Sec. IV. Details of the ^1H relaxation experiments for diluted systems are given in Sec. III.

III. EXPERIMENTAL

Dispersion of ^1H spin-lattice relaxation rates, $R_1 = 1/T_1$, for glycerol- h_5 diluted in glycerol- h_0 (i.e., fully deuterated glycerol) was studied in the temperature range of 248 K–348 K by employing the commercial fast (electronic) field cycling spectrometer STELAR FFC 2000,¹ which allows to cover the frequency range of 10^4 Hz– 2×10^7 Hz. Spin-lattice relaxation times down to about 1 ms are accessible for the spectrometer. The temperature was controlled by heating flowing air or evaporating liquid nitrogen. The temperature stability was ± 0.3 K. In all cases a single-exponential relaxation has been observed. The measurements were done for several mole fractions of glycerol- h_5 (CDN Isotopes) in glycerol- h_0 : $x = 1.0, 0.87, 0.56, 0.30$, and 0.22 . Glycerol- h_5 has been used to avoid exchange effects which would likely be present for glycerol- h_8 .

IV. INTERMOLECULAR CONTRIBUTION TO ^1H RELAXATION FOR GLYCEROL

An example of relaxation dispersion data for different mole fractions of glycerol- h_5 is shown in Fig. 2. The overall relaxation rate becomes progressively smaller due to a diminishing contribution of the intermolecular relaxation. While for $x = 1$ one can clearly see an intermolecular contribution to the relaxation at low frequencies (one can notice that the relaxation dispersion contains two components), for $x = 0.22$ this effects is much smaller. Solid lines represent theoretical predictions (fits) which will be discussed later.

To get a qualitative picture of the changes in the ^1H relaxation due to dilution the obtained relaxation dispersion data have been first transformed to the susceptibility representation according to the relationship: $\chi''(\omega) = \omega R_1(\omega)$. Next, the susceptibility results for individual temperatures have been

merged in order to construct a master curve for every concentration, as shown in Fig. 3.^{3,4} The concept of constructing a master curve from individual relaxation data is based on frequency-temperature superposition (FTS), which assumes that the spectral shape of the susceptibility does not significantly change with temperature; only the time constant is different; FTS is assumed to be a generic feature of the dynamics in viscous liquids.²⁷ First, a reference data set showing a maximum (in the susceptibility representation) is chosen and fitted by a Cole-Davidson function and then plotted as a function of $\omega\tau_{\text{rot}}$. The susceptibilities for other temperatures are shifted along the $\omega\tau_{\text{rot}}$ axis until an overlapping is reached.

To check the linear dependence of the overall relaxation rate, R_1 , on the mole fraction x , three values of $\omega\tau_{\text{rot}}$ have been selected; they are marked in Fig. 3 as vertical dashed lines. For these values the ratio between the relaxation rate for the concentration of x , $R_{1,x}$, and the relaxation rate for $x = 1$, $R_{1,x=1}$, has been plotted versus x (Fig. 4) confirming the expected result. Interesting to note is the fact that at low frequencies more than 80% of the total relaxation is due to intermolecular relaxation.

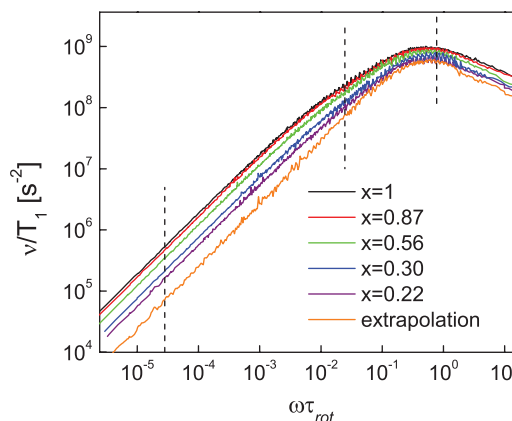


FIG. 3. NMR master curves in the susceptibility representation for glycerol- h_5 dissolved in glycerol- h_0 for different mole fractions x of glycerol- h_5 ; data sets in the temperature range 248 K–348 K have been merged; extrapolation to the zero concentration limit is included. Dashed vertical lines indicate frequencies for which x dependence is checked in Fig. 4.

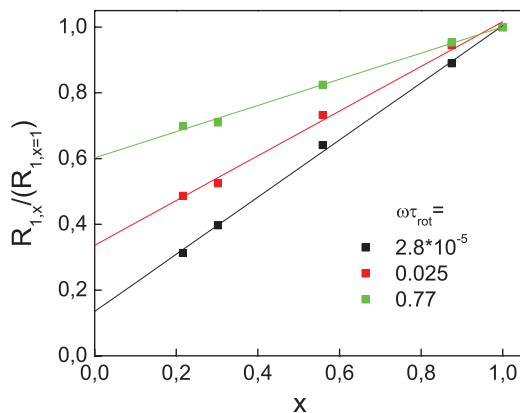


FIG. 4. $R_{1,x}/R_{1,x=1}$ versus mole fraction x for selected $\omega\tau_{rot}$ values (cf. Fig. 3).

The first observation in Fig. 3 is that the low frequency contribution to the overall relaxation (low frequency excess intensity) becomes progressively less pronounced for lower x , and, eventually disappears in the zero concentration limit. This is a direct proof of its intermolecular origin. The second observation is that even for relatively large $\omega\tau_{rot}$, where according to the simulations shown in Fig. 1, one should not expect intermolecular effects, the master curves for different concentrations of glycerol- h_5 differ. This reflects the fact that there is a rotational contribution to the modulations of the intermolecular interactions. Although the simulations have been done for glycerol- h_8 (to avoid discussing HD intra-molecular contributions present for partially deuterated molecules) they also apply to glycerol- h_5 – only the intra-molecular contribution is smaller in the last case.

To disclose the full spectral shape of the intermolecular relaxation the master curves shown in Fig. 3 have been extrapolated to the zero concentration limit ($x \rightarrow 0$). In this way the intramolecular contribution to the entire relaxation has been obtained (red open squares in Fig. 5). One should be aware at this stage that it also contains the 1H - 2H intermolecular contribution, which is, however, not significant. The intramolecular susceptibility can be well fitted by a Cole-Davidson function as is expected for the rotational dynamics in viscous liquids (cf. Fig. 5). Next, the intramolecular master curve has been subtracted from the total relaxation ($x = 1$) to reveal the intermolecular contribution (blue solid spheres in Fig. 5). One clearly sees that the contribution of the intermolecular relaxation around the maximum of the total master curve is still significant in contrary to the theoretical predictions of the hard-sphere-force-free model. In addition, this high-frequency part of the intermolecular susceptibility corresponds to the position of the intramolecular maximum. This can be interpreted as a consequence of the rotational effects on the fluctuations of the intermolecular dipole-dipole couplings.

To take into account the rotational effects we modify the expression for $J_{inter}(\omega)$ (Eq. (5)) as follows:

$$\begin{aligned} \tilde{J}_{inter}(\omega) &= J_{trans}(\omega) + f J_{rot}(\omega) \\ &= \left[72 \frac{3}{4\pi} \int_0^\infty \frac{u^2}{81+9u^2-2u^4+u^6} \frac{u^2 \tau_{trans}}{u^4+(\omega\tau_{trans})^2} du \right] \end{aligned}$$

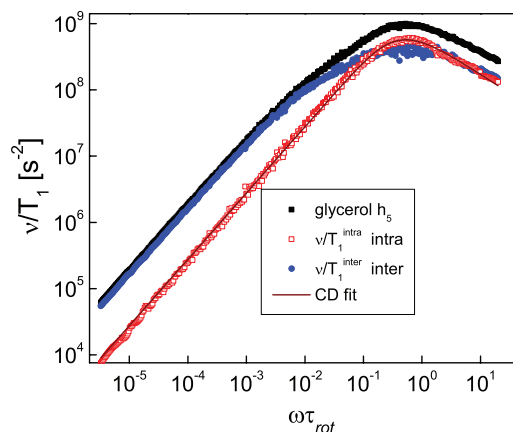


FIG. 5. Decomposition of the master curve of the entire relaxation for $x = 1$ (black squares) into intramolecular (red squares) and intermolecular (blue spheres) contributions. The intramolecular contribution (red squares) has been obtained by extrapolating the experimental results to the limit $x \rightarrow 0$, while the intermolecular contribution (blue spheres) is given as a difference between the results for $x = 1$ (black squares) and for $x \rightarrow 0$; $f = 2.68$, $\beta = 0.6$, $\tau_{trans}/\tau_{rot} = 52$.

$$+ f \left[\frac{\sin[\beta \arctan(\omega\tau_{CD})]}{\omega [1 + (\omega\tau_{CD})^2]^{\frac{\beta}{2}}} \right], \quad (8)$$

where the parameter f is a measure of the rotational contribution; \tilde{J} indicates a non-normalized spectral density. The parameter f is, in fact, related to an effective eccentricity factor^{21–23} in the sense, that for centrally placed spins $f = 0$ and it increases for spins more distant from the central position. This expression is a kind of simplification because it treats the translational and rotational effects on the intermolecular interactions as independent of each other. We consider it as a pragmatic way to include the rotational effects. In Fig. 6 the intermolecular master curve has been decomposed into translational and rotational parts according to Eq. (8). One notices here the relatively large contribution of the rotational part. Since the translational and rotational spectral densities of Eq. (8) are normalized, the factor $f = 2.68$ directly shows the substantial contribution of the rotational term.

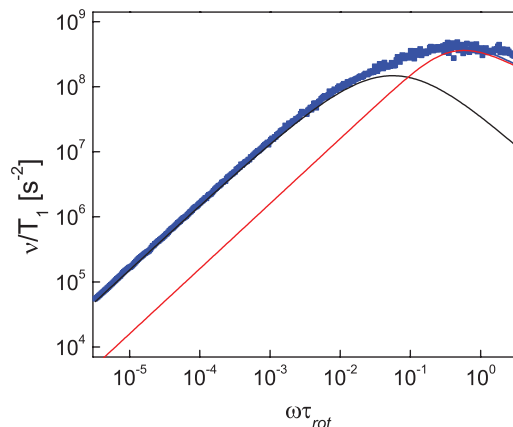


FIG. 6. Intermolecular master curve reproduced as a sum of translational (black) and rotational (red) parts according to Eq. (8).

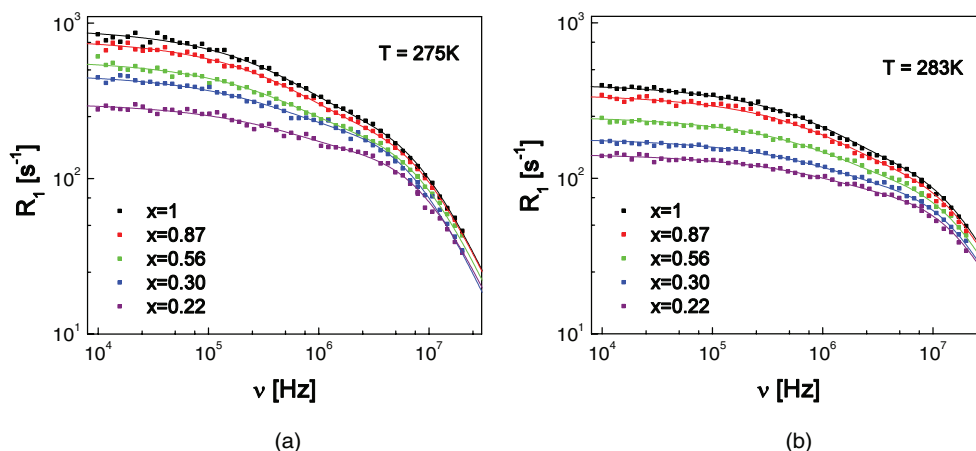


FIG. 7. Relaxation dispersion data for glycerol-h₅/glycerol-h₈ for different mole fractions of the partially protonated molecules at $T = 275$ K (a) and $T = 283$ K (b). Solid lines: fits according to Eq. (9). The parameters are given in Table I.

The analysis in terms of master curves reflects averaged relations between the translational and rotational parameters. To investigate in detail their temperature dependence for solutions with different dilution ratios, the individual relaxation dispersion data are analyzed.

Inserting Eq. (8) into Eq. (7) one can express the total relaxation rate R_1^H in terms of $J_{\text{rot}}(\omega)$ and $J_{\text{trans}}(\omega)$:

$$\begin{aligned}
 R_1^H(\omega_H) = & \frac{2}{5} I_H (I_H + 1) \left[(C_{\text{intra}}^{HH,\text{red}})^2 + f n x N \frac{4\pi}{3} \frac{1}{d^3} \right. \\
 & \times \left. \left(\frac{\mu_0}{4\pi} \gamma_H^2 \hbar \right)^2 \right] [J_{\text{rot}}(\omega_H) + 4J_{\text{rot}}(2\omega_H)] \\
 & + \frac{2}{15} I_D (I_D + 1) \left[(C_{\text{intra}}^{HD})^2 \right. \\
 & \left. + f \left((1 - nx) N \frac{4\pi}{3} \frac{1}{d^3} \left(\frac{\mu_0}{4\pi} \gamma_H \gamma_D \hbar \right)^2 \right) \right] \\
 & \times [J_{\text{rot}}(\omega_H - \omega_D) + 3J_{\text{rot}}(\omega_H) \\
 & + 6J_{\text{rot}}(\omega_H + \omega_D)] \\
 & + \frac{2}{5} I_H (I_H + 1) n x N \frac{4\pi}{3} \frac{1}{d^3} \left(\frac{\mu_0}{4\pi} \gamma_H^2 \hbar \right)^2 \\
 & \times [J_{\text{trans}}(\omega_H) + 4J_{\text{trans}}(2\omega_H)] \\
 & + \frac{2}{15} I_D (I_D + 1) (1 - nx) \\
 & \times N \frac{4\pi}{3} \frac{1}{d^3} \left(\frac{\mu_0}{4\pi} \gamma_H \gamma_D \hbar \right)^2 \\
 & \times [J_{\text{trans}}(\omega_H - \omega_D) + 3J_{\text{trans}}(\omega_H) \\
 & + 6J_{\text{trans}}(\omega_H + \omega_D)]. \quad (9)
 \end{aligned}$$

This expression has been applied to interpret ^1H relaxation dispersion data for individual temperatures for glycerol-h₅/glycerol-h₀ for different mole fractions x . Examples of the analysis are shown in Figs. 7(a) and 7(b) for 275 K and 283 K, respectively. The following fitting strategy has been applied. The coupling constants $C_{\text{intra}}^{HH,\text{red}}$ and C_{intra}^{HD} have been treated as global fit parameters for all concentrations and temperatures;

the same concerns the relative contributions of the translational and rotational parts to the intermolecular spectral density, f , and the distance of closest approach d . The correlation time, $\tau_{\text{rot}} = \beta \tau_{\text{CD}}$, has been allowed to change depending on the temperature and concentration, the ratio $\tau_{\text{trans}}/\tau_{\text{rot}}$ as well as β have been treated as dependent only on temperature. The same fitting strategy has been applied to the data shown in Fig. 2. The parameters obtained are summarized in Table I. From the large values of the $\tau_{\text{trans}}/\tau_{\text{rot}}$ ratio one should not conclude that the elementary translational jump time is significantly longer from that of the rotational displacements; τ_{trans} merely defines the time scale of the decay of the translational correlation function.

Comparing the present results with those obtained in Ref. 4 by applying solely the force-free-hard-sphere model to describe intermolecular relaxation (that means $f = 0$) one notices that now the intramolecular coupling constant $(C_{\text{intra}}^{HH,\text{red}})^2 = 1.1 \times 10^{10} \text{ Hz}^2$ is smaller than previously ($(C_{\text{intra}}^{HH,\text{red}})^2 = 1.55 \times 10^{10} \text{ Hz}^2$) because now it has been recognized that part of the relaxation which was previously treated as intramolecular is, in fact, of the intermolecular origin.

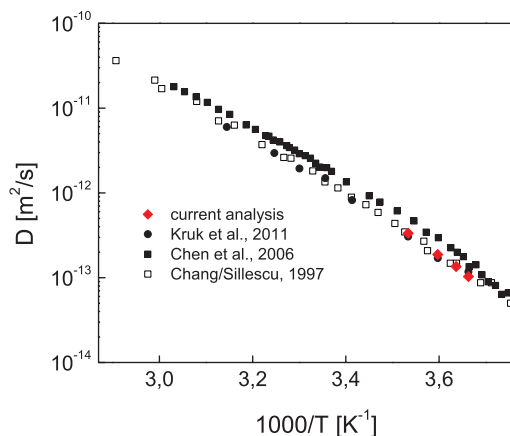


FIG. 8. Comparison of translational diffusion coefficient D obtained from pulse field gradient NMR (Refs. 9 and 10) and NMR relaxometry (Kruk et al.⁴ with the current analysis).

TABLE I. Parameters obtained by fitting the relaxation dispersion data in terms of Eq. (9). The global parameters are: $(C_{\text{intra}}^{HH,\text{red}})^2 = 1.1 \times 10^{10} \text{ Hz}^2$, $(C_{\text{intra}}^{HD})^2 = 6.5 \times 10^7 \text{ Hz}^2$, $f = 2.68$, and $d = 3.50 \text{ \AA}$.

T (K)	τ_{rot} (ns)					β	$\tau_{\text{trans}}/\tau_{\text{rot}}$
	$x = 1$	$x = 0.87$	$x = 0.56$	$x = 0.30$	$x = 0.22$		
273	10.0	9.4	9.8	11.9	8.5	0.61	60
275	8.2	7.7	7.9	9.4	7.2	0.60	57
278	6.3	6.1	5.7	6.9	6.0	0.60	52
283	4.1	3.9	3.9	4.0	3.7	0.60	47

The obtained distance of closest approach, d , has been used to calculate the translational diffusion coefficient, D from the relationship $D = d^2/2\tau_{\text{trans}}$. These diffusion coefficients are compared with the results of NMR pulse field gradient experiments and with the values obtained in Ref. 4 from the analysis of ^1H relaxation dispersion data under the assumption that the intermolecular interactions are entirely modulated by the translational diffusion.⁴ The comparison is shown in Fig. 8 (the diffusion coefficients from the current analysis are given as values averaged over all x); all results are in good agreement. In spite of the strong intermolecular rotational contribution the extracted D values are not significantly altered. One can see from Table I that the values of the correlation time, τ_{rot} , somewhat scatter with the mole fraction x for a given temperature. We attribute that to temperature instability.

V. DISCUSSION

As already explained, the concept of the intermolecular interactions being entirely modulated by the translational dynamics is highly simplified. Applying it for glycerol- h_8 , glycerol- h_5 , and glycerol- h_3 in our previous work,⁴ we have, nevertheless, obtained translational diffusion coefficients which are in good agreement with those from our present analysis and also from pulse field gradient NMR. However, the treatment of Ref. 4 has led to temperature dependent values of the distance of closest approach, d . A systematic trend has been observed; for higher temperatures d became shorter. Also for glycerol- h_5 the averaged d value was shorter than for glycerol- h_3 . One can understand this finding as follows. ^1H nuclei in glycerol- h_3 are placed further away from the molecular center than in glycerol- h_5 . In consequence, the rotational influence on the intermolecular relaxation is more pronounced; in other words, the intermolecular spectral density becomes more “rotational-like.” A larger d value reflects the fact that the relative contribution of the purely translational dynamics compared to the rotational one becomes smaller due to the increasing role of the molecular tumbling for the intermolecular relaxation.

The current description is also (as in Ref. 4) based on a superposition of Cole-Davidson and translational spectral densities, but now the Cole-Davidson spectral density is partitioned between the intramolecular and intermolecular relaxation. This means that the weight of overall Cole-Davidson contribution now also depends partly on the distance of closest approach. In consequence, it was possible in the present

analysis to keep d temperature independent, as one expects. This indicates that using ^1H NMR relaxometry as a source of information on the translational dynamics one should consider the rotational influence on the intermolecular relaxation. This statement does not contradict the conclusion that even the simple model^{7,8} attributing the fluctuations of the intermolecular interactions entirely to the translational motion leads to diffusion coefficients which are in good agreement with those from pulse field gradient NMR. The reason for that is that the translational part of the intermolecular interaction is spectrally separated from the rotational contributions.

Finishing this section we note that the present approach still leads (as in Ref. 4) to a temperature dependent ratio $\tau_{\text{trans}}/\tau_{\text{rot}}$. This dependence cannot be explained by violating the rotation-translation coupling, because the trend is opposite: the obtained $\tau_{\text{trans}}/\tau_{\text{rot}}$ is smaller for higher temperatures. This suggests that this effect should be still attributed deficiencies of the applied motional models, assuming a superposition of translational and rotational components for the intermolecular spectral density.

VI. CONCLUSIONS

^1H NMR relaxation dispersion studies have been performed for glycerol- h_5 diluted in glycerol- h_0 versus the mole fraction of glycerol- h_5 . By extrapolating the results to the zero concentration limit the spectral shape of the intermolecular relaxation has been revealed. For polyatomic molecules with nuclei at non-central positions the intermolecular dipole-dipole interactions are modulated by both translational and rotational dynamics. Therefore, in addition to a contribution caused by translational motion a strong contribution associated with rotational dynamics of the molecules has been observed which clearly demonstrates the important role of eccentricity effects. Both contributions appear to be spectrally separated. The intermolecular spectral density has been described as a sum of purely translational and rotational parts. This additive model allows interpreting the relaxation dispersion data for individual temperatures as well as the NMR master curve obtained by applying FTS. Translational diffusion coefficients $D(T)$ have been determined from the analysis based on the bimodal form of the intermolecular spectral density. The values obtained are in good agreement with those of pulse field gradient NMR. The results also agree with the D values obtained from NMR relaxometry in our previous work⁴ under the assumption that the intermolecular interactions are modulated entirely by the translational motion. Thus, regarding the determination of the diffusion coefficient this simple analysis still allows to extract reliable D values. Having clarified the role of inter- and intramolecular relaxation in liquids, ^1H NMR relaxometry has the potential to become a routine technique determining the diffusion coefficient. Finishing this section, we wish to note that there are liquids, for instance, in o-terphenyl, for which no spectrally separated intermolecular relaxation contribution has been found.³ With the experience gained from this work we attribute this feature to large eccentricity effects that lead to a rotational-like shape of the intermolecular spectral densities.

ACKNOWLEDGMENTS

The authors appreciate financial support of the Deutsche Forschungsgemeinschaft (DFG) (Grant No. RO 907/16).

- ¹R. Kimmich and E. Ansaldo, *Prog. NMR Spectrosc.* **44**, 257 (2004).
²D. Kruk, A. Hermann, and E. A. RöSSLer, *Prog. NMR Spectrosc.* (in press).
³R. Meier, R. Kahlau, D. Kruk, and E. A. RöSSLer, *J. Phys. Chem. A* **114**, 7847 (2010).
⁴D. Kruk, R. Meier, and E. A. RöSSLer, *J. Phys. Chem. A* **115**, 951 (2011).
⁵P. Lunkenheimer, U. Schneider, R. Brand, and A. Loidl, *Contemp. Phys.* **41**, 15 (2000).
⁶A. Kudlik, S. Benkhof, T. Blochowicz, C. Tschirwitz, and E. RöSSLer, *J. Mol. Struct.* **479**, 201 (1999).
⁷L. P. Hwang and J. H. Freed, *J. Chem. Phys.* **63**, 4017 (1975).
⁸Y. Ayant, E. Belorizky, J. Alizon, and J. Gallice, *J. Phys. (Paris)* **36**, 991 (1975).
⁹I. Chang and H. Sillescu, *J. Phys. Chem.* **101**, 8794 (1997).
¹⁰B. Chen, E. E. Sigmund, and W. P. Halperin, *Phys. Rev. Lett.* **96**, 145502 (2006).
¹¹J. P. Kintzinger and M. D. Zeidler, *Ber. Bunsenges. Phys. Chem.* **77**, 98 (1972).
¹²H. C. Torrey, *Phys. Rev.* **92**, 962 (1953).
¹³A. Abragam, *The Principles of Nuclear Magnetism* (Clarendon, Oxford, 1961), p. 302.
¹⁴F. Fujara, B. H. Sillescu, and G. Fleischer, *Z. Phys. B: Condens. Matter* **88**, 195 (1992).
¹⁵H. E. Heinze and H. Pfeiffer, *Z. Phys.* **192**, 329 (1966).
¹⁶J. F. Harmon, *Chem. Phys. Lett.* **7**, 207 (1970).
¹⁷J. F. Harmon and B. H. Muller, *Phys. Rev.* **82**, 400 (1969).
¹⁸P. Lindner, E. RöSSLer, and H. Sillescu, *Makromol. Chem.* **182**, 3653 (1981).
¹⁹M. Pöschl and H. G. Hertz, *J. Phys. Chem.* **98**, 8195 (1994).
²⁰M. Kehr, N. Fatkullin, and R. Kimmich, *J. Chem. Phys.* **126**, 094903 (2007).
²¹Y. Ayant, E. Belorizky, P. Fries, and J. Rosset, *J. Phys. (Paris)* **38**, 325 (1977).
²²J. P. Albrand, M. C. Taieb, P. H. Fries, and E. Belorizky, *J. Chem. Phys.* **75**, 2141 (1981).
²³J. P. Albrand, M. C. Taieb, P. H. Fries, and E. Belorizky, *J. Chem. Phys.* **78**, 5809 (1983).
²⁴C. J. F. Böttcher and P. Bordewijk, *Theory of Electric Polarization* (Elsevier, Amsterdam, 1973), Vol. 2.
²⁵D. Kruk, T. Nilsson, and J. Kowalewski, *Mol. Phys.* **99**, 1435 (2001).
²⁶D. Kruk and J. Kowalewski, *J. Chem. Phys.* **130**, 174104 (2009).
²⁷W. Götze, *Complex Dynamics of Glass-Forming Liquids* (Oxford University Press, Oxford, England, 2009).

Publication 3

Nuclear Magnetic Resonance Relaxometry as a Method of Measuring
Translational Diffusion Coefficients in Liquids.

Kruk, D; Meier, R.; Rössler, E.A.

Phys. Rev. E **2012**, 85, 020201.

Copyright 2012 by The American Physical Society

DOI: 10.1103/PhysRevE.85.020201

Nuclear magnetic resonance relaxometry as a method of measuring translational diffusion coefficients in liquids

D. Kruk,^{1,2} R. Meier,¹ and E. A. Rössler^{1,*}

¹*Experimentalphysik II, Universität Bayreuth, D-95440 Bayreuth, Germany*

²*Faculty of Mathematics & Computer Science, University of Warmia & Mazury in Olsztyn, PL-10710 Olsztyn, Poland*

(Received 14 October 2011; published 23 February 2012)

By application of the field-cycling technique, we measure the dispersion of the ¹H nuclear magnetic resonance (NMR) spin-lattice relaxation time $T_1(\omega)$ for a series of molecular liquids. We demonstrate that such NMR relaxometry studies can be used for determining diffusion coefficients. A broad frequency range of 10 kHz–20 MHz is covered. By scanning $T_1(\omega)$ one directly probes the spectral density of the diffusion processes. The value of the diffusion coefficient D can be determined from a linear dependence of the ¹H spin-lattice relaxation rate on the square root of the frequency at which it is measured. The power of this method lies in its simplicity, which allows one to determine $D(T)$ independently of the diffusive model. The results obtained are in very good agreement with those of field gradient NMR methods.

DOI: [10.1103/PhysRevE.85.020201](https://doi.org/10.1103/PhysRevE.85.020201)

PACS number(s): 66.10.cg, 76.60.Pc, 61.25.Em, 76.60.Es

Nuclear magnetic resonance (NMR) is a phenomenon that gives rise to a variety of specific experimental methods which are very valuable as sources of information on dynamical properties of molecular systems. In recent decades NMR field gradient diffusometry has become the key method of measuring translational diffusion coefficients D in liquids [1]. In order to probe the translational motion the sample is placed in an inhomogeneous magnetic field characterized by a linear, well-controlled field gradient. The position of a nucleus possessing a spin (an NMR-active nucleus) is monitored by changes in its Larmor frequency (precession frequency) which depend on the location of the traced nucleus. The range of D accessible by field gradient NMR methods is 10^{-6} – 10^{-14} m² s⁻¹ [1,2]. The higher bound of D refers to diffusion in gases while the lower one corresponds to moderately viscous (supercooled) liquids.

In this paper we demonstrate, focusing on liquids, that ¹H NMR relaxometry can be treated as a method complementary to field gradient diffusometry. The idea of NMR relaxation experiments is as follows [3,4]. First, the sample is polarized in a strong external magnetic field. The generated magnetization is proportional to the difference in the equilibrium populations of the ¹H Zeeman quantum states determined by the Boltzmann distribution. Then the field is switched to a lower value (relaxation field B_{rel}) and the energy levels repopulate according to the new equilibrium conditions. As a result the ¹H magnetization decreases in time, reaching eventually the value determined by the lower field B_{rel} . The magnetization decay is in most cases exponential with a time constant referred to as the spin-lattice relaxation time T_1 . The spin transitions are induced by stochastic fluctuations of magnetic dipole-dipole interactions between pairs of protons (this is in most cases the dominating relaxation mechanism), and one has to distinguish between proton sites on the same molecule (intramolecular) and on different molecules (intermolecular). In consequence, the measured value of the relaxation rate R_1 ($R_1 = 1/T_1$) is the sum of two contributions resulting from intramolecular and

intermolecular dipolar interactions, respectively [3]:

$$R_1(\omega) = R_{1,\text{intra}}(\omega) + R_{1,\text{inter}}(\omega), \quad (1)$$

where $\omega = \gamma_{\text{H}} B_{\text{rel}}$ (γ_{H} is the proton gyromagnetic factor). The intramolecular relaxation is associated with molecular rotation changing the orientation of the vector connecting the interacting nuclei (within a molecule) with respect to the direction of the external magnetic field. The relaxation rates depend on the spectral density of these fluctuations (as well as on the dipolar interaction strength). In the case of intermolecular relaxation the dipolar interactions are mediated by the relative translational motion of the molecules, which leads not only to fluctuations of the orientation of the internuclear axis, but also to changes in their separation, as reflected by the intermolecular dipolar correlation function $C_{\text{inter}}(t)$ [3,5,6]:

$$C_{\text{inter}}(t) \propto \left\langle \frac{Y_m^{2*}(\Omega(t)) Y_m^2(\Omega(0))}{r^3(t)} \right\rangle. \quad (2)$$

Here, the spherical harmonics $Y_m^2(\Omega)$ describe the molecular orientation via the Euler angle Ω , while r is the interspin distance. For isotropic liquids the rotational and translational dynamics averages the dipole-dipole interactions to zero. For dipolar relaxation of nuclei with spin quantum number $\frac{1}{2}$ the intermolecular relaxation rate $R_{1,\text{inter}}(\omega)$, measured at the angular frequency $\omega = 2\pi\nu$, is related to the intermolecular spectral density J_{inter} [which is a Fourier transform of the correlation function $C_{\text{inter}}(t)$] in a simple way according to the well-known relaxation formula [3]

$$R_{1,\text{inter}}(\omega) = \frac{3}{10} N \left(\frac{\mu_0}{4\pi} \gamma_{\text{H}}^2 \hbar \right)^2 [J_{\text{inter}}(\omega) + 4J_{\text{inter}}(2\omega)], \quad (3)$$

where N is the proton density (number of protons per unit volume). This number can be obtained from the relation $N = n N_A \rho / M_{\text{mol}}$, where M_{mol} is the molecular mass, ρ is the density of the liquid, n is the number of hydrogen atoms per molecule, and N_A is the Avogadro number. Thus by varying the relaxation field the spectral density is scanned.

Until recently, field-dependent relaxation experiments had not been routinely possible. Due to the recent commercial

*ernst.roessler@uni-bayreuth.de

availability of STELAR NMR field-cycling (FC) spectrometers, which cover about three orders of magnitude in the frequency (10 kHz–20 MHz for ^1H), NMR relaxometry gained new momentum [4,7]. The FC technique employs repetitive changes in the magnetic field: the external magnetic field is switched from a polarization field to a relaxation one and back to a high detection field. The measured frequency dependence of the spin-lattice relaxation rate $R_1 = T_1^{-1}$ is referred to as relaxation dispersion. An expression analogous to Eq. (3) can be written for the intramolecular relaxation rate $R_{1,\text{intra}}(\omega)$, but including intramolecular spectral densities that are associated with molecular rotation [3,7]. Thus the key dynamical processes, translation and rotation, can be monitored, in principle, with ^1H NMR relaxometry simultaneously, which is a unique and great advantage of this method, as shown in [7,8].

The rotational dynamics of a liquid can be probed by other methods, for instance dielectric spectroscopy (DS) [9]. The DS spectral density obtained from the imaginary part of the complex permittivity via $J_{\text{DS}}(\omega) = \varepsilon''/(\Delta\varepsilon\omega)$, where $\Delta\varepsilon$ is linked to the static dielectric constant ε_s [$(\varepsilon_s - \varepsilon_\infty) = \Delta\varepsilon$, where ε_∞ is the high-frequency permittivity], is often modeled by a Cole-Davidson spectral density which reflects its non-Lorentzian character. It gives as a limit a Lorentzian spectral shape that corresponds to an exponential correlation function (force-free isotropic tumbling). As dielectric spectroscopy is indifferent to translational motion, a comparison between NMR and DS results is of great value for differentiating between the contributions to the ^1H relaxation associated with rotation and translation. Recently, we have compared results of FC ^1H NMR relaxometry and DS for several viscous liquids such as glycerol [5,10]. ^1H NMR relaxation dispersion data compared with the DS results show a low-frequency excess contribution. To confirm its intermolecular (translational) origin, a series of ^1H NMR relaxation experiments for isotopically diluted systems (for instance glycerol- h_5 dissolved in glycerol- d_8) has been performed (for a full account see [11]). In Fig. 1 we show that the low-frequency contribution becomes progressively suppressed for a decreasing concentration of the ^1H -containing molecules. As ^1H - ^2H dipole-dipole interactions are much weaker than those between proton pairs (^1H - ^1H), this observation gives an ultimate proof of the intermolecular origin of the excess relaxation contribution. The intramolecular relaxation dispersion (obtained by extrapolating the relaxation data to the zero-concentration limit of glycerol- h_5) and the dielectric spectral density shapes are essentially identical as in both cases the rotational dynamics is solely probed. In conclusion, the dilution experiment shows that there is a considerable time scale separation of inter- and intramolecular relaxation contributions.

Different motional models have been applied to quantitatively describe the translational motion in condensed matter [12]. A closed form expression for the intermolecular correlation function referred to as the hard-sphere force-free diffusion model has been derived in [5,6]:

$$C_{\text{inter}}(t) = 72 \frac{1}{d^3} \int_0^\infty \frac{u^2}{81 + 9u^2 - 2u^4 + u^6} \exp\left(-\frac{u^2 t}{\tau_{\text{trans}}}\right) du, \quad (4a)$$

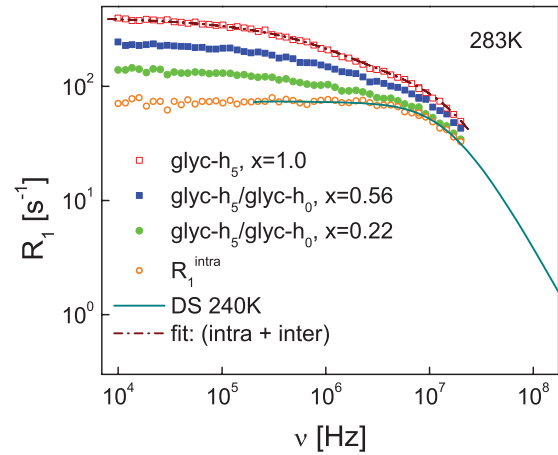


FIG. 1. (Color online) ^1H relaxation dispersion data for glycerol- h_8 and glycerol- h_5 -glycerol- h_0 mixtures with a mole fraction $x = 100\%$, 56% , 22% , and 0% (extrapolated) of glycerol- h_5 . Dashed-dotted line, fit in terms of the model presented in [8]. In the last case the low-frequency contribution disappears and only the intramolecular relaxation part (associated solely with rotational dynamics) remains. For comparison the dielectric spectral density is included (solid line). As it well agrees with the relaxation dispersion for $x = 0\%$ the translational origin of the low-frequency relaxation contribution is again confirmed.

which leads to the spectral density [8]

$$J_{\text{inter}}(\omega) = 72 \frac{1}{d^3} \int_0^\infty \frac{u^2}{81 + 9u^2 - 2u^4 + u^6} \frac{u^2 \tau_{\text{trans}}}{u^4 + (\omega \tau_{\text{trans}})^2} du, \quad (4b)$$

where u is an integration variable. This model assumes that the interacting nuclei are placed in the centers of the molecules that undergo Fick diffusion (force-free) with a uniform distribution of the molecules (treated as hard spheres) outside the distance of closest approach, d . The correlation time τ_{trans} is defined as $\tau_{\text{trans}} = d^2/D_{12}$, where D_{12} is the relative translational diffusion coefficient defined as the sum of self-diffusion coefficients of the participating molecules (thus for identical molecules it is twice larger than the self-diffusion coefficient, $D_{12} = 2D$). It has been shown by computer simulations that the effects of structural correlation present in liquids affect the intermolecular correlation function [13]. In addition, the intermolecular dipolar interactions are not only mediated by the translational motion, they are also affected by the molecular tumbling if the interacting nuclei were not placed in the molecular centers; this is referred to as eccentricity effects [14,15]. As we are going to extract the diffusion coefficients from the low-frequency range of the relaxation dispersion which corresponds to long times (via the inverse Fourier transform relationship) these effects become irrelevant [13,16,17]. For long times the intermolecular correlation function $C_{\text{inter}}(t)$ follows a power law $\propto t^{-3/2}$ that is characteristic of free diffusion. This time power law implies the form of the low-frequency expansion of the corresponding spectral

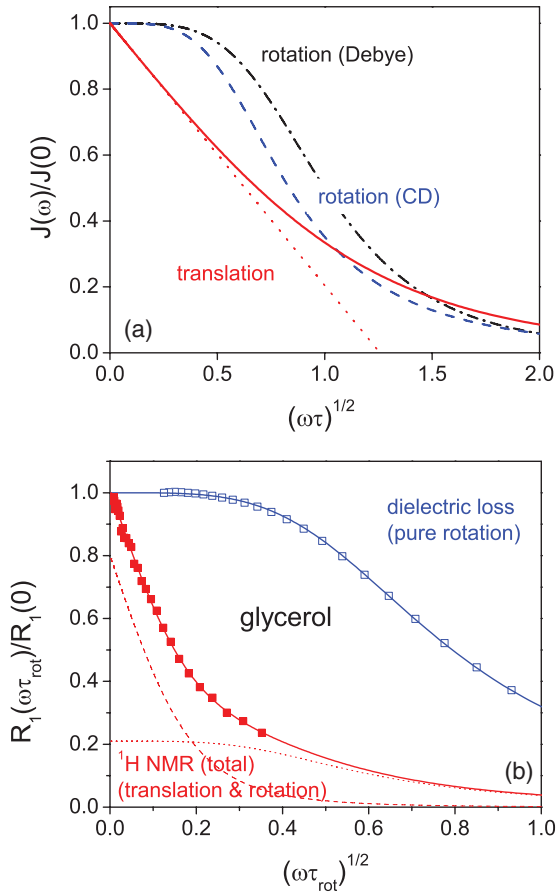


FIG. 2. (Color online) (a) Low-frequency behavior of the translational spectral density for the hard-sphere force-free model [5,6] compared with those of rotational spectral densities modeled as Debye and Cole-Davidson functions; dotted straight line, the limiting linear dependence predicted by Eq. (2). (b) Normalized ^1H NMR relaxation rate R_1 and dielectric spectral density for glycerol as functions of $\sqrt{\omega\tau_{\text{rot}}}$. The decomposition of the ^1H relaxation dispersion into intermolecular (dashed) and intramolecular (dotted) parts [8] shows that the first one controls the low-frequency shape of the entire relaxation curve.

density [5,12,18–21]:

$$J_{\text{inter}}(\omega) = a - b\sqrt{\omega}. \quad (5)$$

This expansion applies when $\omega\tau_{\text{trans}} < 1$. The seminal fact is that the constant b depends only on the diffusion coefficient D ; it does not include any details of the diffusion model [12,17,21]. Besides the very simple mathematical formulation, which makes the task of determining the diffusion coefficient values straightforward, an important consequence of this relation is that for the intermolecular relaxation contribution there is no frequency-independent low-field region. This is illustrated in Fig. 2(a) where the intermolecular spectral density (obtained from the hard-sphere force-free model) is compared with Cole-Davidson and Debye (Lorentzian) spectral densities describing intramolecular relaxation associated with rotational motion, both plotted as functions of $\sqrt{\omega\tau}$ (τ denotes here the characteristic correlation time; it has been set as $\tau_{\text{trans}} = \tau_{\text{rot}} = \tau$.) While J_{inter} in the low-frequency range shows the linear dependence of Eq. (5), the intramolecular spectral

density J_{intra} follows a Gaussian-like limiting dependence; for a Debye function (which is a special case of the Cole-Davidson function) one gets $J_{\text{intra}} \propto [1 - (\omega\tau_{\text{rot}})^2]$. Thus, from the low-frequency shape of the spectral density (relaxation rate) one can clearly distinguish between rotational and translational dynamics. To confirm this theoretically predicted feature we compare in Fig. 2(b) the ^1H relaxation dispersion $R_1(\omega)$ for glycerol with the corresponding DS results, both plotted as functions of $\sqrt{\omega\tau_{\text{rot}}}$. One sees that the limiting low-frequency behavior of $R_1(\omega)$ is indeed linear (it is determined by the translational contribution) whereas the DS results show a different frequency dependence.

The translational diffusion coefficient can be obtained from the model-independent relation $b = \pi/9D^{3/2}$. This implies [in combination with Eq. (3)] that for $\omega\tau_{\text{trans}} < 1$ the relaxation dispersion follows the relation

$$\begin{aligned} R_1(\nu) &\cong R_1(0) - B\sqrt{\nu} \\ &= R_1(0) - N \left(\frac{\mu_0}{4\pi} \gamma_{\text{H}}^2 \hbar \right)^2 \left(\frac{\sqrt{2} + 8}{30} \right) \left(\frac{\pi}{D} \right)^{3/2} \sqrt{\nu}, \end{aligned} \quad (6)$$

where the intramolecular contribution has been included into $R_1(0)$ as there is no visible dispersion of the intramolecular relaxation in the linear range of the intermolecular contribution. The fact that the intramolecular relaxation contribution can be included into $R_1(0)$ is ensured by the relationship between the rotational and translational correlation times. For the idealized case of mono-atomic molecules modeled as hard spheres with the nucleus placed in the molecular center, it has been theoretically predicted that $\tau_{\text{trans}}/\tau_{\text{rot}} = 9$ [3]. Investigating a variety of liquids, we have found that this ratio is considerably larger (40–70) [10] (which makes the time scale separation of these two processes even more easily discernible, as is also seen in Fig. 1 for glycerol). As a result, the diffusion coefficient can be straightforwardly calculated from the slope B (which contains only the spin density N and the diffusion coefficient D) of the limiting linear dependence of $R_1(\nu)$ on $\sqrt{\nu}$. We wish to stress that, although relaxation dispersion data contain both the intramolecular and intermolecular components (which makes them a unique source of information about the rotational and translational motion at the same time), for determining the translational diffusion coefficient there is no need to separate these contributions.

Although the feature of the low-frequency intermolecular relaxation dispersion encoded in Eq. (6) has been known for years, its advantages have not been appreciated so far. The relationship has been used to determine the diffusion coefficient for paramagnetic species in solutions [17]. In all cases the focus was on the dynamics of the paramagnetic molecules and the electron spin relaxation. In fact, the relationship of Eq. (6) was once applied to determine the diffusion coefficient of molecular liquids a long time ago [19]; however, this possibility was not, to our knowledge, further exploited until now. The reason likely lies in experimental difficulties—field-dependent relaxation studies have become routinely available only recently.

We have collected ^1H spin-lattice relaxation dispersion data for several liquids. In Fig. 3, as an example, the ^1H relaxation data for xylitol [$\text{HOCH}(\text{CH}_2\text{OH})_3\text{CH}_2\text{OH}$] obtained in a broad

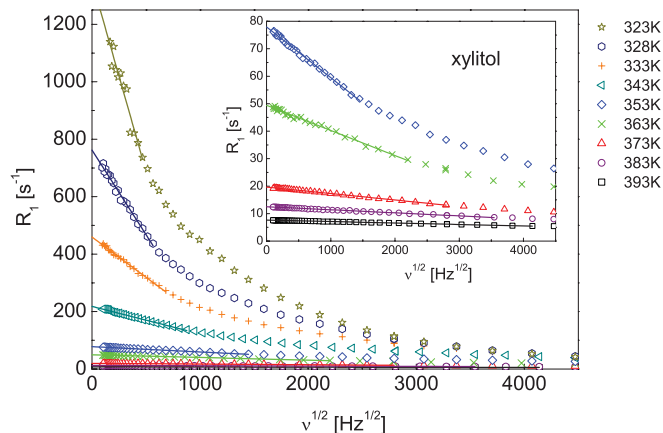


FIG. 3. (Color online) ^1H relaxation dispersion of the liquid xylitol plotted as a function of $\sqrt{\nu}$; the slope of the linear part at low frequencies yields the diffusion coefficient $D(T)$ [cf. Eq. (6)]; the inset shows enlarged high-temperature data.

temperature range are plotted against $\sqrt{\nu}$. The linear range of this dependence progressively extends to higher frequencies when the motion becomes faster (higher temperatures). The values of the diffusion coefficients extracted from the linear part are compared with those from NMR field gradient diffusometry [22–24] in Fig. 4. The results follow the Vogel-Fulcher-Tammann expression [10] as is typical of viscous liquids. A very good agreement between NMR relaxometry and diffusometry is reached, encouraging us to explore further the potential of ^1H NMR relaxometry by applying it to other systems. The results for other liquids also are in a very good agreement with those of field gradient diffusometry. It is worth mentioning that recently we have applied a full relaxation theory combined with the force-free hard-sphere diffusion model to reproduce the whole relaxation dispersion including the determination of the rotational time constants—cf. Fig. 1 [8,11].

As far as fast diffusional motion is concerned, the limit of NMR relaxometry is determined only by the fact that a perceptible (beyond the experimental inaccuracy of the FC technique) relaxation dispersion has to be seen in the accessible frequency range (up to 20 MHz). Using conventional NMR spectrometers operating at higher frequencies (say up to 600 MHz), this range can be considerably extended. Nevertheless, NMR relaxometry loses its sensitivity for fast diffusion processes of the order of water diffusion (10^{-9} m²/s). The slow diffusion limit is determined by two factors. The first one is that using this type of spectrometer one cannot measure relaxation times shorter than 1 ms. In the low-field range the relaxation time decreases when the correlation times becomes longer, eventually reaching this limit. The second limitation is that the linear

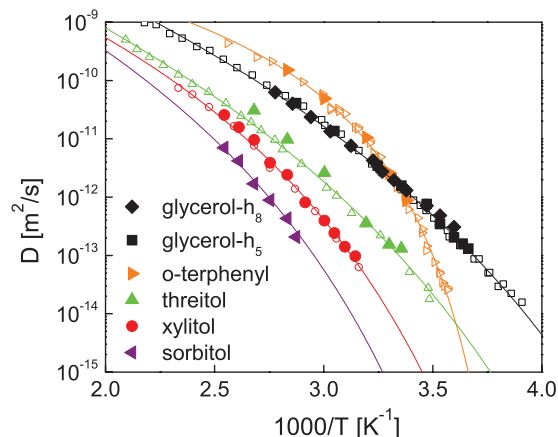


FIG. 4. (Color online) Translational diffusion coefficient D as obtained from ^1H NMR relaxometry (full symbols) for several liquids versus the reciprocal temperature; for comparison data from field gradient NMR (open symbols) are displayed [22–24]; the data are interpolated via the Vogel-Fulcher-Tammann expression [10].

range of the relaxation dispersion is observed when the condition $\omega\tau_{\text{trans}} < 1$ is fulfilled. This implies that to be able to detect the linear part of the relaxation dispersion at the low-frequency limit of 10 kHz, the correlation time τ_{trans} must not be longer than approximately 5×10^{-6} s. Using the relation $\tau_{\text{trans}} = d^2/2D$ introduced in the force-free hard-sphere model, where d defined as the distance of closest approach is close to the molecular diameter, one can estimate the upper limit of the accessible values of the diffusion coefficient. For a molecule of diameter of the order of 3 Å one reaches $D \cong 10^{-14}$ m²/s, which is at the limit of field gradient NMR diffusometry. We have thus demonstrated that ^1H NMR relaxometry can serve as a highly advantageous method of determining values of diffusion coefficients in a broad range. Taking into account the simplicity of the mathematical operations required, one can say that the diffusion coefficients are accessible in a (almost) direct way. The proposed method of determining diffusion coefficients can be used in a variety of areas—from industrial applications (such as, for instance, probing oil properties) to various research fields. Although we concentrated on ^1H relaxometry, other nuclei, such as, for instance ^{19}F , can also be exploited, which enlarges its potential. Nevertheless, when other (than dipole-dipole) relaxation mechanisms are of importance (for instance, hyperfine interactions for paramagnetic systems), Eq. (6) has to be modified according to a relaxation theory appropriate for the system of interest.

The authors appreciate financial support by the Deutsche Forschungsgemeinschaft (DFG) through Grant No. RO 907/15.

- [1] W. S. Price, *NMR Studies of Translational Motion* (Cambridge University Press, Cambridge, 2009).
 [2] F. Fujara, B. Geil, H. Sillescu, and G. Fleischer, *Z. Phys. B* **88**, 195 (1992).

- [3] A. Abragam, *The Principles of Nuclear Magnetism* (Clarendon Press, Oxford, 1961).
 [4] R. Kimmich and E. Anordo, *Prog. Nucl. Magn. Reson.* **44**, 257 (2004).

- [5] L. P. Hwang and J. H. Freed, *J. Chem. Phys.* **63**, 4017 (1975).
- [6] Y. Ayant, E. Belorizky, J. Alizon, and J. Gallice, *J. Phys. (France)* **38**, 325 (1977).
- [7] D. Kruk, A. Herrmann, and E. A. Rössler, *Prog. Nucl. Magn. Reson.*, doi:10.1016/j.pnmrs.2011.08.001 (2011).
- [8] D. Kruk, R. Meier, and E. A. Rössler, *J. Phys. Chem. B* **115**, 951 (2011).
- [9] C. J. F. Böttcher and P. Bordewijk, *Theory of Electric Polarization* (Elsevier Amsterdam 1973), Vol. 2.
- [10] R. Meier, R. Kahlau, D. Kruk, and E. A. Rössler, *J. Phys. Chem. A* **114**, 7847 (2010).
- [11] R. Meier, D. Kruk, and E. A. Rössler, *J. Chem. Phys.* **136**, 034508 (2012).
- [12] C. A. Sholl, *J. Phys. C* **14**, 447 (1981).
- [13] M. Odellius, A. Laaksonen, M. H. Levett, and J. Kowalewski, *J. Magn. Reson. A* **105**, 289 (1993).
- [14] J. P. Albrand, M. C. Taieb, P. H. Fries, and E. Belorizky, *J. Chem. Phys.* **78**, 5809 (1983).
- [15] Y. Ayant, E. Belorizky, P. Fries, and J. Rosset, *J. Phys. (France)* **38**, 325 (1977).
- [16] J. F. Harmon and B. H. Muller, *Phys. Rev.* **182**, 400 (1969).
- [17] E. Belorizky, D. G. Gillies, W. Gorecki, K. Lang, F. Noack, C. Roux, J. Struppe, L. H. Sutcliffe, J. P. Travers, and X. Wu, *J. Phys. Chem. A* **102**, 3674 (1998).
- [18] J. F. Harmon, *Chem. Phys. Lett.* **7**, 207 (1970).
- [19] P. H. Fries and E. Belorizky, *J. Phys.* **39**, 1263 (1983).
- [20] E. Belorizky and P. H. Fries, *J. Phys. C* **14**, 521 (1981).
- [21] P. H. Fries, *Mol. Phys.* **48**, 503 (1983).
- [22] I. Chang and H. Sillescu, *J. Phys. Chem.* **101**, 8794 (1997).
- [23] F. Fujara, B. Geil, H. Sillescu, and G. Z. Fleischer, *Z. Phys. B: Condens. Matter* **88**, 195 (1992).
- [24] A. Döb, M. Paluch, H. Sillescu, and G. Hinze, *J. Chem. Phys.* **117**, 6582 (2002).

Publication 4

Inter- and Intramolecular Relaxation in Molecular Liquids by Field Cycling
 ^1H NMR Relaxometry.

Meier, R.; Kruk, D; Bourdick, A.; Schneider, E.; Rössler, E.A.

Appl. Magn. Reson. **2012**, *44*, 153.

Copyright 2012 by Springer-Verlag Wien

DOI: 10.1007/s00723-012-0410-1

Inter- and Intramolecular Relaxation in Molecular Liquids by Field Cycling ^1H NMR Relaxometry

R. Meier · D. Kruk · A. Bourdick · E. Schneider ·
E. A. Rössler

Received: 26 July 2012 / Revised: 17 September 2012
© Springer-Verlag Wien 2012

Abstract Field cycling ^1H nuclear magnetic resonance (NMR) relaxometry is applied to study rotational as well as translational dynamics in molecular liquids. The measured relaxation rates, $T_1^{-1}(\omega) \equiv R_1(\omega)$, contain intra- and intermolecular contributions, $R_{1,\text{intra}}(\omega)$ and $R_{1,\text{inter}}(\omega)$. The intramolecular part is mediated by rotational dynamics, the intermolecular part by translation as well as rotation. The rotational impact on the intermolecular relaxation (eccentricity effect) is due to the spins not located in the molecule's center. The overall relaxation rate is decomposed into $R_{1,\text{intra}}(\omega)$ and $R_{1,\text{inter}}(\omega)$ by isotope dilution experiments. It is shown that the eccentricity model (Ayant et al. in *J. Phys. (Paris)* 38:325, 1977) reproduces fairly well the bimodal shape of $R_{1,\text{inter}}(\omega)$ for *o*-terphenyl and glycerol. As the relaxation contribution associated with translational dynamics dominates at lower frequencies, the overall relaxation rate shows a universal linear behavior when plotted versus square root of frequency. This allows determining the self-diffusion coefficient, D , in a model-independent way. It is demonstrated that the shape of NMR master curves comprising relaxation data for different temperatures, linked by frequency–temperature superposition, reflects the relative strength of translational and rotational contributions.

1 Introduction

Field cycling (FC) nuclear magnetic resonance (NMR) relaxometry has become a powerful tool for investigating dynamics in condensed matter, in particular in

R. Meier · D. Kruk · A. Bourdick · E. Schneider · E. A. Rössler (✉)
Experimentalphysik II, Universität Bayreuth, 95440 Bayreuth, Germany
e-mail: ernst.roessler@uni-bayreuth.de

D. Kruk
Faculty of Mathematics and Computer Science, University of Warmia and Mazury in Olsztyn,
Śloneczna 54, 10710 Olsztyn, Poland
e-mail: danuta.kruk@matman.uwm.edu.pl

viscous liquids and polymers [1, 2]. One distinguishes mechanical and electronic FC. Mechanical FC can be combined with high-resolution NMR [3–5], whereas in electronic FC usually only the total amplitude of the NMR signal is monitored. Due to recent availability of commercial (electronic) FC spectrometers the technique has gained new momentum [1, 2]. Currently FC ^1H NMR relaxometry allows routine measurements of spin–lattice relaxation time dispersion $T_1 = T_1(\omega)$ in a frequency range of 10 kHz–20 MHz.

Recently, we have compared the results of FC ^1H NMR relaxometry and dielectric spectroscopy (DS) for several viscous liquids [6]. Such liquids can easily be supercooled and thereby their viscosity, diffusion coefficient, D , and re-orientational correlation time, τ_{rot} , change in a super-Arrhenius manner [7–9]. It is well known that DS spectra for these systems can be described in terms of a Cole–Davidson (CD) spectral density which provides a phenomenological interpolation of the non-exponential (stretched) correlation function of the highly cooperative re-orientational dynamics involved in the structural relaxation (α -process) of liquids [10]. The ^1H NMR susceptibility [11, 12], i.e., relaxation dispersion data transformed to the susceptibility representation, $\chi''_{\text{NMR}}(\omega) = \omega/T_1(\omega)$ show, in addition to the α -relaxation peak, a low-frequency excess contribution (of a varying amplitude) which cannot be reproduced by a single CD susceptibility. Figure 1a summarizes our results for a series of different liquids (some of the data have already been published previously [6, 13]). Whereas, for instance, glycerol shows a pronounced low-frequency excess contribution, in the case of *o*-terphenyl such a contribution is almost missing, and NMR and DS curves agree well. The results shown in Fig. 1a stem from combining the relaxation dispersion data collected at different temperatures by means of frequency–temperature superposition (FTS). This allows constructing NMR master curves, $\chi''_{\text{NMR}}(\omega\tau_{\alpha})$, covering several decades of the reduced frequency $\omega\tau_{\text{rot}}$, where $\tau_{\text{rot}} \equiv \tau_{\alpha}$ is the (re-orientational) time constant attributed to the α -process. Applying FTS one assumes that the spectral shape of the

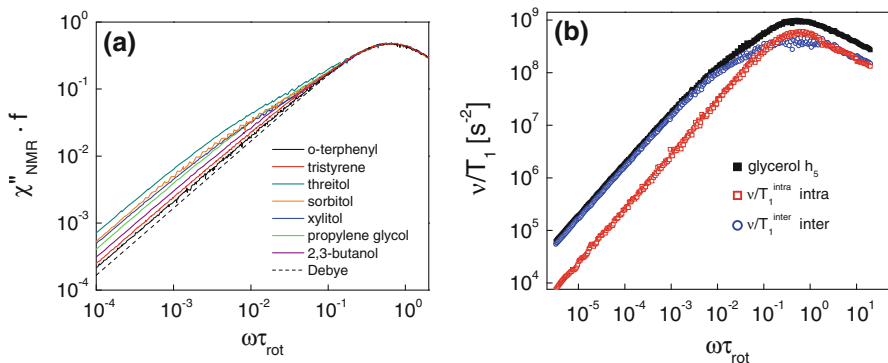


Fig. 1 **a** Susceptibility master curves for different liquids. Note the low-frequency excess contribution with respect to a Debye curve (*dashed line*), **b** total (*black filled squares*), intra- (*red open squares*) and intermolecular (*blue circles*) NMR susceptibility of glycerol obtained from isotope dilution experiments; the inter-contribution shows a *bimodal spectral shape* reflecting the eccentricity effect (color figure online)

susceptibility does not change significantly with temperature, which is actually a generic feature of the cooperative motion in highly viscous liquids [9, 14].

As ^1H NMR relaxation probes fluctuations of dipole–dipole interactions, one has to distinguish between protons within the same molecule (intramolecular) and in different molecules (intermolecular). In consequence, the overall relaxation rate $R_1 = 1/T_1$ is a sum of both rates, $R_{1,\text{intra}}$ and $R_{1,\text{inter}}$, $R_1 = R_{1,\text{intra}} + R_{1,\text{inter}}$ [15]. We have attributed the excess low-frequency contribution to the intermolecular relaxation mediated by translational motion of the molecules, while the main relaxation peak stems from rotational dynamics associated with both inter- and intermolecular relaxation [13, 16]. Performing isotope dilution experiments we have shown that indeed the excess contribution is suppressed, when the protonated molecules are substituted by their deuterated counterpart. The intra- and intermolecular relaxation contributions are spectrally separated with the intermolecular part dominating at low frequencies. So far such isotope dilution experiments have been rarely performed by FC ^1H NMR [17–19].

In Fig. 1b the separated $R_{1,\text{intra}}(\omega)$ and $R_{1,\text{inter}}(\omega)$ relaxation contributions for glycerol are displayed [16]. The intramolecular part (red open squares) can be well reproduced by a CD function, while the spectral shape of the intermolecular relaxation (blue circles) can be described as bimodal. Its low-frequency part is dominated by translational modulations of the intermolecular dipole–dipole interactions, whereas the high-frequency part reflects the rotational influence on the intermolecular interaction resulting from the non-central positions of the nuclei in the molecule. In our first attempt [13], this eccentricity effect has been described by treating the intermolecular spectral density as a sum of a translational part described by the hard sphere free diffusion (HSFD) model introduced by Hwang and Freed [20] and Ayant et al. [21], and a rotational part described by a CD function. The HSFD model describes the translational dynamics in terms of free (Fick) diffusion with appropriate boundary conditions introducing a distance of closest approach d which is expected to be on the order of the molecular size. For the hydrodynamic model of a (molecular) sphere rotating and translating in a viscous medium one gets $r = \tau_{\text{trans}}/\tau_{\text{rot}} = 9$ [15] where $\tau_{\text{trans}} = d^2/2D$. Experimentally we have observed $r = 30 - 60$ [13, 16]. This ratio is essentially temperature-independent as expected for the translational–rotational coupling to hold for moderately viscous liquids [22]. Thus, as $\tau_{\text{trans}} > \tau_{\text{rot}}$, the translational modulations of the intermolecular interactions are responsible for the low-frequency shoulder of the overall relaxation rate $R_1(\omega)$ from which the diffusion coefficient $D(T)$ can be extracted [23].

For long times the intermolecular correlation function follows the power-law $\propto t^{-3/2}$, which is characteristic for free diffusion [24]. The time power-law implies the form of the low-frequency expansion of the corresponding spectral density [24–28].

$$R_1(\omega) = R_1(0) - B \cdot \frac{1}{D^{3/2}} \cdot \sqrt{\omega}, \quad \omega\tau_{\text{trans}} < 1. \quad (1)$$

The important fact is that in addition to standard physical constants, the factor B depends only on the spin density N , i.e., the number of spins per unit volume. It does not include any details of the diffusion model [24]. This makes the task of determining

the diffusion coefficient straightforward, there is no frequency-independent (low-frequency) region for the intermolecular relaxation contribution (the extreme narrowing condition does not apply). Although Eq. (1) is well known, for quite a long time it has never been exploited systematically for liquids (except of the diffusion of paramagnetic species in solutions [29, 30]), probably due to missing technical possibilities of obtaining the dispersion of the NMR relaxation. Now, with the emergence of commercially available FC spectrometers, its potential can be fully exploited. Since, as already said, $\tau_{\text{trans}} > \tau_{\text{rot}}$, the translational diffusion always controls the low-frequency behavior of the relaxation dispersion as the rotational part is constant there. Thus, Eq. (1) can be applied for extracting the diffusion coefficient in protonated liquids without taking recourse of the isotope dilution experiment. In the present contribution this approach is further applied to determine $D(T)$ for several liquids, extending the results presented in Ref. [23]. Moreover, given that the translational–rotational coupling applies, Eq. (1) allows constructing NMR master curves, from which the ratio $r \equiv \tau_{\text{trans}}/\tau_{\text{rot}}$ as well as relative magnitudes of the intermolecular and intramolecular dipole–dipole couplings can be estimated for different liquids.

As mentioned above, in the susceptibility data of *o*-terphenyl essentially no low-frequency excess contribution is observed (cf. Fig. 1) and it is interesting to ask what spectral shape is found for $R_{1,\text{intra}}(\omega)$ and $R_{1,\text{inter}}(\omega)$ in this case. Thus, we will present results of an isotope dilution experiment for *o*-terphenyl, once again demonstrating the importance of the intermolecular relaxation contribution also in this case. Ayant et al. [31] have developed a general expression for the intermolecular relaxation rate $R_{1,\text{inter}}(\omega)$ accounting for the eccentricity of the spin positions. We will refer to this expression when attempting to describe $R_{1,\text{inter}}(\omega)$ quantitatively.

2 Theoretical Background

2.1 Eccentricity Effects and Intermolecular Relaxation

The HSFD model of translational dynamics assumes spherical particles with one spin placed at their centers. Ayant et al. [31] have extended this description to spherical molecules carrying an off-centered spin and undergoing rotational diffusion which now also contributes to the modulation of the intermolecular interactions. The model assumes isotropic rotational diffusion. Although this assumption is not fully adequate for the cooperative dynamics of viscous liquids [2, 7–9, 14], it is definitely worthwhile to discuss the model of Ayant et al. [31] in more detail. As the resulted expression for the intermolecular spectral density is quite cumbersome, we refrain from quoting it again and refer to Ref. [31]. Using it, the intermolecular NMR susceptibility $\chi''_{\text{inter}}(\nu) \equiv 2\pi\nu \cdot J_{\text{inter}}(\nu)$ can be calculated depending on the eccentricity parameter $e \equiv 2\rho/d$ (ρ denotes the distance of the spin from the center of a spherical molecule) and the ratio between the translational and rotational correlation times $r \equiv \tau_{\text{trans}}/\tau_{\text{rot}}$; Fig. 2 shows some examples for $r \equiv \tau_{\text{trans}}/\tau_{\text{rot}} = 9$ (Fig. 2a) and $r = 50$ (Fig. 2b). The value $r = 9$ corresponds to

the hydrodynamic model of a sphere (molecule) rotating in a viscous medium [15], $r = 50$ is close to the experimental value obtained for glycerol [16]. For $e = 0$ the model reduces to the HSF model [20, 21] (black line), while with increasing of the eccentricity parameter, e , an additional contribution rises on the high-frequency flank of $\chi''_{inter}(\nu)$ reflecting the rotational contribution to the intermolecular relaxation. The latter is more resolved for $r = 50$ (cf. Fig. 2b).

Phenomenologically, the intermolecular spectral density, $\tilde{J}_{inter}(\omega)$, calculated applying the eccentricity model of Ayant et al. can be separated into two terms:

$$\tilde{J}_{inter}(\omega) = J_{trans}(\omega) + f \cdot J_{rot}(\omega), \tag{2}$$

where J_{trans} is given by the HSF model ($e = 0$), while $f \cdot J_{rot}(\omega)$ is the additional part which arises from eccentricity. J_{trans} and J_{rot} are normalized: $\int_0^\infty J(\omega)d\omega = \pi/2$; thus $\tilde{J}_{inter}(\omega)$ is not normalized $\int_0^\infty \tilde{J}_{inter}(\omega)d\omega = \pi/2 \cdot (1 + f)$.

The separation according to Eq. (2) has been done in Fig. 3. One gets the rotational contribution $f \cdot J_{rot}(\omega)$ by subtracting the corresponding HSF susceptibility from the total one. Attempts to reproduce the rotational contribution by means of a Debye or CD spectral density fail, because of its broadened shape. Although the model assumes that the rotational dynamics is described by Lorentzian spectral densities, the fact that the description includes rotational correlation times of different orders leads to a broadening of the rotational contribution. A CD function can partially mimic the broadening; however, the eccentricity model predicts a high-frequency behavior $\propto \omega^{-1}$ at $\omega\tau_{rot} > 1$ which cannot be reproduced in this way (cf. Fig. 3).

The parameter f has been obtained by integrating the rotational part. Figure 4a shows the f parameters obtained for different e values; obviously, $f(e = 0) = 0$. For small e values the factor f rises quite slowly and $f = 1$ is reached only for $e \approx 0.56$. For larger eccentricity the rotational contribution and thus the f factor grows rapidly. In the (unphysical) case of spins located on the surface of the (molecular) sphere, i.e., $e = 1$, the rotational contribution to intermolecular relaxation will be 50 times larger than the translational one.

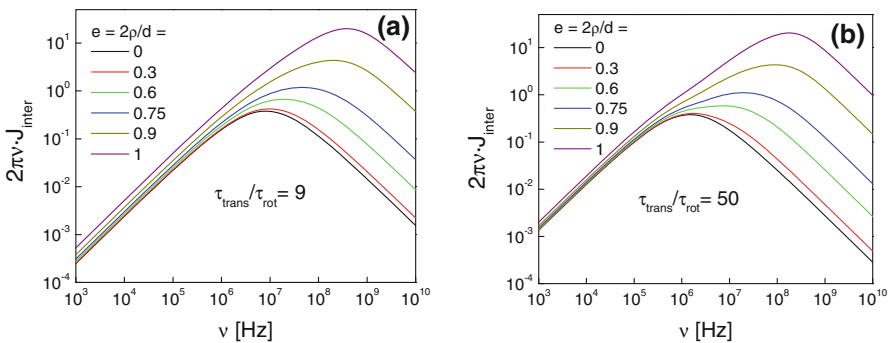


Fig. 2 Intermolecular NMR susceptibility, $2\pi\nu \cdot J_{inter}(\nu)$, for different eccentricity parameters e $r = 9$ (a), and $r = 50$ (b)

Fig. 3 Separation of the intermolecular NMR susceptibility (solid black line) into rotational (solid red line) and translational (solid blue line) parts; attempts to reproduce the rotational part via Debye (dashed dark cyan line) and CD (dotted green line) spectral densities (color figure online)

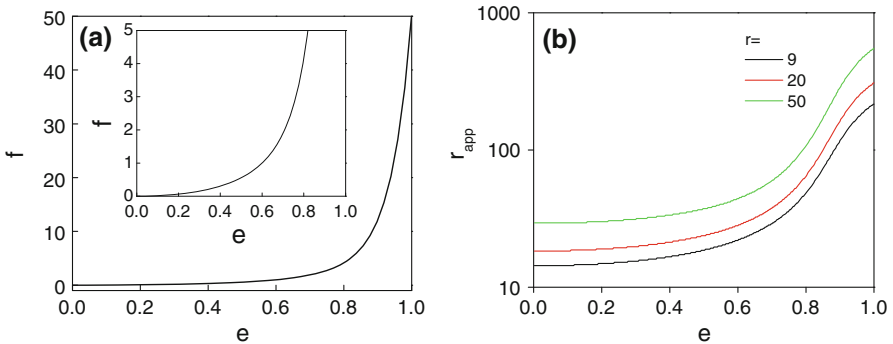
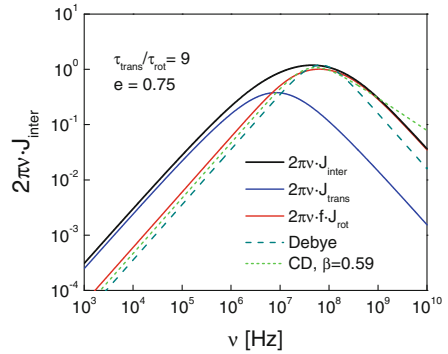


Fig. 4 **a** Dependence of f (cf. Eq. 2) on eccentricity $e \equiv 2\rho/d$ as given by the eccentricity model [33], **b** the apparent ratio $r_{app} = \tau_{trans}/\tau_{rot,app}$ versus e . The apparent rotational time constant $\tau_{rot,app}$ was derived from the peak maximum of the rotational contribution

One can see in Fig. 2 that the rotational peak shifts to higher frequencies with increasing e . Hence the apparent ratio $r_{app} = \tau_{trans}/\tau_{rot,app}$ can be discussed as a function of eccentricity e (cf. Fig. 4b). The time constant $\tau_{rot,app}$ is obtained from the peak position ($\omega\tau_{rot,app} = 1$) of the rotational part (obtained by subtraction of the HSDF contribution from the total spectral density). The apparent ratio r_{app} initially rises slowly (for low e), but for higher e it grows much faster. This can be explained by the larger linear velocity (a faster loss of correlation) of more off-centered spins. For $r = 9$ the apparent ratio varies between $r_{app} \approx 14$ for $e \rightarrow 0$ and $r_{app} \approx 200$ for $e = 1$. As the model includes rotational correlation times of different ranks (which are related to the assumed rank-two correlation time τ_{rot}), one does not get $\tau_{rot,app} = \tau_{rot}$. Thus, the experimentally observed rather higher ratio r_{app} may actually correspond to a smaller r value combined with large eccentricity e .

2.2 The Low-Frequency Limit of the Overall ^1H Spin–Lattice Relaxation Rate

The total spin–lattice relaxation rate of systems containing only protons can be written as:

$$R_1(\omega) = R_{1,\text{intra}}(\omega) + R_{1,\text{inter}}(\omega) = R_{1,\text{intra}}(\omega) + R_{1,\text{inter}}^{\text{rot}}(\omega) + R_{1,\text{inter}}^{\text{trans}}(\omega), \quad (3)$$

when one accepts that the intermolecular spectral density can be approximated as a sum of translational and rotational contributions (Eq. (2)) with

$$R_{1,\text{inter}}^{\text{trans}}(\omega) = \frac{K_{\text{inter}}}{5} [J_{\text{trans}}(\omega) + 4J_{\text{trans}}(2\omega)], \quad (4)$$

$$R_{1,\text{intra}}(\omega) + R_{1,\text{inter}}^{\text{rot}}(\omega) = \frac{K_{\text{intra}} + fK_{\text{inter}}}{5} [J_{\text{rot}}(\omega) + 4J_{\text{rot}}(2\omega)], \quad (5)$$

where

$$K_{\text{inter}} = 2\pi \left(\frac{\mu_0}{4\pi} \hbar \gamma \right)^2 \frac{N}{d^3}. \quad (6)$$

As mentioned, N denotes the spin density. Expanding the translational and rotational spectral densities, $J_{\text{trans}}(\omega)$ and $J_{\text{rot}}(\omega)$ (in Debye approximation) up to the rank-two terms one gets:

$$J_{\text{trans}}(\omega) = \frac{4\tau_{\text{trans}}}{9} \left(1 - \frac{3}{4\sqrt{2}} (\omega\tau_{\text{trans}})^{1/2} + \frac{1}{12\sqrt{2}} (\omega\tau_{\text{trans}})^{3/2} + \dots \right), \quad (7)$$

$$J_{\text{rot}} = \tau_{\text{rot}} \left(1 - (\omega\tau_{\text{rot}})^2 + \dots \right). \quad (8)$$

These expansions hold for $\omega\tau_{\text{trans}} < 1$ and $\omega\tau_{\text{rot}} < 1$, respectively. Substituting Eq. (7) into Eq. (4); Eq. (8) into Eq. (5) and then adding the terms according to Eq. (3), one obtains for the total rate $R_1(\omega)$:

$$R_1(\omega) \cong R_1(0) + R_1^{(1)}(\omega) + R_1^{(2)}(\omega), \quad (9)$$

where

$$R_1(0) = R_1^{(0)}(\omega) = (K_{\text{intra}} + fK_{\text{inter}})\tau_{\text{rot}} + \frac{4}{9}K_{\text{inter}}\tau_{\text{trans}}, \quad (10a)$$

$$\begin{aligned} R_1^{(1)}(\omega) &= -\frac{4}{15} \left(\frac{\sqrt{2}}{8} + 1 \right) K_{\text{inter}}\tau_{\text{trans}}(\omega\tau_{\text{trans}})^{1/2} \\ &= -\frac{\pi}{30} \left(1 + 4\sqrt{2} \right) \left(\frac{\mu_0}{4\pi} \hbar \gamma \right)^2 \frac{N}{D^{3/2}} \sqrt{\omega}, \end{aligned} \quad (10b)$$

$$R_1^{(2)}(\omega) = -\frac{17}{5} (K_{\text{intra}} + fK_{\text{inter}})\tau_{\text{rot}}(\omega\tau_{\text{rot}})^2 + \frac{1}{135} \left(1 + 8\sqrt{2} \right) K_{\text{inter}}\tau_{\text{trans}}(\omega\tau_{\text{trans}})^{3/2}. \quad (10c)$$

As already discussed in Sect. 1, Eq. (10b) once again demonstrates that the pre-factor of $\sqrt{\omega}$ depends only on the self-diffusion coefficient D and the spin density N .

To reveal the universality of the relaxation dispersion in the low-frequency range we shall consider the ratio $R_1(\omega)/R_1(0)$, which yields:

$$\frac{R_1(\omega)}{R_1(0)} \cong 1 - \frac{\frac{4}{15} \left(\frac{\sqrt{2}}{8} + 1\right) K_{\text{inter}} \tau_{\text{trans}} (\omega \tau_{\text{trans}})^{1/2}}{(K_{\text{intra}} + fK_{\text{inter}}) \tau_{\text{rot}} + \frac{4}{9} K_{\text{inter}} \tau_{\text{trans}}} + \frac{\frac{1}{135} (1 + 8\sqrt{2}) K_{\text{inter}} \tau_{\text{trans}} (\omega \tau_{\text{trans}})^{3/2} - \frac{17}{5} (K_{\text{intra}} + fK_{\text{inter}}) \tau_{\text{rot}} (\omega \tau_{\text{rot}})^2}{(K_{\text{intra}} + fK_{\text{inter}}) \tau_{\text{rot}} + \frac{4}{9} K_{\text{inter}} \tau_{\text{trans}}} \quad (11)$$

The first order term in Eq. 11 can be rewritten as:

$$\frac{R_1(\omega)}{R_1(0)} \cong 1 - \frac{3(\sqrt{2} + 8)}{40} \sqrt{\omega \tau'} \cong 1 - 0.7 \cdot \sqrt{\omega \tau'}, \quad (12)$$

where one defines a rescaled correlation time τ' as:

$$\tau' = \tau_{\text{trans}} \left(\frac{4\xi r}{4\xi r + 9} \right)^2, \quad \xi = \frac{K_{\text{inter}}}{K_{\text{intra}} + fK_{\text{inter}}}. \quad (13)$$

This shows that the low-frequency part of the relaxation dispersion can indeed be mapped to a universal linear dependence versus $\sqrt{\omega \tau'}$, and D is given as:

$$D = \left(\frac{\frac{4\pi}{9} \left(\frac{\mu_0}{4\pi} \hbar \gamma_H^2\right)^2 N_H}{R_1(0) \sqrt{2\tau'}} \right)^{2/3}. \quad (14)$$

First deviations from the low-frequency linear behavior observed at higher frequencies are determined by the second-order term in Eq. (11), they go in the upward direction (second derivative positive) or in the downward direction (second derivative negative) depending on the interplay between the rotational and translational contributions. When the rotational contribution prevails, the direction is downward, and upward otherwise. The second term vanishes when

$$c \equiv \xi \cdot r^{-5/2} \approx 40, \quad (15)$$

where the last equality has been obtained taking into account that the rotational contribution shows significant dispersion only at frequencies for which $\omega \tau_{\text{rot}} \approx 1$. Equation (15) gives the condition under which the square root term dominates the relaxation dispersion over a large frequency range.

Figure 5a shows reduced relaxation rates, $R_1(\omega)/R_1(0)$ versus $0.7 \cdot \sqrt{\omega \tau'}$ for different parameter ξ , $r \equiv \tau_{\text{trans}}/\tau_{\text{rot}} = 9$ is kept constant as predicted by Stokes–Einstein–Debye law [15]; the rotational contribution is described by a Debye spectral density and the translational one by the HSFD model. For $c = 40$ the reduced relaxation rate follows the linear behavior up to rather high frequencies, while for c larger or smaller than about 40, the curves bend up or down from the linearity, respectively. In Fig. 5b ξ has been fixed to a small value which means that the coupling constant associated with the rotational dynamics, $K_{\text{intra}} + fK_{\text{inter}}$, dominates the coupling constant for the translational spectral density K_{inter} . For $r \equiv \tau_{\text{trans}}/\tau_{\text{rot}} = 9$ the relaxation curves bend down, but this changes with increasing r . The shape of the relaxation dispersion is highly sensitive to r as it enters Eq. (15) with an exponent 5/2. Below, we will demonstrate that the different relaxations

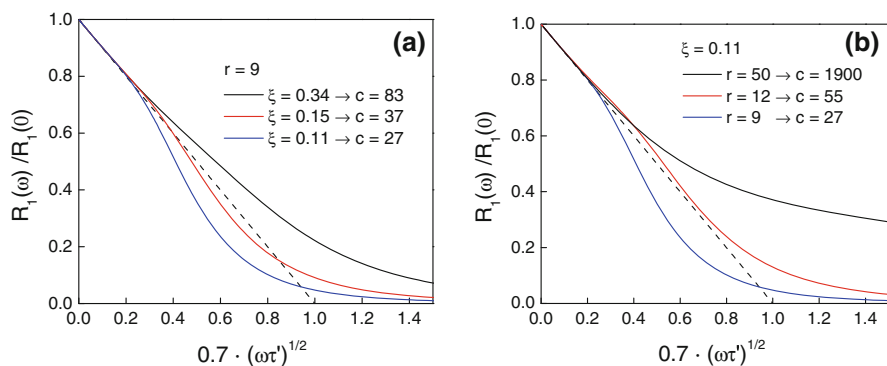


Fig. 5 Reduced relaxation rates, $R_1(\omega)/R_1(0)$ versus $0.7 \cdot \sqrt{\omega\tau}$ for **a** $r = 9$ and different ζ values, **b** fixed ζ and different ratios r ; *dashed line* low-frequency limit

characteristics (deviations from the low-frequency linearity) are actually found experimentally.

3 Experimental

The dispersion of the ^1H spin–lattice relaxation rate, $R_1 = 1/T_1$, was studied in the temperature range of 200–400 K (depending somewhat on the system) by employing a commercial fast (electronic) FC spectrometer STELAR FFC 2000 [1] which allows one to cover the frequency range of 10^4 – $2 \cdot 10^7$ Hz. Spin–lattice relaxation times down to about 1 ms are accessible. The temperature was controlled by heating flowing air or evaporated liquid nitrogen. The temperature stability was ± 0.3 K. In all cases a single-exponential relaxation has been observed. In the case of *o*-terphenyl, the fully protonated liquid *o*-terphenyl- h_{14} was diluted with the fully deuterated *o*-terphenyl- h_0 . The measurements were done for several mole fractions of *o*-terphenyl- h_{14} in *o*-terphenyl- h_0 $x_{\text{H}} = 1.0, 0.75, 0.5$ and 0.25 . The susceptibility data measured at different temperatures were merged by shifting the data ν/T_1 along the frequency axis to get the best overlap. Fitting a CD function to the susceptibility master curve allows determining the time constant τ_{rot} and consequently $\chi''_{\text{NMR}}(\omega\tau_{\text{rot}})$ is obtained.

4 Results

4.1 Isotope Dilution Study of *o*-Terphenyl

As mentioned above, the ^1H relaxation dispersion of *o*-terphenyl does not show a discernible low-frequency contribution and therefore, in analogy to the dielectric spectra it can be approximated by a CD function (cf. Fig. 1). Thus, it is of interest to single out the $R_{1,\text{intra}}(\nu)$ and $R_{1,\text{inter}}(\nu)$ contributions. We have diluted *o*-terphenyl- h_{14} by its deuterated counterpart, *o*-terphenyl- h_0 . Relaxation dispersion profiles for

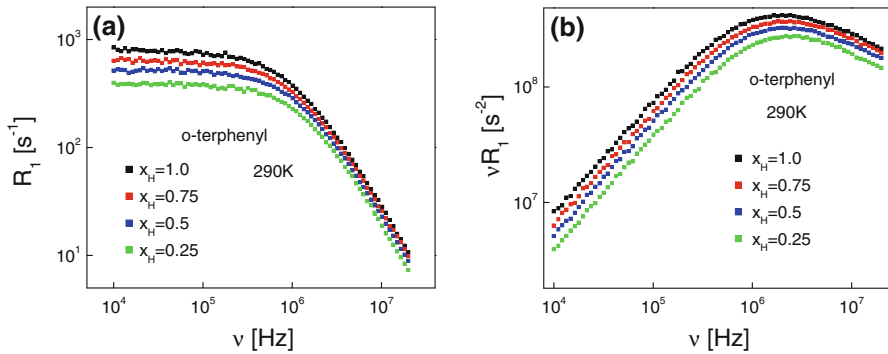


Fig. 6 **a** ^1H spin–lattice relaxation rate of *o*-terphenyl as a function of frequency, **b** the same data in the susceptibility representation

different mole fractions x_H at $T = 290$ K are shown in Fig. 6a and in the susceptibility representation $\chi''_{\text{NMR}}(\nu) = \nu/T_1(\nu)$ in Fig. 6b. In Fig. 7a the corresponding susceptibility master curves $\chi''_{\text{NMR}}(\omega\tau_{\text{rot}})$ (cf. Sect. 1) are displayed. The corresponding shift factor of the individual data sets can be identified with the correlation time τ_{rot} . The rotational correlation times obtained in this way agree well with those obtained from ^2H NMR [32] and light scattering [33] (cf. Fig. 7b). Moreover, in Figs. 6b and 7b no influence of the ratio x_H on the dynamics is seen as there is no visible shift of the susceptibility peaks (cf. Fig. 6b).

The amplitude of the master curves in Fig. 7a decreases linearly with x_H (cf. inset Fig. 7a) as expected, however, one should note that the fraction of the intermolecular relaxation contribution does not strongly change with ω . Extrapolating to $x_H \rightarrow 0$ yields the intramolecular part $R_{1,\text{intra}}(\nu)$, while the intermolecular contribution is obtained according to $R_{1,\text{inter}}(\nu) = R_1(\nu) - R_{1,\text{intra}}(\nu)$ [16]. The results are displayed in Fig. 8a. Regarding the amplitude, the intramolecular (red symbols) and intermolecular (blue symbols) contributions are quite similar, once again

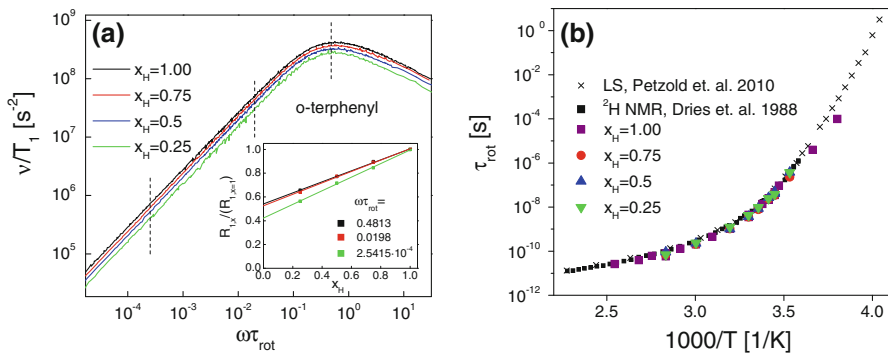


Fig. 7 **a** Susceptibility ^1H NMR master curves obtained from relaxation dispersion data measured over the temperature range of 283–353 K, *inset* the reduced relaxation rate as a function of the mole fraction x_H , **b** rotational time constants τ_{rot} of *o*-terphenyl as obtained from FC ^1H NMR by constructing the master curves, compared to those from ^2H NMR [32] and dynamic light scattering [33]

demonstrating the relevance of the intermolecular relaxation in molecular liquids. The time constants τ_{rot} extracted when constructing the master curves for each x_{H} are (as expected) virtually the same independently of x_{H} (cf. Fig. 7b). Also the spectral shapes of both contributions look very similar; however, at low frequencies small but systematic differences between $R_{1,\text{inter}}(\nu)$ and $R_{1,\text{intra}}(\nu)$ are revealed which are better disclosed when the original relaxation rates (at 290 K) are plotted as a function of $\sqrt{\nu}$ (cf. Fig. 9). Whereas, the intramolecular part exhibits a flat low-frequency behavior, the intermolecular relaxation contribution as well as the total relaxation rate exhibit the same linear low-frequency behavior. Thus, although $R_{1,\text{inter}}(\nu)$ and $R_{1,\text{intra}}(\nu)$ look rather similar when displayed double logarithmically as a function of ν , they can be well distinguished by their limiting behavior at low

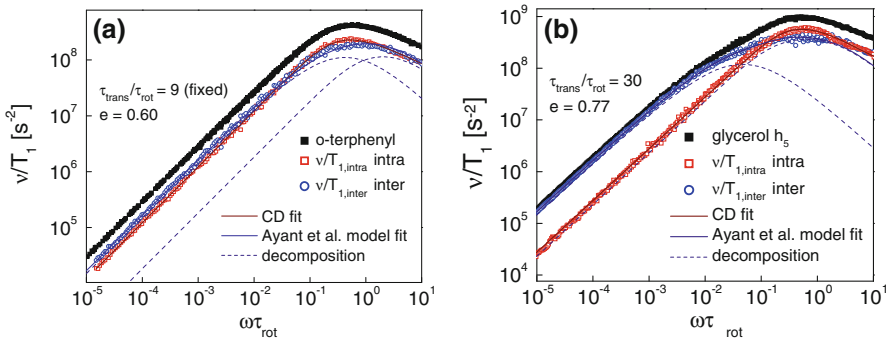


Fig. 8 **a** Susceptibility master curves $\chi''_{\text{NMR}}(\omega\tau_{\text{rot}})$ of the total (black solid squares), the intra- (red open squares) and the intermolecular relaxation contribution (blue open circles) for *o*-terphenyl; interpolation of intermolecular part by the eccentricity model of Ayant et al. [31] (solid blue line) and the intramolecular part by a Cole–Davidson function (solid red line); decomposition of intermolecular relaxation into the purely translational part given by the hard sphere free diffusion model [20, 21] and the remaining contribution due to eccentricity effects (dashed blue lines), **b** analog data for glycerol [16] (color figure online)

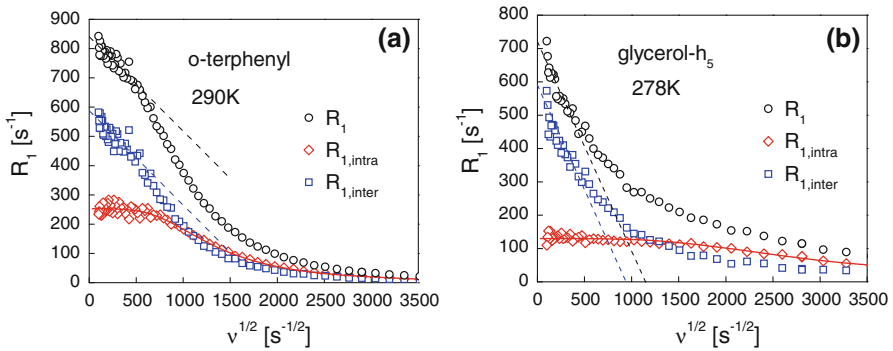


Fig. 9 **a** Relaxation rates R_1 versus square root of frequency $\sqrt{\nu}$ of *o*-terphenyl at 290 K (black circles) and their separation in intra- and intermolecular contributions (red and blue circles); red line CD fit, **b** analogous figure for glycerol- h_5 at 278 K (color figure online)

frequencies when plotted versus $\sqrt{\nu}$. Moreover, the linear behavior in $\sqrt{\nu}$ still survives for the total relaxation rate $R_1(\sqrt{\nu})$, since $\tau_{\text{trans}} > \tau_{\text{rot}}$ always holds.

For comparison, in Fig. 8b we included once again our result from the isotope dilution experiment for glycerol. In this case, as discussed above, the total relaxation rate $R_1(\nu)$ shows a low-frequency shoulder which is absent in the intramolecular part (red symbols), what confirms its intermolecular origin. In contrast to *o*-terphenyl, for glycerol also the intermolecular part (blue symbols) shows a bimodal spectral shape with a strong maximum at high frequencies which originates from the rotational influence due to eccentricity effects. In both cases, *o*-terphenyl and glycerol, the intermolecular contributions can be reproduced by the model of Ayant et al. [31] (cf. Sect. 2.1) see Fig. 8. Overall, the fits are satisfying although, as said, this model does not reproduce the high-frequency behavior ($\omega\tau_{\text{rot}} > 1$), since it does not take into account the non-Debye character of the rotational dynamics in viscous liquids. For glycerol the obtained ratio $r = 30$ is somewhat smaller than the previously reported $r_{\text{app}} \approx 50$ [16] which in any case is significantly beyond the Stokes–Einstein–Debye limit $r = 9$.

The eccentricity $e = 0.77$ suggests that the average distance of a spin to the center of the molecule is about three quarters of its radius. The diameter (or distance of closest approach) is found $d = 3.5 \cdot 10^{-10}\text{m}$. Again this is in agreement with the previously reported values (cf. Table 1) [34]. With *o*-terphenyl the corresponding parameters are less conclusive. Here one has to fix the ratio r to get a convergence of the fitting procedure; we fixed it to the hydrodynamic value $r = 9$. Then the eccentricity $e = 0.60$ and the diameter $d = 3.72 \cdot 10^{-10}\text{m}$ are rather small with respect to values reported from other techniques (cf. Table 1). In contrast to glycerol- h_5 , for *o*-terphenyl the positions of the maxima of the intramolecular relaxation and the part of intermolecular contributions which is associated with rotation do not coincide (cf. Fig. 8a). This might stem from the fact that although the model of Ayant et al. [31] is an exact mathematical solution of the problem of intermolecular spectral density, it assumes spherical molecules.

Regarding the experimental finding of $r_{\text{app}} \approx 50$, for glycerol and other liquids [13, 16] one could argue that this large apparent separation could be in agreement with the Stokes–Einstein–Debye relation $r = 9$, but under the condition of a large eccentricity. This is indeed possible, but the required value $e \approx 0.9$ seems to be too large especially for glycerol- h_5 .

A comparison of Fig. 9a, b also visualizes the impact of the rotationally driven relaxation contributions on the shape of the total relaxation curves. One sees that for

Table 1 Diameters of glycerol and *o*-terphenyl molecules obtained by applying the eccentricity model of Ayant et al. [31] compared to the values obtained from diffusion coefficient measurements by field gradient NMR diffusometry and to van der Waals diameter from gas phase data [34]

Diameter	van der Waals [34] (Å)	Field gradient NMR [34] (Å)	Eccentricity model (Å)
Glycerol	4.4	3.2	3.5
<i>O</i> -Terphenyl	7.6	4.6	3.72

glycerol-h₅ (cf. Fig. 9b) the intramolecular relaxation (red open circles) does not exhibit dispersion, until reaching quite high frequencies; obviously the same is expected for the rotationally mediated part of the intermolecular contribution. In consequence, the total rate $R_1(\sqrt{\nu})$ (as well intermolecular part $R_{1,inter}(\sqrt{\nu})$) departs from the linear behavior in upward direction due to the dispersion of the relaxation rate associated with the translational dynamics. For *o*-terphenyl $R_1(\sqrt{\nu})$ bends downwards due to the dispersion of the rotationally driven relaxation which is observed at much lower frequencies than for glycerol. Thus, the fact that $R_{1,inter}(\sqrt{\nu})$ is also affected by the rotational dynamics is now clearly seen as it also bends downwards (cf. Fig. 9a). But yet at lower frequencies the linear behavior due to translation still prevails in both curves $R_1(\sqrt{\nu})$ and $R_{1,inter}(\sqrt{\nu})$ (cf. dashed lines in Fig. 9a).

4.2 Master Curves for the Total Relaxation Rate

The discussion of Sect. 2.2 implies that the reduced total relaxation rate $R_1(\nu)/R_1(0)$ plotted versus $0.7 \cdot \sqrt{\omega\tau'}$ (Eq. 12) yields a master curve provided that translational–rotational coupling holds. In Fig. 10a the glycerol relaxation rates measured at different temperatures plotted versus square root of the frequency are shown. The linear behavior at low frequencies is well visible and allows for extrapolating to the $R_1(0)$ limit. Given $R_1(0)$ the time constants τ' can be chosen in such a way that the individual data form the master curve described by Eq. (12). This is demonstrated in Fig. 10b; data collected in a broad temperature range coincide.

In Fig. 11 analogous master curves obtained for different liquids are shown. They all coincide in the linear, low-frequency range, but they show quite different behaviors beyond this limit. Whereas the curves for *o*-terphenyl and tristyrene bend downwards, all other curves bend upwards with respect to the low-frequency limit.

As demonstrated in Sect. 2.2, the character of the deviations from the linearity depends on the interplay between the rotationally and translationally driven relaxation contributions (cf. Fig. 5) and thus varies for different liquids. Glycerol, its homologues (DL-threitol, xylitol, sorbitol) and propylene glycol show translation-

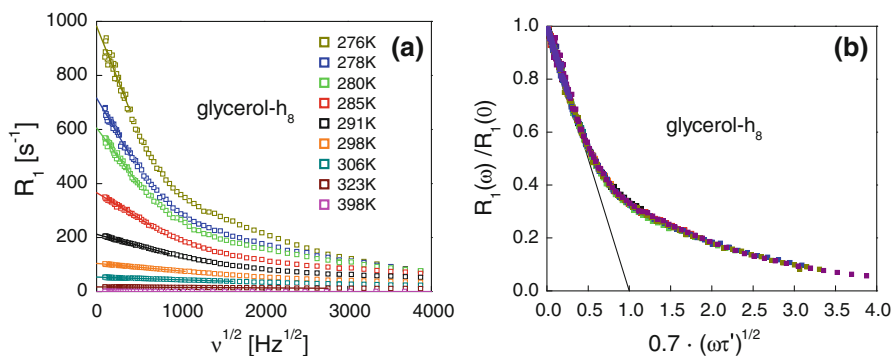


Fig. 10 **a** ¹H relaxation rates of glycerol at different temperatures versus $\sqrt{\nu}$, **b** master curve constructed from the data shown in **a**; the straight line indicates the limiting behavior at low frequencies

dominated (bending upwards from linear behavior) relaxation curves. It is known that for these liquids the ratio $r = \tau_{\text{rot}}/\tau_{\text{trans}}$ is rather large [13, 16]. On the other hand, the rotational shape (the relaxation curve bending downwards) is observed only for *o*-terphenyl and tristyrene. This indicates a rather small r and a relatively large contribution of the rotationally driven terms which may originate from large eccentricity and/or strong intramolecular coupling. Finally, the master curve of 2,3-butanol has an intermediate shape.

The data shown in Fig. 11 have been used for extracting translational diffusion coefficients according to the procedure applied by us previously to other liquids [23]. Figure 12 comprises the diffusion coefficients D for the new results and the

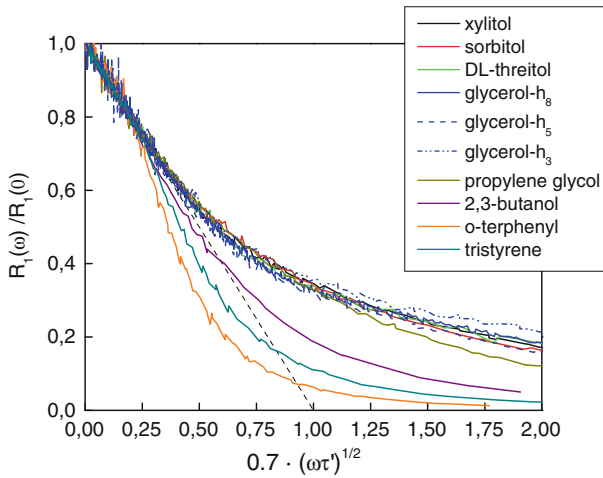


Fig. 11 ¹H NMR master curves for different liquids: reduced relaxation versus square root of rescaled frequency; *dashed line* low-frequency limit

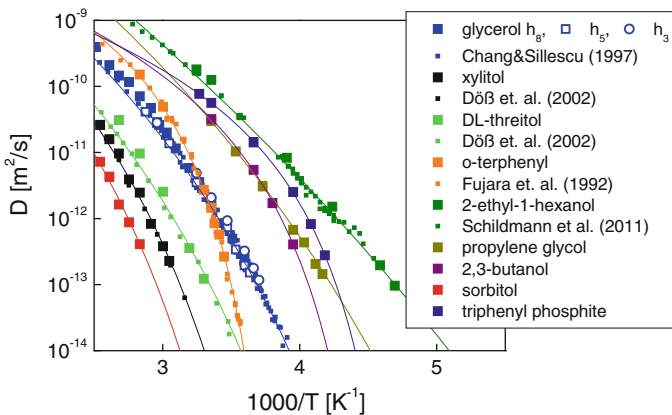


Fig. 12 Translational diffusion coefficient D (*large symbols*) as function of reciprocal temperature and comparison with diffusion data (*small symbols*) obtained from field gradient NMR [22, 34–36]

previous ones plotted versus reciprocal temperature. The results of NMR relaxometry agree very well with the values obtained by field-gradient NMR diffusometry [22, 34–36].

5 Conclusions

Performing ^1H FC NMR relaxometry experiments for isotopically (^2H) diluted glycerol and *o*-terphenyl, the overall relaxation has been unambiguously decomposed into intra- and intermolecular parts. It has been demonstrated that the intermolecular relaxation stems from a combined effect of translational and rotational dynamics modulating intermolecular dipole–dipole interactions. The rotational influence on the intermolecular relaxation originating from non-central positions of the interacting spins (eccentricity effects) has been described in terms of the eccentricity model proposed by Ayant et al. [31], which provides mathematical form of the intermolecular spectral density including the joint effect of translation and rotation. The spectral density of the model can be decomposed in a sum of purely translational and purely rotational terms. Describing the rotational term as a CD function one can, to a certain extent, mimic the broadening of the spectral density predicted by Ayant et al. [31] as a result of rotational correlation times of different ranks entering the exact expression. Yet, the eccentricity model assumes rotational diffusion which does not apply in viscous liquids, and the CD function provides a better description at high frequencies. Finally, a criterion has been derived which allows for resolving which motional process gives the dominant contribution to the relaxation. Applying the criterion to several liquids, it has been shown that for glycerol and its homologues (threitol, xylitol, sorbitol) and propylene glycol the dominating influence on the intermolecular relaxation stems from translation, while for *o*-terphenyl and tristyrene the rotational effects prevail. Qualitatively, this can be explained by large eccentricity of protons in these molecules.

Acknowledgments We appreciate financial support of the Deutsche Forschungsgemeinschaft through the grant RO 907/15.

References

1. R. Kimmich, E. Anordo, *Prog. NMR Spectrosc.* **44**, 257 (2004)
2. D. Kruk, A. Herrmann, E.A. Rössler, *Prog. NMR Spectrosc.* **63**, 33 (2012)
3. S. Grosse, F. Gubaydullin, H. Scheelken, H.-M. Vieth, A. Yurkovskaya, *Appl. Magn. Reson.* **17**, 211–225 (1999)
4. K.L. Ivanov, A.V. Yurkovskaya, H.-M. Vieth, *J. Chem. Phys.* **129**, 234513 (2008)
5. S. Korchak, K. Ivanov, A. Yurkovskaya, H.-M. Vieth, *J. Chem. Phys.* **133**, 194502 (2012)
6. R. Meier, R. Kahlau, D. Kruk, E.A. Rössler, *J. Phys. Chem. A* **114**, 7847 (2010)
7. P. Lunkenheimer, U. Schneider, R. Brand, A. Loidl, *Contemp. Phys.* **41**, 15 (2000)
8. A. Kudlik, S. Benkhof, T. Blochowicz, C. Tschirwitz, E. Rössler, *J. Mol. Struct.* **479**, 201 (1999)
9. T. Blochowicz, A. Brodin, E.A. Rössler, *Adv. Chem. Phys.* **133 Part A**, 127 (2006)
10. C.J.F. Böttcher, P. Bordewijk, *Theory of Electric Polarization*, Vol. 2. (Elsevier, Amsterdam, 1973)

11. S. Kariyo, C. Gainaru, H. Schick, A. Brodin, V.N. Novikov, E.A. Rössler, *Phys. Rev. Lett.* **97**, 207803 (2006)
12. S. Kariyo, A. Brodin, C. Gainaru, A. Herrmann, J. Hintermeyer, H. Schick, V.N. Novikov, E.A. Rössler, *Macromolecules* **41**, 5322 (2008)
13. D. Kruk, R. Meier, E.A. Rössler, *J. Phys. Chem.* **115**, 951 (2011)
14. W. Götz, *Complex Dynamics of Glass-Forming Liquids* (Oxford University Press, Oxford, 2009)
15. A. Abragam, *The Principles of Nuclear Magnetism* (Clarendon Press, Oxford, 1961), p. 302
16. R. Meier, D. Kruk, J. Gmeiner, E.A. Rössler, *J. Chem. Phys.* **136**, 034508 (2012)
17. J.P. Kintzinger, M.D. Zeidler, *Ber. Bunsenges. Phys. Chem.* **77**, 98 (1972)
18. M. Kehr, N. Fatkullin, R. Kimmich, *J. Chem. Phys.* **126**, 094903 (2007)
19. A. Herrmann, B. Kresse, M. Wohlfahrt, I. Bauer, A.F. Privalov, D.Kruk, N. Fatkullin, F. Fujara, E.A. Rössler, *Macromolecules* **45**, 6516 (2012)
20. L.P. Hwang, J.H. Freed, *J. Chem. Phys.* **63**, 4017 (1975)
21. Y. Ayant, E. Belorizky, J. Alizon, J. Gallice, *J. Phys. (Paris)* **36**, 991 (1975)
22. F. Fujara, B.H. Sillescu, G. Fleischer, *Z. Phys. B Condens. Matter* **88**, 195 (1992)
23. D. Kruk, R. Meier, E.A. Rössler, *Phys. Rev. E* **85**, 020201 (R) (2012)
24. E. Belorizky, P.H. Fries, *Chem. Phys. Lett.* **145**, 1 (1988)
25. H.C. Torrey, *Phys. Rev.* **92**, 962 (1953)
26. H.E. Heinze, H. Pfeiffer, *Z. Phys.* **192**, 329 (1966)
27. J.F. Harmon, B.H. Muller, *Phys. Rev.* **400**, 182 (1969)
28. C.A. Sholl, *J. Phys. C* **14**, 447 (1981)
29. E. Belorizky, D.G. Gilies, W. Gorecki, K. Lang, F. Noack, C. Roux, J. Struppe, L.H. Sutcliffe, J.P. Travers, X. Wu, *J. Phys. Chem. A* **102**, 3674 (1998)
30. U. Stark, E. Cebe, K. Meise-Gresch, W. Müller Warmuth, *J. Mol. Liq.* **52**, 67 (1992)
31. Y. Ayant, E. Belorizky, P. Fries, J. Rosset, *J. Phys. (Paris)* **38**, 325 (1977)
32. Th Dries, F. Fujara, M. Kiebel, E. Rössler, H. Sillescu, *J. Chem. Phys.* **88**, 2139 (1988)
33. N. Petzold, E.A. Rössler, *J. Chem. Phys.* **133**, 124512 (2010)
34. I. Chang, H. Sillescu, *J. Phys. Chem.* **101**, 8794 (1997)
35. A. Döß, M. Paluch, H. Sillescu, G. Hinze, *J. Chem. Phys.* **117**, 6582 (2002)
36. S. Schildmann, A. Reiser, R. Gainaru, C. Gainaru, R. Böhmer, *J. Chem. Phys.* **135**, 174511 (2011)

Publication 5

Long-Time Diffusion in Polymer Melts Revealed by ^1H NMR
Relaxometry.

Meier, R; Herrmann, A.; Kresse, B.; Privalov, A.F.; Kruk, D.; Fujara, F.; Rössler, E.A.
ACS Macro Lett. **2013**, 2, 96.

Copyright 2013 by The American Chemical Society

DOI: 10.1021/mz300571t

Long-Time Diffusion in Polymer Melts Revealed by ^1H NMR Relaxometry

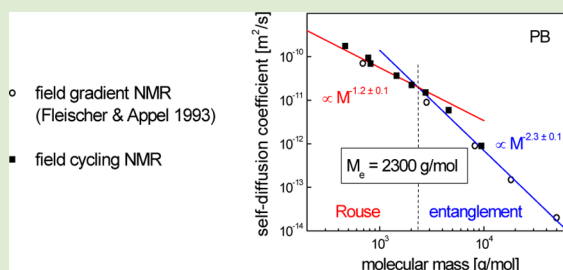
R. Meier,[†] A. Herrmann,[†] B. Kresse,[‡] A. F. Privalov,[‡] D. Kruk,[§] F. Fujara,[‡] and E. A. Rössler^{*,†}

[†]Experimentalphysik II, Universität Bayreuth, 95440 Bayreuth, Germany

[‡]Institut für Festkörperphysik, Technische Universität Darmstadt, Hochschulstr. 6, 64289 Darmstadt, Germany

[§]University of Warmia and Mazury in Olsztyn, Faculty of Mathematics and Computer Science, Sloneczna 54, PL-10710 Olsztyn, Poland

ABSTRACT: We demonstrate that field-cycling ^1H NMR relaxometry can be used as a straightforward method of determining translational diffusion coefficient $D = D(M)$ in polymer systems. The ^1H spin–lattice relaxation dispersion for polybutadiene of different molecular masses M ($446 < M/(\text{g mol}^{-1}) < 9470$) is measured at several temperatures ($233 < T/\text{K} < 408$) in a broad frequency range. The diffusion coefficient $D(T)$ is determined from the intermolecular contribution to the overall spin–lattice relaxation rate $R_1(\omega)$, which dominates in the low-frequency range and follows a universal dispersion law linear in $\sqrt{\omega}$. The extracted diffusion coefficients are in good agreement with the values obtained previously by field gradient NMR. The molecular mass dependence $D = D(M)$ exhibits two power laws: $D \propto M^{-1.3 \pm 0.1}$ and $\propto M^{-2.3 \pm 0.1}$. They show a crossover for $M = 2300$, a value that is close to the entanglement molecular mass M_e of polybutadiene. The corresponding power-law exponents are close to the prediction of the tube-reptation model.



Field-cycling (FC) ^1H NMR relaxometry has become a powerful tool for investigating dynamics of polymers.^{1,2} By varying the external magnetic field B , the frequency dependence of the spin–lattice relaxation rate $R_1(\omega) = T_1^{-1}(\omega)$ can be measured up to five decades in frequency if an earth field compensation is employed.^{3,4} By converting the relaxation dispersion into the susceptibility representation $\chi''_{\text{NMR}}(\omega) = \omega \cdot R_1(\omega)$ and then applying frequency–temperature superposition (FTS), master curves $\chi''_{\text{NMR}}(\omega\tau_s)$ are obtained; τ_s denotes the correlation time of the segmental (local) dynamics.^{2,5,6} As at low temperatures the NMR relaxation is solely determined by the segmental dynamics (other dynamical processes are too slow to act as an effective relaxation mechanism), τ_s is directly accessible. FTS is an important property of cooperative dynamics in condensed matter and has been applied for a long time, for example, in rheology of polymers. This procedure allows extending the covered frequency range and including both the polymer and the segmental dynamics into the master curve. Consequently, converting then the master curve into the time domain, the dipolar correlation function $C_{\text{DD}}(t)$ is obtained for a time range encompassing 10 decades. Characteristic power-law regimes of the correlation function can be identified and compared with the prediction of polymer theories, for example, the Doi–Edwards tube-reptation model.⁷ Moreover, the segmental mean square displacement of the polymer can be accessed in the subdiffusive regime.^{8,9}

The proton spin–lattice relaxation rate, $R_1(\omega)$, consists of intramolecular and intermolecular parts: $R_1(\omega) = R_1^{\text{intra}}(\omega) +$

$R_1^{\text{inter}}(\omega)$.¹⁰ The intramolecular contribution stems from protons belonging to the same molecule, while the intermolecular contribution originates from dipole–dipole interactions between protons of different molecules. Thus, $R_1^{\text{intra}}(\omega)$ is solely associated with molecular rotation, whereas $R_1^{\text{inter}}(\omega)$ is predominantly mediated by translational diffusion. This enables ^1H NMR relaxometry to probe the translational motion, which has recently been demonstrated for low molecular mass liquids.^{11,12} A comparison of the ^1H NMR relaxation results in the susceptibility representation with dielectric spectroscopy data has revealed that the NMR susceptibility shows a low-frequency excess contribution (of varying amplitude) in addition to the primary or α -relaxation peak.¹³ We have confirmed that the excess contribution originates from the intermolecular relaxation contributions to the total relaxation rate $R_1(\omega)$.¹⁴ The ultimate proof has been given by isotope dilution experiments,¹⁵ that is, the excess contribution disappears when the protonated molecules are substituted by their deuterated counterpart, whose interactions with protons are much weaker. The extrapolation of the relaxation data to zero concentration limit gives $R_1^{\text{intra}}(\omega)$ and, hence, also $R_1^{\text{inter}}(\omega)$.

The translational dipolar correlation function $C_{\text{inter}}(t) = \langle Y_m^{2*}(\Omega(t))Y_m^2(\Omega(0))/r^3(t)r^3(0) \rangle$ describes fluctuations of the interspin distance r and the orientation of interspin axis with

Received: October 26, 2012

Accepted: December 13, 2012

Published: January 11, 2013

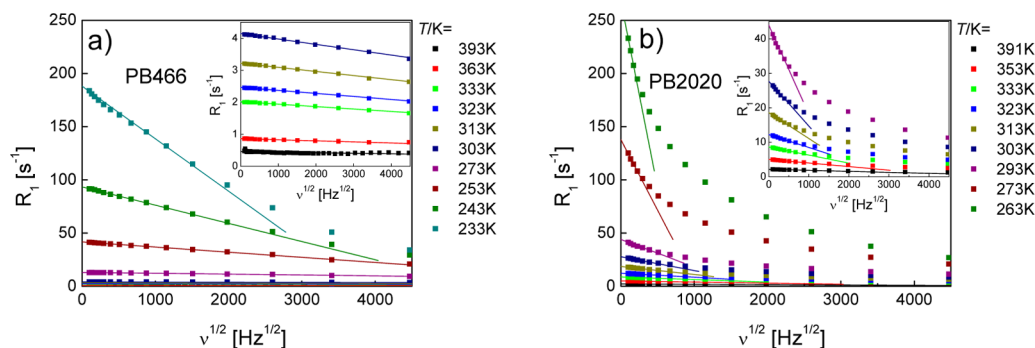


Figure 1. ¹H spin–lattice relaxation rates R_1 of polybutadiene (PB) $M = 466$ (a) and $M = 2020$ (b) plotted as a function of the square root of the Larmor frequency $\sqrt{\nu}$ in the temperature range as indicated (data from ref 3).

respect to the direction of the external magnetic field via the angle Ω encoded in spherical harmonics of rank two Y_m^2 . At long times, the correlation function follows the power law $C_{\text{inter}}(t) \propto t^{-3/2}$, which is characteristic of free diffusion.¹⁶ As a result, the spectral density (Fourier transform of the correlation function) and thus $R_1(\omega)$ depends linearly on the square root of the resonance frequency, $\sqrt{\omega}$.^{16–19} As shown for low- M liquids,¹¹ the rotational correlation time is significantly shorter than the corresponding correlation time for translational motion, as expected. Combining this dependence of the spectral density with the expression for the total ¹H spin–lattice relaxation rate,¹⁰ the low-frequency expansion (up to the first-order term and in absence of other NMR active nuclei) of the relaxation dispersion is given by^{16–19}

$$R_1(\omega) = R_1^{\text{intra}}(\omega) + R_1^{\text{inter}}(\omega) = R_1(0) - \frac{B}{D^{3/2}} \cdot \sqrt{\omega} \quad (1)$$

with

$$B = \frac{\pi}{30} \cdot (1 + 4\sqrt{2}) \cdot \left(\frac{\mu_0}{4\pi} \hbar \gamma_{\text{H}}^2 \right)^2 \cdot N$$

where γ_{H} is the proton gyromagnetic ratio and N is the spin density, that is, the number of spins per unit volume. The intramolecular contribution associated with reorientational dynamics is included in $R_1(0)$. This is allowed as the rotational contribution is frequency independent in the low-frequency range, that is, $\omega\tau_{\text{rot}} \ll 1$ (τ_{rot} denotes the rotational correlation time).

The important fact is that, besides the standard physical constants, the factor B only depends on N . It does not include any details of a diffusion model.¹⁶ Although eq 1 is well-known, its potential could have been fully exploited only lately due to commercial availability of FC spectrometers. Recently, diffusion coefficients of several liquids have been determined via eq 1 and they are in excellent agreement with those of field gradient (FG) NMR diffusometry.^{11,12}

In the present contribution, we demonstrate that the described approach can also be applied to polymer systems, and polybutadiene melts of different molecular masses M (mass average) are used as an example. There eq 1 applies for $\omega \ll 1/\tau_t$, where τ_t is the terminal relaxation time, that is, the Rouse time or the disengagement time of the tube-reptation model for nonentangled and entangled polymers, respectively (where one assumes that $\tau_t \propto D^{-1}$).

The dispersion of the spin–lattice relaxation above 10 kHz was measured by an electronic field cycling spectrometer

Spinmaster FFC 2000 manufactured by STELAR. Experiments were performed in the temperature range $233 < T/\text{K} < 408$. The relaxometer covers a ¹H frequency range from $\nu = \omega/2\pi = 10$ kHz to 20 MHz (for ¹H), while the switching time from high polarization field to relaxation field is 3 ms. Lower ¹H frequencies were reached using a home-built spectrometer in Darmstadt operating down to 400 Hz.³ The low frequencies were achieved by utilizing a three-dimensional resistive coil arrangement for compensating for the earth field and other magnetic stray fields.⁴ The relaxation rate R_1 was determined by an exponential fit of the magnetization decay curve. The results have been published previously in the susceptibility representation.³ In the present contribution we display and analyze the corresponding relaxation dispersion curves.

Figure 1a presents the spin–lattice relaxation rate R_1 plotted against the square root of the frequency $\sqrt{\nu}$ for polybutadiene (PB) with rather small molecular mass $M/(\text{g}\cdot\text{mol}^{-1}) = 466$ (PB 466). The polymer chains are still so short that essentially no polymer dynamics is discovered and the system relaxes like a low-molecular mass liquid.^{2,3} The solid lines at low frequencies indicate the limiting, linear part of the relaxation dispersion. At higher frequencies, the relaxation dispersion deviates from linearity, and the linear part shrinks with decreasing temperature (cf. inset in Figure 1a). The deviation from the linear behavior is caused by the increasing importance of higher order terms of the expansion of the translational spectral density (eq 1) and by a dispersion of the intramolecular relaxation contribution for which the extreme narrowing condition ($\omega\tau_{\text{rot}} \ll 1$) does not hold any longer.

Figure 1b shows the relaxation rates R_1 versus $\sqrt{\nu}$ for PB of $M = 2020$ which is close to the entanglement molecular mass $M_e \cong 1800$.²⁰ Again, the solid lines indicate the linear part of the relaxation dispersion observed at low frequencies. Compared to the low- M system, PB 466, the range in which $R_1(\sqrt{\nu})$ behaves linearly is rather small, but it becomes larger at high temperatures (cf. inset of Figure 1b). The pronounced difference from the data of low- M polybutadiene in Figure 1a is caused by a significantly slower as well as by a stronger relaxation dispersion due to polymer specific dynamics (cf. below).

We analyzed the relaxation dispersion for a series of polybutadienes of molecular masses $M = 466, 777, 816, 1450, 2020, 2760, 4600, 9470$ at several temperatures (data from ref 3). The procedure cannot be applied to higher M values as the linear regime in Figure 1 becomes too small or is even beyond the accessible frequency range. The relaxation data are shown as master curves in Figure 4 and discussed further below. The values of the diffusion coefficients, $D = D(T)$, are extracted

from the slope of the linear part in Figure 1 and from corresponding plots for the polybutadienes with different molecular masses using eq 1, and displayed in Figure 2. For all

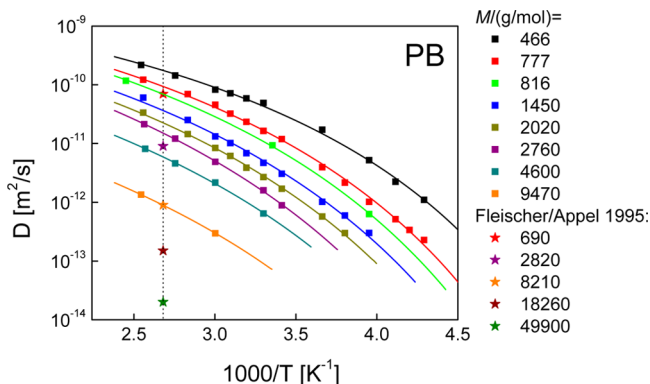


Figure 2. Diffusion coefficient $D(T)$ for polybutadiene of different molecular masses M as indicated extracted applying eq 1. Lines: interpolation by VFT equation. Stars: results from field gradient NMR at $T = 373$ K reported by Fleischer and Appel.²¹

polybutadienes, the spin density $N = 5.75 \times 10^{28} \text{ m}^{-3}$ was taken as provided by the mass density $\rho = 0.86 \text{ g/cm}^3$.²⁰ The temperature dependence of N is marginal when comparing diffusion coefficients on logarithmic scales. A super-Arrhenius temperature dependence of the diffusion coefficients is observed, and for each molecular mass $D(T)$ can be well interpolated by the Vogel–Fulcher–Tammann (VFT) equation. There is a trend that the M dependence becomes stronger at high M . Note that the temperature range in which the diffusion coefficients can be determined narrows with increasing M . For comparison, we included the results of Fleischer and Appel, which have been obtained at 373 K by applying FG NMR which is presently the standard method measuring diffusion coefficients in polymers.²¹

The M dependence of D is presented in Figure 3 and is obtained by interpolating $D(T)$ from FC NMR at $T = 373$ K (dashed line in Figure 2). The results from both FC and FG NMR nicely agree though the FC data appear to be systematically slightly higher. Two power-laws $D \propto M^{-\alpha}$ are

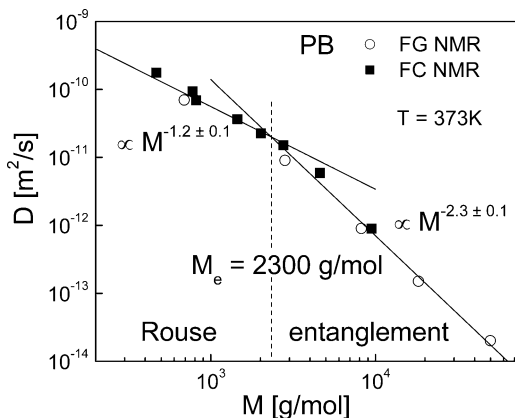


Figure 3. Dependence of the diffusion coefficient D on molecular mass M , as obtained by field cycling (FC) NMR relaxometry and by field gradient (FG) NMR;²¹ solid lines: power laws with exponents as indicated; arrow marks the crossover at a molecular mass being close to M_e .

revealed with a crossover at $M \cong 2300$, which is quite close to the entanglement molecular mass $M_e \cong 1800$.²⁰ The tube-reptation model predicts $\alpha = 1$ for the Rouse regime and $\alpha = 2$ for the entanglement regime. Fleischer and Appel have attributed all their data points to the latter regime and have reported an exponent $\alpha = 2.0$.²¹ Considering the combined results of NMR relaxometry and diffusometry, it seems that for low M the Rouse regime is already seen. By interpolating both data sets (straight lines), it has been obtained: $\alpha = 1.2 \pm 0.1$ for $M < M_e$ and $\alpha = 2.3 \pm 0.1$ for $M > M_e$. To our knowledge, this is the first time that the crossover in $D(M)$ has been found for PB. In another work, Fleischer and Appel found two regimes in the case of polydimethylsiloxane (PDMS) and polyethylene oxide (PEO).²² In the entanglement region, the exponent is similar to that found for polystyrene²³ and hydrogenated polybutadiene.²⁴ It is well-known that the tube-reptation model needs some modifications to account for effects such as constraint release or contour length fluctuations.⁷

Equation 1 implies that ^1H relaxation dispersion results obtained at different temperatures can be scaled to follow a master curve, at least at low frequencies where the expansion in eq 1 applies.¹² Thus, eq 1 can be rewritten in a master curve form:

$$R_1(\omega)/R_1(0) = 1 - \sqrt{\omega\tau_{\text{res}}} \quad (2)$$

where

$$\tau_{\text{res}} = \left(\frac{\frac{\pi}{30}(1 + 4\sqrt{2}) \left(\frac{\mu_0 \hbar \gamma^2}{4\pi} \right)^2 N}{R_1(0)D^{3/2}} \right)^2$$

In Figure 4, such master curves are displayed for a series of polybutadienes investigated in the temperature range as

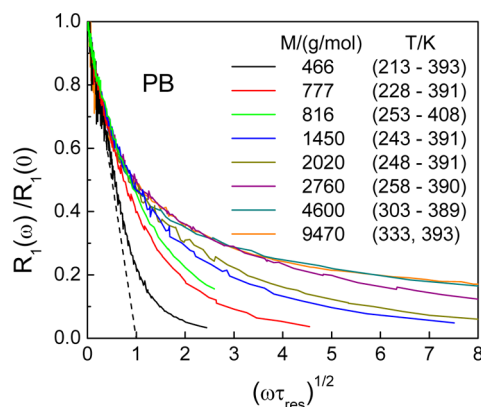


Figure 4. Master curves of PB of different M constructed from ^1H spin–lattice relaxation dispersion data obtained in the indicated temperature ranges along eq 2; dashed line: universal linear low-frequency limit.

indicated. Note that the master curves contain all relaxation data discussed in the present paper (taken from ref 3), and for a given M value, the data collapse even at high frequencies beyond the linear low-frequency regime. This is a consequence of the fact that translational-rotational coupling or more generally FTS applies in good approximation for polymer melts. The master curves for different M coincide in the linear low frequency range but systematically differ at higher reduced frequencies $(\omega\tau_{\text{res}})^{0.5}$. Whereas for PB 466 the reduced

relaxation rate $R_1(\omega)/R_1(0)$ follows the linear dependence in a wide frequency range, for the high- M polymers this regime is significantly smaller and eventually, for $M > 9470$, vanishes. The progressing bending over of $R_1 = R_1(\sqrt{\omega})$ for increasing M stems from increasing contributions of polymer specific relaxation terms reflecting Rouse and entanglement dynamics to the overall relaxation. In terms of their time-scale, they are located between the terminal relaxation and the segmental relaxation as demonstrated in our previous publications.^{2,3}

In conclusion, the present study demonstrates that the method of determining the diffusion coefficient from the low-frequency slope of the ^1H spin–lattice relaxation dispersion, as already applied to low-molecular mass liquids,^{11,12} can also be used for neat polymers. An extension to polymer solutions is not straightforward as the method probes the relative translational displacements among the proton bearing species. NMR relaxometry allows probing rotational and translational dynamics of polymer systems in a single experiment. The rotational dynamics has been discussed in our previous works, in which the temperature and molecular mass dependencies of the segmental (reorientational) contribution dominating the high-frequency behavior of the relaxation rate were analyzed in addition to the polymer specific.^{2,3,5,6} In the present work, the low-frequency features of the ^1H relaxation rate were used to complete the analysis of the polymer dynamics by extracting the diffusion coefficients and inquire into their dependence on temperature and molecular mass. Note that this evaluation is only possible by attaining the relaxation rate at extremely low frequencies. The obtained $D(M)$ data agree well with those reported by FG NMR, thus making FC NMR a further technique probing diffusion of condensed matter.

AUTHOR INFORMATION

Corresponding Author

*E-mail: ernst.roessler@uni-bayreuth.de.

Notes

The authors declare no competing financial interest.

REFERENCES

- (1) Kimmich, R.; Fatkullin, N. *Adv. Polym. Sci.* **2004**, *170*, 1–113.
- (2) Kruk, D.; Herrmann, A.; Rössler, E. A. *Prog. NMR Spectrosc.* **2012**, *63*, 33–64.
- (3) Herrmann, A.; Kresse, B.; Gmeiner, J.; Privalov, A. F.; Kruk, D.; Fujara, F.; Rössler, E. A. *Macromolecules* **2012**, *45*, 1408–1416.
- (4) Kresse, B.; Privalov, A. F.; Fujara, F. *Solid State Nucl. Magn. Reson.* **2011**, *40*, 134–137.
- (5) Kariyo, S.; Gainaru, C.; Schick, H.; Brodin, A.; Novikov, V. N.; Rössler, E. A. *Phys. Rev. Lett.* **2006**, *97*, 207803. Erratum: Herrmann, A.; Gainaru, C.; Schick, H.; Brodin, A.; Novikov, V. N.; Rössler, E. A. *Phys. Rev. Lett.* **2008**, *100*, 109901.
- (6) Kariyo, S.; Brodin, A.; Gainaru, C.; Herrmann, A.; Schick, H.; Novikov, V. N.; Rössler, E. A. *Macromolecules* **2008**, *41*, 5313–5321.
- (7) Doi, M.; Edwards, S. F. *The Theory of Polymer Dynamics*; Oxford Science Publications: Oxford, 1986.
- (8) Kehr, M.; Fatkullin, N.; Kimmich, R. *J. Chem. Phys.* **2007**, *127*, 084911.
- (9) Herrmann, A.; Kresse, B.; Wohlfahrt, M.; Bauer, I.; Privalov, A. F.; Kruk, D.; Fatkullin, N.; Fujara, F.; Rössler, E. A. *Macromolecules* **2012**, *45*, 6516–6526.
- (10) Abragam, A. *The Principles of Nuclear Magnetism*; Clarendon Press: Oxford, U.K., 1961.
- (11) Kruk, D.; Meier, R.; Rössler, E. A. *Phys. Rev. E* **2012**, *85*, 020201(R).
- (12) Meier, R.; Kruk, D.; Bourdick, A.; Schneider, E.; Rössler, E. A. *Appl. Magn. Reson.* **2012**, DOI: 10.1007/s00723-012-0410-1.
- (13) Meier, R.; Kahlau, R.; Kruk, D.; Rössler, E. A. *J. Phys. Chem. A* **2010**, *114*, 7847–7855.
- (14) Kruk, D.; Meier, R.; Rössler, E. A. *J. Phys. Chem. B* **2011**, *115*, 951–957.
- (15) Meier, R.; Kruk, D.; Gmeiner, J.; Rössler, E. A. *J. Chem. Phys.* **2012**, *136*, 034508.
- (16) Belorizky, E.; Fries, P. H. *Chem. Phys. Lett.* **1988**, *145*, 33–38.
- (17) Torrey, H. C. *Phys. Rev.* **1953**, *92*, 962–969.
- (18) Heinze, H. E.; Pfeiffer, H. Z. *Z. Phys.* **1966**, *192*, 329–339.
- (19) Harmon, J. F.; Muller, B. H. *Phys. Rev.* **1969**, *182*, 400–410.
- (20) Fetters, L. J.; Lohse, D. J.; Richter, D.; Witten, T. A.; Zirkel, A. *Macromolecules* **1994**, *27*, 4639–4647.
- (21) Fleischer, G.; Appel, M. *Macromolecules* **1995**, *28*, 7281–7283.
- (22) Fleischer, G.; Appel, M. *Macromolecules* **1993**, *26*, 5520–5525.
- (23) Antonietti, M.; Fölsch, K. J.; Sillescu, H. *Makromol. Chem.* **1987**, *188*, 2317–2324.
- (24) Lodge, T. P. *Phys. Rev. Lett.* **1999**, *83*, 3218–2321.

Publication 6

Iso-Frictional Mass Dependence of Diffusion of Polymer Melts Revealed
by ^1H NMR Relaxometry.

Meier, R; Herrmann, A.; Hofmann, M.; Schmidtke, B.; Kresse, B.; Privalov, A.F.; Kruk, D.;
Fujara, F.; Rössler, E.A.

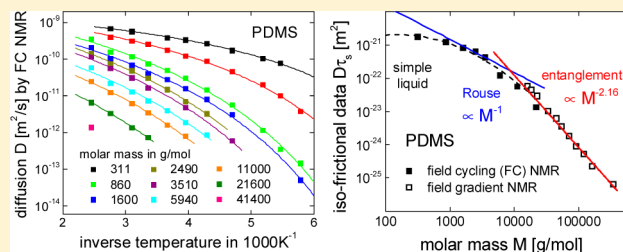
Macromolecules **2013**, *46*, 5538.

Copyright 2013 by The American Chemical Society

DOI: 10.1021/ma400881c

Iso-Frictional Mass Dependence of Diffusion of Polymer Melts Revealed by ^1H NMR RelaxometryR. Meier,[†] A. Herrmann,[†] M. Hofmann,[†] B. Schmidtke,[†] B. Kresse,[‡] A. F. Privalov,[‡] D. Kruk,[§] F. Fujara,[‡] and E. A. Rössler^{†,*}[†]Experimentalphysik II, Universität Bayreuth, 95440 Bayreuth, Germany[‡]Institut für Festkörperphysik, TU Darmstadt, Hochschulstrasse 6, 64289 Darmstadt, Germany[§]Faculty of Mathematics & Computer Science, University of Warmia & Mazury in Olsztyn, 10710 Olsztyn, Poland

ABSTRACT: We extract the translational diffusion coefficient $D(T, M)$ from field cycling (FC) ^1H NMR relaxometry which provides the relaxation dispersion of poly(dimethylsiloxane), 1,4-poly(butadiene), poly(styrene), 1,4-poly(isoprene), and poly(propylene glycol) with various molecular masses M . Oligomers with very low M , nonentangled ($M < M_e$), and entangled ($M > M_e$) polymers are included. The low-frequency ^1H NMR relaxation dispersion is dominated by translational dynamics and allows extracting D via benefiting from an universal dispersion power-law characteristic of free diffusion. In order to correct for the additional mass dependence of the monomeric friction coefficient observed at low M and controlled by the M dependence of the glass transition, the segmental correlation time $\tau_s(T, M)$ is taken from previous analyses of the FC susceptibility master curves. Consequently, we present the temperature independent, iso-frictional quantity $D\tau_s \propto F(M)$, which reveals the M -dependence of the pure collective polymer dynamics. While at the lowest M the quantity $D\tau_s$ displays a trend to become M independent typical of simple liquids, it crosses over to a behavior characteristic of Rouse dynamics. In most systems, however, this crossover manifests itself in a rather narrow M interval as entanglement dynamics takes over at $M > M_e$. Thus, pure Rouse behavior is difficult to identify, yet the approach allows one to decide when a molecule becomes a polymer, in terms of the (smallest) Rouse unit.



1. INTRODUCTION

Characterizing translational diffusion in condensed matter is an important issue in many areas of science and technology. In particular, understanding the slow diffusion in polymer melts is of great interest. Here, the Rouse model¹ and de Gennes' reptation idea² provide the most accepted framework for nonentangled ($M < M_e$) and entangled ($M > M_e$) melts of linear polymers, respectively, where M_e denotes a polymer specific crossover molecular mass. The full theory of polymer melts has been formulated by Doi and Edwards in terms of the so-called tube-reptation model.³ Depending on the chain length or the molecular mass M , the diffusion coefficient $D(M)$ exhibits a characteristic power-law dependence which is explained semiquantitatively. The model has been refined by introducing effects such as contour length fluctuations^{4,5} and constraint release.^{6,7} It offers not only an explanation for the long-time diffusion, i.e., the M dependence of D , but also for the subdiffusive translation of a polymer segment at times much shorter than the terminal relaxation time τ_d . Specifically, different power-law regimes are forecast for the mean square displacement as a function of time and they can be probed piece-wise for example by neutron scattering⁸, field gradient (FG) nuclear magnetic resonance (NMR)^{9–11} and recently by field cycling (FC) ^1H NMR relaxometry.^{12,13}

Regarding the determination of the diffusion coefficient D , FG NMR diffusometry has become the key method of

measuring translational motion in condensed matter.^{14,15} The range of D accessible by FG NMR methods is 10^{-6} – 10^{-14} $\text{m}^2 \text{s}^{-1}$.¹⁵ In low-molecular mass systems the lower bound of D refers to moderately viscous or supercooled liquids. Regarding polymer systems, such D values are found at comparatively high temperatures in systems with a low glass transition temperature T_g such as poly(butadiene) (PB).

We have recently shown that FC ^1H NMR relaxometry has the potential to become an alternative, straightforward route for measuring D in bulk liquids as well as in polymers.^{16–19} The idea of FC NMR is as follows:^{20–23} First, the sample is polarized in a strong, external magnetic field. The generated magnetization is proportional to the difference in the populations of the ^1H Zeeman quantum states determined by the Boltzmann distribution. Then the field is switched to a lower value (relaxation field) and the energy levels repopulate according to the new equilibrium conditions. The magnetization decay is usually exponential with a time constant denoted as the spin–lattice relaxation time T_1 . The spin transitions are induced by stochastically fluctuating interactions between the magnetic dipole moments of the protons. The transition probability and in consequence T_1 depends on the

Received: April 29, 2013

Revised: June 7, 2013

Published: July 2, 2013

strength and the spectral density of these fluctuations, *i.e.*, for a given relaxation field on the spectral density at multiples of the Larmor frequency. By varying the relaxation field which is proportionally linked to the ^1H frequency, the spectral density is scanned via the relaxation dispersion $R_1(\omega) = 1/T_1(\omega)$.

As ^1H NMR relaxation reflects fluctuations of the magnetic dipole–dipole interactions between pairs of protons, one has to distinguish between protons on the same molecule and on different molecules.²⁴ Thus, the measured relaxation rate $R_1(\omega)$ is a sum of two contributions which result from intra- and intermolecular dipolar interactions, respectively. The intramolecular relaxation is associated with molecular rotation changing the orientation of the vector connecting the interacting nuclei. The intermolecular dipolar interactions are additionally mediated by the relative translational motion of the molecules which leads not only to fluctuations of the orientation of the internuclei axis, but also to changes in their distance. This implies that translation as well as rotation can be monitored by ^1H NMR relaxometry simultaneously provided that a sufficiently broad range of (Larmor) frequencies is covered.

Until recently field dependent relaxation experiments have not routinely been possible. Because of the commercial availability of STELAR FC NMR relaxometers which cover about 3 orders of magnitude in the frequency (10 kHz to 20 MHz for ^1H), this has changed and NMR relaxometry gained new momentum.^{20–23} By performing FC ^1H NMR experiments on several liquids and polymers we have demonstrated^{16–19} (in particular by applying the isotope dilution technique^{25–30}) that the limiting low-frequency behavior of $R_1(\omega)$ is determined solely by the intermolecular relaxation controlled by translational diffusion of the protons. Moreover, a universal dispersion law, explicitly $R_1(\omega) = R_1(0) - A\omega^{1/2}$ holds for ^1H NMR in the low-frequency limit as a consequence of free diffusion dominating translational dynamics in liquids at long times.^{31–34} The constant A depends only on the diffusion coefficient D and on the spin density (apart from physical constants). This dispersion law is an important fact; it implies that no frequency independent relaxation rate is observed even at the lowest frequencies in contrast to the often discussed so-called extreme narrowing condition which actually is reached only for the intramolecular relaxation contribution.^{17,18} In the case of PB we have been able to extract $D(M,T)$ from the low-frequency behavior of $R_1(\omega)$ covering the range $446 < M/(\text{g mol}^{-1}) < 9470$ and $230 < T/\text{K} < 410$.¹⁹ The obtained D values complement those reported by FG NMR,³⁵ and the crossover from Rouse to entanglement dynamics has been clearly identified by a change of the power-law dependence of $D(M)$.

In the present contribution we extend the analysis of our previous FC ^1H NMR experiments in order to extract $D(M,T)$ and include also the polymers poly(styrene) (PS), poly(dimethylsiloxane) (PDMS), poly(propylene glycol) (PPG), and 1,4-poly(isoprene) (PI). In addition to employing the commercial spectrometer STELAR FFC 2000, only with the help of a home-built spectrometer^{13,36,37} sufficiently low-frequency dispersion was compiled to allow the present analysis. As only at high M the monomeric friction coefficient becomes independent of M , which is equivalent to the fact, that the glass transition temperature T_g becomes independent of M , the diffusion data at a given temperature have to be corrected for the M dependence of the friction coefficient in order to test the scaling laws of the tube-reptation model. The correction is in particular important for low M in the Rouse regime. This is

easily possible, since FC ^1H NMR provides in addition to D also the segmental correlation time $\tau_s(T,M)$ ^{38–44} which can be taken proportional to the friction coefficient. Iso-frictional diffusion data have only been presented in rare cases, for example, by Colby and co-workers for PB,⁴⁵ where the approach has also been called iso-free-volume correction. Thus, in the present contribution we analyze the M dependence of the product $D\tau_s$ which allows testing the M dependence of the structural factor, *i.e.*, the function representing solely the behavior of the collective polymer dynamics. As we will show, the inclusion of low- M systems in our analysis also enables us to estimate the crossover to simple liquid dynamics, that is, in principle, the onset of polymer dynamics in terms of the dynamic bead size; *i.e.*, the Rouse molecular mass M_R can be given.

2. THEORETICAL BACKGROUND

It has recently been demonstrated that the low-frequency dispersion of the ^1H spin–lattice relaxation rate $R_1(\omega) = 1/T_1(\omega)$ of a liquid is dominated by the intermolecular dipolar relaxation contribution mediated by translational motion of the molecules, while at higher frequencies both inter- and intramolecular contributions are relevant.^{12,16–19} In a liquid, self-diffusion at long times is Fickian which yields a power-law $C_{\text{trans}}(t) \propto t^{-3/2}$ of the intermolecular NMR correlation function.³⁴ Therefore, the total relaxation rates (including intra- and intermolecular contribution) can be expanded at low-frequencies providing a universal dispersion law^{17,18}

$$R_1(\omega) = R_1^{\text{intra}}(\omega) + R_1^{\text{inter}}(\omega) = R_1(0) - \frac{B}{D^{3/2}}\sqrt{\omega} \quad (1)$$

with

$$B = \frac{\pi}{30}(1 + 4\sqrt{2})\left(\frac{\mu_0}{4\pi}\hbar\gamma_{\text{H}}\right)^2 N$$

where γ_{H} is the proton gyro-magnetic ratio and N the spin density, *i.e.*, the number of spins per volume unit. The intramolecular (reorientational) contribution is included in $R_1(0)$ as the rotational contribution is frequency independent in the low-frequency range, *i.e.*, at $\omega\tau_{\text{rot}} \ll 1$. In other words, the corresponding spectral density is flat at low-frequencies. Thus, at sufficiently high temperatures a linear regime of $R_1(\sqrt{\nu})$ (with $\nu = \omega/2\pi$) is expected at low frequencies and confirmed experimentally for several liquids^{17,18} as well as for polymers.^{19,23} With given spin density N , the diffusion coefficient $D(T)$ can be directly extracted from the slope of a linear fit of the relaxation rate plotted versus $\sqrt{\nu}$ at low frequencies. In the present work the approach is applied to measure the diffusion coefficient $D(T,M)$ of several polymers as a function of temperature and molecular mass M .

In our previous works we rescaled the susceptibility data $\chi''(\omega) \equiv \omega/T_1(\omega)$ by applying frequency–temperature superposition (FTS) (see also below),^{38–44} however, also the relaxation rate $R_1(\omega)$ itself measured at different temperatures can be merged into a single master curve.^{18,19} On the basis of the universal dispersion law (eq 1), one can rescale $R_1(\omega)$ reaching a common low-frequency behavior

$$R_1(\omega\tau_{\text{res}})/R_1(0) = 1 - \sqrt{\omega\tau_{\text{res}}} \quad (2)$$

where the rescaling time τ_{res} is given by

Table 1. Applied Spin Densities N for Poly(dimethylsiloxane), Poly(butadiene) and Poly(isoprene) Calculated from Mass Densities ρ , Number of Hydrogen Atoms n_H per Monomer, and Molar Mass M of the Monomer via Eq 6 and Their Entanglement Masses M_e

	ρ [g/cm ⁻³]	n_H	M [g/mol]	N [10 ²⁸ m ⁻³]	M_e^{47} [g/mol]
polydimethylsiloxane	0.965	6	74.17	4.70	12 000
polybutadiene	0.86	6	54.09	5.75	1900
polyisoprene	0.92	8	69.06	6.42	6400

Table 2. Details on the Polystyrene (PS) Samples: Molar Mass (Mass Average) M_w , Polydispersity M_w/M_n (with M_n Number Averaged Molar Mass), Molar Mass M used in Eq 6, Number of Protons n_H , Density ρ , and Spin Density N

sample	M_w [g/mol]	M_w/M_n	M [g/mol]	n_H	ρ [g/cm ⁻³]	N [10 ²⁸ m ⁻³]
ethylbenzene	106.17	1.00	106.17	10	0.8665 ⁵⁷	4.91
PS 370	371.47	1.00	371.47	35	1.065 ⁵⁸	6.04 ^b
PS 690	690	1.09	104.15 ^a	8 ^a	1.04 ⁵⁹	4.81
PS 1380	1380	1.05	104.15 ^a	8 ^a	1.04	4.81
PS 1920	1920	1.08	104.15 ^a	8 ^a	1.04	4.81

^aPer monomer. ^bHigher due to a tertiary butyl end group.

$$\tau_{\text{res}} = \left(\frac{B}{R_1(0)D^{3/2}} \right) \quad (3)$$

Polymer theories, most prominently the tube-reptation model,^{3,46,47} provide characteristic M dependences for transport quantities in polymer melts. Depending on the molecular mass being above or below the entanglement mass M_e , characteristic power-law behavior is forecast for $D(M)$, specifically $D(M) \propto M^{-1}$ ($M < M_e$) and $D(M) \propto M^{-2}$ ($M > M_e$). Experiments covering usually the entanglement regime have essentially confirmed the prediction, yet, the magnitude of the exponent has turned out to be somewhat larger than 2 (*i.e.*, 2.2–2.4).^{46,47} The entanglement mass M_e varies among different polymers; typical values are $M_e = 17000$ for PS⁴⁷ or $M_e = 3500$ for PPG,⁴⁸ for example. For the other polymers considered M_e can be found in Table 1.

In order to test the predictions of the polymer theory one has to consider “iso-frictional” dynamics, *i.e.*, dynamics with a constant monomeric friction coefficient ζ instead of constant temperature T since ζ depends not only on temperature but also on M , in particular for short chains. This behavior is caused by the M dependence of the glass transition phenomenon controlling the “local” or “glassy” dynamics at short times and is reflected in the M dependence of the glass transition temperature T_g . In many cases the function $T_g(M)$ saturates only at high M .^{45,46} Whether the saturation is connected with onset of entanglement at $M > M_e$ is debated.^{49–51} Consequently, the mass and temperature dependence of the diffusion coefficient can be factorized:^{46,47,52}

$$D(T, M) = F(M)/\zeta(T, M) \quad (4)$$

Here ζ depends on both mass and temperature, whereas the structural factor F depends only on M and reflects the M dependence of the collective polymer dynamics. For short chains the M dependence of D is influenced by both quantities, whereas with increasing M the sensitivity of ζ to M vanishes ($\zeta(T, M) \xrightarrow{\text{large } M} \zeta^\infty(T)$). Thus, for long chains iso-thermal and iso-frictional quantities are equivalent in terms of their M dependence. Yet, for low M one has to correct D with the friction coefficient in order to establish the structural factor $F(M)$. As the segmental time constant τ_s is proportional to ζ one has to consider the product $D\tau_s$ to unravel the behavior of

$F(M)$. As mentioned such an analysis was only carried out in rare cases.⁴⁵

Reformulating the Bloembergen, Purcell, Pound expression⁵³ the NMR relaxation data are converted to the susceptibility representation according to the equation:

$$\omega R_1(\omega) = K[\chi''(\omega_H) + 2\chi''(2\omega)] \cong 3K\chi''_{DD}(\omega) \quad (5)$$

where K is an effective NMR coupling constant. The index “DD” stands for dipolar coupling which, as discussed, contains intra- and intermolecular contributions. Applying FTS as often done, *e.g.*, in rheological studies,^{46,47} $\chi''_{DD}(\omega)$ can be expressed as $\chi''_{DD}(\omega\tau_s)$, where τ_s is the segmental (“local”) correlation time.^{38–44} In other words, master curves can be constructed by shifting the susceptibilities measured at different temperatures solely along the frequency axis to provide the best overlap among the individual spectra collected. FTS reflects a fundamental feature of cooperative dynamics in condensed matter.⁵⁴ While at low-frequency diffusion dominates the dispersion of the ¹H NMR relaxation rate, at high frequencies (and low temperatures) local (or glassy) dynamics determine the relaxation rate. Thus, the time constant τ_s is directly accessed at certain temperatures by fitting the data by a Cole–Davidson function.⁵⁵ Extending the measurements over a large temperature range, the construction of the master curves yields $\tau_s(T)$, and the corresponding data for the polymers considered here (except for PS) have partly been published previously.^{38–44,56} Determining $D(M, T)$ from an analysis of the low-frequency dispersion of $R_1(\sqrt{\nu})$ and plotting the product $D(T, M)\tau_s(M, T)$ the function $F(M)$ is extracted (*cf.* Equation 4) and can be checked against the predictions of the tube-reptation model. The current study investigates molecular masses as low as possible (crystallization has to be avoided) and it is also the aim to find out whether the function $F(M)$ allows to determine the crossover from Rouse to simple liquid dynamics at the lowest M .

3. EXPERIMENTAL SECTION

Samples of linear polystyrene (PS) with a narrow molecular mass distribution were purchased from Polymer Standards Service, Mainz, Germany. Table 2 gives an overview of molecular masses and polydispersities M_w/M_n . Note that in the following M_w in g/mol denotes the mass average molecular mass. The samples of 1,4-poly(butadiene) (PB), poly(dimethylsiloxane) (PDMS), 1,4-poly(isoprene) (PI), and poly(propylene glycol) (PPG) were investigated

Table 3. Details on the Poly(propylene glycol) (PPG) Samples: Molar Mass (Mass Average) M_w , Polydispersity M_w/M_n (with M_n Number Averaged Molar Mass), Molar Mass M used in Eq 6, Number of Protons n_H , Density ρ , and Spin Density N

sample	M_w [g/mol] ^b	M_w/M_n ^b	M [g/mol]	n_H	ρ [g/cm ⁻³]	N [10 ²⁸ m ⁻³]
propylene glycol	76.09	1.00	76.09	8	1.04 ⁶⁰	6.58
di(propylene glycol)	134.173	1.00	134.173	14	1.0206 ⁶¹	6.41
tri(propylene glycol)	192.26	1.00	192.26	20	1.02 ⁶²	6.39
PPG 455	455	1.06	58.08 ^a	6 ^a	1.005 ⁶³	6.25
PPG 790	790	1.03	58.08 ^a	6 ^a	1.005	6.25
PPG 1000	1000	1.03	58.08 ^a	6 ^a	1.005	6.25
PPG 3080	3080	1.03	58.08 ^a	6 ^a	1.005	6.25
PPG 5300	5300	1.06	58.08 ^a	6 ^a	1.005	6.25

^aPer monomer. ^bCf. ref 43.

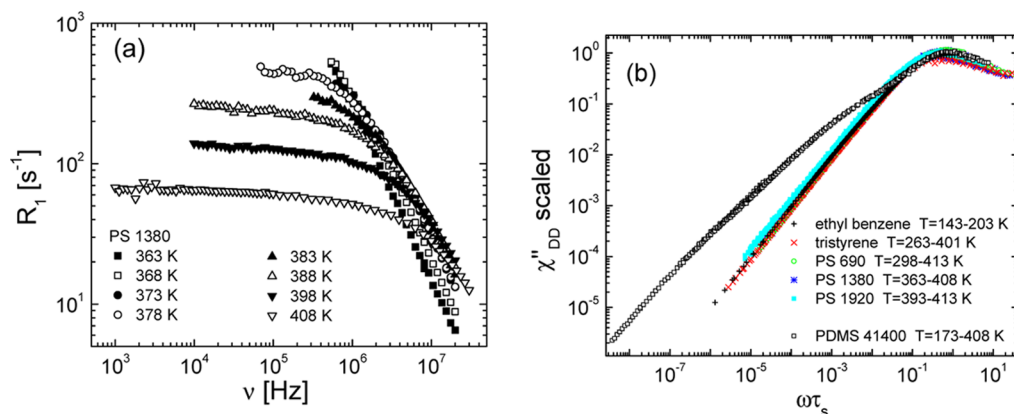


Figure 1. (a) Relaxation rate $R_1(\nu)$ of polystyrene (PS) with molecular mass $M = 1380$ at various temperatures as indicated. The data at 408 K were measured at the home-built spectrometer allowing to access lower frequencies. (b) Susceptibility master curves $\chi''_{DD}(\omega\tau_s)$ of all the polystyrenes in the temperature range investigated; in addition, the master curve for a high molecular mass PDMS is included.^{42,43}

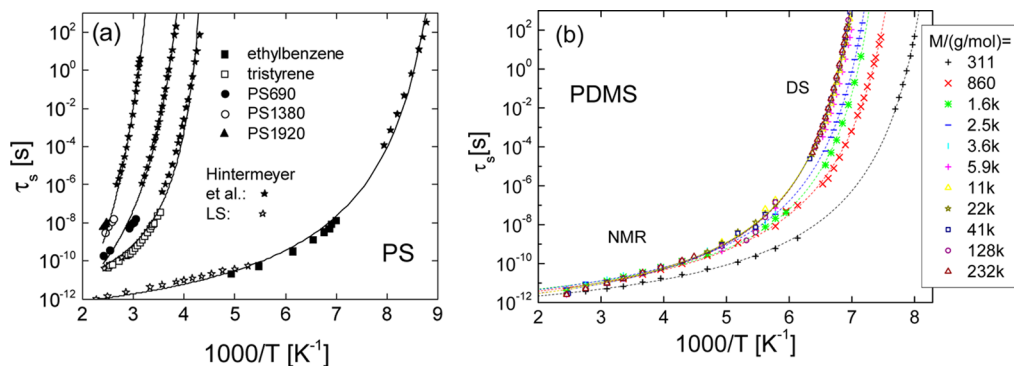


Figure 2. (a) Segmental time constants τ_s as a function of the inverse temperature for PS with $M = 377, 690, 1380,$ and 1920 compared to those reported by dielectric spectroscopy (DS)⁵⁰ and depolarized light scattering (LS); (b) Corresponding time constants for PDMS at M values indicated.⁴³ Data are interpolated by the Vogel–Fulcher–Tammann formula (cf. Table 4).

over a broad range of molecular masses M . Details of the samples and the results in the susceptibility representation were already published in refs 38–43. Furthermore, Table 3 gives an overview over molecular masses and polydispersities for PPG also taken from ref 43.

The ¹H NMR spin–lattice relaxation experiments were performed with two different electronic field cycling relaxometers, a commercial one (STELAR Spinmaster FFC2000) at Bayreuth University and a home-built one^{36,37} at the Technische Universität Darmstadt. With the first equipment experiments were performed at temperatures from 173 to 408 K; with the latter, ¹H NMR spin–lattice relaxation rates from 403 to 413 K were measured. The Stelar relaxometer covers a ¹H frequency range from $\nu = \omega/2\pi = 10$ kHz to 20 MHz while the switching time from high polarization field to relaxation field was 3 ms. Lower ¹H frequencies can only be reached with the home-built relaxometer where frequencies down to 400 Hz and up to 30 MHz

were accomplished for the present project. The low frequencies were attained by utilizing a three-dimensional resistive coil arrangement for compensating the earth field, other magnetic stray fields, and field drifts.³⁷ Switching times of 3 or 6 ms were achieved when the compensation system is not used ($\nu > 1$ kHz) or when it is employed ($\nu \leq 1$ kHz), respectively. The relaxation time T_1 was determined by an exponential fit of the magnetization decay curve. When measuring at the Stelar relaxometer the sample was in a 10 mm tube with a filling height of about 15 mm, whereas it was in 5 mm tubes with a filling height of around 10 mm in case of the low frequency experiments in Darmstadt.

In order to determine the diffusion coefficient along eq 1 one needs the spin density which is given by the formula

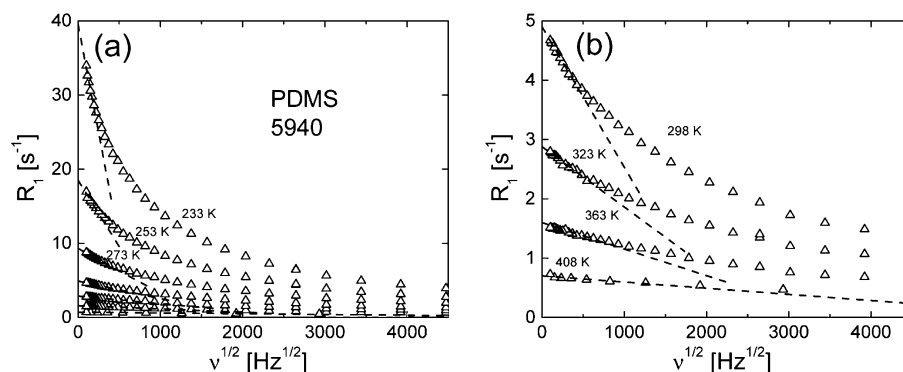


Figure 3. (a) Relaxation rate R_1 as a function of $\sqrt{\nu}$ for PDMS with $M = 5940$ at different temperatures as indicated. Dashed lines: linear interpolations at low frequencies (cf. Equation 1). (b) Magnification of the high temperature curves.

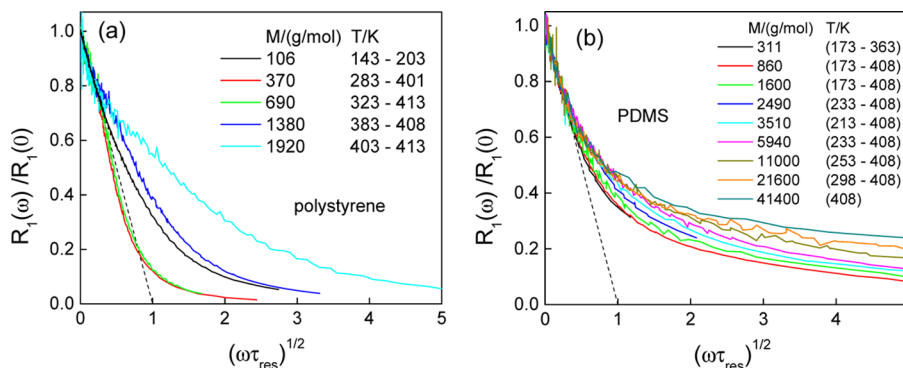


Figure 4. (a) Relaxation rate master curves for polystyrene as a function of $\sqrt{(\omega\tau_{\text{res}})}$ obtained from eq 2 for molecular masses and temperature ranges as indicated. Dashed line: linear limit at low frequencies. (b) Master curves for PDMS (data from ref 43).

$$N = n_{\text{H}} \frac{\rho N_{\text{A}}}{M} \quad (6)$$

where n_{H} denotes the number of hydrogen atoms, M the molar mass, ρ the density and N_{A} the Avogadro constant. Table 1 lists the applied values and the resulting spin number densities for PDMS, PB and PI. For PS and PPG they are listed in Table 2 and 3, respectively. The error of the evaluated diffusion coefficients was in many cases smaller than the size of the points; exemplarily for PDMS 162 error bars are included (cf. Figure 6a).

In order to test the applicability of FTS for the analysis of the NMR relaxation data some polystyrenes were also studied by depolarized light scattering (LS). For details, the reader is referred to ref 64.

4. RESULTS

In Figure 1a, the dispersion of the spin–lattice relaxation rate $R_1(\nu)$ of PS with molecular mass $M = 1380$ is displayed on double–logarithmic scales for the temperature range from 363 to 408 K. With increasing temperature, the frequency dependence of $R_1(\nu)$ gets weaker toward lower frequencies and the slower relaxation processes are shifted into the experimentally accessible frequency window. Note that for the highest temperature ($T = 408$ K), $R_1(\nu)$ was measured with the home-built Darmstadt relaxometer by employing the stray field compensation system, which extends the frequency range by one decade toward low frequencies.

By applying FTS the susceptibility is shifted solely in frequency to provide a master curve as a function of the reduced frequency $\omega\tau_s$ (see Figure 1b). Thereby the effective frequency window of the technique is significantly extended and the segmental time constants $\tau_s(T)$ are provided (Figure 2). The master curves $\chi''_{\text{DB}}(\omega\tau_s)$ exhibit a peak at $\omega\tau_s \approx 1$

which is identified with the segmental or local dynamics governed by the α -process of the glass transition. For polymers at $\omega\tau_s < 1$, an excess intensity with respect to the spectrum of a simple liquid is observed, which is on the one hand due to the slower, M -dependent segmental polymer dynamics^{38–44} and on the other hand due to the intermolecular relaxation contribution.¹³ Actually, in the case of PS the effect of the polymer specific relaxation is almost not discernible as no higher M can be studied due to the quickly rising T_g of PS. For PS, however, the crossover to the “monomeric liquid” ethylbenzene can be studied. As we have reported on the polymer relaxation dispersion of PB, PI, PPG, and PDMS in a series of papers^{38–44} we refrain to show the data again; just one example for a high- M PDMS is included in Figure 1b.^{42,43} Clearly, in the case of PDMS a strong excess low-frequency contribution is recognized and attributed to the collective polymer dynamics.

Figure 2a shows the time constants $\tau_s(T)$ of segmental motion for all the PS samples investigated (cf. Table 2) as obtained by constructing the susceptibility master curves in Figure 1b. They are compared with the results from dielectric spectroscopy (DS).⁵⁰ While FC ^1H NMR provides time constants at high temperature, DS gives results at low temperatures close to T_g . Both techniques complement each other. For a given temperature, the dynamics is slowing down with increasing M . A drastic change is observed for ethylbenzene for which the $\tau_s(T)$ curve is strongly shifted to low temperatures. Here $T_g = 117$ K is found while in the high M limit of polystyrene $T_g = 373$ K is reported.⁵⁰ Thus, $T_g(M)$ changes strongly when crossing over from the simple liquid limit to the high- M polymer. As T_g quickly becomes very high

polymer dynamics cannot be accessed by ^1H FC NMR beyond about $M \cong 2000$. For tristyrene and ethylbenzene we compare $\tau_s(T)$ with the results from depolarized light scattering (LS) which are collected in the same temperature range. An almost perfect agreement is found which demonstrates that the construction of the FC NMR master curves provides reliable segmental correlation times. For comparison $\tau_s(T, M)$ of PDMS is shown in Figure 2b.⁴³ Again, the agreement between DS⁵⁰ and FC ^1H NMR is very good as it has been demonstrated also for PB,⁴⁰ PI^{43,56} and PPG.⁴³ The joint data sets in Figure 2 of DS, NMR, and LS are interpolated by a Vogel–Fulcher–Tammann function, *i.e.*, $\tau_s(T) = \tau_0 e^{B/(T-T_0)}$, (VFT; solid-lines) for each M . The fitting parameters τ_0 , B , and T_0 are given in Table 4 (Appendix).

The diffusion coefficient $D(T)$ is extracted from the relaxation dispersion data by plotting R_1 as a function of $\sqrt{\nu}$ (*cf.* eq 1). This is shown exemplarily in Figure 3a for the relaxation rate of PDMS with $M = 5940$ at low temperatures, while Figure 3b presents the data at higher temperatures. The low-frequency range in which $R_1(\sqrt{\nu})$ can be linearly interpolated is increasing with temperature. The straight (dashed) lines in Figure 3 represent the linear fits from which $D(T)$ has been determined.

Figure 4 shows master curves of the relaxation rate R_1 constructed according to eq 2 for PS (Figure 4a) and PDMS (Figure 4b). They contain all relaxation data for different molecular masses collected in the indicated temperature range. For a given value of M the data coincide even beyond the linear low-frequency limit which proves that FTS generally applies for polymer melts including both polymer specific as well as local (glassy) dynamics, a fact already demonstrated in the master curve representation $\chi''_{\text{DD}}(\omega\tau_s)$ (*cf.* Figure 1b). For different M universal low-frequency behavior is observed (dashed line). At higher reduced frequencies $\sqrt{(\omega\tau_{\text{res}})}$ the scaled relaxation rate $R_1(\omega)/R_1(0)$ increasingly bends up with increasing M . We have previously shown (*cf.* ref 18) that a progressing upward turn suggests a larger spectral separation between the translational and rotational/segmental dynamics and in the case of polymers (here PDMS in Figure 4b) a systematically growing contribution of polymer specific relaxation due to Rouse and entanglement dynamics. The latter, regarding their time scale, occurs between the segmental dynamics and the terminal relaxation, which is associated with free translational diffusion. Similar results as for PDMS have already been reported for PB.¹⁹

The situation for the oligomers of PS is somewhat different (Figure 4a). In tristyrene and PS690 the spectral separation of rotational and translational dynamics seems to be quite narrow and even a downward curvature with respect to the limiting low-frequency behavior is observed at intermediate rescaled frequencies as found in other simple liquids like *o*-terphenyl.¹⁸ The PS samples with higher M show a somewhat similar trend with M as PDMS. The relaxation behavior of ethylbenzene does not fit in this systematics. Here, details of the inter- and intramolecular coupling determine the master curve. Although important differences are observed in the master curves of PS in Figure 4a, the actual polymer specific relaxation distribution is rather small when compared to PDMS where relaxation for samples of much higher M values were measured (*cf.* Figure 1b).

Finally, we show in Figure 5 the full dipolar correlation function, *i.e.* $C_{\text{DD}}(t) = \langle (D_{0,m}^2(\Omega(t))/r^3(t))(D_{0,m}^2(\Omega(0))/r^3(0)) \rangle$ where $D_{0,m}^2(\Omega)$ denotes Wigner rotation matrices

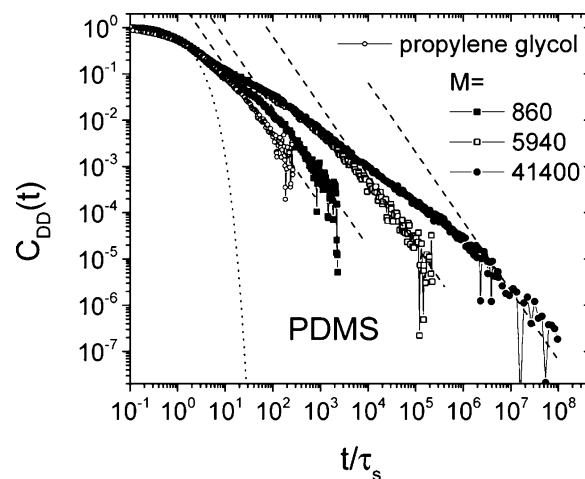


Figure 5. Dipolar correlation functions $C_{\text{DD}}(t)$ vs. reduced time t/τ_s for different molecular masses (M) of PDMS; for comparison the result for propylene glycol is included; dashed straight lines: power laws $\propto t^{-3/2}$ characteristic of free diffusion. Dotted line: Kohlrausch function expected for reorientational dynamics controlled solely by the glassy dynamics.

and r the inter spin distance, obtained for PDMS after Fourier transformation of the susceptibility master curves (*cf.* Figure 1b). By applying the isotope dilution technique, which allows to single out intra- and intermolecular relaxation contributions, it has recently been demonstrated that in the case of PDMS the intermolecular relaxation is rather strong, *i.e.*, it dominates the total relaxation already at $\omega\tau_s < 1$.¹³ Although we could not explain this difference with respect to all the other polymers studied so far then, now we suppose that this effect results from fast methyl group rotation in PDMS which preaverage predominately the intramolecular dipolar coupling. Thus, PDMS is best suited to demonstrate the relevance of intermolecular relaxation caused by translational diffusion. As seen in Figure 5, the higher M the more retarded is the correlation loss due to the increasing polymer dynamics appearing at $t/\tau_s \gg 1$. As $M_e = 12000$ ⁴⁷ the dynamics essentially reflects Rouse dynamics (*cf.* also ref 43). At longest times the correlation function bends down to a faster decay which, however, is not (stretched) exponential as expected for a dominating intramolecular relaxation but rather described by the universal long-time power-law $C_{\text{trans}}(t) \propto t^{-3/2}$ characteristic of free diffusion as indicated by the dashed lines.³⁴ In Figure 5, the correlation functions are compared to that of the simple liquid propylene glycol which shows a similar long-time behavior but the relaxation is much less extended in time compared to those of the polymers. The expected Kohlrausch decay typical of reorientational dynamics dominated by glassy (local) dynamics is indicated by the dotted curve; it controls the dynamics at short times for all polymers. In simple liquids it can only be singled out via an isotope dilution experiment^{16,18} or by performing FC ^2H NMR.¹³

In Figure 6a, the diffusion coefficient $D(T, M)$ of PDMS in the temperature range $T = 163 \text{ K} - 408 \text{ K}$ is shown as obtained from the analysis of the low-frequency relaxation dispersion. For all M a constant spin density was taken (*cf.* Table 1) for the application of eq 1. As expected, D is reduced by several decades with increasing M . For each M a super-Arrhenius temperature dependence of $D(T)$ is observed, which is again interpolated by the VFT formula (solid lines), *i.e.*, $D(T) = D_0 e^{-B/(T-T_0)}$. In Table 5 (Appendix) the applied parameters D_0

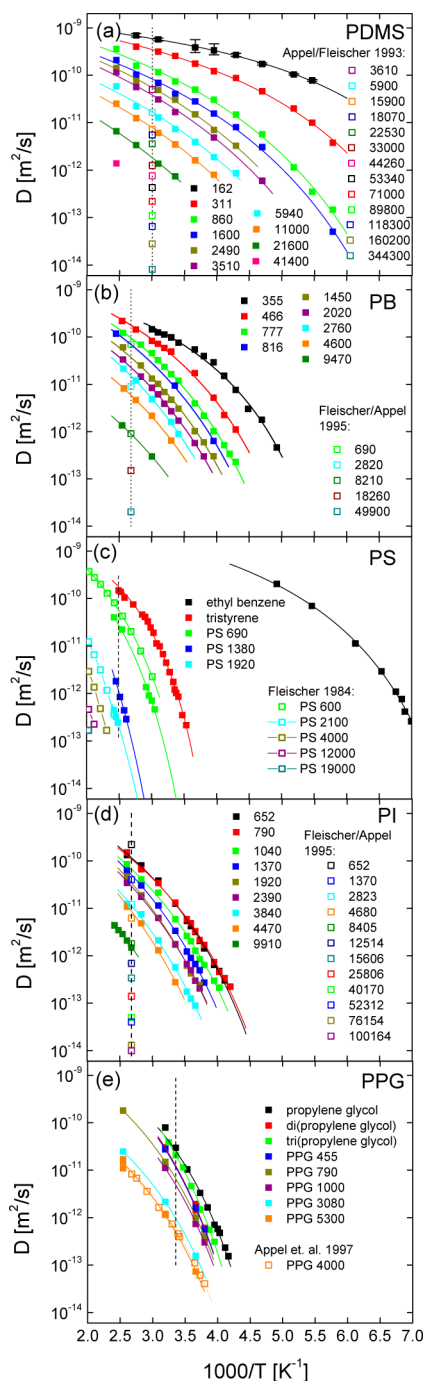


Figure 6. Diffusion coefficients $D(T, M)$ obtained from FC ^1H NMR (full symbols) as a function of inverse temperature for (a) poly(dimethylsiloxane) (PDMS) compared to field gradient (FG) data (open symbols) taken at $T = 333 \text{ K}$ ⁶⁵ (b) 1,4-poly(butadiene) (PB) and FG data at $T = 373 \text{ K}$ ³⁵ (c) poly(styrene) (PS) and FG data⁶⁶ (d) 1,4-poly(isoprene) (PI) and FG data at $T = 373 \text{ K}$,³⁵ and (e) poly(propylene glycol) (PPG) and FG data⁶⁷ with molecular masses M in g/mol as indicated. In most cases, the error bars are smaller than symbol size. Solid lines: Vogel–Fulcher–Tammann interpolation. Dashed lines: cuts at a given T providing $D(M)$.

, B and T_0 for PDMS and the other polymers are given. One observes a trend that the M dependence becomes stronger at higher M . For comparison we included literature data from FG NMR actually only taken at a single temperature $T = 333 \text{ K}$.⁶⁵

In general, for PDMS a very similar picture is rendered as in the case of PB, which has been reported previously,¹⁹ and the data are again shown in Figure 6b for comparison. The results for PS are presented in Figure 6c. As discussed before the M range of PS is restricted to $M < 2000$ as T_g becomes too high and the relevant temperature range of the segmental and polymer dynamics is beyond the current experimental possibilities. The corresponding FG NMR results⁶⁶ include somewhat higher M . Here, the D data for the low- M limit ethylbenzene are strongly shifted to lower temperatures. This reflects the fact that T_g is very low in the low- M limit. Parts d and e of Figure 6 display the diffusion coefficient for PI and PPG, respectively, and the corresponding FG data from the literature for comparison.^{35,67} Again a very similar systematic mass and temperature dependence is observed. For all the polymers investigated the results from FC ^1H NMR relaxometry and the literature data fit well.

In Figure 7, the M dependence of the diffusion coefficient is shown for the different polymers (black diamonds) by evaluating the corresponding $D(T, M)$ curves of Figure 6 at a given temperature (in most cases where the literature data were also available). While the FC ^1H NMR data extend to lower M the overall agreement between FC and FG ^1H NMR is very satisfactory. From the combined results a clear crossover between two apparent power-laws, $\propto M^{-\alpha'}$, can be seen for PDMS, PB, and PI. The observed exponents for high M , $\alpha' \approx 2.2$, are in accord with literature data⁶ and somewhat above the predictions of the tube-reptation model. They reflect the regime of entanglement dynamics. The crossover molecular mass is close to the M_e values reported in the literature (cf. Table 1) as also indicated in Figure 7. In the case of PPG, samples of high M were not available, thus the crossover is not observed. For PS, as said, only a few low M values can be analyzed. However, apart from PDMS the power-laws found for low M values do not at all agree with the prediction of the Rouse theory (i.e., $\propto M^{-1}$) but show higher exponents $\alpha' > 1$. For PS we even find $\alpha' \approx 4$ apparently due to its prominent M dependence of T_g mentioned above. This points out to the necessity of analyzing an iso-frictional quantity in order to test the collective polymer effects in the low- M limit.

Exemplarily for PDMS Figure 8 presents the quantity $D\tau_s$, determined at different temperatures. The values of the time constants τ_s are taken from Figure 2b. As expected (cf. Section 2), at fixed $M D\tau_s$ is essentially temperature independent, which proves the cancellation of the monomeric friction $\zeta(T, M)$. Here, we note that usually according to Einstein, or Doi–Edwards in the case of polymers, the product $D\tau_s$ should be proportional to temperature. In Figure 8 one finds no systematic temperature dependence. This we also take as an indication that in the (high) temperature range studied terminal and segmental dynamics are not decoupled. The horizontal lines are the mean values $D\tau_s(M)$ of the particular molecular masses M . Thus, $D\tau_s(M) \propto F(M)$ is an iso-frictional quantity and allows to probe the structural function $F(M)$ (cf. eq 4) which reflects solely the M dependence of the collective polymer dynamics.

The right-hand axis of Figure 7 presents $D\tau_s(M)$ for all polymer systems considered. For PS the applied time constants τ_s can be found in Figure 2a, for the other polymers $\tau_s(T)$ is taken from works published previously.^{38–44} Starting again with the results for PDMS and comparing the power-law exponent of $F(M) \propto M^{-\alpha}$ in the Rouse regime ($M < M_e$) it drops continuously below $\alpha = 1$ (dotted line in Figure 7) when M

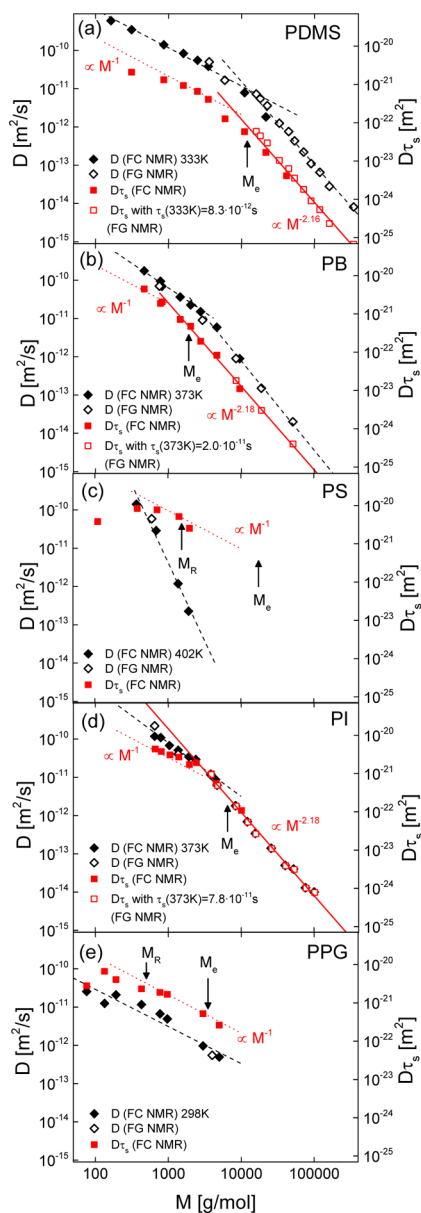


Figure 7. Diffusion coefficients D obtained from FC ^1H NMR (full black diamonds, left scale) as a function of the molecular mass M for (a) PDMS, (b) PB, (c) PS, (d) PI, and (e) PPG at temperatures as indicated, for comparison data from FG NMR from refs 35 and 65–67 (open black diamonds), dashed straight lines: apparent power-laws gpt for $D(M)$. Iso-frictional quantity $D\tau_s(M) \propto F(M)$ (right axis and full red squares), corresponding data from FG NMR^{35,65} (open squares) with τ_s taken from FC ^1H NMR, red straight solid lines: fitted power-laws for entanglement dynamics ($M > M_e$) with exponents as indicated; dotted straight lines: expected power-law for Rouse dynamics.

reaches low values. In contrast, $D(M)$ itself follows essentially an apparent power-law. Actually, in the case of PS, the formerly striking M -dependence disappears completely at lowest M indicating that only for $M = 1920$ first effects from polymer dynamics are revealed. PS (as well as PPG) are the rare cases for which relaxation data down to the monomeric simple liquid are accessible.

In the case of PB, the results between $D(M)$ and $F(M)$ are not very different while for PI the M dependence again crosses over to a rather weak M dependence; *i.e.*, it is significantly

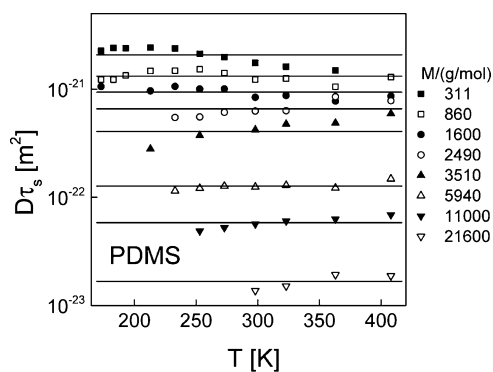


Figure 8. Iso-frictional quantity $D\tau_s(M) \propto F(M)$ for PDMS plotted versus inverse temperature, horizontal lines represent average value of $D\tau_s$.

weaker than that of $D(M)$ and the exponent α becomes lower than 1 at lowest M . For PPG a nonsystematic behavior is observed for the simple liquid limit, a fact well-known also for $T_g(M)$.^{43,68} In any case, the M dependence essentially disappears also in this case at lowest M . Thus, correcting to get iso-frictional data, $F(M)$ depends more weakly on M than $D(M)$ at $M < M_e$ (from literature), *i.e.*, the behavior expected for Rouse dynamics does not clearly show up; its apparent presence in $D(M)$, *e.g.*, in PDMS, has to be taken as accidental. In addition, for most polymers the Rouse regime extends over a too narrow M interval since entanglement dynamics quickly takes over at high M . In the latter regime, the iso-friction correction does not change the power-law exponent, and in all cases one observes $\alpha' \approx 2.2$ which is somewhat above the prediction of the tube-reptation model, a well-known fact.

5. DISCUSSION AND CONCLUSIONS

Benefiting from the universal low-frequency dispersion of the ^1H spin–lattice relaxation characteristic of free diffusion we have extracted the temperature and mass dependence of the diffusion coefficient D for a series of different polymers (PDMS, PB, PS, PI, PPG). Very satisfactory agreement is found when compared to the results provided by field gradient NMR which so far is the major technique to determine diffusion in liquids and in particular in polymer melts. In the case of PDMS with its comparatively strong intermolecular dipolar coupling a range of diffusion coefficient $10^{-9} > D/(\text{m}^2/\text{s}) > 10^{-13} \text{ m}^2/\text{s}$ is covered by FC ^1H NMR which is close to the range accessed by FG NMR. However, deep in the entanglement regime the currently accessible frequencies of FC NMR are not sufficiently low to detect the terminal relaxation.

As FC ^1H NMR allows to measure the full dipolar correlation function probing glassy, Rouse as well as entanglement dynamics (as long as M is not too high), the relaxation analysis provides the segmental correlation time τ_s in addition which is a measure for the monomeric friction coefficient. Of course, the full correlation function is only accessible when exploiting FTS and constructing susceptibility master curves. Yet, the procedure works particularly well above T_g as confirmed by comparing the extracted time constants τ_s with those reported from other techniques like dielectric spectroscopy or depolarized light scattering. The temperature dependence of τ_s is controlled by the glass transition phenomenon and its M dependence in polymers is different from that of translational diffusion. Thus, FC ^1H NMR relaxometry offers the unique possibility to access the iso-frictional quantity $D\tau_s(M) \propto F(M)$

which solely reflects the effect of collective polymer dynamics, actually within the same experiment. While the results for high M ($M > M_c$) remain unchanged, the correction becomes relevant at short chains, and the correction effect is stronger the stronger the M dependence of T_g is, which, in the case of polystyrene, is very strong. As a consequence one observes a continuous crossover from an M -independent $F(M)$ in the low- M limit toward an exponent α close to the one expected for the Rouse regime. In most polymers, however, this power-law manifests itself (if at all) in a rather narrow M range as entanglement effects take over at higher M .

Regarding the crossover to an M -independent structural factor $F(M)$ at lowest M , it is only observed for PS and for PPG. Here, the low- M limit of the monomeric liquid has been included in the present analysis. For the other polymers this limit cannot experimentally be reached either since no such oligomers are available or they show a high tendency to crystallize or the current temperature interval of FC spectrometer does not extend to sufficiently low temperatures. Remarkably, in the case of PS first indications of polymer dynamics are reflected in $F(M)$ only beyond, say, $M = 1500$ (cf. Figure 7), and one may take this value as an estimate of the Rouse mass or dynamic bead size M_R . In the case of PPG, one can estimate $M_R = 500$ from Figure 7. Here, we mention that Sokolov and co-workers^{49,69} have argued that the Kuhn length being a static quantity is not an appropriate measure when characterizing the dynamic bead size. Indeed, it is well-known from neutron scattering that the onset of Rouse dynamics is observed for length scales significantly larger (about a factor 4 in many polymers) than the Kuhn length.⁷⁰ In particular, the authors speculated that in the case of PS the dynamic bead size is about $M = 5000$. This has surely been a too large estimate, but still about 15 monomer units ($M_R \cong 1500$) are needed that first collective polymer dynamics can be observed in PS which is rather large when compared to the other polymers. In the case of PB, polymer dynamics set in only at $M > 500$.⁴⁰ In the case of PDMS 162, we are not able to access $\tau_s(T)$ as T_g is shifted to too low temperatures. In any case, inspecting the structural factor $F(M)$ or the low-frequency contribution in the susceptibility/spectral density in the low- M limit may be taken as a way to answer the question when does a liquid become a polymer melt; and it can be addressed by FC ^1H NMR. Finally, we note studying the M dependence of the viscosity Gray et al.⁷¹ have observed three M regimes and the one at lowest M has been attributed to the simple liquid limit.

All in all, the present work demonstrates that FC ^1H NMR relaxometry is a versatile technique which allows to probe local as well as collective dynamics in polymers. Because of the dominance of intermolecular relaxation in the low-frequency limit the diffusion coefficient can be determined by a straightforward analysis of the relaxation dispersion, and a wealth of diffusion data can be collected within short measuring time. Thus, in many cases FC ^1H NMR may become a promising alternative to FG NMR.

6. APPENDIX

Applied parameters for the Vogel–Fulcher–Tammann (VFT) fits are given in Tables 4 and 5.

AUTHOR INFORMATION

Corresponding Author

*E-mail: (E.A.R.) ernst.roessler@uni-bayreuth.de.

Table 4. Applied Parameters for the Vogel–Fulcher–Tammann (VFT) Fits of Segmental Time Constant $\tau_s(T)$ in Figure 2

sample	τ_0 [s]	B [K]	T_0 [K]
ethylbenzene	2.378×10^{-13}	484.6	100.6
tristyrene	9.110×10^{-13}	829.5	209.0
PS 690	4.079×10^{-15}	2014	209.0
PS 1380	1.011×10^{-18}	3816	229.4
PDMS 311	7.415×10^{-13}	418.4	111.9
PDMS 860	1.029×10^{-12}	505.1	118.0
PDMS 1600	1.487×10^{-12}	451.2	124.3
PDMS 2490	1.203×10^{-12}	500.5	124.4
PDMS 11 000	6.591×10^{-13}	549.4	127.3
PDMS 21 600	8.484×10^{-13}	520.4	128.3
PDMS 41 400	7.057×10^{-13}	526.0	128.4
PDMS 232 000	7.455×10^{-13}	514.2	128.9

Table 5. Applied Parameters for the Vogel–Fulcher–Tammann (VFT) Fits of the Diffusion Coefficient $D(T)$ in Figure 6

sample	D_0 [10^{-10} m ² /s]	B [K]	T_0 [K]
PDMS 311	17.49	245.7	105.0
PDMS 860	22.42	424.7	105.0
PDMS 1600	27.69	680.2	105.0
PDMS 2490	18.65	709.3	105.0
PDMS 3510	21.45	834.7	105.0
PDMS 5940	17.10	866.3	105.0
PDMS 11 000	8.678	901.9	105.0
PDMS 21 600	6.019	989.8	105.0
PDMS 41 400	3.204	1178	105.0
PB 355	24.58	517.1	142.5
PB 466	46.89	754.4	142.5
PB 777	53.31	926.9	142.5
PB 816	50.55	989.4	142.5
PB 1450	35.21	1051	142.5
PB 2020	27.72	1107	142.5
PB 2760	28.75	1211	142.5
PB 4600	8.995	1158	142.5
PB 9470	1.642	1203	142.5
ethylbenzene	80.60	349.6	109.0
tristyrene	79.13	700.1	216.8
PS 690	163.1	1174	216.8
PS 1380	2841	2294	216.8
PS 1920	409.0	2243	216.8
PI 652	111.5	1034	146.1
PI 790	86.38	991.7	146.1
PI 1040	87.98	1105	146.1
PI 1370	126.3	1251	146.1
PI 1920	134.5	1355	146.1
PI 2390	90.38	1301	146.1
PI 3840	57.11	1409	146.1
PI 4470	84.85	1562	146.1
PI 9910	19.19	1619	146.1
propylene glycol	212.1	886.0	166.3
di(propylene glycol)	593.2	1116	166.3
tri(propylene glycol)	861.5	1097	166.3
PPG 455	529.8	1110	166.3
PPG 790	174.6	1037	166.3
PPG 1000	124.0	1032	166.3
PPG 3080	22.64	1022	166.3
PPG 5300	15.01	1057	166.3

Notes

The authors declare no competing financial interest.

ACKNOWLEDGMENTS

The financial support of Deutsche Forschungsgemeinschaft (DFG) through Priority Program SPP 1369 "Polymer-Solid Contacts: Interfaces and Interphases" (RO 907/16) and Grant FU 308/14 is acknowledged.

REFERENCES

- (1) Rouse, P. E. *J. Chem. Phys.* **1953**, *21*, 1272–1280.
- (2) de Gennes, P. G. *J. Chem. Phys.* **1971**, *55*, 572–579.
- (3) Doi, M.; Edwards, S. F. *The Theory of Polymer Dynamics*; Oxford Sci. Publications: Oxford, U.K., 1986.
- (4) Doi, M. *J. Poly. Sci. Polym. Lett. Ed.* **1981**, *19*, 265–273.
- (5) Milner, S. T.; McLeish, T. C. B. *Phys. Rev. Lett.* **1998**, *81*, 725–728.
- (6) Rubinstein, M.; Colby, R. H. *J. Chem. Phys.* **1988**, *89*, 5291–5306.
- (7) Likhtman, A. E.; McLeish, T. C. B. *Macromolecules* **2002**, *35*, 6332–6343.
- (8) Wischniewski, A.; Monkenbusch, M.; Willner, L.; Richter, D.; Kali, G. *Phys. Rev. Lett.* **2003**, *90*, 058302.
- (9) Pahl, S.; Fleischer, G.; Fujara, F.; Geil, B. *Macromolecules* **1997**, *30*, 1414–1418.
- (10) Komlosh, M. E.; Callaghan, P. T. *J. Chem. Phys.* **1998**, *109*, 10053–10067.
- (11) Fischer, E.; Kimmich, R.; Fatkullin, N.; Yatsenko, G. *Phys. Rev. E* **2000**, *62*, 775–782.
- (12) Kehr, M.; Fatkullin, N.; Kimmich, R. *J. Chem. Phys.* **2007**, *126*, 094903.
- (13) Herrmann, A.; Kresse, B.; Wohlfahrt, M.; Bauer, I.; Privalov, A. F.; Kruk, D.; Fatkullin, N.; Fujara, F.; Rössler, E. A. *Macromolecules* **2012**, *45*, 6516–6526.
- (14) Fujara, F.; Geil, B.; Sillescu, H.; Fleischer, G. *Z. Phys. B Condens. Matter* **1992**, *88*, 195–204.
- (15) Price, W. S. *NMR Studies of Translational Motion*; Cambridge University Press: Cambridge, U.K., 2009.
- (16) Meier, R.; Kruk, D.; Gmeiner, J.; Rössler, E. A. *J. Chem. Phys.* **2012**, *136*, 034508.
- (17) Kruk, D.; Meier, R.; Rössler, E. A. *Phys. Rev. E* **2012**, *85*, 020201.
- (18) Meier, R.; Kruk, D.; Bourdick, A.; Schneider, E.; Rössler, E. A. *Appl. Magn. Reson.* **2013**, *44*, 153–168.
- (19) Meier, R.; Herrmann, A.; Kresse, B.; Privalov, A. F.; Kruk, D.; Fujara, F.; Rössler, E. A. *ACS Macro Lett.* **2013**, *1*, 96–99.
- (20) Kimmich, R.; Anardo, E. *Prog. Nucl. Magn. Reson. Spectrosc.* **2004**, *44*, 257–320.
- (21) Kimmich, R.; Fatkullin, N. *Adv. Polym. Sci.* **2004**, *170*, 1–113.
- (22) Kruk, D.; Herrmann, A.; Rössler, E. A. *Prog. NMR Spectrosc.* **2012**, *63*, 33–64.
- (23) Rössler, E. A.; Fatkullin, N.; Stapf, S. *Curr. Opin. Colloid Interface Sci.* **2013**, *18*, 173.
- (24) Abragam, A. *The Principles of Nuclear Magnetism*; Clarendon Press: Oxford, U.K., 1961.
- (25) Bonera, G.; Rigamonti, A. *J. Chem. Phys.* **1965**, *42*, 171–174.
- (26) Zeidler, M. D. *Ber. Bunsen-Ges. Phys. Chem.* **1965**, *69*, 659–668.
- (27) Kintzinger, J. P.; Zeidler, M. D. *Ber. Bunsen-Ges. Phys. Chem.* **1972**, *77*, 98–103.
- (28) Morita, M.; Ando, I.; Nishioka, A.; Sato, K.; Kato, Y.; Suzuki, S. *Polym. Sci., Polym. Lett. Ed.* **1980**, *18*, 109–113.
- (29) Collignon, J.; Sillescu, H. *J. Polym. Sci., Polym. Lett. Ed.* **1980**, *18*, 669–672.
- (30) Lindner, P.; Rössler, E.; Sillescu, H. *Makromol. Chem.* **1981**, *182*, 3652–3669.
- (31) Torrey, H. C. *Phys. Rev.* **1953**, *92*, 962–969.
- (32) Heinze, H. E.; Pfeiffer, H. *Z. Phys.* **1966**, *192*, 329–339.
- (33) Harmon, J. F.; Muller, B. H. *Phys. Rev.* **1969**, *182*, 400–410.
- (34) Belorizky, E.; Fries, P. H. *Chem. Phys. Lett.* **1988**, *145*, 33–38.
- (35) Fleischer, G.; Appel, M. *Macromolecules* **1995**, *28*, 7281–7283.
- (36) Lips, O.; Privalov, A. F.; Dvinskikh, S.; Fujara, F. *J. Magn. Reson.* **2001**, *149*, 22–28.
- (37) Kresse, B.; Privalov, A. F.; Fujara, F. *Solid State Nucl. Magn. Reson.* **2011**, *40*, 134–137.
- (38) Kariyo, S.; Gainaru, C.; Schick, H.; Brodin, A.; Novikov, V. N.; Rössler, E. A. *Phys. Rev. Lett.* **2006**, *97*, 207803. Erratum: Kariyo, S.; Herrmann, A.; Gainaru, C.; Schick, H.; Brodin, A.; Novikov, V. N.; Rössler, E. A. *Phys. Rev. Lett.* **2008**, *100*, 109901.
- (39) Kariyo, S.; Brodin, A.; Gainaru, C.; Herrmann, A.; Hintermeyer, J.; Schick, H.; Novikov, V. N.; Rössler, E. A. *Macromolecules* **2008**, *41*, 5322.
- (40) Kariyo, S.; Herrmann, A.; Gainaru, C.; Schick, H.; Brodin, A.; Novikov, V. N.; Rössler, E. A. *Macromolecules* **2008**, *41*, 5313.
- (41) Herrmann, A.; Novikov, V. N.; Rössler, E. A. *Macromolecules* **2009**, *42*, 2063–2068.
- (42) Herrmann, A.; Kariyo, S.; Abou Elfadl, A.; Meier, R.; Gmeiner, J.; Novikov, V. N.; Rössler, E. A. *Macromolecules* **2009**, *42*, 5236–5243.
- (43) Hofmann, M.; Herrmann, A.; Abou Elfadl, A.; Kruk, D.; Wohlfahrt, M.; Rössler, E. A. *Macromolecules* **2012**, *45*, 2390–2401.
- (44) Herrmann, A.; Kresse, B.; Gmeiner, J.; Privalov, A. F.; Kruk, D.; Fujara, F.; Rössler, E. A. *Macromolecules* **2012**, *45*, 1408–1416.
- (45) Colby, R. H.; Fetters, L. J.; Graessley, W. W. *Macromolecules* **1987**, *20*, 2226–2237.
- (46) Graessley, W. W. *Polymeric Liquids and Networks: Dynamics and Rheology*; Taylor & Francis Group: New York, 2008.
- (47) Rubinstein, M.; Colby, R. *Polymer Physics*; Oxford University Press: New York, 2008.
- (48) Smith, B. A.; Samulski, E. T.; Yu, L.; Winnik, M. A. *Macromolecules* **1985**, *18*, 1901.
- (49) Ding, Y.; Kisliuk, A.; Sokolov, A. P. *Macromolecules* **2004**, *37*, 161.
- (50) Hintermeyer, J.; Herrmann, A.; Kahlau, R.; Goiceanu, C.; Rössler, E. A. *Macromolecules* **2008**, *41*, 9335–9344.
- (51) Agapov, A. L.; Sokolov, A. P. *Macromolecules* **2009**, *42*, 2877–2878.
- (52) Berry, G. C.; Fox, T. G. *Adv. Polym. Sci.* **1986**, *5*, 261.
- (53) Bloembergen, N.; Purcell, E. M.; Pound, R. V. *Phys. Rev.* **1948**, *73* (7), 679.
- (54) Petzold, N.; Schmidtke, N.; Kahlau, R.; Bock, D.; Meier, R.; Micko, B.; Kruk, D.; Rössler, E. A. *J. Chem. Phys.* **2013**, *138*, 12A510.
- (55) Böttcher, C. J. F.; Bordewijk, P. *Theory of electric polarization*; Elsevier: Amsterdam, 1973; Vol. 2.
- (56) Abou Elfadl, A.; Kahlau, R.; Herrmann, A.; Novikov, V. N.; Rössler, E. A. *Macromolecules* **2010**, *43*, 3340–3351.
- (57) Indication on the web site: <http://en.wikipedia.org/wiki/Ethylbenzene>.
- (58) Data sheet from Polymer Standards Service, Mainz, Germany.
- (59) Indication on the web site: <http://de.wikipedia.org/wiki/Polystyrol>.
- (60) Indication on the web site: <http://de.wikipedia.org/wiki/1,2-Propandiol>.
- (61) Indication on the web site: http://en.wikipedia.org/wiki/Dipropylene_glycol.
- (62) Indication on the web site: <http://www.chemicaland21.com/industrialchem/solalc/TRIPROPYLENE%20GLYCOL.htm>.
- (63) Indication on the web site: <http://de.wikipedia.org/wiki/Polypropylenglycol>.
- (64) Petzold, N.; Rössler, E. A. *J. Chem. Phys.* **2010**, *133*, 124512.
- (65) Appel, M.; Fleischer, G. *Macromolecules* **1993**, *26*, 5520–5525.
- (66) Fleischer, G. *Polym. Bull.* **1984**, *11*, 75–80.
- (67) Appel, M.; Fleischer, G.; Kärger, J.; Chang, I.; Fujara, F.; Schönhals, A. *Colloid Polym. Sci.* **1997**, *275*, 187–191.
- (68) Gainaru, C.; Hiller, W.; Böhmer, R. *Macromolecules* **2010**, *43*, 1907–1914.
- (69) Agapov, A.; Sokolov, A. P. *Macromolecules* **2010**, *43*, 9126–9130.
- (70) Richter, D.; Monkenbusch, M.; Arbe, A.; Colmenero, J. *Adv. Polym. Sci.* **2005**, *174*, 1–221.

(71) Gray, R. W.; Harrison, G.; Lamb. *J. Proc. R. Soc. London A* **1977**, *356*, 77–102.

Bibliography

- [1] Cummins, H.Z.; Li, G.; Hwang, Y.H.; Shen, G.Q.; Du, W.M.; Hernandez, J.; Tao, N.J. *Z. Phys. B* **1997**, *103*, 501.
- [2] Adichtchev, S.; Benkhof, S.; Blochowicz, T.; Novikov, V. N.; Rössler, E.A.; Tschirwitz, C.; Wiedersich, J. *Phys. Rev. Lett.* **2002**, *88*, 055703.
- [3] Brodin, A; Rössler, E.A. *J. Chem. Phys.* **2006**, *125*, 114502.
- [4] Schmidtke, B.; Petzold, N.; Kahlau, R.; Rössler, E.A. *J. Chem. Phys.* **2013**, *139*, 084504.
- [5] Böttcher, C. J. F.; Bordewijk, P. *Theory of electric polarization, Vol. 2*; Elsevier: Amsterdam, **1973**.
- [6] Kudlik, A.; Benkhof, S.; Blochowicz, T.; Tschirwitz, C.; Rössler, E.A. *J. Mol. Struc.* **1999**, *479*, 201.
- [7] Lunkenheimer, P.; Schneider, U.; Brand, R.; Loidl, A. *Contemp. Phys.* **2000**, *41*, 15.
- [8] Hansen, J.P.; MacDonald, I.R. *Theory of Simple Liquids*; Academic Press: London, **2006**.
- [9] Khintchine, A. *Mathematische Annalen* **1934**, *109*, 604.
- [10] Gainaru, C.; Kahlau, R.; Rössler, E.A.; Böhmer, R. *J. Chem. Phys.* **2009**, *131*, 184510.
- [11] Davidson, D.W.; Cole, R.H. *J. Chem. Phys.* **1950**, *18*, 1417.
- [12] Davidson, D.W.; Cole, R.H. *J. Chem. Phys.* **1951**, *19*, 1484.
- [13] Palade, L.-I.; Yerney, V.; Attan, P. *Rheologica Acta* **1996**, *35*, 265.
- [14] Götze, W. *J. Phys. Condens. Matter* **1999**, *11*, A1.
- [15] Götze, W. *Complex Dynamics in Glass-Forming Liquids*, Oxford University Press: Oxford, **2009**.
- [16] Kivelson, D.; Kivelson, S. A.; Zhao, X. L.; Nussinov, Z.; Tarjus, G. *Physica A* **1995**, *219*, 27.
- [17] Vogel, H. *Phys. Z.* **1921**, *22*, 645.
- [18] Fulcher, G.S. *J. Am. Ceram. Soc.* **1925**, *6*, 339.
- [19] Tammann, G.; Hesse, W.Z. *Z. Anorg. Allg. Chem.* **1926**, *156*, 245.
- [20] Gainaru, C.; Böhmer, R.; Williams, G. *Eur. Phys. J. B* **2010**, *75*, 209.

- [21] Abragam, A. *The Principles of Nuclear Magnetism*, Clarendon Press, Oxford **1961**.
- [22] Kowalewski, J; Mäler, L. *Nuclear Spin Relaxation in Liquids*, Taylor and Francis, New York **2006**.
- [23] Bloembergen, N; Purcell, E.M.; Pound, R.V. *Phys. Rev.* **1948**, *73*, 679.
- [24] Solomon, I. *Phys. Rev.* **1955**, *99*, 559.
- [25] Gainaru, C.; Lips, O.; Troshagina, A.; Kahlau, R.; Brodin, A.; Fujara, F.; Rössler, E. A. *J. Chem. Phys.* **2008**, *128*, 174505.
- [26] Diezemann, G.; Sillescu, H. *J. Chem. Phys.* **1999**, *111*, 1126.
- [27] Dries, Th.; Fujara, F.; Kiebel, M.; Rössler, E.A.; Sillescu, H. *J. Chem. Phys.* **1988** *88*, 2139.
- [28] Blochowicz, T; Kudlik, A; Benkhof, S; Senker, J; Rossler, E.A.; Hinze, G *J. Chem. Phys.* **1999**, *110*, 12011.
- [29] Brodin, A.; Rössler, E.A. *Eur. Phys. J. B* **2005**, *44*, 3.
- [30] Petzold, N.; Rössler, E.A. *J. Chem. Phys.* **2010**, *133*, 124512.
- [31] Petzold, N.; Schmidtke, B.; Kahlau, R.; Bock, D.; Meier, R.; Micko, B.; Kruk ,D; Rössler, E.A. *J. Chem. Phys.* **2013**, *138*, 12A510.
- [32] Adishchev, S.; Bock, D.; Gainaru, C.; Kahlau, R.; Micko, B.; Petzold, N.; Pötzschner, B.; Rössler, E.A. *Z. Phys. Chem.* **2012**, *226*, 1149.
- [33] Stapf, S.; Kimmich, R.; Seitter, R.-O. *Phys. Rev. Lett.* **1995**, *75*, 2855.
- [34] Herrmann, A.; Kresse, B.; Wohlfahrt, M.; Bauer, I.; Privalov, A.F.; Kruk, D.; Fatkullin, N.; Fujara, F.; Rössler, E. A. *Macromolecules* **2012**, *45*, 6516.
- [35] Noack, F.; Preissing, G. *Z. Naturforsch* **1969**, *24 a*, 143.
- [36] Preissing, G.; Noack, F.; Kosfeld, R.; Gross, B. *Z. Physik* **1971**, *246*, 84.
- [37] Hausser, R; Noack, F. *Z. Physik* **1964**, *182*, 93.
- [38] Meier, R.; Kahlau, R.; Kruk, D.; Rössler, E.A. *J. Phys. Chem. A* **2010**, *114*, 7847.
- [39] Grosse, S.; Gubaydullin, F.; Scheelken, H.; Vieth, H.-M.; Yurkovskaya, A. *Appl. Magn. Reson.* **1999**, *17*, 211.
- [40] Ivanov, K.L.; Yurkovskaya, A.V.; Vieth, H.-M. *J. Chem. Phys* **2008**, *129*, 234513.
- [41] Korchak, S.; Ivanov, K.; Yurkovskaya, A.; Vieth, H.-M. *J. Chem. Phys.* **2012**, *133*, 194502.
- [42] Noack, F. *Prog. Nucl. Magn. Reson. Spectrosc.* **1986**, *18*, 171.
- [43] Kimmich, R.; Anorado, E. *Prog. Nucl. Magn. Reson. Spectrosc.* **2004**, *44*, 257.

- [44] Spinmaster FFC – 2000 Fast Field Cycling NMR Relaxometer Reference Manual. Stelar s.r.l.: via E. Fermi, 4. 27035 Mede (PV). Italy, 2001.
- [45] Lips, O.; Privalov, A.F.; Dvinskikh, S.V. Fujara, F. *J. Mag. Res.* **2001**, *149*, 22.
- [46] Kresse, B. Privalov, A.F.; Fujara, F. *Solid State Nucl. Magn. Reson.* **2011**, *40*, 134.
- [47] Sholl, C.A. *J. Phys. C* **1981**, *14*, 447.
- [48] Torrey, H.C. *Phys. Rev.* **1953**, *92*, 962.
- [49] Ayant, Y.; Belorizky, E.; Alizon, J.; Gallice, J. *J. Phys. (Paris)* **1975**, *36*, 991.
- [50] Hwang, L.P.; Freed, J.H. *J. Chem. Phys.* **1975**, *63*, 4017.
- [51] Ayant Y.; Belorizky E.; Fries P.; Rosset J. *Journal de Physique* **1977**, *38*, 325.
- [52] Albrand J.P.; Taieb, M.C.; Fries, P.; Belorizky, E. *J. Chem. Phys.* **1981**, *75*, 2141.
- [53] Giulotti, L.; Lanzi, G.; Tosca, L. *J. Chem. Phys.* **1956**, *24*, 632.
- [54] Mitchell, R.W.; Eisner, M. *J. Chem. Phys.* **1960**, *33*, 86.
- [55] Mitchell, R.W.; Eisner, M. *J. Chem. Phys.* **1961**, *34*, 651.
- [56] Hill, N.E. *Proc. Phys. Soc. B* **1955**, *68*, 209.
- [57] Bonera, G.; Rigamonti, A. *J. Chem. Phys.* **1965**, *42*, 171.
- [58] Harmon, J.F.; Muller, B.H. *Phys. Rev.* **1969**, *182*, 400.
- [59] Kintzinger, J.P.; Zeidler, M.D. *Ber. Bunsenges. Phys. Chem.* **1973**, *77*, 98.
- [60] Friedrich, A.; Dölle, A.; Zeidler M.D. *Magn. Reson. Chem.* **2003**, *41*, 813.
- [61] Collignon, J.; Sillescu, H. *J. Polym. Sci., Polym. Lett. Ed.* **1980**, *18*, 669.
- [62] Lindner, P.; Rössler, E.A.; Sillescu H. *Makromol. Chem.* **1981**, *182*, 3653.
- [63] Kehr, M.; Fatkullin, N.; Kimmich, R.J. *Chem. Phys.* **2007**, *126*, 094903.
- [64] Henritzi, P.; Bormuth, A.; Vogel, M. *Solid State Nucl. Magn. Reson.* **2013**, *54*, 32.
- [65] Harmon, J.F. *Chem. Phys. Lett.* **1970**, *7*, 207.
- [66] Chang, I.; Sillescu, H. *J. Phys. Chem. B* **1997**, *101*, 8794.
- [67] Fujara, F.; Geil, B.; Sillescu, H.; Fleischer, G. *Z. Phys. B* **1992**, *88*, 195.
- [68] Fries, P.H.; Belorizky, E.; Minier M.; Albrand, J.P.; Taieb, M.C. *Mol. Phys.* **1982**, *47*, 1153.
- [69] Stark, U.; Cebe, E.; Meise-Greisch, K.; Müller Warmuth, W. *J. Mol. Liq.* **1992**, *52*, 67.
- [70] Belorizky, E.; Gillies, D.G.; Gorecki, W.; Lang, K.; Noack, F.; Roux, C.; Struppe, J.; Sutcliffe, L.H.; Travers, J. P.; Wu, X. *J. Phys. Chem. A* **1998**, *102*, 3674.
- [71] Kruk, D.; Korpała, A.; Kowalewski, J.; Rössler, E.A.; Moscicki, J. *J. Chem. Phys.* **2012**, *137*, 044512.

- [72] Kruk, D.; Korpała, A.; Kubica A.; Meier, R.; Rössler, E.A. *J.Chem. Phys.* **2013**, *138*, 024506.
- [73] Heitjans, P.; Schirmer, A.; Indris, S. in *Diffusion in Condensed Matter: Methods, Materials, Models*; Heitjans, P., Kärger, J., Eds.; Springer: Berlin, **2005**; 369.
- [74] Kuhn, A; Sreeraj, P.; Pöttgen, R.; Wiemhöfer, H.-D.; Martin Wilkening, M.; Heitjans, P. *J. Am. Chem. Soc.* **2011**, *133*, 11018.
- [75] Posch, H.A.; Dardy H.D.; Litovitz, T.A. *Ber. Bunsenges. Physik. Chem.* **1977**, *81*, 744.
- [76] Dux, H.; Dorfmueller, T. *Chem. Phys.* **1979**, *40*, 219.
- [77] Chen, B.; Sigmund, E.E.; Halperin, W.P. *Phys. Rev. Lett.* **2006**, *96*, 145502.
- [78] Rouse, P.E. *J. Chem. Phys.* **1953**, *21*, 1272.
- [79] Kruk. D.; Herrmann, A.; Rössler, E.A. *Prog. NMR Spectrosc.* **2004**, *63*, 33.
- [80] Doi, M.; Edwards, S.F. *The Theory of Polymer Dynamics*; Oxford Sci. Publications: Oxford, U.K., **1986**.
- [81] Rubinstein, M.; Colby, R. *Polymer Physics*; Oxford University Press: New York, **2008**.
- [82] Kircher, O.; Böhmer, R.; Alba-Simionesco, C. *J. Mol. Struc.* **1999**, *479*, 195.
- [83] Schnauss, W.; Fujara, F.; Sillescu, H. *J. Chem. Phys.* **1992**, *97*, 1378.
- [84] Graessley, W.W. *Polymeric Liquids and Networks: Dynamics and Rheology*; Taylor & Francis Group: New York, **2008**.
- [85] Kariyo, S.; Gainaru, C.; Schick, H.; Brodin, A.; Novikov, V.N.; Rössler, E.A. *Phys. Rev. Lett.* **2006**, *97*, 207803. Erratum: Kariyo, S.; Herrmann, A.; Gainaru, C.; Schick, H.; Brodin, A.; Novikov, V.N.; Rössler, E.A. *Phys. Rev. Lett.* **2008**, *100*, 109901.
- [86] Kariyo, S.; Herrmann, A.; Gainaru, C.; Schick, H.; Brodin, A.; Novikov, V.N.; Rössler, E.A. *Macromolecules* **2008**, *41*, 5313.
- [87] Kariyo, S.; Brodin, A.; Gainaru, C.; Herrmann, A.; Hintermeyer, J.; Schick, H.; Novikov, V.N.; Rössler, E.A. *Macromolecules* **2008**, *41*, 5322.
- [88] Herrmann, A.; Novikov, V.N.; Rössler, E.A. *Macromolecules* **2009**, *42*, 2063.
- [89] Herrmann, A.; Kariyo, S.; Abou Elfadl, A.; Meier, R.; Gmeiner, J.; Novikov, V.N.; Rössler, E.A. *Macromolecules* **2009**, *42*, 5236.
- [90] Herrmann, A.; Kresse, B.; Gmeiner, J.; Privalov, A.F.; Kruk, D.; Fujara, F.; Rössler, E.A. *Macromolecules* **2012**, *45*, 1408.

- [91] Hofmann, M.; Herrmann, A.; Abou Elfadl, A.; Kruk, D.; Wohlfahrt, M.; Rössler, E.A. *Macromolecules* **2012**, *45*, 2390.
- [92] Hintermeyer, J.; Herrmann, A.; Kahlau, R.; Goiceanu, C.; Rössler, E.A. *Macromolecules* **2008**, *41*, 9335.

Acknowledgements

I would like to thank very much my supervisor Ernst Rößler for the great opportunity to work in this field. I appreciated the pleasant atmosphere in the group which was very inspiring. By allowing certain latitudes on the one hand and by kindly giving constructive suggestions on the other hand he creates a unique room where fruitful research can be achieved.

Many thanks go to Danuta Kruk for the friendly and enjoyable collaboration. Her wide knowledge on the theory of spin systems was very profitable.

Furthermore I am very grateful to Franz Fujara for the opportunity to measure in his lab in Darmstadt and to Benjamin Kresse who patiently introduced me to the relaxometer there, which provided very valuable data in the case of polymers.

Finally, I am indebted to Jürgen Gmeiner who helped me with the preparation of the glycerol samples, which is not trivial due to its hygroscopicity.